SEISMIC REHABILITATION OF REINFORCED MASONRY COLUMNS USING CFRP AND GFRP WRAPS

Nima Farnia

A Thesis

In the Department

of

Building, Civil, and Environmental Engineering

Presented in Partial Fulfillment of the Requirements
For the Degree of
Doctor of Philosophy (Civil Engineering) at

Concordia University

Montréal, Québec, Canada

November 2011

CONCORDIA UNIVERSITY
SCHOOL OF GRADUATE STUDIES

This is to certify that the thesis prepared

By: Nima Farnia

Entitled: Seismic Rehabilitation of Reinforced Masonry Columns Using CFRP and GFRP Wraps

and submitted in partial fulfillment of the requirements for the degree of

Doctor of Philosophy (Civil Engineering)

complies with the regulations of the University and meets the accepted standards with respect to originality and quality.

Signed by the final examining committee:

Dr. G. Butler — Chair

Dr. M. Saatcioglu — External Examiner

Dr. S.V. Hoa — External to Program

Dr. M. Nokken — Examiner

Dr. A. Bagchi — Examiner

Dr. K. Galal and Dr. O. A. Pekau — Thesis Supervisor

Approved by

Chair of Department or Graduate Program Director

Dean of Faculty

ABSTRACT

SEISMIC REHABILITATION OF REINFORCED MASONRY COLUMNS USING CFRP AND GFRP WRAPS

NIMA FARNIA - Ph.D.
Concordia University 2011

Compared to reinforced concrete, there are relatively fewer experimental and analytical studies that address the behaviour of masonry columns under combined axial load and cyclic flexure. There exist reinforced concrete masonry (RCM) columns that are part of the moment resisting system of masonry structures that are in need for seismic upgrade. Wrapping such susceptible RCM columns with carbon fibre-reinforced polymer (CFRP) or glass fibre-reinforced polymer (GFRP) composites is expected to enhance the seismic behaviour of reinforced masonry columns considerably. This study focuses on assessing the seismic performance of RCM columns wrapped with CFRP or GFRP composites.

In the experimental phase of this study, nine 1.4 m reinforced masonry columns were constructed and tested when subjected to constant axial force and cyclic lateral excitations. The columns have a cross-section of 390mm×390mm and were constructed using bull-nosed concrete units. The first column had no FRP wraps and was used as a control specimen while the other eight columns were wrapped using different number of layers of CFRP (or GFRP) sheets or different wrapping schemes. From the tests, the effect of FRP wraps on improving the ductile behaviour, strength and energy dissipation capacity of RCM columns were quantified.

Furthermore, the experimental program extended to develop a stress-strain model for grouted concrete masonry strengthened with carbon fiber-reinforced polymer (CFRP) composites. Twelve five-block high prisms were constructed using bull-nose concrete blocks. As the study focuses on evaluating the contribution of FRP wraps in enhancing concrete masonry behaviour, the test variable was set to be the volumetric ratio of FRP material, and via detailed instrumentation, tests were conducted to measure the confining effect of the FRP material.

Finally, a macro model that is capable of simulating the cyclic lateral load-deformation response of FRP-strengthened reinforced concrete masonry (RCM) columns is proposed. The data obtained from experimental results and the proposed strain-stress model were used for developing the nonlinear macro model, and it is shown that there is a good correlation between the experimental results and the predictions of the proposed model be it the load-deformation backbone curve or the full load-deformation hysteretic response of FRP-strengthened RCM columns.

ACKNOWLEDGEMENT

First of all, I would like to thank my supervisors Dr. Khaled Galal and Dr. Oscar Pekau for their academic and financial support. I am especially grateful to Dr. Khaled Galal for the tremendous help in experimental techniques and approaches. This work would have been impossible to be complete without his help.

I would like to acknowledge the financial supports of Natural Sciences and Engineering Research Council of Canada (NSERC), le Fonds Québécois de la Recherche sur la Nature et les Technologies (FQRNT), and Centre d' Études Interuniversitaire sur les Structures sous Charges Extrêmes (CEISCE).

The experimental phase of this project became possible with the endless support and sincere collaboration of l'Association des Entrepreneurs en Maçonnerie du Québec (AEMQ), Normand Turenne (Président) and Denis Brisebois (Directeur Général). Furthermore, Canada Masonry Design Centre (CMDC) is greatly acknowledged for their contribution in enlightening us with ideas at the very beginning of this project.

I would also like to to extend my sincere gratitude to all my other colleagues namely; Alp, Amir, Behnam, Hany, Hosein, Hossam, Mossab, and Ricky for supporting me and helping me in the structural laboratory to complete my experimental work.

I also would like acknowledge the assistance and technical support of laboratory technicians Mark Elie, Jaime Yeargans, and Tiberiu Aldea. Their ideas helped me during the experimental phase of this thesis.

To my beloved family

TABLE OF CONTENTS

LIST OF FIGURES

LIST OF TABLES

LIST OF ACRONYMS

ACI	American Concrete Institute
ASTM	American Society of Testing and Materials
CFRP	Carbon Fibre-Reinforced Polymer
CSA	Canadian Standards Association
FRP	Fibre-Reinforced Polymer
GFRP	Glass Fibre-Reinforced Polymer
AFRP	Aramid Fibre-Reinforced Polymer
ISIS	Intelligent Sensing for Innovative Structures
MSJC	Specification for Masonry Structure
NCMA	National Concrete Masonry Association
RBM	Reinforced Brick Masonry
RC	Reinforced Concrete
RM	Reinforced Masonry
RCM	Reinforced Concrete Masonry
RMC	Reinforced Masonry Column
URM	Unreinforced Masonry

LIST OF SYMBOLS

The following symbols are used in this study:

A_e: Effective confined area

A_g: Gross section area

b: Section width

b_f: Width of CFRP strips in partial wrapping

c: Neutral axis depth

C: nonlinear function order (P-M model)

C_F: Unloading stiffness shape factor

d: Depth of the cross section

d_b: Rebar diameter

d_{cr}: Column top lateral displacement at cracking point

$d_{\max}$: Maximum lateral displacement in each cyclic loop

d_y: Column top lateral displacement at yield point

d_u: Column top lateral displacement at ultimate state

D_e: Equivalent diameter of rectangular section

E_m: Modules of Elasticity of concrete masonry

E_f: Modules of Elasticity of FRP

E_s: Modules of Elasticity of steel rebars

$f_{l,eff}$: Lateral confining pressure at peak compressive strength

f_l : Lateral confining pressure

f_m : Masonry axial stress

f_m' : Maximum compressive strength of unconfined masonry

f_{mc} : Maximum compressive strength of confined masonry

$f_{\max}$: Maximum compressive strength of masonry

f_s : Stress in steel rebars

f_{sy} : Yield tensile stress in steel rebars

f_{su} : Ultimate tensile stress in steel rebars

f_t : Modulus of rupture of the concrete masonry

$F_.$ Adjusted lateral load

F_{cr} : Lateral force at cracking point

$F_{\max}$: Maximum lateral force in each cyclic loop

F_u : Lateral force at ultimate state

F_y : Lateral force at yield point

g_m : Masonry mass-density

h: Section height

h_2: Distance between two hinges on the top of the column

h_p : Height of the plastic hinge

I_g : Gross section moment of inertia

k: Column stiffness (kN/mm)

k_1: Empirical constant

k_2: Empirical constant

K_{avg}: Stiffness in one cycle

l_d: Development length

n: empirical constant

N: number of CFRP layers

P: Axial Force

r: corner's radius

S_f: Pitch in partial wrapping

t_j: Thickness of CFRP jacket

u: Top displacement of the column

u_b: Elastic bond stress

$u_b^{'}$: Inelastic bond stress

V: Applied lateral load

Z_m: Empirical constant

Δ: Lateral displacement of the tip of the column

Δ_{slip}: Bond-slip deformation

Δ_y: Flexural deformation at yield

Δ_u: Ultimate displacement

δ: Lateral drift (%)

ε_c: Axial strain of a concrete section

ε_{fu} : Ultimate FRP strain (rupture strain)

ε_{fc} : FRP tensile strains at capacity failure

α : Non-dimensional coefficients

ε_{l} : Lateral strain

ε_{j} : Transverse strain of the jacket

ε_{m} : Masonry axial strain

ε_{m0} : Axial strains recorded at peak strength for unconfined masonry

ε_{mcc} : Axial strains recorded at capacity failure for confined masonry

ε_{mc} : Axial strains recorded at peak strength for confined masonry

ε_{mcu} : Axial strains recorded at ultimate failure for confined masonry

ε_{v} : Volumetric strain

ρ_{FRP} : Volumetric ratio of FRP reinforcement

μ_{Δ} : Displacement ductility

ν_{0} : Initial Poisson's ratio

CHAPTER 1

INTRODUCTION

1.1 Background and problem definition

Masonry materials are one of the most important construction materials as they have been widely used in building construction over centuries. The term masonry refers generally to tuff or clay brick, concrete block, etc. that are bonded with mortar and grout. From a structural engineering perspective, masonry is classified as either unreinforced or reinforced masonry. Unreinforced masonry has high compressive carrying capacity, but like unreinforced concrete, unreinforced masonry possesses little tensile strength, and it cannot be used as an efficient building material for structures or structural elements subjected to direct tensile stress or tensile stresses associated with flexure. To improve this inefficiency in masonry, it is reinforced with reinforcing bars (usually steel), which enhances strength of masonry in tension.

While reinforced masonry structures generally provide good performance under gravity loads, there are still several aspects of their behaviour when subjected to high lateral forces that occur in seismic events need to be understood. The current National Building Code of Canada, (NBCC) (2010), defines four types of reinforced masonry structures based on their seismic force resisting system. These types are: moderate ductile shear walls, limited ductile shear walls, shear walls (conventional construction), and moment resisting frames. Regardless of the utilized lateral load resisting system (being either moment-resisting frame or combination of shear walls and columns), the overall behaviour of the structure is greatly affected by the performance of reinforced masonry

columns. In moment resisting frames made of concrete blocks, reinforced concrete masonry (RCM) columns are expected to resist the moment reversals associated with the seismic excitation besides resisting the axial loads. Furthermore, RCM columns that are used in combination with shear walls (mainly due to presence of openings) will be subjected to cyclic excitations that will induce inelastic deformations. In both above-mentioned scenarios, the masonry column should possess high ductility and energy dissipation capacity in order to prevent its failure which may lead to progressive collapse of part of, or the whole, masonry structure.

In seismic events, existing reinforced masonry columns are expected to deform well into their inelastic range when subjected to a seismic load. This inelastic (nonlinear) deformation can be either ductile or non-ductile. Prior to the enforcement of ductile design philosophy of 1970's, RCM columns were designed on the basis of strength. Once the ultimate strength of a column is reached, abrupt non-ductile failure follows, which reduces the energy dissipating capacity of that column and consequently the structure and results in brittle failure. Performance-based seismic engineering is the modern approach to earthquake resistant design. Seismic performance *(performance level)* is described by designating the maximum allowable damage state *(damage indices)* for an identified seismic hazard *(hazard level)* (FEM A273/274, 1997 and Vision 2000 Committee, 1995). Overall lateral deflection, ductility demand, and inter-storey drift are the most commonly used damage indices. One method of upgrading the seismic performance level of existing non-ductile RCM columns is to increase their ductility.

The increase in ductility can be achieved by using fibre-reinforced polymer (FRP) composite materials as a confining material. Moreover, besides improving the ductility,

FRP confinement increases lateral load carrying capacity of confined members, and can be used for strengthening purposes.

Fibre-reinforced polymer (FRP) composite materials have become a popular material in strengthening of reinforced concrete and masonry elements in recent decades. They offer attractive characteristics such as high strength and high stiffness–to-weight ratio, as well as light weight for ease of application with minimal interruption to occupants. Most research efforts in retrofitting deficient masonry structural elements using FRP were directed to masonry walls, and less work has been conducted in the past on retrofitting reinforced masonry columns. On the other hand, there has been significant effort in evaluating the performance of FRP-rehabilitated plain and reinforced concrete (RC) columns (e.g. Shrive et al. 2003, Galal et al. 2005, and Paultre et al. 2008). In general, previous research showed that wrapping non-ductile RC columns with FRP sheets is an effective form of increasing the column's ductility and, hence, its seismic performance.

In recent years, strengthening different types of masonry columns with FRP material attracted the attention of different researchers. Micelli et al. (2004) studied the behaviour of brick masonry columns with different masonry materials and external FRP wrapping to quantify the compressive strength of confined masonry columns. Krevaikas and Traintafillou (2005) proposed a strength model for FRP wrapped rectangular columns made of clay bricks. Also, FRP confinement of rectangular specimens made of limestone and clay bricks were studied by Aiello et al. (2009). Recently, Ludovico et al. (2010) provided more data for behaviour of FRP-wrapped tuff and clay brick masonry section.

In this research, the performance of wrapped reinforced concrete masonry (RCM) columns when subjected to constant axial load and increasing cyclic lateral excitations is investigated experimentally and analytically. It is noteworthy to say that, up to the author's knowledge, the literature survey did not reveal similar experimental or analytical programs on the behaviour of concrete FRP-wrapped masonry columns.

1.2 Objectives

This research has two main objectives. The first objective is to examine experimentally the overall seismic performance of FRP-confined rectangular reinforced concrete masonry (RCM) columns subjected to axial and lateral load excitations, and to generate enough experimental data to develop a non-linear macro model to predict the behaviour of RCM columns. The second objective is to develop an accurate analytical model based on experimental tests to represent stress-strain relation of the CFRP-confined concrete masonry in axial compression which is needed for development of non-linear macro model.

1.3 Scope

In order to achieve the objectives of this research, the scope of research is to:

1. Carry out auxiliary tests in order to obtain the mechanical characteristics of the constituent materials such as concrete block, mortar, grout, steel reinforcement, CFRP and GFRP sheets, and also to obtain masonry assemblage properties, namely, compressive and tensile strength of masonry assemblage.

2. Construct and test nine full-size masonry columns under axial and cyclic lateral loads. The first column acts as a control column and the rest of the columns will be wrapped with different number of layers of CFRP or GFRP sheets, or with different wrapping schemes.
3. Test twelve 5-block high prisms wrapped with CFRP sheets under compressive load. Based on the results of tested prisms, an analytical model is developed to obtain stress-strain relation of rectangular confined RCM columns.
4. Develop a non-linear macro model to predict the hysteretic behaviour of FRP-jacketed RCM columns subject to combined axial and cyclic lateral loads.

1.4 Organization of the thesis

This thesis is divided into seven chapters. The following is a brief description of the contents of each chapter.

Chapter one is an introductory chapter, provides brief information regarding the importance and objectives of this research and followed with a summary of organization of the thesis.

Chapter two reviews the pervious research in strengthening of masonry columns and application of FRP material in improving the confinement of masonry columns. Also at the end of this chapter common methods in design of masonry construction are summarized and current Canadian codes and standards in the field of masonry are introduced.

Chapter three presents the first phase of the experimental programs which consists of tests conducted to obtain properties of concrete blocks, steel reinforcement, mortar and

grout. Furthermore, tests conducted on auxiliary specimens to obtain compressive strength and flexural strength of masonry assemblage is explained. Moreover, chapter three reviews aspects associated with the testing of full-sized RCM columns including design, and fabrication. The test setup utilized for testing of full-sized RCM columns is described. Finally, the criteria adopted to define failure mechanism during testing of the full-sized columns are explained at the end of this chapter.

In chapter four, the effectiveness of CFRP wraps in modifying the failure mechanism and improving compression strain ductility of masonry blocks is quantified. Results of the experimental study along with data available in the literature were used to propose refined confinement model for CFRP-wrapped rectangular masonry prisms. Moreover, the developed model is validated by comparing the section capacity of tested CFRP-wrapped columns with analytical results obtained from using the developed model.

Chapter five (along with details in Appendix B) presents the results obtained from testing nine full-scale reinforced masonry column and compares the overall seismic behaviour of the tested columns. The detailed behaviour of each column such as strains in the rebars, ties, and FRP jacket are presented in Appendix B. Comparisons are made to assess the effect of different number and type of CFRP (or GFRP) sheets on improving the lateral load carrying capacity, ductility, energy absorption, and stiffness.

Chapter six focuses on developing a macro model to simulate the cyclic lateral load-deformation response of CFRP-strengthened reinforced concrete masonry (RCM) columns with limited computational effort. The macro model shows a general good

correlation between obtained experimental and proposed monotonic and hysteretic models.

Chapter seven includes the conclusions and contributions of this study followed by a list of recommendations for future studies.

CHAPTER 2

LITERATURE REVIEW

2.1 Introduction

This chapter covers four topics relevant to the research conducted in this thesis. First part of this chapter provides general information about masonry columns. In the second part, a brief review of literature associated with different techniques for strengthening of masonry columns is presented. The third part of this chapter briefly reviews common approaches for predicting the contribution of confinement material to the strength capacity or stress-strain relations of masonry sections. Finally, in the last part of this chapter, general concepts used in the design of masonry structures are explained briefly, also Canadian codes and other important available standards in masonry design are introduced.

2.2 Definition of masonry columns

A masonry column is a vertical compression member that has a height greater than $5(t+10)$ mm and a length less than $3(t+10)$ mm, where t is the column thickness (width). As shown in Figure 2.1, a masonry column is usually built as a separate supporting member. Where such a column is contained within a wall, it is commonly referred to as a pier. Piers can be enlarged in the out-of-plane direction of the wall for added strength and stability. If a column is built integrally with the wall and interacts with the wall to resist an out-of-plane lateral load, it is called a pilaster. A pilaster within a wall may be constructed to be flush, or more commonly, can project from either or both

faces of the wall. It serves to resist concentrated vertical load and to stiffen the wall against lateral buckling. In addition, the wall can span horizontally between pilasters to carry lateral loads. In this case, the pilaster must be designed to span vertically and resist these loads by bending in the vertical direction.

Columns and pilasters can be unreinforced or reinforced. However, due to the high vulnerability of columns and their structural significance to overall building stability, it is recommended that, even when reinforcement is not required by CSA S304.1 (2004), masonry columns should have minimum reinforcement of 0.25% of the gross-sectional area with at least four reinforcing bars. Figure 2.2 shows the typical layout and reinforcement details for masonry columns and pilasters. Columns and pilasters can be constructed using standard block and brick or by using special pilaster or chimney units. Although conventional practice has been to allow ties to be placed in the mortar joints away from direct contact with vertical reinforcement, the more recent trend is to require ties to be directly contact with the vertical reinforcement to prevent buckling and improve ductile behaviour.

2.3 Review of available techniques for strengthening of masonry columns

Experimental research shows that masonry columns subjected to axial load fail in one of three modes (Drysdale and Hamid, 2005):

- Overall vertical splitting and crushing of the masonry shell and the grout core (for unreinforced columns)

- Simultaneous splitting of the masonry shell, curling of the grout core, buckling of vertical reinforcement between ties.
- Same as the second mode, but with pulling out of lateral tie hooks and buckling of vertical reinforcement over two or more courses.

Since the 1980's, different techniques have been developed for preventing/delaying any of above modes of failure for masonry columns that are subjected to compressive forces. Strengthening of masonry columns have been achieved by utilizing steel confinement, concrete jacket confinement, and FRP confinement. It should be noted that when it comes to strengthening, similar to the concrete members, as shown in Figure 2.3, the response of masonry varies depends on the method used for strengthening, and it is important to understand the changes in the behaviour of the confined section which directly affects the design outcome.

2.3.1 Steel and concrete-confined masonry columns

Priestley and Elder (1983) conducted experimental tests on grouted concrete masonry prisms in order to obtain stress-strain curves of unconfined and confined concrete masonry. In their study, confinement was provided by placing stainless steel confining plates in mortar bed joints. Figure 2.4 shows the dimensions of tested prisms. Prisms were tested under axial load up to the failure, and it was observed that average stress-strain curves obtained from the test program agreed well with a modified form of Kent-Park curve (Priestley and Elder, 1983) for unconfined and confined concrete. More details about modified Kent-Park model are given in section 2.4 of this chapter.

Khalaf et al. (1993) conducted an experimental program to determine the strength and the behaviour of block masonry columns; also, the effect of lateral ties and different percentage of vertical bars was investigated. Short stack-bonded fully bedded block-work masonry columns (similar to the one showed in Figure 2.5) were constructed and tested under axial load to study the mechanism of failure and to determine ultimate strength. In their study, they concluded that strength of columns with 6- and 8-mm-Φ ties were 17.7 and 17.6 percent higher than the unreinforced columns due to confinement provided by lateral ties. Furthermore, they proposed a new formula to calculate the ultimate load of block masonry columns based on the compressive strength of masonry assemblage (f'_m) and contribution of vertical bars.

Finally, as an alternative approach, Kog et al. (2001) conducted an experimental program by adding concrete jacketing to confine brick masonry columns, as shown in Figure 2.6. In their research, a tremendous increase in the load-bearing capacity was noted when the columns were strengthened by concrete jackets reinforced with longitudinal steel and stirrups. The tested columns exhibited two-stage behaviour, one before and another after the cracking of the concrete jacket. The peak load-bearing capacity was proportional to the amount of stirrups in the jacket, grade of concrete, and amount of longitudinal steel. Moreover, the researchers proposed an analytical method to predict the axial load bearing capacity of concrete jacketed brick masonry columns.

2.3.2 FRP-confined masonry columns

Tegola et al. (2003) investigated the mechanical behaviour of masonry elements confined by FRP material. In their study, columns with natural stone blocks were

strengthened with internal pultruded aramid fibre-reinforced polymer (AFRP) composite rods inserted in every horizontal joint and wrapped with one layer of CFRP laminate. By adding pultruded AFRP rods, transversally inserted similar to traditional steel dowels, confinement effectiveness was increased, and consequently columns failure under increasing compressive load was delayed. As shown in Figure 2.7, the researchers concluded that the proposed strengthening technique is effective in enhancing stiffness, strength and ductility.

In another experimental study, Masia and Shrive (2003) aimed to quantify the increase in strength of CFRP wrapped square masonry columns. Figure 2.8 shows some of the 18 columns made of clay masonry units that were tested under axial load. Note that in this study, masonry columns were rehabilitated with CFRP sheets after they got damaged under axial load. Masia and Shrive observed that, in general, the axial load bearing capacity increased by wrapping masonry columns; however, due to limited number of tests they could not draw quantify the effectiveness of CFRP wraps.

Krevaikas and Traintafillou (2005) studied the effect of number of layers, radius of the corners, cross section ratios, and type of fibres in strengthening of masonry columns, as some of these variables are shown in Figure 2.9. In their study, 42 specimens made of clay bricks were tested under axial load, and it was observed that the confinement provided by FRP considerably improves both the load-carrying capacity and deformability of rectangular masonry columns. Furthermore, Krevaikas and Traintafillou (2005) proposed a simple confinement model to develop stress-strain curves of FRP-confined masonry. More details about the proposed model are given in section 2.4 of this chapter.

Shaheen and Shrive (2005) studied the strengthening of masonry columns by spraying them with glass fiber reinforced polymer (GFRP). Twenty-four reinforced columns were constructed with Type S mortar and straight and bull nose masonry units and tested under increasing axial loads. Figure 2.10 shows the process of spraying GFRP on the surface of masonry column. In their conclusions, the researchers indicated that ultimate loads of columns sprayed with GFRP did not increase substantially; however, there is a general improvement in the load-carrying capacity of the columns by increasing the sprayed GFRP thickness and steel reinforcement. Furthermore, they noted that large increases in ultimate strains were obtained for all strengthened specimens.

Aiello et al. (2007 and 2009) investigated the effectiveness of CFRP and GFRP confinement in improving the axial load-carrying capacity of both circular and rectangular masonry columns (see Figure 2.11). Columns were built out of clay or calcareous blocks. Different schemes such as wrapping only at location of bed joints with CFRP strips instead of providing continuous wrap along the height tested. Similar to previous research, increased strength and deformability were observed. Moreover, Aiello et al. (2009) proposed a confinement model to develop stress-strain curves of FRP-confined masonry. More details about the proposed model are given in section 2.4.4 of this chapter.

In a more recent study, Ludovico et al. (2010) investigated the effectiveness of wrapping columns with uniaxial glass FRP (GFRP), carbon FRP (CFRP) and basalt FRP (BFRP) laminates by testing 18 square masonry scaled columns made of tuff or clay bricks under increasing axial load. The specimen dimensions and FRP wrapping scheme are shown in Figure 2.12. It was shown that the investigated confining systems are able to

provide significant gains in terms of both compressive strength and ductility of masonry columns. Furthermore, Ludovico et al. (2010) proposed refined equations for theoretical predictions of strength increase in the wrapped masonry columns.

2.4 Review of stress-strain relations of unconfined and CFRP-confined masonry sections

2.4.1 General behaviour of FRP-confined concrete masonry section

The stress-strain behaviour of FRP-confined concrete masonry is usually obtained by assuming a behaviour that is similar to that of FRP-confined concrete sections. Figure 2.13 shows a typical stress-strain curve in the axial compression and the lateral dilatancy directions for concrete (or concrete masonry) material. The FRP-confined concrete masonry response is expressed by the dashed lines; and the unconfined concrete masonry response is expressed by the solid lines. In Figure 2.13, f_m and ε_m are the axial stress and strain of unconfined concrete masonry, f_{mc} and ε_{mc} are the axial stress and strain of the FRP confined concrete masonry, $f_m^{'}$ and $f_{mc}^{'}$ are maximum strength of unconfined and confined concrete masonry, respectively. Also the relation between the confining pressure f_l and the lateral strain ε_l is shown. The following sections describe the means of evaluating the above parameters based on the previous experimental studies.

2.4.2 Priestly and Elder model for unconfined concrete masonry (1983)

Priestley and Elder (1983) introduced stress-strain curves for both unconfined and confined concrete masonry by modifying the Kent-Park (1982) model that was originally

developed for concrete elements. Priestley and Elder (1983) developed stress-strain curves of confined and unconfined concrete masonry by conducting tests on number of concrete masonry prisms (see 2.3.1 in this chapter). Their stress-strain model for unconfined masonry is used as a guideline to obtain the behaviour of unconfined concrete masonry in this study (see Chapter 5). However, in their research, confinement was provided by placing steel plates in mortar bed joints which in general behaves differently in comparison to confinement provided by FRP wraps; therefore, their model for confined masonry concrete is not suitable for the analytical phase of this thesis.

As can be seen from Figure 2.14, Priestly and Elder (1983) model for unconfined concrete consists of three portions:

- A parabolic rising curve:

$$f_m = 1.067 f_m^{'}\left[\frac{2\varepsilon_m}{0.002} - \left(\frac{\varepsilon_m}{0.002}\right)^2\right] \quad : \text{For } \varepsilon_m \le 0.0015 \qquad 2.1$$

where, ε_m and f_m are axial strain and stress in masonry respectively, and $f_m^{'}$ is the maximum compressive strength of concrete masonry assemblage.

- A linear falling branch:

$$f_m = f_m^{'}[1 - Z_m(\varepsilon_m - 0.0015)] \quad :\text{For } \varepsilon_m > 0.0015 \qquad 2.2$$

where, parameter Z_m indicates the slope of falling branch and obtained from experimental tests. Parameter Z_m is described by Kent-Park as:

$$Z_m = \frac{0.5}{\left[\frac{3 + 0.29 f_m^{'}}{145 f_m^{'} - 1000}\right] - 0.002} \qquad 2.3$$

- Final horizontal plateau (constant stress):

For strains in masonry (ε_m) that f_m obtained from Equation 2.2 is smaller than $0.2f_m^{'}$, f_m is assumed equivalent to $0.2f_m^{'}$.

2.4.3 Krevaikas and Traintafillou model for confined masonry (2005)

Krevaikas and Traintafillou (2005) studied the effect of confinement to improve the overall behaviour of rectangular masonry columns (for more details see section 2.3.2). As suggested by Krevaikas and Traintafillou (2005) the basis of the FRP contribution to the strength and deformability of confined masonry is, by analogy to confined concrete, the transverse passive pressure f_l developing in the masonry in response to the jacket forces. This pressure is, in general, non-uniform, especially near the corners of rectangular cross sections. As an average value for f_l in a cross section with dimensions b and h, Krevaikas and Traintafillou (2005) suggested (Figure 2.15):

$$f_l = \frac{\sigma_{l,h} + \sigma_{l,b}}{2} = \frac{1}{2} k_e \left(\frac{2t_f}{h} E_f \varepsilon_f + \frac{2t_f}{b} E_f \varepsilon_f\right) = k_e \frac{(b+h)}{bh} t_f E_f \varepsilon_f \qquad 2.4$$

where E_f=elastic modulus of FRP; ε_f=circumferential FRP strain; t_f=thickness of FRP; and k_e=effectiveness coefficient.

For continuous FRP jackets with fibers in the direction perpendicular to the member axis, k_e is defined as the ratio of the effectively confined area (A_e in Figure 2.16) to the total cross-sectional area A_g as follows:

$$k_e = 1 - \frac{b'^2 + h'^2}{2A_g} \qquad 2.5$$

Compressive failure of FRP-confined masonry occurs when the FRP jacket fractures at a hoop stress that is equal to the hoop tensile strength, $f_{fe} = E_f \varepsilon_f$, which is in general less than the uniaxial tensile strength of FRP (due to the multi-axial state of stress, stress concentrations, etc.).

The model proposed by Krevaikas and Traintafillou (2005) for FRP-confined masonry is based on the well-known form of models typically adopted for FRP-confined concrete (see, for instance, De Lorenzis and Tepfers (2003), for a comparative study of confinement models):

$$f_{mc} = f_m(\alpha + k_1 \frac{f_l}{f_m}) \qquad 2.6$$

where, f_{mc}=compressive strength of confined masonry; f_m =compressive strength of unconfined masonry; unconfined masonry; k=empirical constant, and $\alpha < 1$ to ensure continuity of f_{mc} at the level of confining stress beyond which $f_{mc} \geq f_m^{'}$.

Experimental evidence both for concrete and for masonry confined with low volumetric fractions of transverse (confining) reinforcement suggests that for very low values of the confining stress the confined compressive strength does not exceed the unconfined value.

The aforementioned confinement model for masonry is defined fully by determining the empirical constant k_1 and α from testing. Experimental tests resulted in α=0.6 and k_1=1.65. Substituting these values in Equation (2.6) and taking $f_{mc}/f_m = 1$, the ratio f_l / f_m becomes equal to 0.24. Hence the proposed model for strength is written as follows:

$$f_{mc} = f_m \text{ if } \frac{f_l}{f_m} \leq 0.24 \quad 2.7$$

$$f_{mc} = f_m(0.6 + 1.65\frac{f_l}{f_m}) \text{ if } \frac{f_l}{f_m} \geq 0.24 \quad 2.8$$

2.4.4 Aiello and Micelli model for confined masonry (2009)

Aiello and Micelli (2009) studied the effect of confinement to improve the overall behaviour of rectangular masonry columns. In their experimental study, they tested 33 masonry columns made of clay or calcareous blocks. Specimens were tested under axial load only. In Aiello and Micelli's study (2009), to evaluate compressive strength of confined masonry (f_{mc}), the following general equation was used:

$$f_{mc} = f_m + k'.f_{l,eff} \quad 2.9$$

where k' =hardening factor for compressive strength; and $f_{l,eff}$ =effective lateral confining pressure. Due to lack of detailed analysis, k' equal to $g_m/1000$ is assumed, where g_m =specific mass/density of masonry expressed in kg/m^3. The effective pressure $f_{l,eff}$ is a function of the cross section shape and the FRP system and it is expressed as:

$$f_{l,eff} = k_{eff}.f_l = k_H.k_V.f_l \quad 2.10$$

where k_{eff} = value of the effectiveness coefficient that is a product between the two terms k_H and k_V related, respectively, to the horizontal and vertical effectiveness; and f_l = ultimate value of the FRP-confining pressure that is estimated in a different way for circular and rectangular columns.

For rectangular columns, with cross-sectional dimensions *b* and *d* (see Figure 2.17), the ultimate value of the FRP-confining pressure is expressed as:

$$f_l = \frac{1}{2}.\min\{\rho_{f,x}E_f + 2.\rho_{b,x}.E_b; 2.\rho_{f,y}E_f + 2.\rho_{b,y}.E_b\}.\varepsilon_{fu} \qquad 2.11$$

where $\rho_{f,x}$, $\rho_{f,y}$, $\rho_{b,x}$, $\rho_{b,y}$ =reinforcement ratio:

$$\rho_{f,x} = \frac{4.t_f.b_f}{d.p_f}, \rho_{f,y} = \frac{4.t_f.b_f}{d.p_f}, \rho_{b,x} = \frac{n_{b,x}.A_b}{d.p_b}, \rho_{b,Y} = \frac{n_{b,y}.A_b}{d.p_b} \qquad 2.12$$

where $n_{b,x}, n_{b,y}$ = number of bars disposed in one course respectively along the *x* and *y* directions, E_f = Young modulus of FRP, E_b = Young modulus of reinforcement, and ε_{fu} = ultimate design strain for FRP.

In the case of continuous wrapping, the confining pressure is estimated by Equation (2.11) assuming:

$$\rho_f = \frac{4.t_f}{\max\{b,d\}} \quad \text{and} \quad \rho_b = 0 \qquad 2.13$$

The value of k_H is given from the relationship between the confined area of the cross section and the total one:

$$k_H = 1 - \frac{b'^2 + d'^2}{3.A_m} \qquad 2.14$$

where b', e, d' =dimension shown in Figure 2.17, and r_c = corner radius. The value of k_V is equal to 1 for continuous jacketing, while in the case of FRP strips it is given by:

$$k_V = \left(1 - \frac{p'_f}{2.\min\{b,d\}}\right)^2 \qquad 2.15$$

where $p_f^{'}$ = vertical spacing between the FRP strips (see Figure 2.17)

2.5 Design methods and masonry codes in Canada

With the advancement of knowledge, there has been an evolution in the methods for design of masonry structures. The design methods mainly differ based on how safety factors are defined. These design methods are working stress design, strength design, and limit state design which combines significant features of the preceding two methods.

In working stress design, safety is provided by ensuring that nowhere in the structure the stresses produced by the maximum service or working loads exceed some specified safe values. The stresses are normally evaluated for the actual or service loading by an elastic analysis and compared with some specified percentage of critical stress, such as yielding stress for steel or compressive strength for concrete or masonry. The structure is therefore, designed to prevent over-stressing under service loads.

In Canada, the principle building code, to which provincial and municipal codes make reference, is the National Building Code of Canada (NBCC). This code makes reference to a series of standards developed by the Canadian Standard Association (CSA). Earlier versions of Canadian Masonry Design Code (CSA S304) had been issued in 1977 (imperial version) and 1978 (metric version) followed in 1984 by CSA S304-M84–Masonry Design for Buildings. All three versions of CSA S304 were working stress design standards.

In strength design, safety is provided by ensuring that at no point in the structure is the resistance of that element exceeded by the effect of the service loads magnified by

some factor, referred to as the load factor. The structure is therefore designed to prevent collapse under some specified overloading.

The intent of limit state design (CSA S304.1 1994 and later) is to ensure that various limiting states are not exceeded during reasonable life of the structure. Because these limiting states include stability and strength at specified overload and performance or serviceability (stress levels, cracking, deflections and vibrations) under service loading, limit states design includes the other two methods; however, the bulk of the design is more similar to strength design.

In Canada, seismic design provisions were first introduced in National Building Code (NBC) in 1941 where a simple equation was proposed to calculate the lateral force ($V = CW$) located at the center of gravity of the building (for all type of buildings including masonry buildings) (Mitchell et al., 2010). The first seismic zoning map was introduced in the 1953 NBCC (NRCC, 1953) based on the locations of large historical earthquakes with the highest intensity values across Canada. Furthermore, the lateral force distribution at different levels along the height was defined. The 1965 NBCC (NRCC 1965) introduced different parameters such as seismic regionalization factor, construction factor (for different type of construction including masonry), importance factor, foundation factor, and structural flexibility factor. In 1970, the first truly probabilistic seismic zoning map was developed (NBCC (NRCC 1970)). Moreover, the previously introduced structural flexibility factor was redefined to be dependent to the period of vibration of the structure (period was defined for different types of structures including masonry) and higher mode effects were accounted by adding a portion of the lateral force at the top of the structure and a reduction of the overturning moment. In

1975 the minimum seismic base shear was redefined by including different factors such as horizontal design ground acceleration, seismic response factor, foundation factor, and factors representing type of construction, damping, ductility, and energy absorption for different types of structures (including masonry). In 1977, the main change in the dynamic analysis design procedure was the introduction of a minimum base shear equal to 90% of the base shear determined from the static analysis procedure, to limit the difference between the base shears determined from static and dynamic analyses. The 1985 code introduced the influence of the acceleration–velocity ratio. This change recognized that the spectral shape varies geographically in response to the number and sizes of local earthquakes and the different characteristics of earthquakes in the east and west of Canada. In 1990, significant changes were introduced by replacing factors representing type of construction, damping, ductility, and energy absorption with the force modification factor (R, varies from 1.0 for unreinforced masonry to 4.0 for ductile moment-resisting space frames), and the use of a load factor of 1.0 on the seismic forces to reflect the onset of yielding in the structure. Several major changes were incorporated in the 2005 NBCC. The 2005 NBCC introduced two separate force modification factors, the ductility-related factor R_d and the overstrength-related factor R_o (Mitchell et al. 2010). The ductility-related force modification factor, R_d, reflects the capability of a structure to dissipate energy through inelastic behaviour while the overstrength-related force modification factor, R_o, accounts for the dependable portion of reserve strength in a structure designed according to the 2005 NBCC and the corresponding CSA standards. R_d and R_o are defined for different types of structures including various types of reinforced masonry buildings.

Recognizing the recent-wide spread application of FRPs in strengthening and repairs of masonry structures; the 2004 edition of S304.1 provides guidance on the design of FRP-reinforced masonry. The design is required to conform to CSA S806 Standard (2004), *Design and Construction of Building Components with FRPs*. Furthermore, other design guidelines such as ISIS Canada (2008) and ACI 440-2R (2002) for the applications of FRP in reinforced concrete are already available for the designers; however, a general design code addressing the applications of FRP in the design of reinforced masonry elements has not yet been published.

2.6 Closing remarks

In this chapter, masonry columns and their common layouts were defined and their modes of failure under compressive force were discussed. Since there is a need for strengthening of masonry columns that were constructed prior to the enforcement of newer design codes, different strengthening techniques have been proposed to retrofit masonry columns in last decades. The focus in these strengthening methods was on providing confinement by using techniques such as; strengthening by placing steel plates in mortar joints, adding concrete jackets around masonry column, and finally providing confinement by using FRP. In regards to FRP materials, CFRP wrap, inserted pultruded AFRP rods, and sprayed GFRP were used for improving the confinement of masonry columns.

Since the application of FRP confinement changes the behaviour of concrete masonry, it is needed to have an accurate prediction of stress-strain relations of FRP-strengthened masonry. Previous approaches in evaluating the effect of confinement in

changing stress-strain curves of masonry, and also FRP confinement effect in increasing the strength of masonry columns/sections were discussed briefly. It is needed to emphasize that while one of the main reasons for utilizing FRP material is to decrease seismic vulnerability of masonry columns, the tested masonry columns reported in the literature were subjected to compression only and there is a lack of knowledge in the behaviour of masonry columns under axial and cyclic lateral loading.

Finally, at the end of this chapter the evolution of methods used in the design of masonry structures were summarized and current Canadian standards for design of masonry structures and guidelines for application of FRP in the design of reinforced masonry elements were introduced.

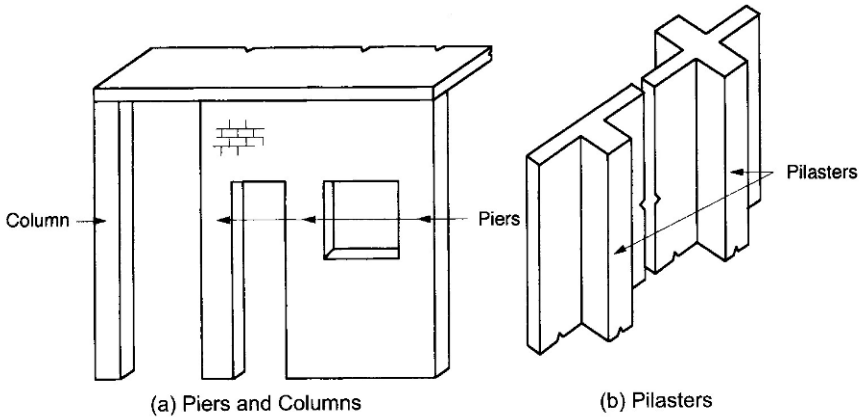

Figure 2.1: Columns and pilasters (Drysdale and Hamid, 2005)

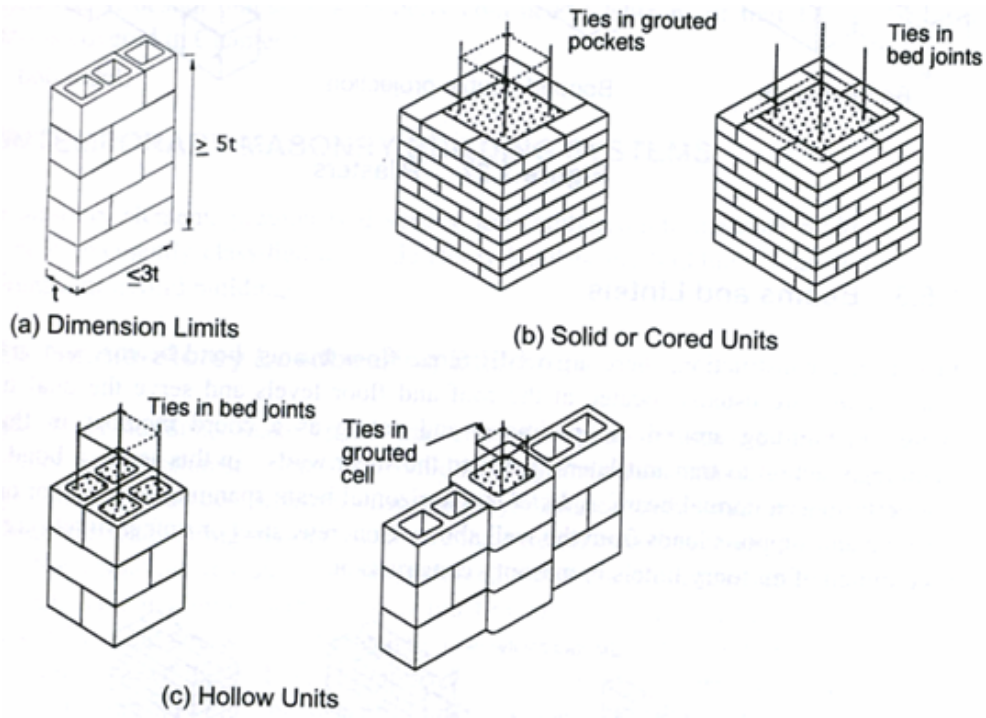

Figure 2.2: Typical layout and reinforcement details of masonry columns (Drysdale and Hamid, 2005)

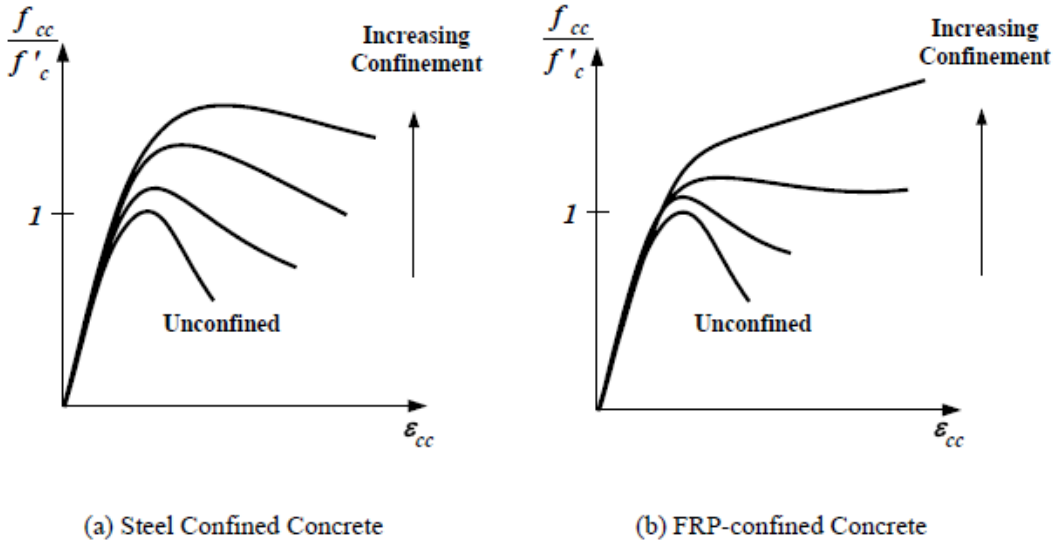

(a) Steel Confined Concrete (b) FRP-confined Concrete

Figure 2.3: Comparing behaviour of steel confined and FRP-confined concrete cylinders (Lee et al., 2006)

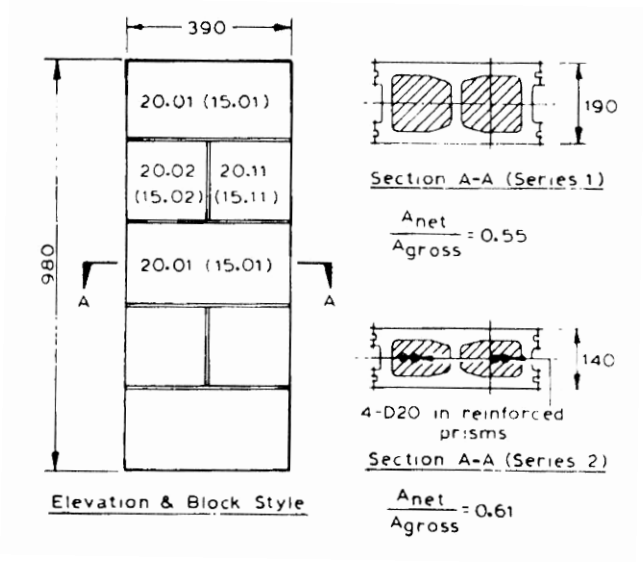

Figure 2.4: Dimensions of tested prisms (Priestley and Elder, 1983)

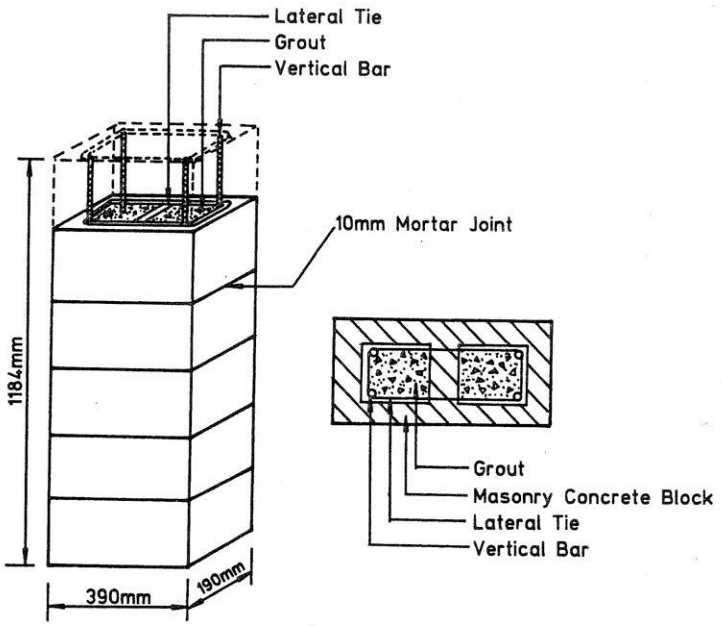

Figure 2.5: Details of block masonry columns tested by Khalaf et al. (1993)

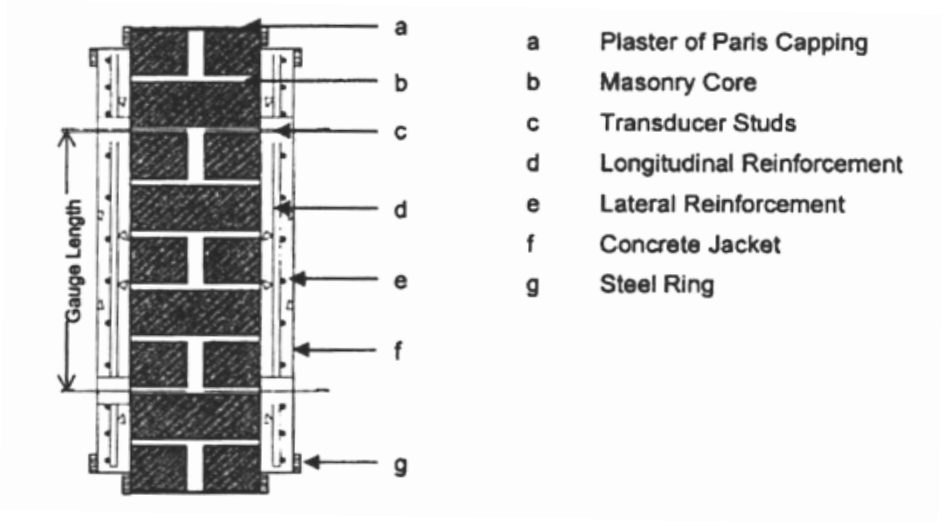

Figure 2.6: Sectional elevation of typical concrete jacketed brick masonry columns (Kog et al., 2001)

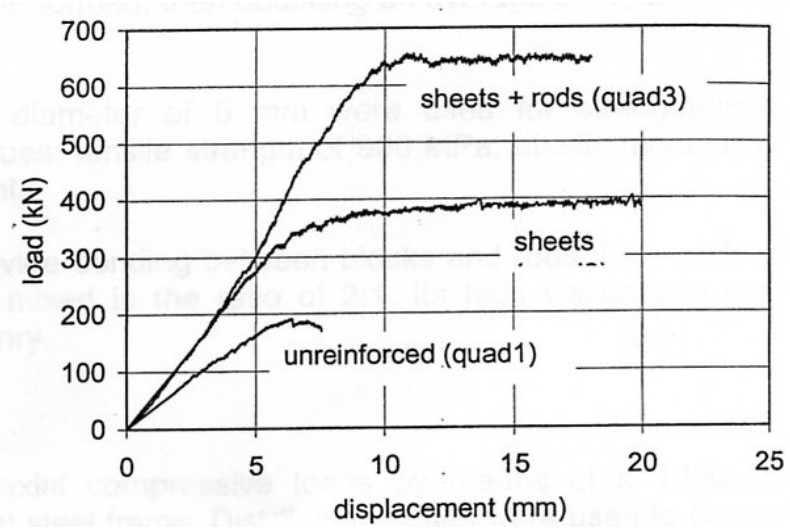

Figure 2.7: Load-displacement curves of tested rectangular masonry columns Tegola et al. (2003)

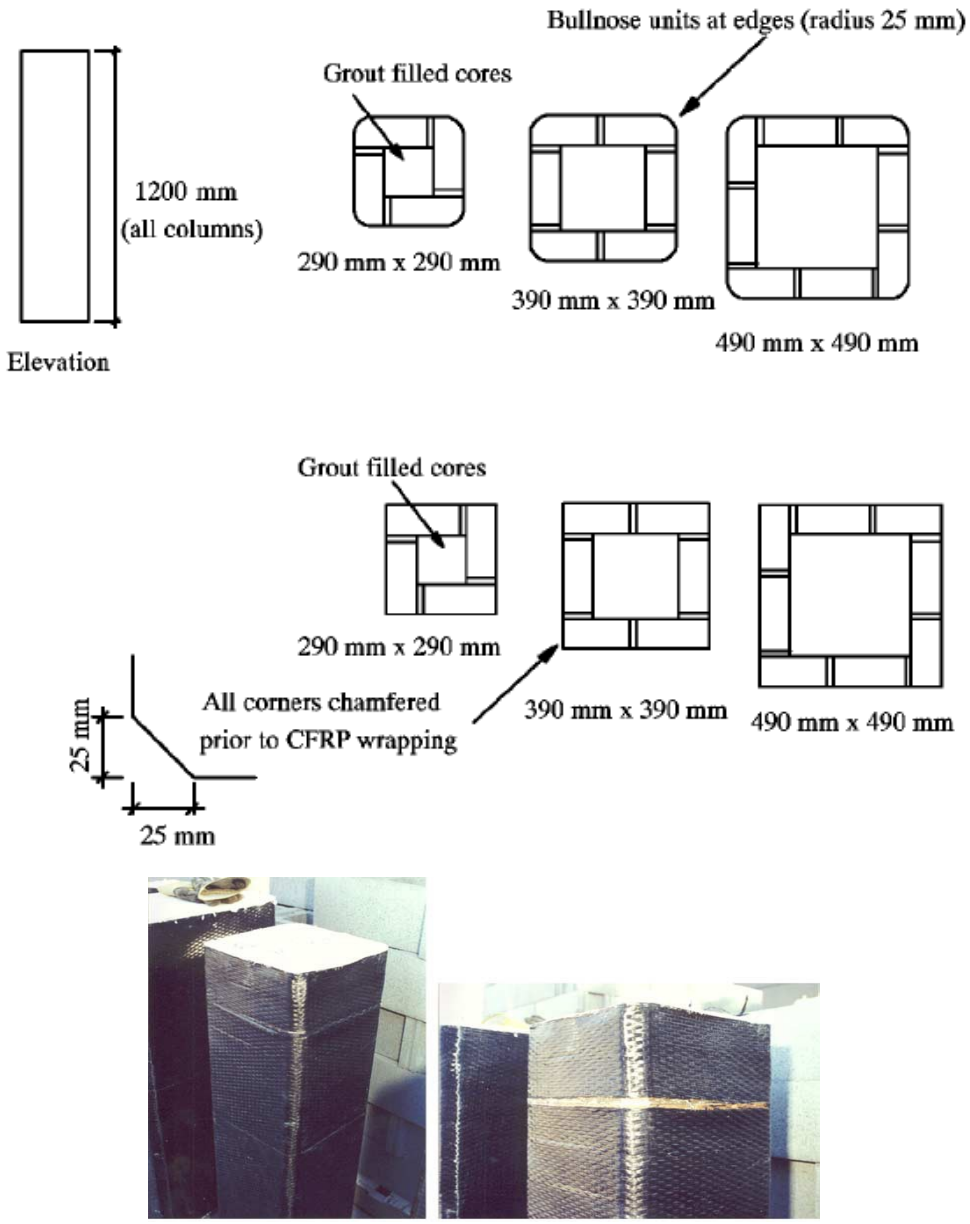

Figure 2.8: Testing wrapped masonry columns under increasing axial load (Masia and Shrive, 2003)

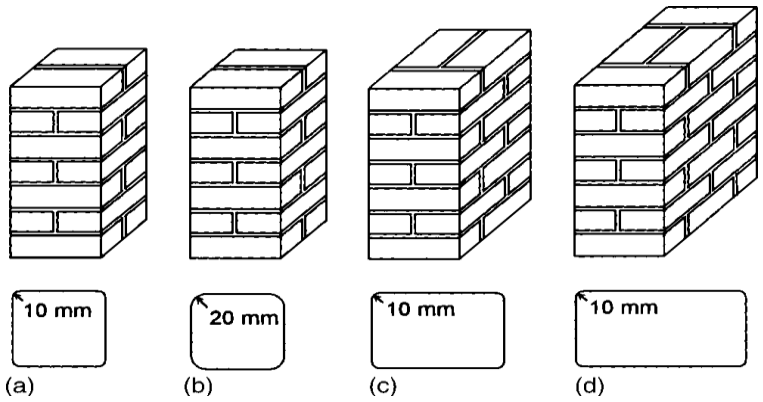

Figure 2.9: Configuration of masonry columns tested by Krevaikas and Traintafillou (2005)

Figure 2.10: (left) GFRP spray process, (right) Failure of GFRP laminates (Shaheen and Shrive, 2005)

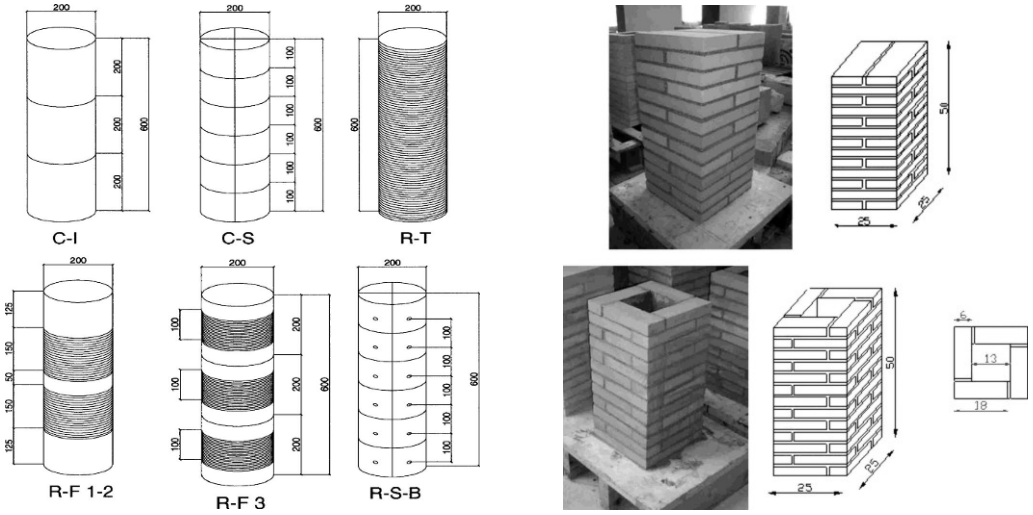

Figure 2.11: Tested circular and rectangular masonry columns with different construction and strengthening schemes (Aiello et al. 2007 and 2009)

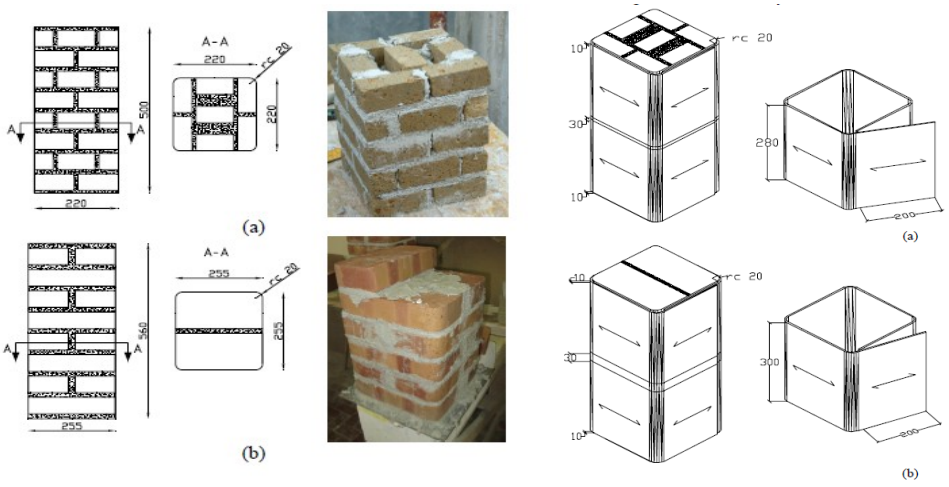

Figure 2.12: Specimens detail (dimensions in mm) and confinement layout for (a) tuff masonry and (b) clay brick masonry (Ludovico et al., 2010)

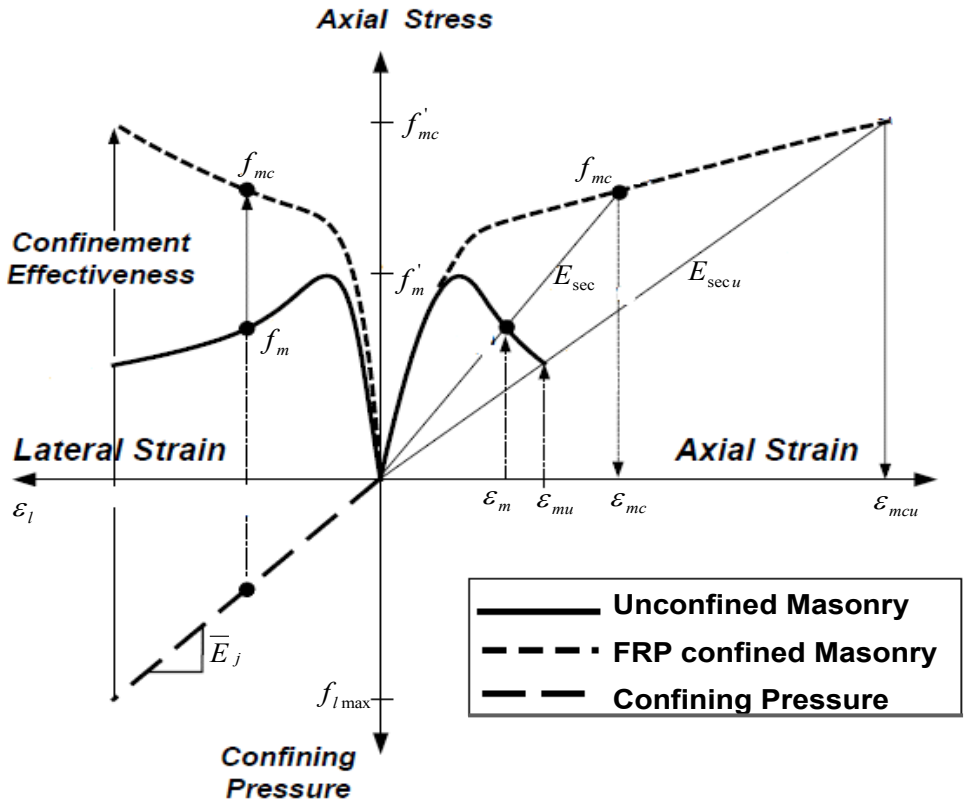

Figure 2.13: Schematic constitutive relation between unconfined and FRP-confined concrete masonry under axial compression (Lee, 2006)

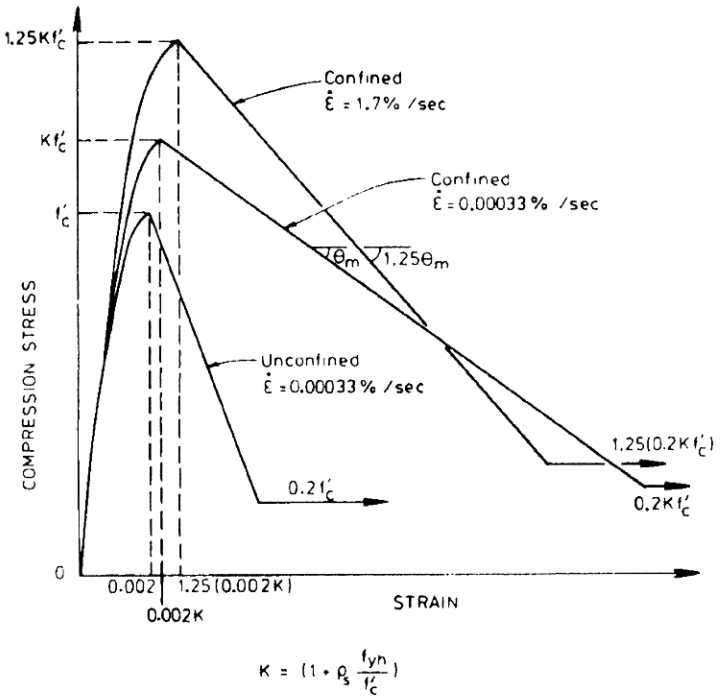

Figure 2.14: Kent-Park curves for unconfined concrete (Priestley and Elder, 1983)

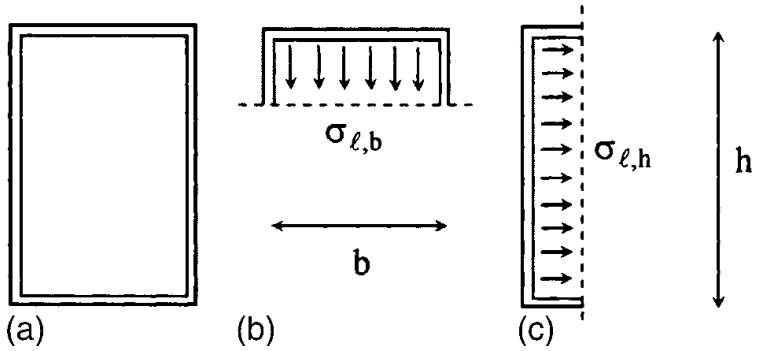

Figure 2.15: Average confining stresses in rectangular cross sections (Krevaikas and Traintafillou, 2005)

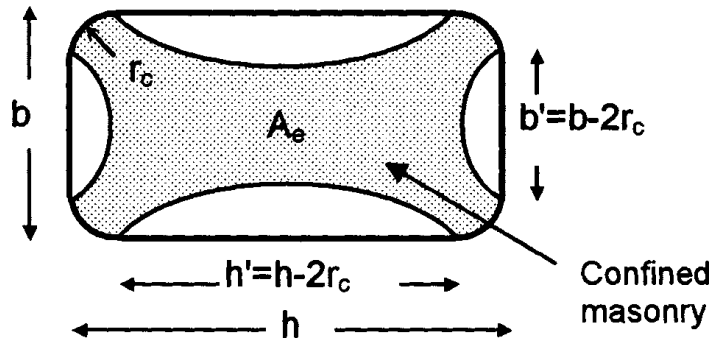

Figure 2.16: Effectively confined masonry in columns with rectangular cross section (Krevaikas and Traintafillou, 2005)

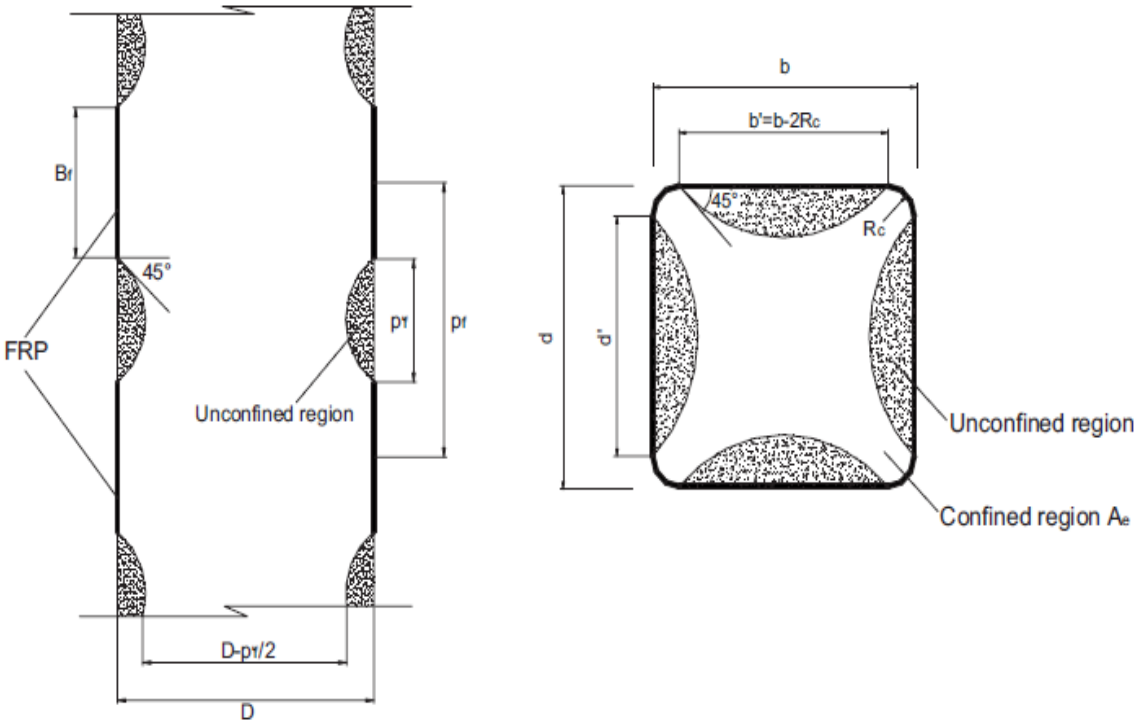

Figure 2.17: Geometry of FRP-confined masonry column (Aiello and Micelli, 2009)

CHAPTER 3

EXPERIMENTAL WORK

3.1 Introduction

This chapter consists of two parts. In the first part of this chapter, the properties of the concrete block, mortar, grout and reinforcements are discussed. Furthermore, tests on auxiliary specimens including compression prism tests and flexural prisms tests are presented. The properties of masonry materials used in constructing reinforced concrete masonry (RCM) columns, 5-block prisms, and the auxiliary specimens are important in this research since the proper interpretation of the test results directly depends on materials' properties. In addition, it is not only meaningful, but also fundamental to provide basic material properties as references for future comparisons. In order to ensure consistency of tests results, all tests were carried out according to the appropriate Canadian and ASTM standards.

In the second part of this chapter, aspects associated with the full-scale RCM columns including design and fabrication is described. The test facility utilized for testing full-scale RCM columns is described. Also, the preparation and the procedure for testing the full-scale RCM columns are outlined. Finally, the criteria adopted to define failure mechanism during testing of the full-sized columns are explained at the end of this chapter.

3.2 Material properties and auxiliary tests

3.2.1 Material properties

To simulate realistic construction practices, all masonry materials used in the test program were commercially available and widely used in the market. These materials are described in the following sections.

3.2.1.1 Concrete masonry units

The standard 190 mm normal-weight bull-nose hollow concrete splitter blocks were used as the basic masonry unit throughout the test program. The standard dimensions are shown in Figure 3.1. Based on these dimensions, a nominal mortar bedded area of 48900 mm^2 was calculated. It should be noted that each block has two round corners on one side with radius of 25 mm.

To obtain compressive strength of concrete blocks, the net area of 48900 mm^2 was used and 5 blocks were crushed under axial load as it is shown in Figure 3.2. For compressive strength tests, gypsum cement capping was used according to ASTM Standard C140-02. Compressive strength of 15.3 MPa with a coefficient of variation of 8.3% for concrete blocks was obtained.

3.2.1.2 Mortar

The primary purpose of mortar in masonry is to bond masonry units into an assemblage that acts as an integral element having desired functional characteristic, it also functions in other ways (National Concrete Masonry Association, NCMA, 1994):

1. Bonds masonry units together into an integral structural assembly,
2. Seals joints against penetration by air and moisture,

3. Prevents small movement within a wall
4. Bonds the joint reinforcement to assist in resisting shrinkage and tension, and
5. Bonds tie and anchor so that all elements perform as an integral unit.

Mortar is sensitive to the mix portions and types of ingredients used. The mortar used throughout the test program was designated and classified as type S in accordance to ASTM standard C270-02 (2002) and CSA A179-04 (2004). Type S mortar that is a mix of 0.5 volumetric unit Type 10 Portland cement, one unit masonry cement, 2.9 units sand, and 0.7 unit water was chosen after several trial mixtures. Mortar mix is summarized in Table 3.1. For trial mixes, six mortar cubes, as it is shown in Figure 3.3, The average 7-day and 28-day compressive strengths were 11.7 MPa and 20.7 MPa, (with coefficient of variation of 9.6% and 4.9%) respectively. The former should not be less than 7.5 MPa and the latter should not be less than 12.5 MPa according to CSA A179-04 (2004) and ASTM C270-02 (2002) for laboratory made mortar cubes.7 days and 28 days strength of tested cubes are summarized in Table 3.2.

3.2.1.3 Grout

Grout is a mixture of cement and aggregate to which sufficient water has been added to achieve required fluidity so it can be proud easily into the cells of the masonry blocks. When poured, it should completely fill the voids (cells) in the masonry, without segregation of the constituents, and completely encase the reinforcement. Grout serves many functions including the following:

- Grout helps develop bond between various masonry units to act together as one unit.

- Grout often is used to structurally bond separate wall elements or wall and column/pier elements. This is most commonly seen in reinforced construction, where grout is used to bond the steel reinforcement to the masonry so the two elements act integrally in resisting load.
- The grouted cells increase the bearing area for resisting area for resisting higher compressive loads.
- The grouted cells increase the stiffness of the masonry elements, and thus increase their resistance to lateral loads. Masonry cantilever walls often are grouted solidly to increase the wall's weight, thereby increasing the resistance to overturning.
- Grout makes the masonry elements more resistance against fire, more sound proof, and increase the heat isolation.

The grout used in this program, categorized as "coarse grout" in accordance with CSA A179-04 (2004) and ASTM C476-02 (2002), was mixture of one volumetric unit Portland cement, 2.8 units fine aggregate (sand), two units coarse aggregates with the maximum size of 7mm (1/4″), and 0.9 unit of water as it is summarized in Table 3.1.

In order to obtain a proper grout mix, six grout cylinders were produced and tested under compression load as shown in Figure 3.4. The average compressive strength at the age of 7 and 28 days were 11.7 MPa and 21.6 MPa (with coefficient of variation of 10.3% and 5.8%) respectively. Seven days and 28 days strength of tested cylinders are summarized in Table 3.3. Slump test of fluid grout was done every day of the construction period ranging from 260 mm to 280 mm slump that passes the lower limit stated in the Canadian code (CSA A179-04 (2004)).

3.2.1.4 Longitudinal and transverse steel reinforcement

The steel reinforcement used in the tested columns was conventional 15M steel rebars (Grade 400) with 462 MPa yield stress. Stirrups were made from steel wires with 4.65mm diameter with yield stress of 240 MPa and they were used as transverse reinforcement.

3.2.1.5 CFRP and GFRP sheets

The CFRP and GFRP sheets and the corresponding epoxy resin used in this research were provided by FYFE Co. (2009). Epoxy mix consists of Component A and Component B that were mixed in laboratory conditions prior to application. Typical dry fibers properties, epoxy material properties and the composite properties are tabulated on Table 3.4.

3.2.2 Auxiliary laboratory tests

Two series of auxiliary specimens were tested to determine strengths and elastic modulus of masonry assemblages. These two series of auxiliary specimen were tested; five-block prisms to obtain compressive strength of masonry assemblage ($f_m^{'}$), and seven-block prisms to get flexural tensile strength of the unreinforced masonry normal to the bed joint (f_t). These tests are discussed in following sections.

3.2.2.1 Compressive strength of masonry assemblage

A series of 5 five-block high and one block wide prisms, laid in running bond, were tested in vertical compression to determine compressive strength according to ASTM C1314-02 (2002a) as it is shown in Figure 3.5. The reason for using five-block

high prism is that five-block prism provides a central zone where uniform stresses can occur due to diminishing effects of end platen restraints. Therefore, it provides a better representation of the actual column situation.

In order to obtain compressive strength of masonry assemblage ($f_m^{'}$), modulus of elasticity, E_m, and Poisson's ratios, ν_m, it was necessary to measure axial load, axial strain, and lateral strain. Therefore, one load cell, as well as several LVDT and potentiometers were installed on each prism as it is shown in Figure 3.5. Unfortunately, lateral strain readings obtained from potentiometers (at the time of testing) were not sufficiently accurate to represent the very small transverse strains (around 3000 micro strain), and it was not possible to estimate the Poisson's ratio, consequently it was decided to use Poisson's ratio equivalent to 0.2 which is widely recommended by the literature for masonry elements.

As can be seen from the tests on the five-block high prisms shown in Table 3.5, an average $f_m^{'}$ equivalent to 11.5 MPa was obtained. Furthermore, load-axial strain relationship for each prism is shown in Figure 3.6. Vertical strain values are the average strains obtained from strain readings measured at the front and back of the prisms.

In order to obtain modulus of elasticity of masonry assemblage, CSA S304.1 (2004) recommendation was followed. CSA S304.1 (2004) (clause 6.5.2) specifies a single value for all masonry assemblages:

$$E_m = 850 f_m^{'} = 850 \times 11.5 = 9775(MPa) \qquad 3.1$$

3.2.2.2 Flexural bond strength of masonry assemblage

For the purpose of estimating the tensile strength of the masonry assemblage, a series of five seven-block high prisms were tested by four-point loading method according to ASTM E518-02. As shown in Figure 3.7, prisms with the height of seven blocks and width of one block were constructed. It is decided to construct seven-block high prisms in order to properly locate the two point loads and supports as and also to provide sufficient span-to-depth ratio (see Figure 3.8), as per the recommendations of CSA S304.1 (2004).

After testing 5 seven-block high prisms, tensile strength f_t (also called modulus of rupture (R)) equivalent to 1.3 MPa was obtained using ASTM E518 (2002) as follows:

$$R = \frac{(0.167P + 0.125P_s)l}{S} \tag{3.2}$$

where, P= maximum axial load applied (in N), P_s = weight of specimen (in N) , l = span (in mm), and S = section modulus of gross net area (in mm^3).

Failure loads and calculated tensile strength for each prism are summarized in Table 3.6. Furthermore, the center deflections of the tested specimens were also determined with a dial gauge (with accuracy of 0.01 mm), and these readings were used for estimating the modulus of elasticity of the specimens in bending parallel to the bed joints. The measured load-mid span deflection relationships are presented in Figure 3.9. As an approximation, it is assumed that seven-block prism behaves like a beam under four-point loading, as shown in Figure 3.9, therefore the modulus of elasticity is equal to:

$$E = \frac{Pa}{24I\Delta_{\max}}(3l^2 - 4a^2) \tag{3.3}$$

where, P= maximum axial load applied, l = span, Δ_{max} = maximum center deflection, and I = gross section inertia, and a = distance between support and loading point (see Figure 3.9). Modulus elasticity equal to 10484 MPa was obtained which can be compared by 9775 MPa obtained in pervious section.

3.3 Preparation for experimental program

This part of chapter 3 describes the construction of the reinforced concrete masonry (RCM) columns, as well as the preparation and the procedure for testing the full-scale RCM columns. Furthermore, the different aspects related to the tests such as lateral loading pattern, and criteria adopted to define failure mechanism during testing of the columns are explained at the end of this chapter.

3.3.1 Construction of full-scale RCM columns

The following sections provide a detailed description of the construction process of the full-scale RCM columns. Nine full-sized 1.4 m high RCM columns were constructed. All columns have dimension of 1.4×0.4×0.4m. The boundary conditions and dimensions of the tested columns represent a 2.8 m high column with fixed-fixed end conditions by maintaining the same moment-to-shear ratio. First column was used as a control specimen and the rest of columns were strengthened with CFRP and GFRP material with different number of layers or wrapping schemes. The wrapping schemes and the details of reinforcement are summarized in Figure 3.10. Also, the assigned designation for each column is shown in Table 3.7.

3.3.1.1 Design of RCM columns

Control column (RMC-0) designed using current Canadian code (CSA S304.1-04) as explained in Appendix A.

3.3.1.2 Construction of RCM columns

Construction, workmanship and consistency of materials are extremely important for research purposes. For comparison to be undertaken, it is crucial that potential sources of variability be avoided. Even when normally identical conditions exist, a natural variability will exist. In order to ensure the workmanship and consistency in construction, specimens were constructed with the help of professional masons from Montréal, Québec, Canada. However, all columns were not built at the same time, and there was a time interval of about 8 month between constructions of each three columns. The steps taken for the fabrication of the masonry columns are described briefly as follows:

1. The first three wood forms for concrete footing were built (see Figure 3.11).
2. Steel cages were prepared for concrete footings. Also four vertical 15M bars that were used in concrete masonry columns were placed in the footings at their locations (see Figures 3.12b). One strain gauge was installed on each vertical rebar at the location of masonry column and concrete footing interface.
3. Concrete was cast, and footings were cured prior to the construction of masonry columns (see Figure 3.12). Hooks were placed inside the concrete footing to provide convenience in handling.
4. Before construction of columns, steel ties were made using 4.75 mm steel rods (see figure 3.13). The diameter of 4.75 mm where used considering Clause 12.1.3

of S304.1-04 which states that the maximum diameter of any reinforcement placed within a mortared bed joint shall not exceed one-half of the bed joint's thickness (i.e. 5 mm). Furthermore, in preparation of ties, strain gauges were installed in number of ties (three for each column). Using 390×190×190mm concrete blocks, the minimum spacing of the ties is forced to be 200 mm. As stated in Clause 12.2.1 of CSA S304.1-04, for reinforcement in compression, the tie spacing shall be the least of:

- 16 times the diameter of the longitudinal bars
- 48 times the diameter of the ties,
- The least dimension of the compression member.

5. Finally, columns were constructed with the help of professional masons. The process followed in the construction of masonry columns is summarized in Figure 3.14. Columns were air cured in the structure lab environment (with approximate temperature of 25°C).

3.3.1.3 CFRP and GFRP overlay technique

For the seismic retrofit of RCM columns, the function of the fibre-reinforced polymer (FRP) composite overlay is to provide additional confinement especially in the plastic-hinge region to prevent spalling of concrete masonry. The overall retrofit objective of the FRP overlay technique is to increase the lateral displacement capacity of columns under lateral loading, which is achieved by enhancing the deformation (rotation) capacity of the column's plastic hinge(s). The steps taken for wrapping of RCM columns are summarized in Figure 3.15. In order to ensure the effectiveness of the wrapping, 150 mm overlap provided as it is recommended by ISIS Canada (2008) design manual. It is

noteworthy to mention that it was observed during wrapping that removing all entrapped air bubbles gets more difficult by increasing the number of CFRP layers. However, there was no such a problem when GFRP material was used.

3.3.2 Preparation of test setup facility

The facility for testing of full-scale masonry columns is located in the structure laboratory of Concordia University. Figure 3.16 shows a schematic of the test set-up. For preparation of the test setup several pieces of setup such as lateral load cell (see Figure 3.17), parts for fixing the footing to strong floor, and parts of lateral and axial loading devices were built in the laboratory. In following sections, some important aspects in preparing the test setup are summarized.

3.3.2.1 Instrumentation

A data acquisition system was used to capture the displacement and strain measurements of the tested columns. As mentioned previously, four strain gauges were installed on vertical rebars at the location column and footing interface. Nine strain gauges were installed on the surface of carbon or glass fiber-reinforced polymer (CFRP or GFRP) wraps at the bottom, middle, and top of the columns. Also, strain gauges were installed on bottom, middle, and top ties. Furthermore, two horizontal linear potentiometers were attached to each side of the columns along the point of application of lateral load, and two horizontal potentiometers were installed to measure the displacements along the height of the columns. Three potentiometers were installed on the RC footing in order to ensure there is no rotation or displacement relative to the

strong floor. All potentiometer used in this experiment had accuracy of 0.1 mm. Finally, for measuring lateral and axial loads, two load cells were calibrated and used.

3.3.2.2 Lateral loading system

The lateral loading system, shown in Figure 3.18, consisted of a Hydraulic Jack which is capable of applying push and pull lateral loads to the tip of the column. The Hydraulic Jack has a push capacity of 600 kN. During the tests, loading of the column was controlled by measured displacement at the tip of the column. The lateral load is transferred to the tip of the column with the help of manufactured steel shaft. As explained in Figure 3.19, this steel shaft was also used as the lateral load cell. Lateral load was applied in a quasi-static manner and two cycles were applied at displacement levels less than 3% drift as it is shown in Figure 3.19.

3.3.2.3 Top loading mechanism

During all tests, constant axial force of 200 kN (equivalent to a stress of 0.11 of the axial compressive capacity of the gross-section area of the tested columns) were applied by using a hydraulic jack with the capacity of 600 kN. An electric pump was used in order to keep the axial load constant during the test. In order to have a simple support at the top of the columns two sets of plates and rollers were made and used in top loading system, as shown in Figure 3.20.

3.3.2.4 Test procedure

After lifting the columns (by using the hooks placed in concrete footing), columns were positioned in the testing frame such that the axial load could be applied right at the

center of the columns' cross-section. For wrapped columns, wrapping process and curing was done before moving the columns into the testing frame. A steel plate was placed on the top of the column and it was leveled by using high strength plaster. This plate had 2.54 mm thickness and dimensions of 400×400mm and it was used for distributing the axial load. After setting the plaster in between the column and top plate, top loading mechanism was mounted on the frame and it was fixed on top of the column. In order to prevent any movement of footing during the test, footing was fixed to the strong floor.

Prior to loading, initial reading of potentiometers, dial gauges, and load cells were calibrated. Tests started by applying the axial load of 200 kN. Then the test continued by applying lateral load. Tests were conducted in a displacement-control mode, where two cycles were applied at each displacement level having 2 mm intervals (i.e. 2 mm, 4 mm, 6 mm, etc.) until 3% lateral drift (40 mm), after which larger displacement intervals of 10 mm were applied. After reaching top lateral displacement of 80 mm, the columns were only pushed or pulled until the test ended either due to failure or limitation in the test setup. It was decided to limit the stroke of lateral loading hydraulic jack to 150 mm for safety concerns. During the tests, any signs of cracks or rupture of FRP wraps were checked and recorded.

3.3.2.5 Failure definition

In this experimental program, failure was defined using two terminologies. The first terminology defines failure as when the lateral load bearing capacity decreased to less than 80% of maximum recorded lateral load during each test. The second terminology of failure is the ultimate failure, and defined with extensive cracking,

spalling of masonry concrete, or as it is shown in Figure 3.21, combination of FRP rupture and crushing of masonry blocks.

3.4 Concluding comments

Based on experimental results in this chapter, properties of the materials that are used in the experimental program and construction of RCM columns are measured. Strength of concrete blocks, mortar, grout, steel reinforcement, CFRP and GFRP materials, compressive strength of masonry assemblage (f'_m), tensile strength of masonry assemblage (f_t), and modulus of elasticity of masonry assemblage (E_m) are obtained.

It is noteworthy to mention that modulus of elasticity assemblage (E_m) was obtained using from two different approach. In the first approach, compressive strength of masonry assemblage (f'_m) was obtained from testing 5 five-block high prisms, and then E_m equivalent to 9775 MPa calculated using CSA S304.1-04 (clause 6.5.2). In the second approach, 5 seven-block high prisms were tested under four-point loading and mid-span deflections where measured. Using measured load mid-span deflections, E_m equivalent to 10488 MPa was calculated.

Furthermore, in this chapter a summary of the steps taken for construction of full-sized RCM columns are provided. Different aspects related to testing procedure such as instrumentation, loading pattern and failure definitions are explained.

Table 3.1: Volumetric ratios of mortar and grout mixes

	Type S mortar cubes	**Coarse grout cylinders**
Compressive strength (MPa)	20.7*	21.6*
	Volumetric ratios of mix	
Cement type 10	1	1
Masonry cement	0.5	-
Sand	2.9	2.8
Coarse aggregates	-	2
Water	0.7	0.9

* 28 days strength

Table 3.2: Mortar cubes Compressive Strength

Cube Number	**7 Days Strength (MPa)**	**28 Days Strength (MPa)**
1	12.89	22.1
2	10.2	19.8
3	12	20.2
Average	11.7	20.7

Table 3.3: Grout Compressive Strength

Cylinder Number	**7 Days Strength (MPa)**	**28 Days Strength (MPa)**
1	11.97	22.1
2	12.52	19.87
3	13.61	22.83
Average	11.7	21.6

Table 3.4: Properties of the (a) Dry carbon fiber, (b) Dry glass fiber, (c) Tyfo SCH-11UP CFRP sheets, (d) Tyfo SEH-51A GFRP sheets, and (e) Tyfo S epoxy (as provided by the supplier, Fyfe Co. 2009)

(a)

	Dry Carbon
Tensile strength	3.79 GPa
Tensile modulus	230 GPa
Ultimate Elongation	1.60%
Density	1.8 gr/cm^3
Weight	315 gr/m^2

(b)

	Dry Glass
Tensile strength	3.24 GPa
Tensile modulus	72.4 GPa
Ultimate Elongation	4.50%
Density	2.55 gr/cm^3
Weight	915 gr/m^2

(c)

	CFRP sheets
Tensile strength	1062 MPa
Tensile modulus	102 GPa
Elongation at break	1.05%
Thickness	0.27 mm

(d)

	GFRP sheets
Tensile strength	575 MPa
Tensile modulus	26.1 GPa
Elongation at break	2.20%
Thickness	1.3 mm

(e)

	Epoxy
Tensile strength	72.4 MPa
Tensile modulus	3.18 GPa
Elongation percent	5%
Flexural strength	123.4 MPa
Flexural modulus	3.12 GPa

Table 3.5: Obtained $f_m^{'}$ from testing 5 five-block high prisms

Prism	Failure Load (kN)	Compressive Strength (MPa)
1	759.4	12.8
2	651.6	11.0
3	536.1	9.0
4	822.8	13.9
5	630	10.6
	Average	**11.5**

Table 3.6: Obtained f_t and modulus of elasticity from testing seven-block prisms

Prisms	Failure Load (N)	Modulus of Rupture (MPa)	Δ_{max} (mm)	E (MPa)
1	14456	1.16	0.7	9500
2	15568	1.25	0.62	11550
3	16680	1.33	0.88	8720
4	17792	1.41	0.7	11690
5	16680	1.33	0.7	10960
	Average	1.3		10484

Table 3.7: Tested RMC columns and their assigned designation

Specimen	Designation
Reinforced **M**asonry **C**olumn : Control Specimen	RMC-0
Reinforced **M**asonry **C**olumn with **1** layer of **C**FRP **W**raps	RMC-CW-1
Reinforced **M**asonry **C**olumn with **2** layers of **C**FRP **W**raps	RMC-CW-2
Reinforced **M**asonry **C**olumn with **3** layers of **C**FRP **W**raps	RMC-CW-3
Reinforced **M**asonry **C**olumn with **1** layer of **C**FRP **S**trips	RMC-CW-1S
Reinforced **M**asonry **C**olumn with **1** layers of **C**FRP **W**rap at **P**lastic hinge	RMC-CW-1P
Reinforced **M**asonry **C**olumn with **1** layer of **G**FRP **W**raps	RMC-GW-1
Reinforced **M**asonry **C**olumn with **2** layers of **G**FRP **W**raps	RMC-GW-2
Reinforced **M**asonry **C**olumn with **1** layer of **G**FRP **S**trips	RMC-GW-1S

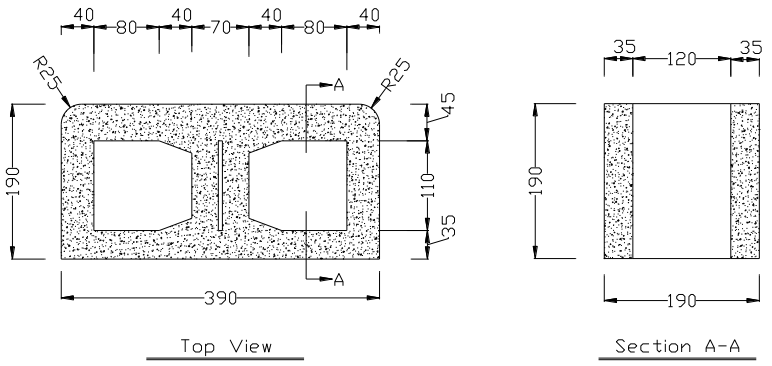

Figure3.1: Bull-nose concrete masonry units (390×190×190 mm) used in experimental work

Figure 3.2: Obtaining compressive strength of concrete masonry units

Figure 3.3: (left) Mortar cube preparation, (middle) Type S mortar cubes, (right)

Obtaining compressive strength of mortar cubes

Figure 3.4: Obtaining compressive strength of grout cylinders

Figure 3.5: (1) Test setup to obtain compressive strength of masonry assemblage (f'_m), (2) and (3) failure modes of five-block prisms under axial load

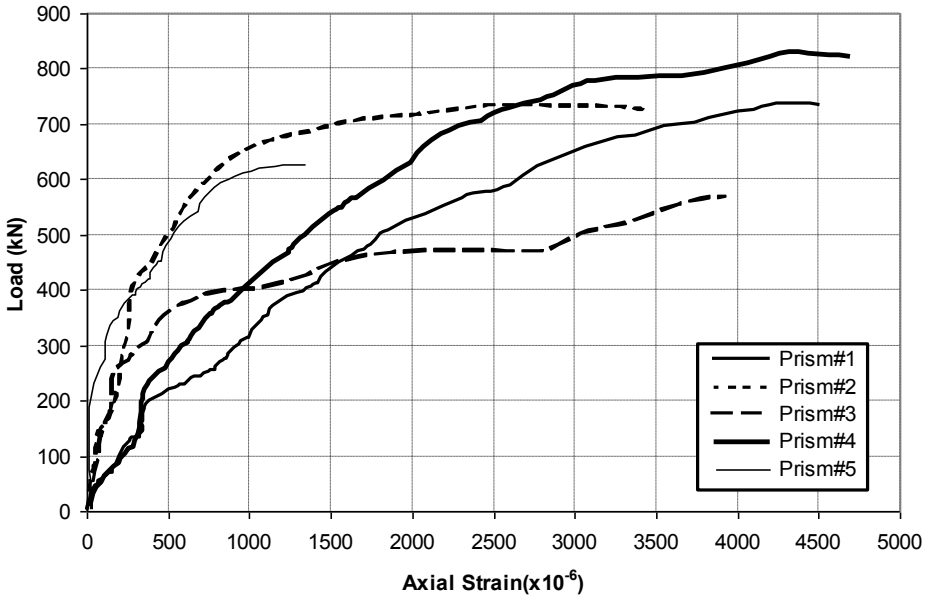

Figure 3.6: Load versus Axial Strain for 5 blocks high prisms

Figure 3.7: Seven-block high prisms

Figure 3.8: (1) test setup to obtain tensile strength of masonry assemblage (f_t), (2) and (3) 7 blocks prisms under third point loading at failure.

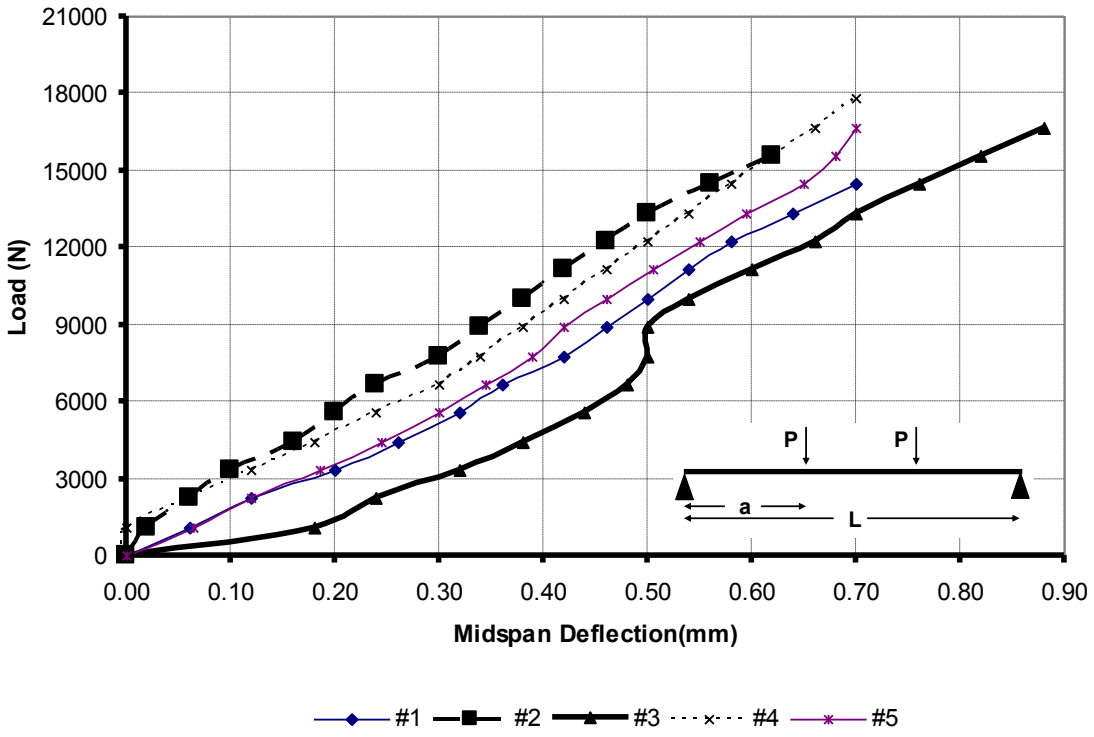

Figure 3.9: Load versus mid span deflections relationship for seven-block prisms

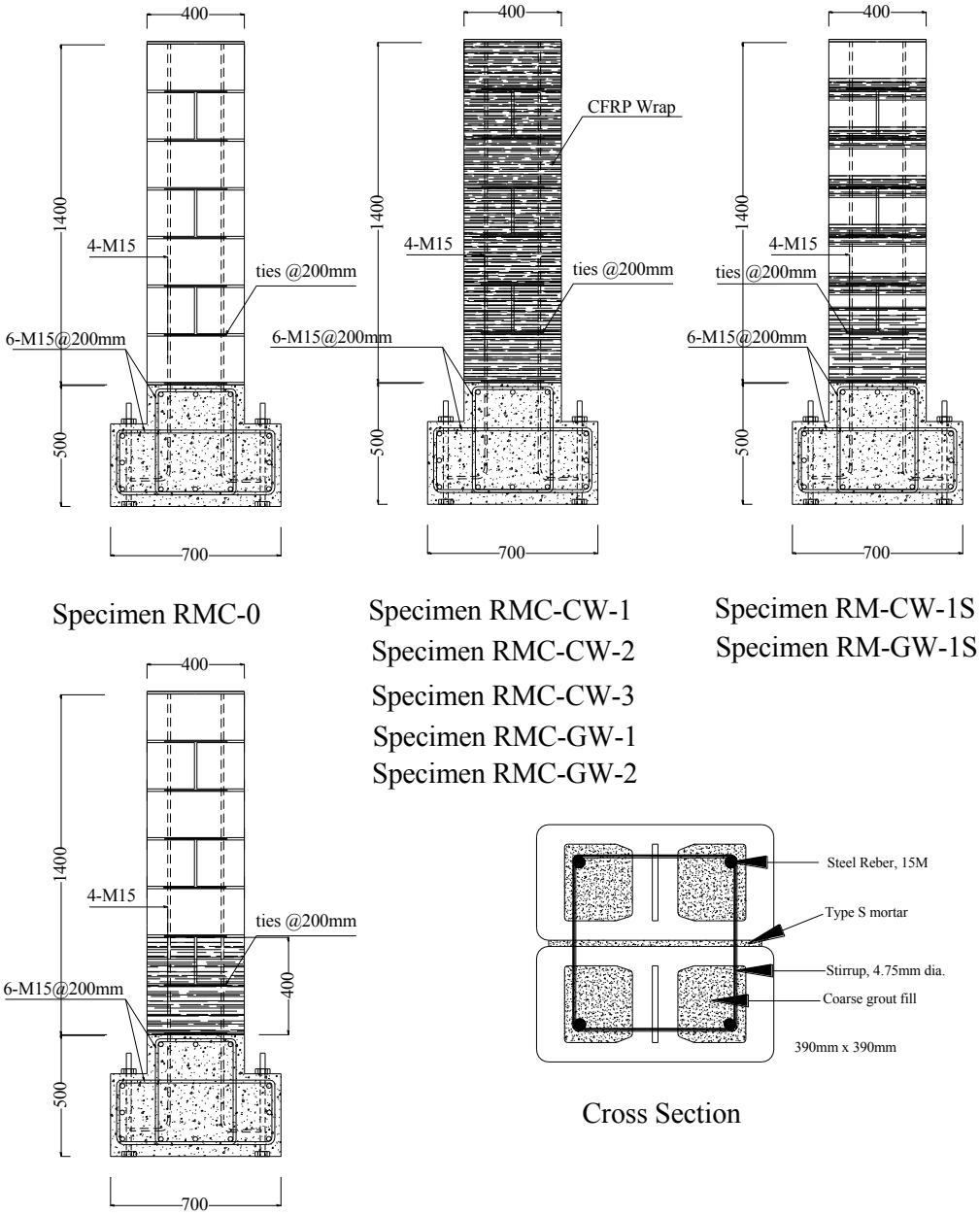

Figure 3.10: Dimensions and details of reinforcement of the 9 constructed RCM columns

Figure 3.11: (a) Prepared wood forms for concrete footings, (b) Steel reinforcement inside the RC footings

Figure 3.12: Three constructed footings prior to construction of masonry columns

Figure 3.13: Steel ties, prepared using steel bars with the diameter of 4.75 mm

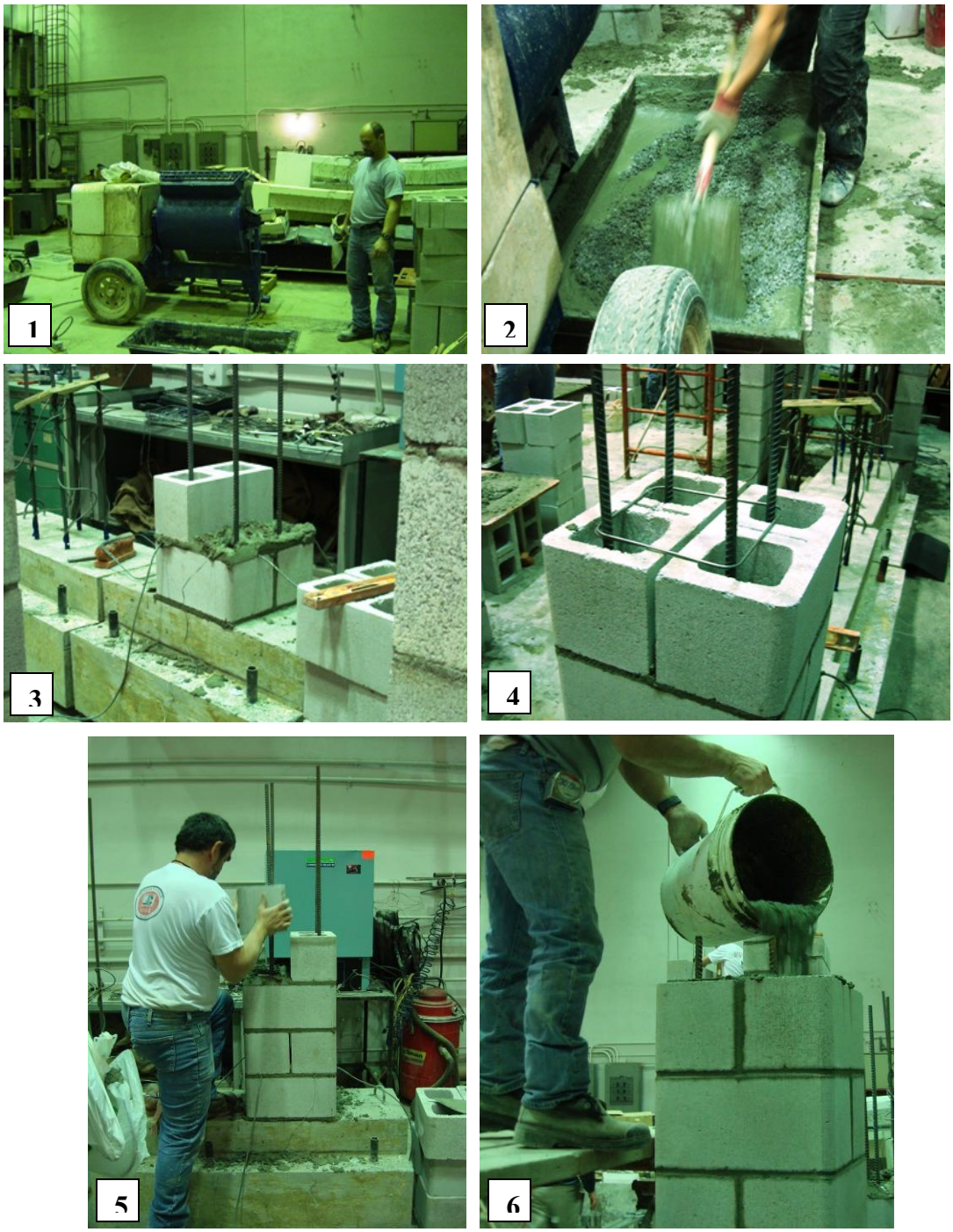

Figure 3.14: (1) Preparation of grout prior to construction, (2) Process of adding pea gravel in the grout mix, (3) Construction of columns and also guiding strain gauges' wires, (4) Placing steel ties in every row at the location of mortar joints (5) Placing blocks along the height (6) Pouring grout at the end of construction

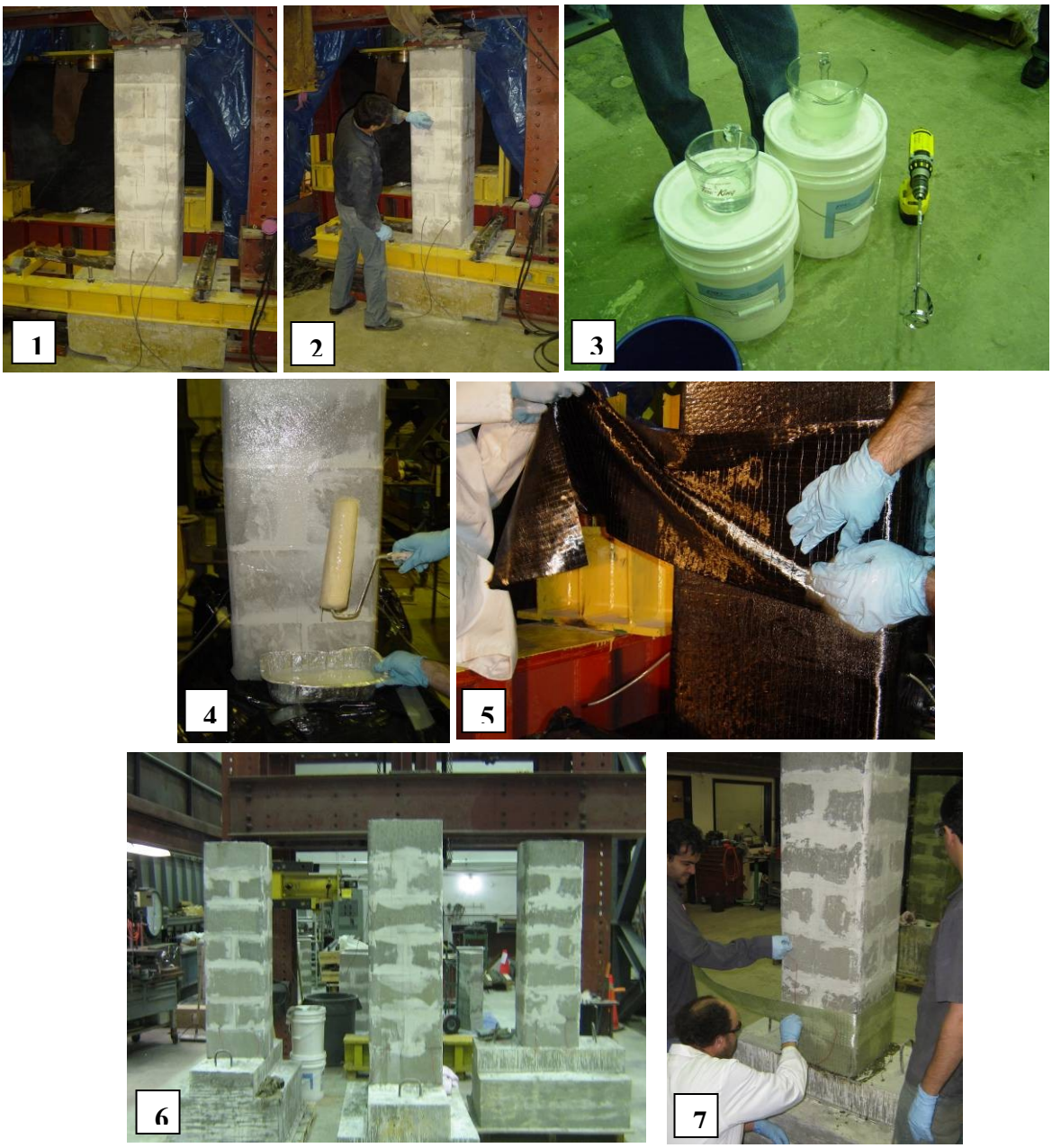

Figure 3.15:(1) Covering all mortar joints and groves with plaster, (2) Removing any unevenness and bump from the surface, (3) Preparing epoxy mix, (4), Saturating the surface of RCM column with epoxy resin before wrapping (5) Overlaying CFRP sheets for column with 2 layers of CFRP, (6) Surface preparation for the three GFRP-wrapped columns, (7) Overlaying GFRP sheets

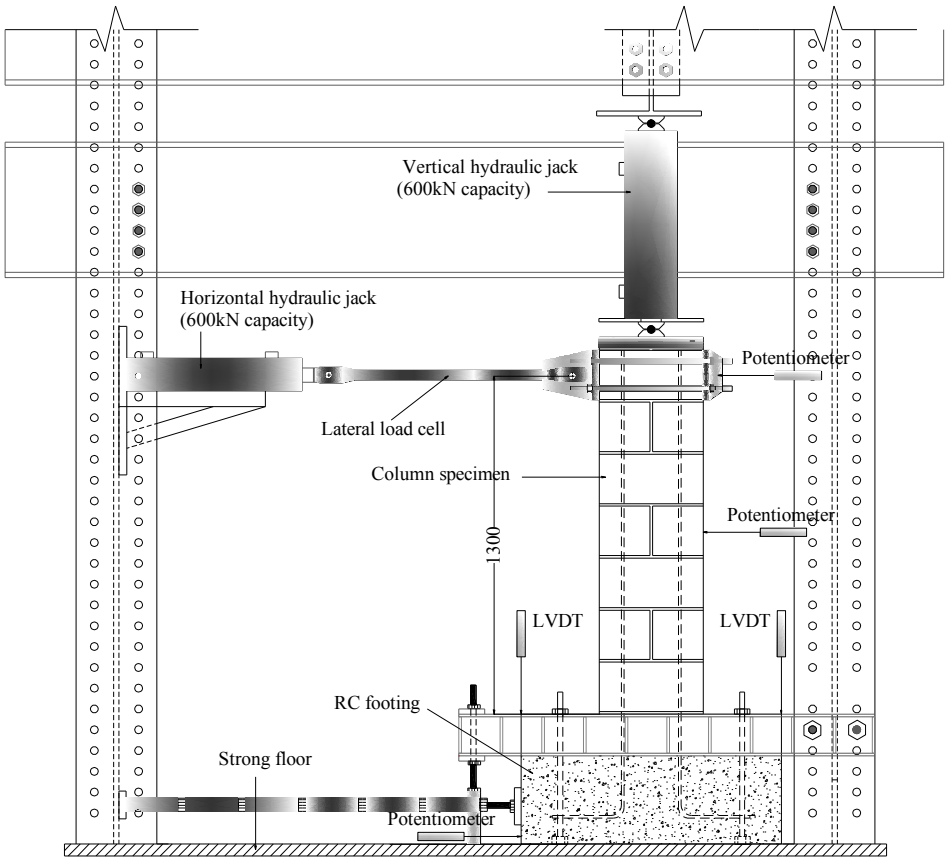

Figure 3.16: Schematic of the test set-up and the location of potentiometers used for displacement measurement.

Figure 3.17: Manufactured lateral load cell for the test setup. Load cell was made by installing four strain gauges and then calibrated before the conducting the first test

Figure 3.18: Test setup and lateral loading system in experimental program. This picture was taken from the test setup of column RMC-CW-3

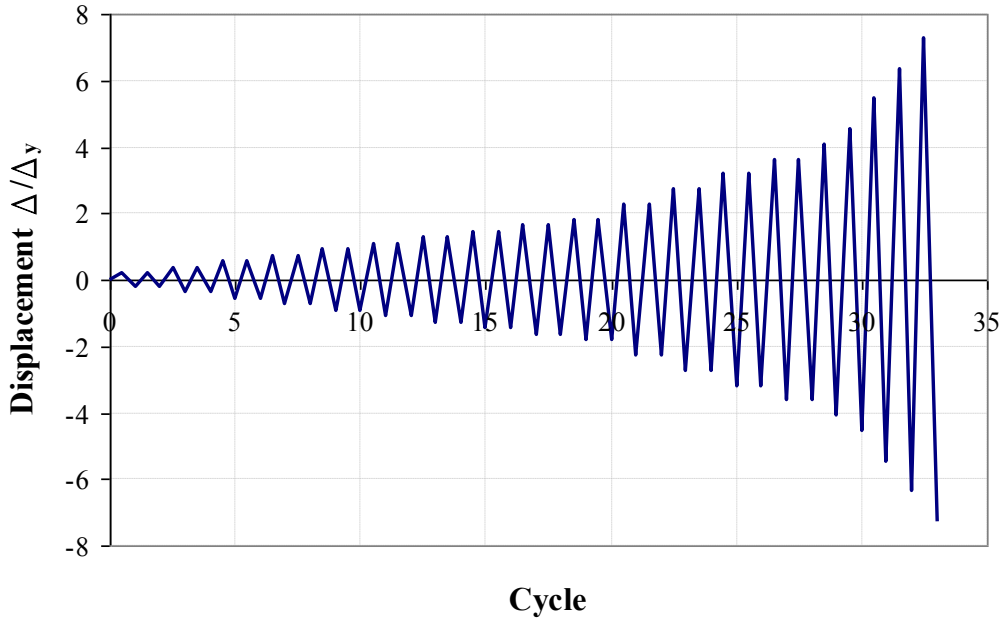

Figure 3.19: Displacement history for column RMC-CW-1

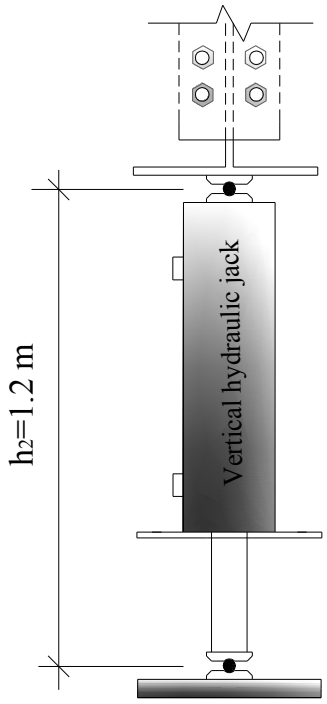

Figure 3.20: Top loading mechanism

Figure 3.21: Observed ultimate failure for column RMC-CW-1S by FRP rupture and crushing of concrete masonry

CHAPTER 4

EXPERIMENTAL RESULTS

4.1 Introduction

In this chapter, the results obtained from the experimental program are discussed and the overall behaviour of the tested columns is compared. The detailed strain gauges readings installed on longitudinal rebars, ties, and FRP jacket of each column like are presented in Appendix B. The comparisons that are presented in this chapter focuses on studying the effect of the content (number of layers and continuity of wrapping) and type of FRP (either CFRP or GFRP) sheets on improving the lateral load bearing capacity, ductility, energy absorption, and stiffness of reinforced masonry columns subjected to axial and lateral loads.

4.2 Test results

4.2.1 CFRP wrapped columns

Figure 4.1 shows the lateral load, F , versus lateral drift hysteretic relations of CFRP wrapped columns. The lateral loads takes into account the contribution of the horizontal component of vertical load to the applied lateral load upon the deformation of the column tip (this contribution increases at high lateral displacement levels). Therefore, adjusted lateral load is defined as:

$$F = V + P.\frac{\Delta}{h_2} \qquad 4.1$$

where, V and P are applied lateral and vertical applied loads, Δ is the lateral displacement of the tip of the column, and h_2 is the distance between two hinges on the top of the column, as it is shown in Figure 4.2. Since displacements are relatively small, contribution of vertical component of V would not have a significant effect on the level of applied axial load.

Prior to the application of the lateral load, columns were first loaded with constant axial load of 200 kN. As shown in Figures 4.3(a) and 4.3(b), the first crack in the control column RMC-0 was observed at 0.7% drift. Cracks widened during the subsequent cycles at the same displacement level. The yielding of vertical rebars started when the column reached a 1% lateral drift. The new diagonal cracks that were formed upon cyclic loading resulted in reduction in the lateral load bearing capacity of the column. It was also observed that the most extensively damaged region shifted above the first mortar bed joint, i.e. about 200 mm away from the column-footing interface due to additional confining effect of the footing. Similar results were observed in the response of reinforced concrete columns tested under seismic and axial loads (Sheikh and Yau, 2002). After reaching a 1.6% lateral drift, Column RMC-0 experienced a significant reduction in the lateral load bearing capacity; thus it was decided to apply a monotonic push load on the column up to failure, which occurred at a 6.6% lateral drift (Figure 4.3(c)).

Due to the confinement provided by one layer of CFRP wrap in column RMC-CW-1, it was not possible to monitor cracking of the original masonry column; however, minor rupture of CFRP wrap was observed at the column-footing interface (see Figure 4.3(d)). The lateral load carrying capacity did not increase after the drift level of 1.5%

and it reduced gradually upon increasing the drift. The maximum lateral load reached during the test was 68 kN at a 1% drift level (see Figure 4.1). The column was considered failed at a 2.8% drift level when the lateral load resistance reduced to less than 80% of the maximum recorded lateral load capacity. Test was stopped at 5% drift level.

As for Column RMC-CW-2, similar to previous column, the lateral load did not increase after a drift of 1.5% after which it started reducing gradually. The maximum lateral load reached during the test was 76 kN at the 0.9% drift level (see Figure 4.1). It should be noted that after 5% drifts level, the specimen was monotonically pushed and the test was stopped at a 6% drift level, and up to that lateral displacement level no rupture or damage have occurred in the CFRP wraps (as it is shown in Figure 4.3(e)); however, few localized debonding of the wrap was observed..

In column RMC-CW-3, the lateral load did not increase after drift of 1.5% and started decreasing gradually after 4% drift (see Figure 4.1). As can be seen in Figure 4.1, the maximum lateral load reached during the test was 79.7 kN at 1.5% drift level. The test was continued until it reached a 10% lateral drift without signs of rupture or damage to the CFRP wraps; however, local debonding of wrap was observed. After removing the CFRP sheets of columns RMC-CW-1, 2, and 3 after being tested, it was observed that the crushed pieces of masonry can be easily removed from the bottom 200 mm of the column.

In an attempt to optimize the CFRP material used in wrapping the columns, another rehabilitation scheme was proposed instead of wrapping masonry column along its full height. RMC-CW-1S was wrapped with one layer of CFRP strips at the plastic hinge zone (bottom 300 mm) and at the bed joints, as shown in Figure 4.3(f). Upon

applying cyclic excitations, the lateral load did not increase after a drift level of 1.2% after which it started reducing gradually (see Figure 4.1). The maximum lateral load reached during the test was 63 kN, which is about 8% less than the maximum recorded lateral load for column RMC-CW-1. Column RMC-CW-1S was considered to be failed at a 3.5% drift when the lateral load reduced to less than 80% of the column's maximum recorded lateral load. After 5% drift, the column was only monotonically pushed, and the ultimate failure occurred at 10% drift due to sudden rupture of CFRP wrap that occurred simultaneously with an explosive crushing of concrete masonry (see Figure 4.3(g)). The most extensive damage occurred at the bottom 300 mm from the column-footing interface.

Since there were no cracks observed above plastic hinge zone while testing column RMC-CW-1S, the column RMC-CW-1P was only wrapped at the base of the column, i.e. at the plastic hinge location, as shown in column 4.3(h). In general, as it is shown in Figure 4.1, this column behaved very similar to column RMC-CW-1S, and the maximum recorded lateral load capacity during the test was 60 kN which is slightly less than the maximum lateral loaded obtained from testing column RMC-CW-1S. As can be seen in Figure 4.3(i), the CFRP jacket opened up at several locations along the height at a 5.7% lateral drift. No cracks were observed above the wrapped zone. Similar to the RMC-CW-1S column RMC-CW-1P failed at a 10% drift when the CFRP wrap ruptured and the masonry concrete crushed at the base of the column (see Figure 4.3(j)).

Figure 4.4 shows the variation of transverse strains on CFRP wrap along the column height for columns RMC-CW-1S and RMC-CW-2. Strain values are obtained from the strain gauges installed on the rounded corners of the wrapped sections. It was

observed that in column RMC-CW-1S, the rupture of the CFRP wrap occurred at a recorded strain of 0.82% where it initiated from one of the column's corners. On the other hand, the maximum transverse strains of RMC-CW-2C did not exceed 0.31% when the test was stopped at 6% lateral drift. These strain readings reflect combined effect of local expansion resulting from concrete confinement and diagonal tension caused by shear. It should be noted that the maximum strains in the CFRP wraps occurred at the location of first mortar bed joint. Similar pattern of CFRP strain readings is reported for reinforced concrete columns confined with CFRP tubes and subjected to axial and lateral loads (Ozbakkaloglu and Saatcioglu, 2006). The distribution of the CFRP tensile strain along the height of the tested rehabilitated columns can be used to determine the plastic hinge length in RCM columns which generally falls within a one column-dimension from the base of the column. Moreover, as it was previously observed, higher content of confining FRP will result in a smaller damaged region (Iacobucci, 2001), and consequently shorter plastic hinge length. The strain readings above the plastic hinge zone, where shear stresses are dominant in comparison to flexure stresses, are very small and almost negligible.

Rupturing strain of 0.82-0.85% was recorded in columns RMC-CW-1S and RMC-CW-1P which is less than rupturing strains obtained from coupon test. This could be attributed to the combined effect of flexural and shear stresses on the CFRP sheets or the presence of a curvature at the corners which made it rupture at lower tensile stress.

4.2.2 GFRP wrapped columns

The testing of GFRP-wrapped columns was conducted similar to the CFRP-wrapped ones. Figure 4.5 shows lateral load, F , versus lateral drift hysteretic relations of the three GFRP-wrapped columns. Moreover, in Figure 4.6, the lateral load versus lateral drift of the three-GFRP wrapped columns are compared with the three CFRP-wrapped columns which have the same wrapping scheme or have the same number of FRP layers.

In Column RMC-GW-1, No cracking or GFRP rupture was observed even at the end of the test and high lateral drifts. However, as it is shown in Figure 4.7(b) longitudinal rebars pullout was observed at high lateral drifts. The lateral load did not increase after the drift level of 1.3% and reduced gradually after. The maximum lateral load reached during the test was 66 kN at the 1% drift level (see Figure 4.5). The column was deemed to reach failure at 2.8% drift level when the lateral load carrying capacity reduced to less than 80% of its maximum recorded lateral load. Test was stopped at 11.6% drift level when the column could not sustain the axial loads.

In general, the columns RMC-GW-2 and RMC-CW-2 behaved similarly, but the column with two layers of GFRP exhibited lower lateral load bearing capacity in compare to the column with 2 layers of CFRP wrap (see Figure 4.6). In this test, lateral load did not increase after the drift of 1% and reduced gradually after. The maximum lateral load reached during the test was 65.2 kN at the 1% drift level (see Figure 4.5). After reaching 5% lateral drift, the column was only pushed up to 11% lateral drift when it was not possible to sustain the axial load safely. After removing the GFRP sheets, it was observed that extensive cracking occurred at the bottom 400 mm of the column.

In Column RMC-GW-1S, similar to the tests on CFRP wrapped columns, it is tried to optimize used GFRP material. Therefore, instead of wrapping the column continuously along the height, only the base of the column (bottom 300 mm) and mortar joints were wrapped with GFRP strips, as it is shown in Figure 4.7(d). Only one layer of GFRP was used for strengthening of column RMC-GW-1S such that the obtained results for this column can be compared with results attained from columns RMC-CW-1S and RMC-GW-1.

In this test, the lateral load did not increase after the drift level of 1.2% and reduced gradually after. Unlike CFRP wrapped column (RMC-CW-1S), no GFRP rupture was observed and no cracks were developed on the surface of the column during the test; therefore, as it is shown in Figure 4.5, the column RMC-GW-1S behaved almost the same as column RMC-GW-1. The maximum lateral load reached during the test was 59.2 kN which is slightly less than maximum recorded lateral load for column RMC-GW-1. Furthermore, this column behaved very similar to column RMC-CW-1S (see Figure 4.6); however, since no GFRP rupture occurred, the degradation of lateral forces were more gradual and without any abrupt decrease in lateral loads (unlike column RMC-CW-1S). Column RMC-GW-1S was considered failed at 4% lateral drift when lateral load reduced to less then 80% of the maximum recorded lateral load. After 5% drift, column was pushed until 12% lateral drift was reached and the test was stopped because of the worry that column might not carry the compressive loads safely.

4.3 Performance of CFRP and GFRP wrapped RCM columns

4.3.1 Improvements to lateral load carrying capacity

Figure 4.9 shows the percentage gain in the lateral load carrying capacity versus equivalent volumetric ratio of FRP material, ρ'_{FRP} , for all the FRP-wrapped columns. In this Figure, maximum lateral load is defined as the average of the maximum lateral load in the push and pull directions. Two relations were defined for volumetric ratio of FRP material. For FRP-wrapped columns, the FRP volumetric reatio, ρ_{FRP} , is calculated as follows (Roca, 2007):

$$\rho_{FRP} = \frac{2.n.t_f(b+h)}{b.h}\frac{b_f}{S_f} \qquad 4.2$$

where, n = number of CFRP layers, t_f = thickness of CFRP jacket, b and h = section dimensions, b_f = width of CFRP strips in partial wrapping, and S_f = Pitch in partial wrapping.

To have a better comparison between CFRP and GFRP wrapped columns, an equivalent volumetric ratio of FRP material (ρ'_{FRP}) is used, which is defined as follows:

$$\rho'_{FRP} = \rho_{FRP}.\frac{E_{FRP}}{E_S} \qquad 4.3$$

where, ρ_{FRP} is defined in Equation (4.2), E_{FRP} is modulus of elasticity of CFRP or GFRP material, and E_S is modulus of elasticity of steel (200 GPa). This equivalent volumetric FRP ratio follows a concept similar to the transformed sections commonly used in the analysis of reinforced concrete sections to transfer steel rebars to equivalent concrete area. The advantage of introducing and using this ratio is the possibility of

identifying the effect of the FRP material's while considering the effect of the modulus of elasticity, E_{FRP}, of the used material. Table 4.1 shows the maximum lateral load capacity and the volumetric ratios of FRP reinforcement (ρ_{FRP} and ρ'_{FRP}) for both CFRP and GFRP wrapped columns.

Figure 4.8 shows the envelope of hysteretic loops for all the CFRP-wrapped columns. From the figure it can be seen that the general trend is that lateral load carrying capacity and the displacement ductility of the rehabilitated columns increases by increasing the number of CFRP layers. It is observed that increasing CFRP wraps from 1 to 2 layers results in increasing the maximum lateral load capacity by about 10.5%. The optimum number of CFRP layers depends on the section dimension and radius of rounded corners (Aiello et al., 2007). Therefore, for the tested columns in this study, it could be said that increasing the CFRP sheets beyond 3 layers would not have significant additional effect on increasing the lateral load carrying capacity.

4.3.2 Improvements to displacement ductility

An important indicator of the seismic performance is the displacement ductility factor, μ_Δ, defined as Δ_u / Δ_y where Δ_y is the yield displacement and Δ_u is the ultimate displacement. In order to determine the yield displacement, an equivalent elasto-plastic relationship is defined. The elastic branch of this system is the secant to the real force-displacement relationship at 75% of the maximum lateral load and is extended to reach the maximum lateral load level in order to estimate the displacement at yield. The failure of the column was defined at the post-peak displacement, Δ_u, where the remaining capacity has dropped to 80% of the peak load (Park, 1989). Table 4.2 shows the ductility

factors for each column in both directions; push and pull. Unlike the slight increase in the load-carrying capacity that the control column experienced, the displacement ductility capacities of the retrofitted columns showed significant increase, where the columns with 2 and 3 layers of CFRP wrap exhibited displacement ductilities that are about 3.5 times higher than that of the control column. As shown in Figure 4.1 and Table 4.2, it is worthy to mention that the confinement from CFRP did not significantly affect the load at yield of the rehabilitated columns, and that all columns' reinforcement yielded at approximately the same level of lateral drift. Similar results were also observed by Binici (2008).

In addition to the percentage gain of lateral load carrying capacity of all tested columns versus equivalent volumetric ratio of FRP material, ρ'_{FRP}, the percentage gain of displacement ductility is also shown in Figure 4.9 which can be useful for design purposes.

4.3.3 Lateral stiffness

Stiffness values were determined by dividing the maximum lateral load reached within a cycle by the corresponding displacement in the positive (push) or negative (pull) direction (see Figure 4.10). The stiffness of a cycle is then idealized by taking the average of stiffness values in positive and negative directions (Park, 1989).

Stiffness degradation diagram for the six tested columns is shown in Figure 4.11. It is observed that retrofitted columns exhibited higher stiffness values than non-retrofitted ones; also it is observed that retrofitted columns with two and three layers of CFRP sheets exhibited very close stiffness values while stiffness values of columns RMC-CW-1, RMC-CW-1S and RMC-CW-1P are situated in between non-retrofitted and

columns RMC-CW-2 and RMC-CW-3. Similar trend in stiffness degradation of GFRP-wrapped columns are also observed and is shown in Figure 4.12. At each level of lateral drift, lower stiffness represents the expansion of section cracks and damages due to applied lateral and axial loads. Based on the obtained stiffness degradation curves the following general equation can be proposed for estimating stiffness values of control and CFRP-strengthened square RCM columns:

$$k = (2.1\rho_{FRP} + 3.2)\delta^{(0.23\rho_{FRP} - 1.04)} \qquad 4.4$$

where, k is the column stiffness (kN/mm), δ is the lateral drift (%), and ρ_{FRP} is the volumetric ratio of CFRP reinforcement. To generate Equation 4.4, first, separate equations were obtained for stiffness degradation versus lateral drift of all specimens, then the changes in the coefficients of each equation were linked to changes in volumetric ratio of CFRP reinforcement (ρ_{FRP}) of the specimens. Although not shown in Figure 4.11 for conciseness and clarity of the curves in the figure, the values of the proposed analytical equation for stiffness have very good correlation with the experimental results with a coefficient of determination value, R^2, of 0.936. These results combined with a strength degradation model can be used for modeling of hysteretic rules of CFRP strengthened rectangular RCM columns. Equation 4.4 can also be used for GFRP wrapped columns using the following modification:

$$k = (2.1\rho'_{FRP} \cdot \frac{E_S}{E_{FRP}} + 3.2)\delta^{(0.23\rho'_{FRP} \cdot \frac{E_S}{E_{FRP}} - 1.04)} \qquad 4.5$$

where, ρ'_{FRP} is defined in Equation 4.3.

4.3.4 Energy dissipation

The resistance of a RCM structure against seismic loads is significantly dependant on the energy dissipation capacity of its columns and walls. The energy dissipation in each cycle is estimated by calculating the area enclosed by the corresponding load-displacement hysteretic loop as shown in Figure 4.10. The cumulative dissipated energy (CDE) was obtained by adding the energy dissipated in consecutive loops, and can be expressed by (Parvin et al., 2010):

$$CDE = \sum_{j=1}^{N} \left[\oint_{cyclej} F \, .du \right] \tag{4.6}$$

where, N = number of response cycles and F = Lateral load obtained from Equation 4.1 and corresponding to the top displacement u.

Figure 4.13 and 4.14 show the drift ratios versus cumulative dissipated energy of CFRP and GFRP wrapped columns respectively. Figure 4.13 also tabulates the increase in accumulated dissipated energy for all CFRP wrapped columns at 5% lateral drift level. It can be seen that the retrofitted columns provided higher energy dissipation as compared to column RMC-0. The wobbles in the energy dissipation curves are caused by elastic energy release at the unloading paths of each cycle (two wobbles per cycle). Furthermore, it is observed that while increasing the number of CFRP layers had a marginal effect in terms of increasing the column's lateral load carrying capacity, a significant increase in terms of energy dissipation capacity is obtained. For instance, it can be observed that wrapping the test column with two layers of CFRP sheet provided an increase of 74% in terms of energy dissipation capacity as compared to the control specimen.

4.4 Conclusions

The effectiveness of CFRP and GFRP confinement in increasing the lateral load carrying capacity, displacement ductility, stiffness, and energy dissipation capacity of RCM columns with square cross section was assessed. This experimental research led to the following findings:

- Wrapping the reinforced masonry control column along its full-height with 1, 2 or 3 layers of CFRP sheets increased the lateral load bearing capacity of the column by about 30%, 46%, and 53%, respectively.
- Wrapping the reinforced masonry control column along its full-height with 1 and 2 layers of GFRP sheets increased the lateral load bearing capacity of the column by about 23 and 25%, respectively.
- Wrapping the reinforced masonry control column along its full-height with 1, 2 or 3 layers of CFRP sheets increased the displacement ductility of the column by about 115%, 260%, and 273%, respectively.
- Wrapping the reinforced masonry control column along its full-height with 1 and 2 layers of GFRP sheets increased the displacement ductility of the column by about 81% and 105%, respectively.
- Wrapping the reinforced masonry control column along its full-height with 1 or 2 layers of CFRP sheets, increased the cumulative energy dissipation capacity of the column at 5% drift by about 32% and 74%, respectively.
- Wrapping the reinforced masonry control column along its full-height with 1 and 2 layers of GFRP sheets, increased the cumulative energy dissipation capacity of the column at 5% drift by about 1% and 26%, respectively.

- It is observed that wrapping the RCM columns at the plastic hinge zone and mortar joints prevents cracking of the columns under the lateral and cyclic loads even at very high lateral drifts. In general, the experimental hysteretic loops in columns RMC-CW-1P, RMC-CW-1S, and RMC-GW-1S were very similar to the ones with one continuous layer of FRP along the height (columns RMC-CW-1, RMC-GW-1) with slightly less increase (about 12%) in lateral load carrying capacity. However, it was observed that this pattern of wrapping is not as effective as continuous wrapping for improving the ductile behaviour of the RCM columns.
- It is observed that by wrapping the RCM columns at plastic hinge zone, no cracks occurred above the wrapped zone when the columns were subjected to cyclic loads, and that the failure occurred through CFRP rupture and crushing of concrete masonry units and it took place at the column's base at very high lateral drifts (10% drift).
- Failure of columns wrapped at the plastic hinge only (RMC-CW-1P) or at the plastic hinge zone and with strips at the mortar bed joints (RMC-CW-1S) occurred due to premature rupture of CFRP wrap. In these columns, CFRP failure occurred at very high lateral drift of 10%.

Table 4.1 Maximum lateral load capacity for each tested column

	Column	No. of FRP layers	F (kN)	ρ_{FRP} (%)	ρ'_{FRP} (%)
CFRP	**RMC-0**	0	52	0	0.00
	RMC-CW-1P	1	60	0.10	0.04
	RMC-CW-1S	1	63	0.16	0.06
	RMC-CW-1	1	68	0.28	0.14
	RMC-CW-2	2	76	0.55	0.28
	RMC-CW-3	3	79.7	0.83	0.42
GFRP	**RMC-0**	0	52.0	-	0.00
	RMC-GW-1S	1	60.9	-	0.07
	RMC-GW-1	1	63.8	-	0.16
	RMC-GW-2	2	65.0	-	0.32

Table 4.2 Displacement ductility factors for tested specimens

		Push			**Pull**		
	Specimen	Δ_{yield} (mm)	Δ_{ult} (mm)	μ_Δ	Δ_{yield} (mm)	Δ_{ult} (mm)	μ_Δ
CFRP	RMC-0	13	22	1.7	10	21	2.1
	RMC-CW-1	14	44	3.1	15	62	4.1
	RMC-CW-2	12	80	6.7	10	72	7.2
	RMC-CW-3	15	102	6.8	13.6	100	7.5
	RMC-CW-1S	13.1	50	3.8	21	52	2.5
	RMC-CW-1P	13	49	3.8	20	50	2.5
GFRP	RMC-GW-1	14	42	3	15	57	3.8
	RMC-GW-2	14	58	4.1	12	52	4.3
	RMC-GW-1S	14	44	3.1	16	58	3.6

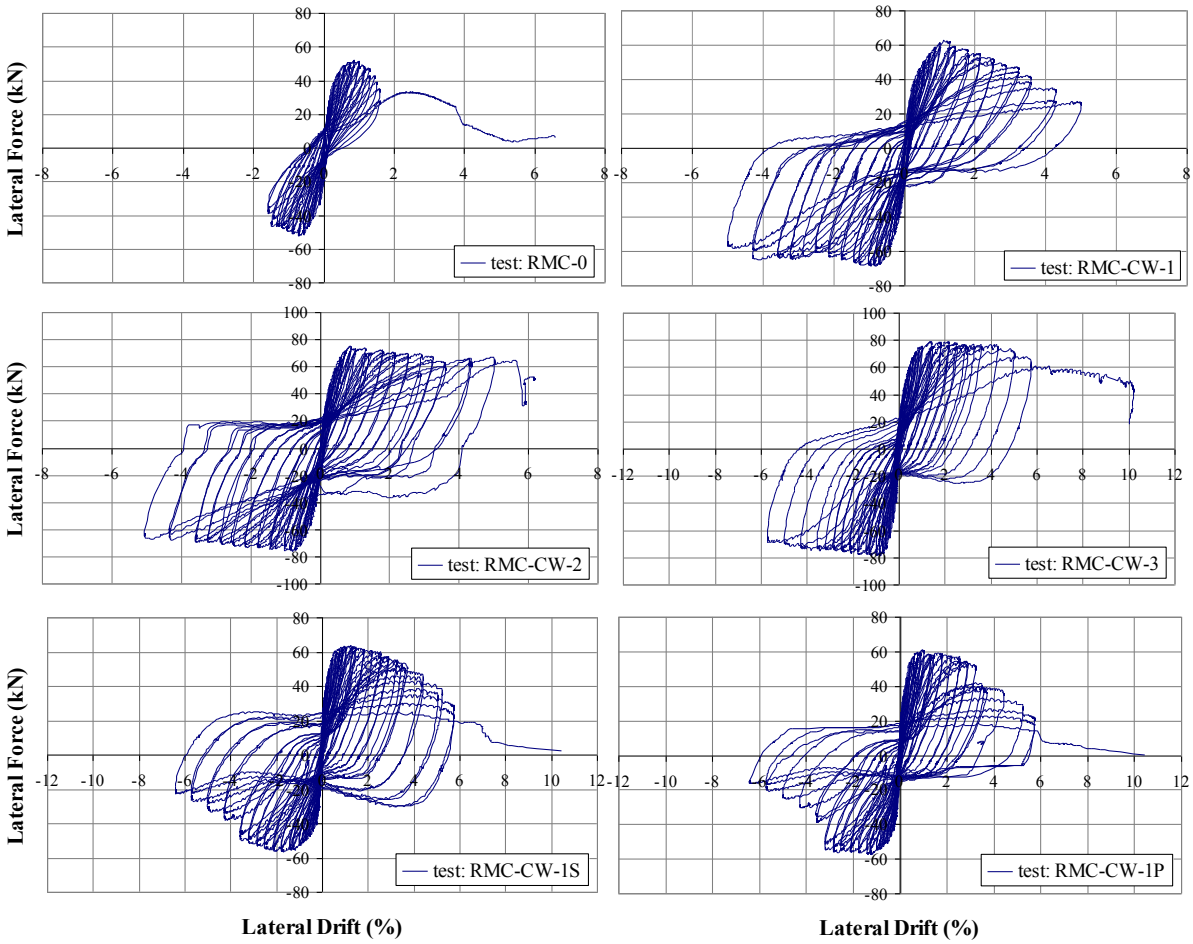

Figure 4.1: Lateral loads-lateral drift relationships of the tested CFRP-wrapped columns

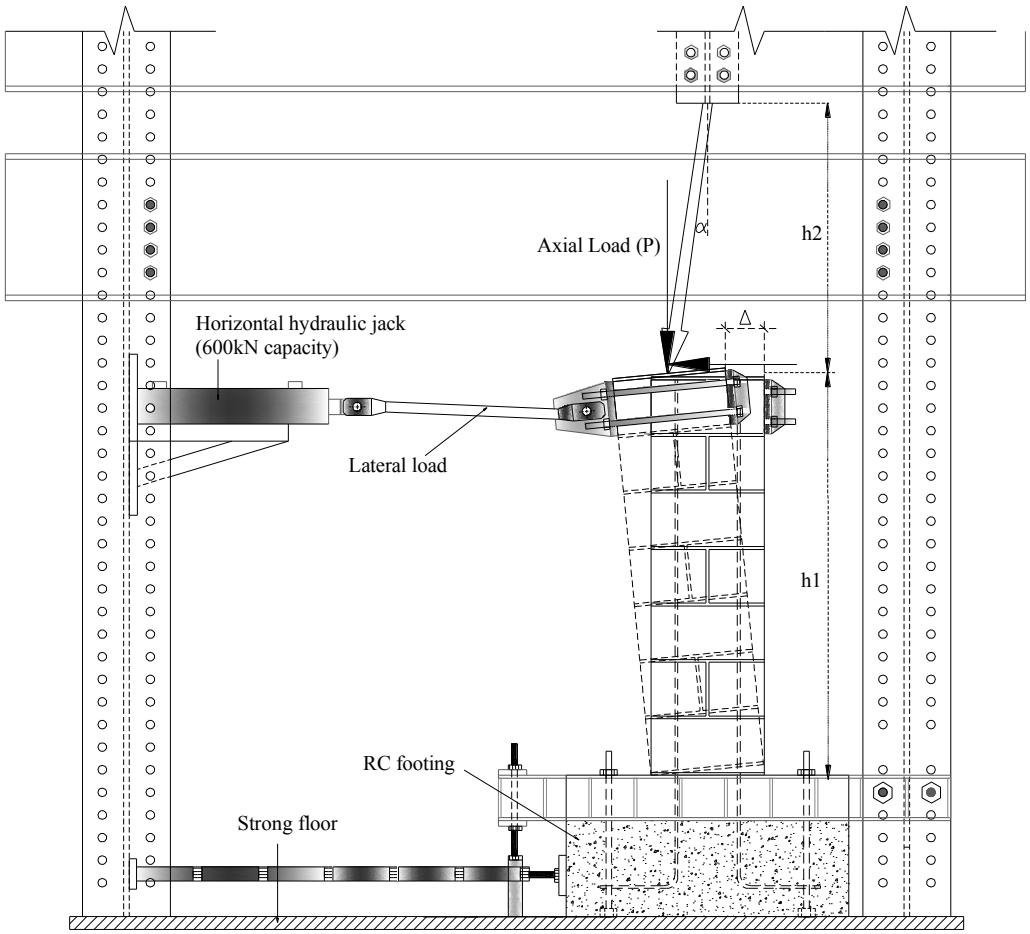

Figure 4.2: Calculation of the lateral load including the effect of inclination of axial load.

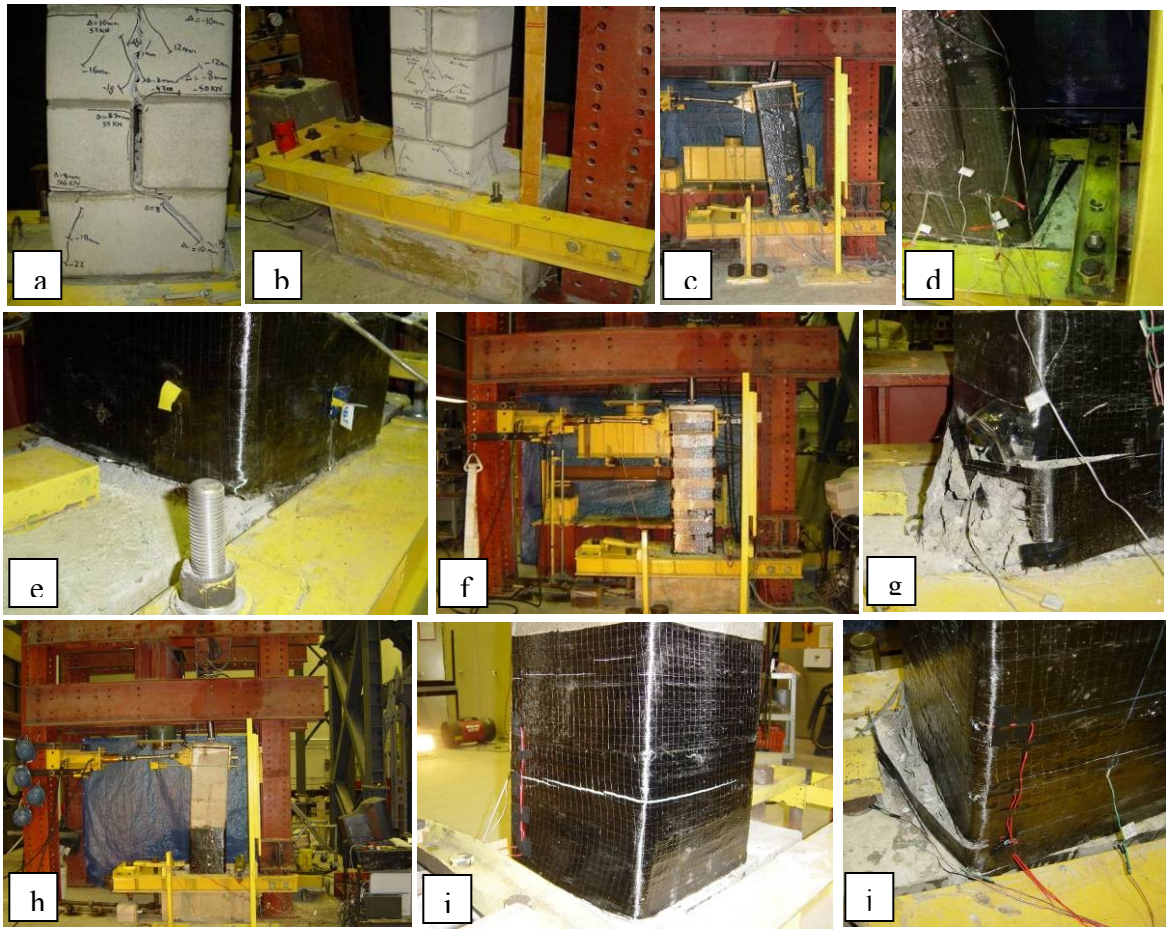

Figure 4.3: Performance of the CFRP-wrapped columns at different stages of the tests including observed cracking pattern and behaviour at failure

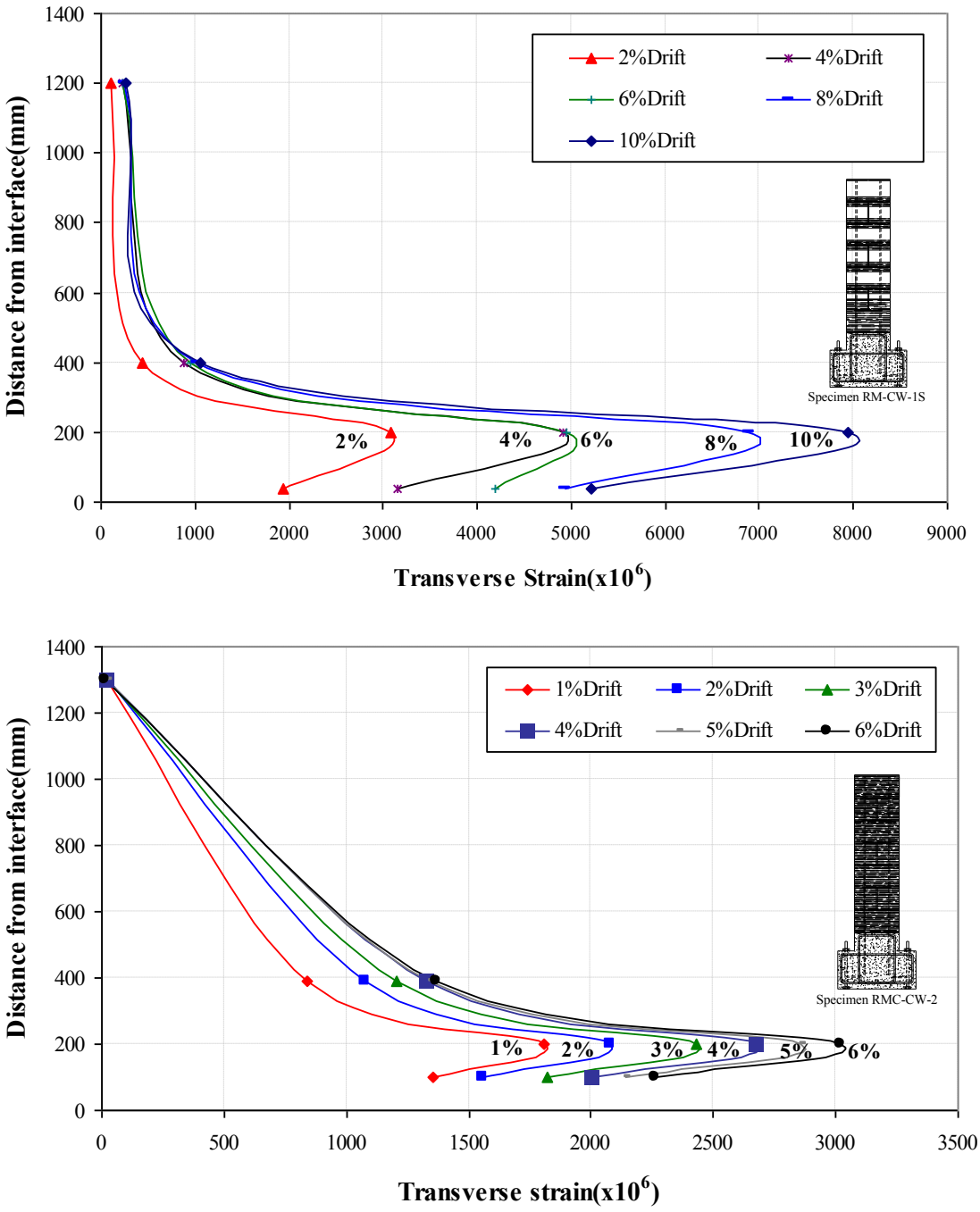

Figure 4.4: Variation of transverse strains on CFRP wraps along column height for columns RMC-CW-1S and RMC-CW-2

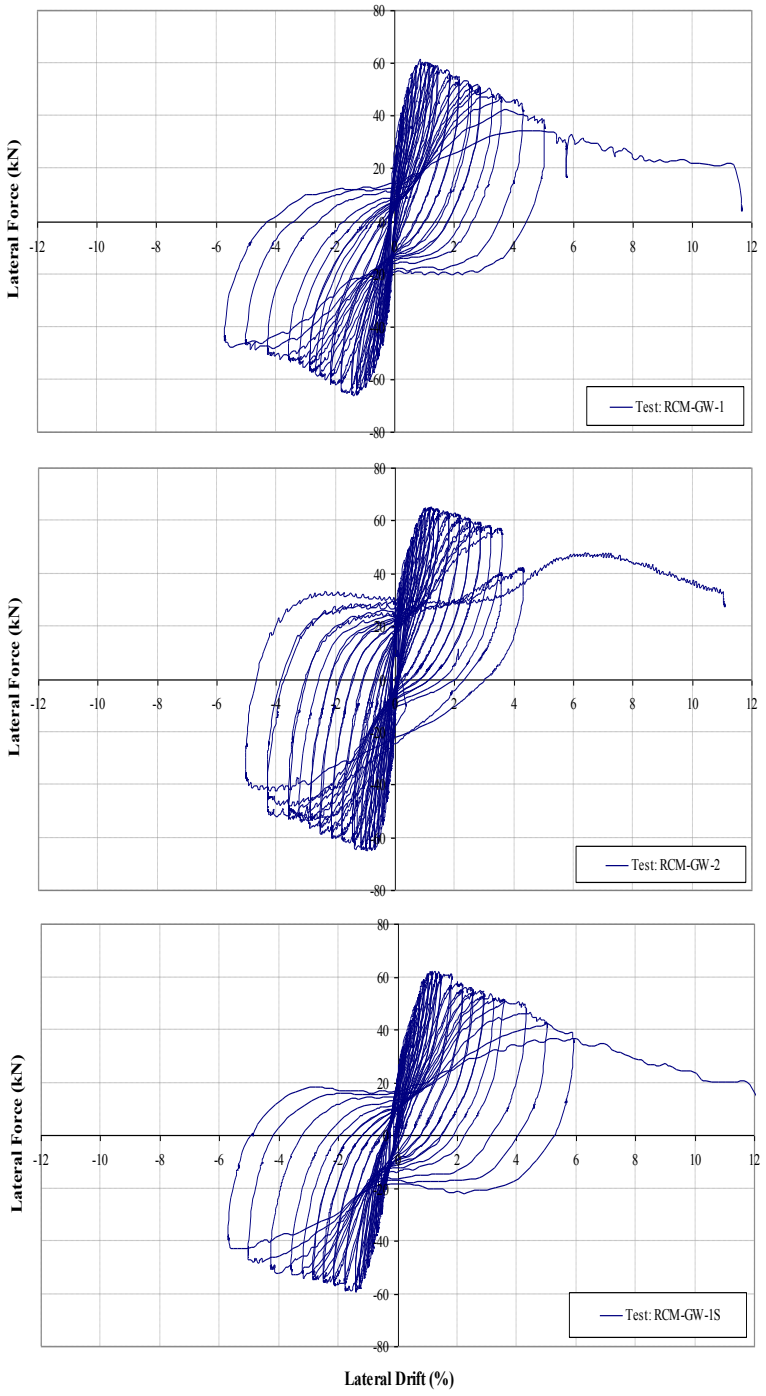

Figure 4.5: Lateral loads-lateral drift relationships of the tested GFRP-wrapped columns

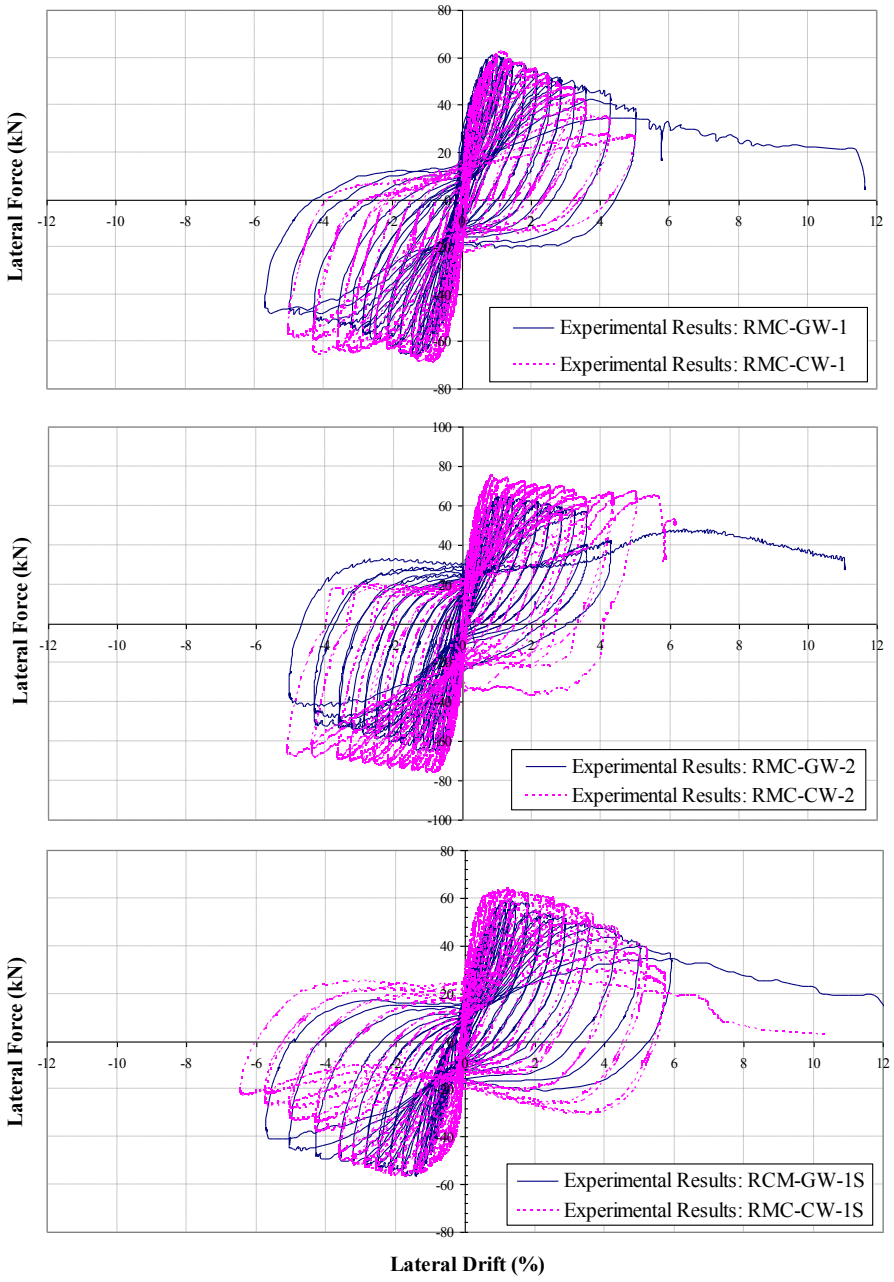

Figure 4.6: Lateral loads-lateral drift relationships of the CFRP and GFRP wrapped columns with similar wrapping scheme or number of layers

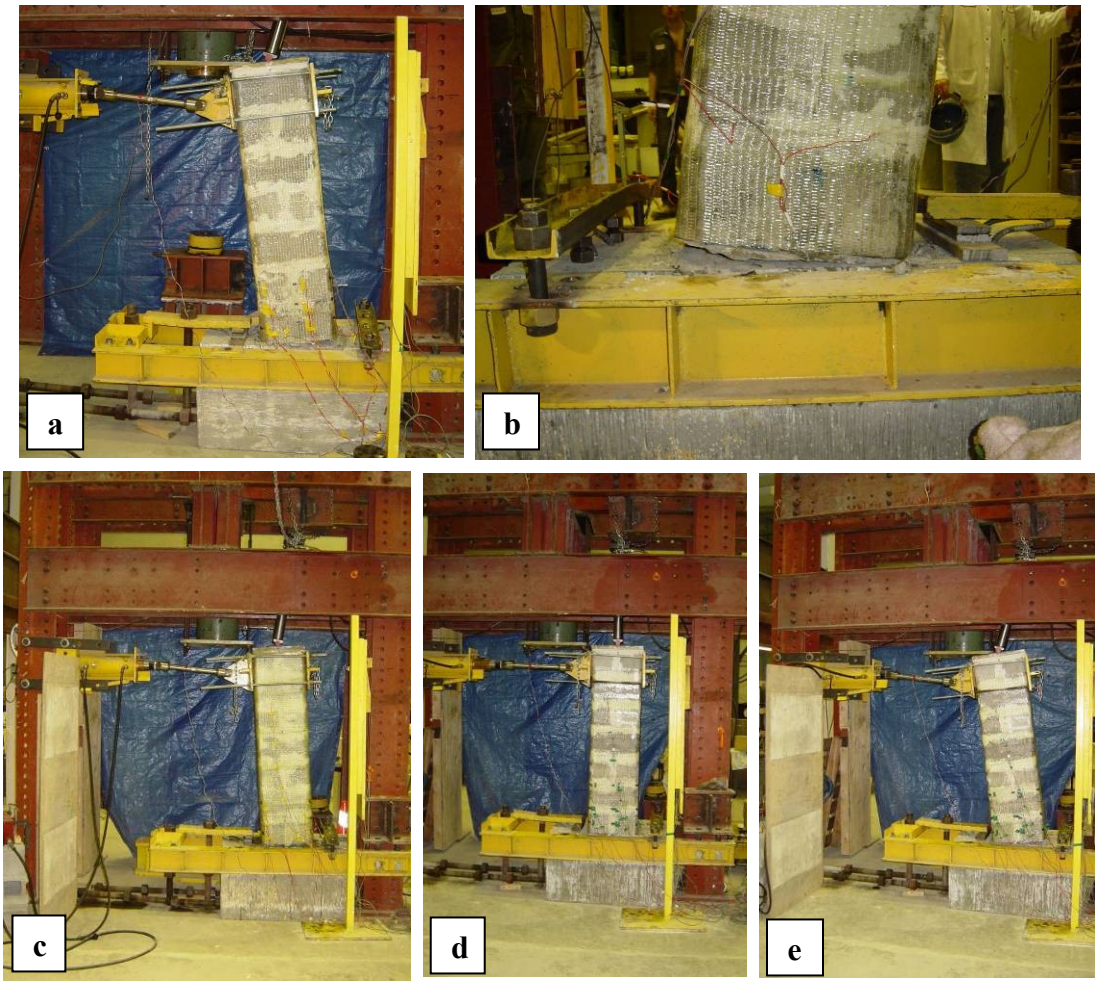

Figure 4.7: a) Column RMC-GW-1 at 6% lateral drift, b) column-footing interface at high lateral drift, c) Column RMC-GW-2 at 6% lateral drift. d) Column RMC-GW-1S before applying lateral loads, e) Column RMC-GW-1S at 6% lateral drift.

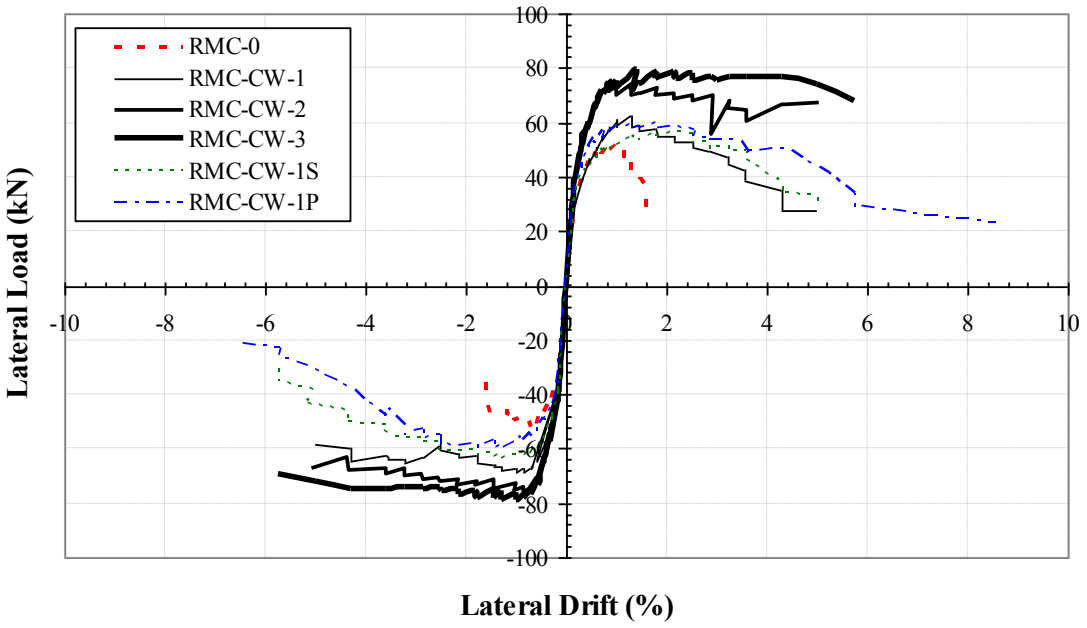

Figure 4.8: Envelope of hysteretic loops of CFRP-wrapped columns

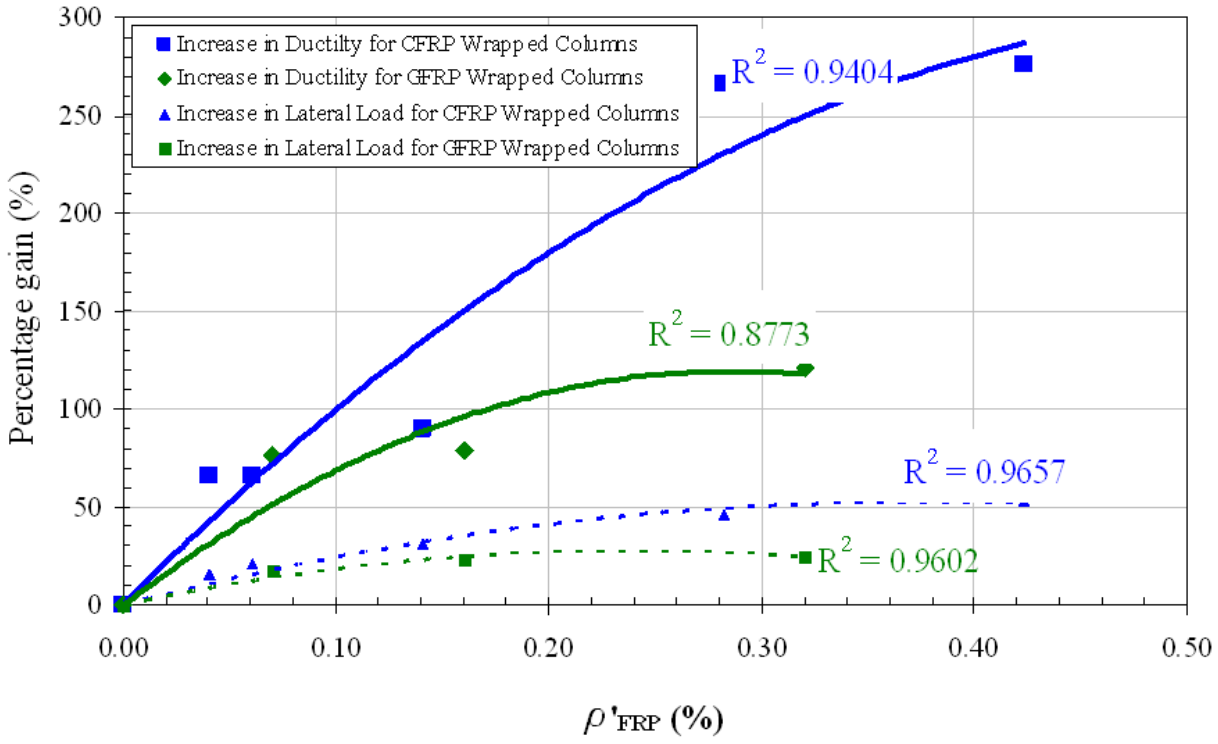

Figure 4.9: Percentage gain in lateral load carrying capacity and displacement ductility versus equivalent volumetric ratio of FRP material (both CFRP and GFRP)

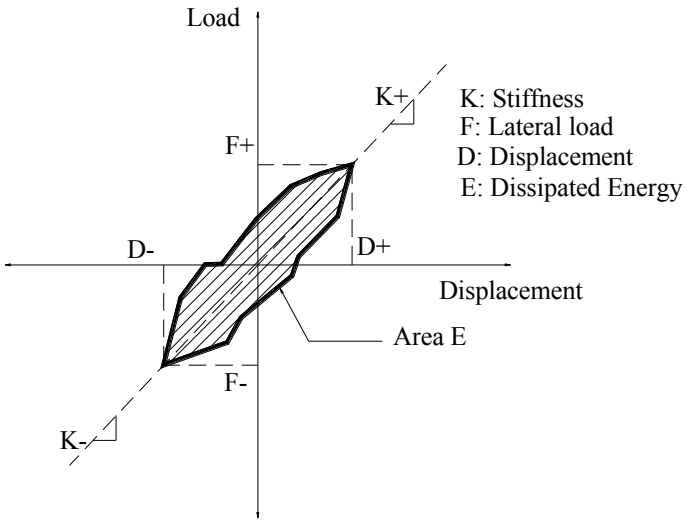

Figure 4.8: Determination of stiffness and energy dissipation for each cycle

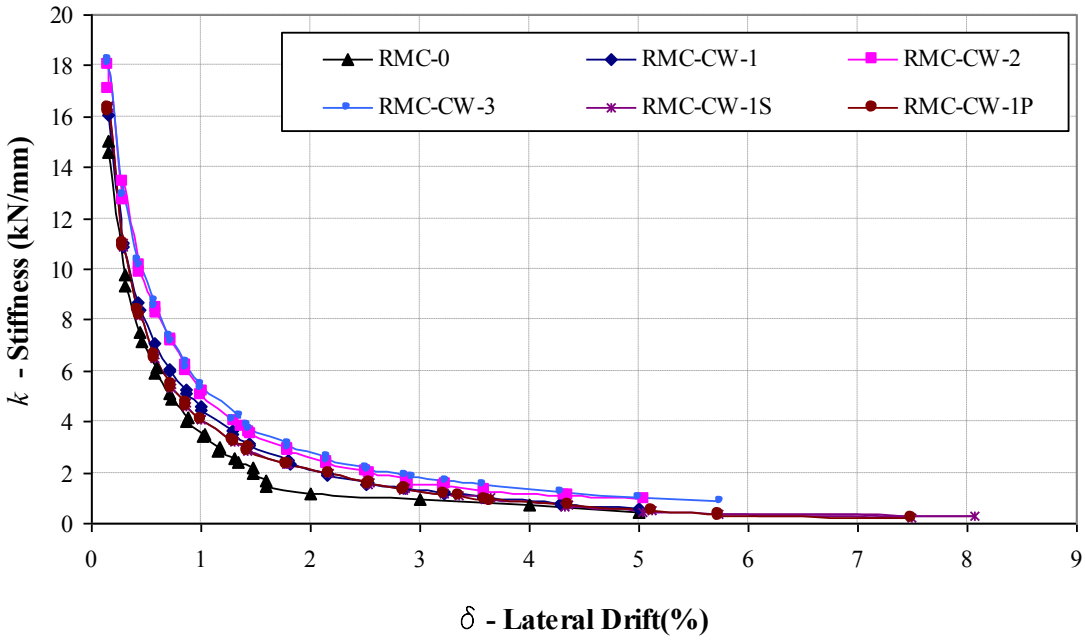

Figure 4.9: Stiffness degradation of the CFRP wrapped column

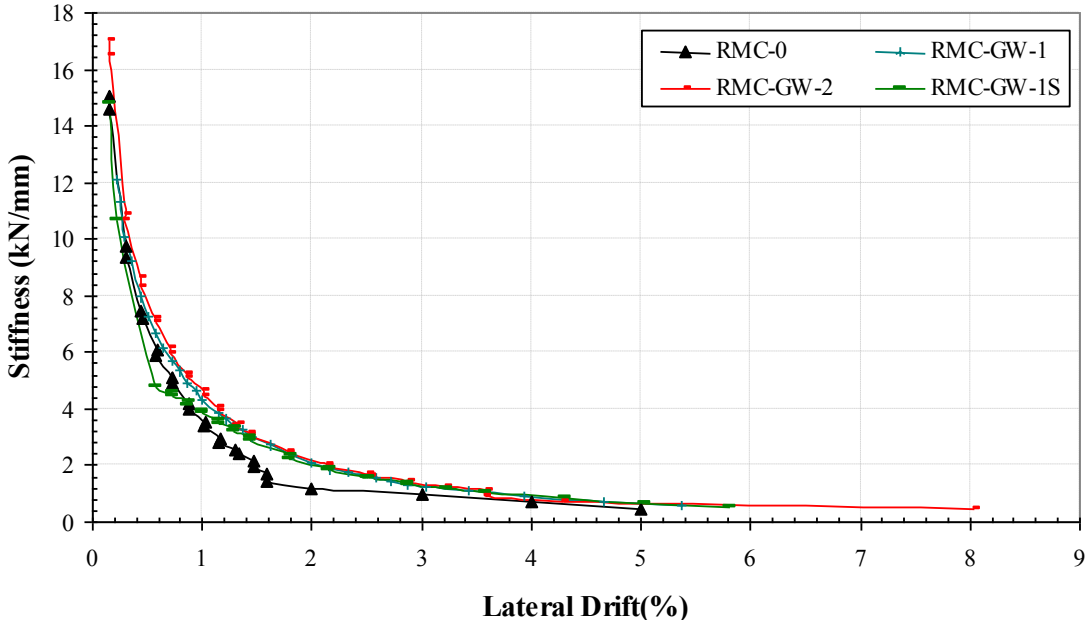

Figure 4.10: Stiffness degradation of the GFRP wrapped column

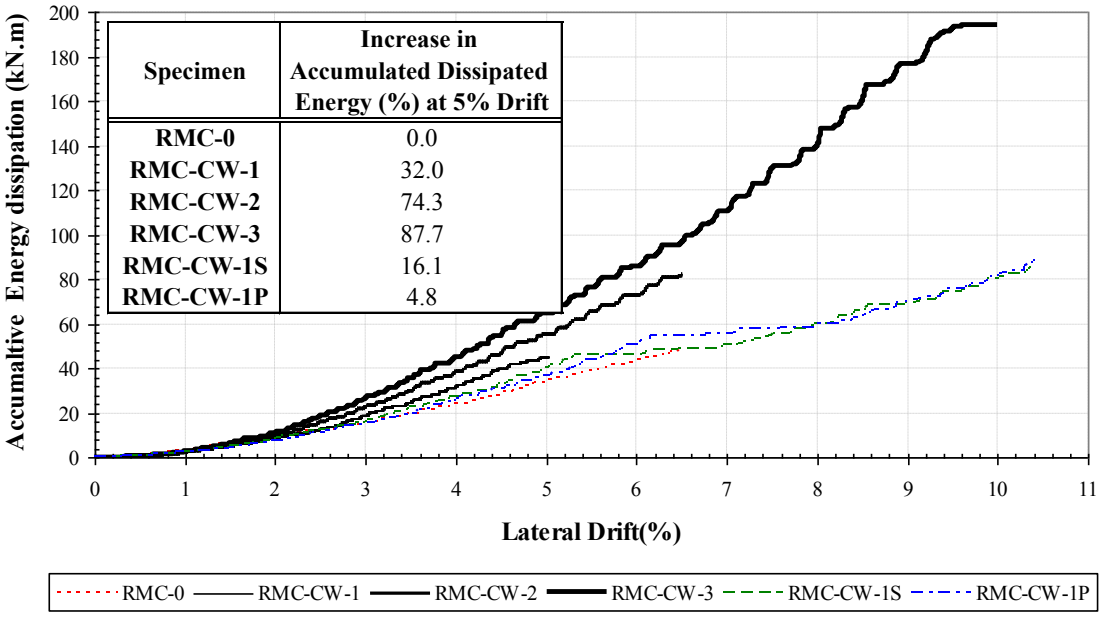

Figure 4.11: Accumulated dissipated energy versus lateral drift for the CFRP wrapped columns

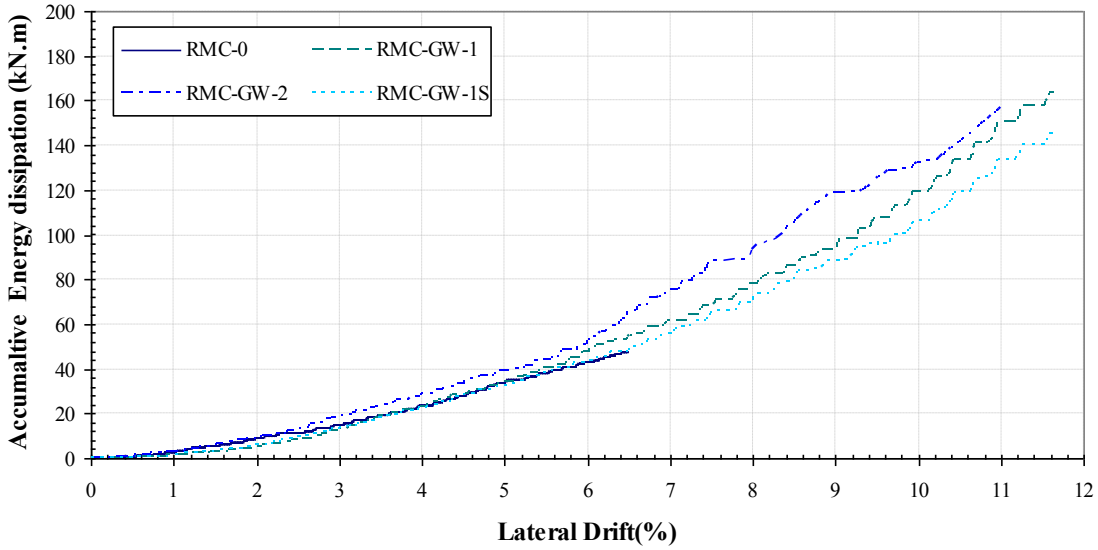

Figure 4.12: Accumulated dissipated energy versus lateral drift for the GFRP wrapped columns

CHAPTER 5

CONFINEMENT MODEL FOR CFRP-WRAPPED CONCRETE MASONRY BLOCK PRISMS

5.1 Introduction

In this chapter, an experimental investigation that led to the development of compression stress-strain characteristics of grouted concrete masonry prisms wrapped with carbon fiber-reinforced polymer (CFRP) composites is described. Twelve five-block high prisms were constructed using bull-nose concrete blocks. Tests were conducted under increasing axial load at low strain rates. As the study focuses on evaluating the contribution of CFRP wraps in enhancing concrete masonry behaviour, the test variable was set to be volumetric ratio of CFRP material. Confining effect of the CFRP material was monitored via detailed instrumentation. In this study, the effectiveness of CFRP wraps in modifying the failure mechanism and improving compression strain ductility of masonry blocks is quantified. Furthermore, the observed experimental results were used to develop a model to predict the stress-strain relationship for unconfined and CFRP-wrapped concrete masonry sections. Comparisons were made between the proposed stress-strain curves for unconfined grouted concrete masonry with other methods available for this type of material. Finally, the proposed strength model and stress-strain relation were validated by comparing the analytical results with the flexural capacity of CFRP wrapped concrete masonry columns described in previous chapter.

5.2 Need for confinement model for FRP-wrapped masonry prisms

In order to be able to predict the inelastic response of masonry structures to extreme events, it is necessary to have detailed information on the complete stress-strain characteristics of masonry including compressive strength and its corresponding strain, slope of the falling branch of the stress-strain curve after peak strength, and ultimate compression strain. These characteristics are available for different types of masonry. Stress-strain relation of unconfined concrete masonry sections were proposed based on experimental investigation, also the effects of confinement by placing steel plates in the mortar bed joints and inserting rolled fine or welded wire mesh into the voids of the hollow concrete masonry prior to grouting were studies (Priestley and Elder, 1983, Dhanasekar and Shrive, 2002). The effect of FRP-strengthening in enhancing the behaviour of masonry columns became a subject of several studies in recent years. The stress-strain characteristic of FRP-wrapped rectangular prisms made of clay bricks was proposed in (Krevaikas and Traintafillou, 2005), a model for stress-strain relation of FRP-wrapped brick masonry columns in compression was proposed in (Corradi et al., 2007), In another similar research, FRP confinement of rectangular specimens made of calcareous stone (limestone) and artificial stone (clay bricks) were studied in (Aiello, 2009), More recently, more data was provided for stress-strain behaviour of tuff and clay brick masonry section in (Ludovico et al., 2010).

On the other hand, considerable research has been directed to establish detailed stress-strain models of FRP wrapped reinforced concrete (RC) sections. The latter models would be considered as a better reference for understanding and simulating the behaviour of FRP wrapped concrete masonry blocks as compared to the models that are developed

for FRP confined brick or stone masonry elements. Various models for FRP-confined concrete columns have been proposed in (Mander et al., 1988, Miyauchi et al., 1997, Xiao and Wu, 2000, Lam and Teng, 2003). Most of the proposed models are empirical in nature and have been calibrated based on experimental tests.

Due to the limited available data reported in the literature, the objective of the research described in this chapter is to provide a stress-strain relationship for CFRP confined rectangular concrete masonry prisms in compression. The model is instrumental in predicting the response of CFRP confined masonry assemblages and columns, especially for concrete masonry members that are designed and constructed following CSA S304.1-04 (2004). Consequently, the proposed stress-strain relations are validated by using them to predict the flexural capacity of the six reinforced masonry columns (one control column, five columns wrapped with CFRP, and three columns wrapped with GFRP) when subjected to axial and lateral excitations.

5.3 Description of test Specimens and their construction

As shown in Figure 5.1, twelve five-course prisms consisting of alternate courses of one full and two half blocks were constructed with the help of a professional mason. The prisms were constructed similar to the prisms that were tested in (Priestley and Elder, 1983). Concrete blocks were grinded to provide round corners with approximate radius of 25mm. Having the amount of CFRP confinement as a test variable, the prisms were divided into 4 groups where each group consisted of three prisms. Prisms designations are shown in Table 5.1. In Table 5.1, the volumetric ratio of CFRP reinforcement (ρ_{FRP}) are also presented (ρ_{FRP} is calculated using Equation 4.2, as it was explained in chapter

4). Details of CFRP installation process are illustrated in Figure 5.2. To ensure the effectiveness of the wrapping, 150 mm overlap provided as recommended by the FRP rehabilitation guidelines (ISIS, 2008).

Before starting the construction of concrete masonry prisms, it was necessary to obtain material properties of concrete masonry blocks, mortar, grout, and CFRP sheets. Therefore, the same material properties that were used in the construction of nine full-scale RCM columns were utilized in the construction of 12 prisms (the details of the material properties were presented in Chapter 3). All prisms were constructed without vertical steel reinforcement. It was observed in a similar previous study (Priestley and Elder, 1983) that masonry stress-strain curves show no significant variation from unreinforced and reinforced prisms, provided that load carried by the reinforcement was subtracted from the total load before calculating masonry stress.

5.4 Test setup/instrumentation and testing procedure

Prisms were tested under monotonically applied axial compressive load with low strain rates of 0.0001 mm/mm/sec resulting in peak stress being reached approximately 200 sec after the start of the test. The test setup used in this experimental study is shown in Figure 5.3. Prior to testing, each prism was bedded into a layer of high strength plaster at its top and bottom between the rigid parallel beams that were used in the test setup. These layers of plaster constrained the rotation of the prism ends and ensured uniform strain along the cross-section of the prism.

A 3000 kN capacity load cell was used to measure the applied axial forces. Two linear variable displacement transducers (LVDTs) were installed. As can be seen in

Figure 5.3, LVDT-1 was used to measure the hydraulic jack's ram travel. Since stroke measurement inevitably incorporates some flexibility in the test setup, LVDT-2 was placed along the front side of the prism, and readings obtained from LVDT-2 were used to correct ram travel readings (LVDT-1) which provided the axial deformation reading of the tested prisms until the end of each test, and it was possible to follow the falling branch of the load-displacement curves. In order to measure tensile strains on the external CFRP confinement, 9 strain gauges were installed on each side of the specimens confined with continuous sheets and 12 strain gauges were installed on each side of the prisms with CFRP strips at mortar joints. Strain gauges were directly applied on the wraps after cleaning the surface and removing a thin layer of epoxy resin. Details of strain gauges locations on each side of the specimens are shown in Figure 5.4.

In the tests, two conditions were used to define the failure of the tested prisms. The failure is classified as a capacity failure when the post-peak axial load carrying capacity of the specimens reaches about 80% of its peak compressive capacity; whereas the failure is classified as an ultimate failure when CFRP rupture or brittle crushing of concrete masonry occurred.

5.5 Results of tested prisms

Figure 5.5 shows the four groups of prisms in the test setup before being tested and at failure. Table 5.2 shows the test results for the 12 prisms in terms of: Maximum strength (f'_{mo} for control specimens, and f'_{mc} for confined specimens), axial strains recorded at peak strength (ε_{mo} for control specimens, ε_{mc} and for confined specimens), and the ultimate strains recorded when CFRP ruptured or crushing of concrete masonry

occurred (ε_{mu} for unconfined masonry, and ε_{mcu} for confined masonry). Also, the table shows the average (AV), standard deviation (SD) and coefficient of variation (COV) values for each group.

The axial stress-strain relationships for all tested specimens are plotted in Figure 5.6. In the tested control prisms it was observed that after maximum strength was attained, face shells started to fall off at different locations and crushing of the coarse grout occurred with a rapid decrease in load. This can be seen in the sharp decreasing branch of the stress-strain curves after achieving to the peak strength. It was observed that in all confined prisms failure was brittle and was triggered by rupture of fibers. Such a failure was mainly due to local stress concentration, and almost in all prisms it was initiated from one of the corners. Moreover, as it is shown in Figure 5.6, tested prisms of groups CM-CW1 and CM-CW-2 demonstrated a softer (less steep) decrease in falling branch of stress-strain curves, and less brittle behaviour especially for specimens with two layers of CFRP wrap. Stress-strain curves of prisms with strips of CFRP at mortar bed joint (CM-CW-1S group) exhibited higher strength properties as compared to the control specimens; however, due to lack of confinement, they did not reduce the brittle behaviour.

Comparison of obtained stress-strain relations (average of the three prisms in each group) are shown in Figure 5.7. It can be observed that the increase in number of CFRP layers contributes directly in increase of peak stress (f'_{mc}), strain at peak strength (ε_{mc}), and strains at ultimate failure (ε_{mcu}) which results in less brittle behaviour.

Figure 5.8 shows the tensile strains recorded at peak compressive strength on the CFRP wrap for one reference specimen of each tested group. The reference prism was

chosen as the one with higher values of recorded strains out of three prisms of each group (prisms CM-CW-1b, CM-CW-2c, and CM-CW-1Sc). In Figure 5.8, the ratio of tensile strains at peak strength of the CFRP reinforcement (ε_{fc}) to the ultimate CFRP rupture strain (ε_{fu}) are reported for each strain gauge. Furthermore, the dashed horizontal lines indicate the average $\varepsilon_{fc}/\varepsilon_{fu}$ values computed with reference to the whole set of strain gauges installed on the specimen. The $\varepsilon_{fc}/\varepsilon_{fu}$ values are summarized in Table 5.3 along with the average values recorded on each specimen; also the average (AV), standard deviation (SD), and coefficient of variation (COV) values related to the each group are shown.

As could be seen from the strain profiles shown in Figure 5.8, the experimental values of $\varepsilon_{fc}/\varepsilon_{fu}$ are greatly non uniform and significantly less than 1 along the CFRP reinforcement perimeter. It is observed that failure is randomly triggered in the rounded corners of the specimens at the point of stress concentrations after which progressive rupture of adjacent fibres occur leading to the failure of the whole specimen. It should be noted that it is difficult to predict the exact location that triggers the ultimate strain in the CFRP along the whole specimen which would explain the relatively low strain in other instrumented locations along the height of the specimens. Similar observations were made in tests on concrete specimens (De Lorenzis and Tepfers, 2003, Matthys et al., 1999).

5.6 Proposed stress-strain relationship for CFRP-wrapped concrete masonry prisms

In this section, based on the data obtained in experimental phase, the following numerical model is proposed to provide a prediction of stress-strain behaviour of unconfined and CFRP-confined rectangular concrete masonry section:

- A parabolic rising curve:

$$f_m = f_{\max}.\left(\frac{2.\varepsilon_m}{0.0017k_1} - \left(\frac{\varepsilon_m}{0.0017k_1}\right)^2\right) \quad :\text{For } \varepsilon_m \le 0.0017k_1 \qquad 5.1$$

where, ε_m and f_m are axial strain and stress in masonry respectively, and $f_{\max}$ is the maximum compressive strength of concrete masonry assemblage(f'_{mo} and f'_{mc} for unwrapped and CFRP-wrapped prisms respectively). Also k_1 is equal to 1 for unconfined masonry, and equal to $k_1 = 1 + 0.64\rho_{FRP} - 0.53\rho_{FRP}^2$, where ρ_{FRP} is volumetric ratio of FRP material (Eq. 4.2)

- A linear falling branch:

$$f_m = f_{\max}[1 - k_2(\varepsilon_m - 0.0017)] \quad :\text{For } \varepsilon_m > 0.0017k_1 \qquad 5.2$$

where, parameter k_2 indicates the slope of falling branch and obtained from experimental tests, and it equals to $k_2 = 487.1 - 480\rho_{FRP}$. In Figure 5.9, stress-strain curves of unconfined concrete masonry obtained from Eq. 5.1 and Eq. 5.2 are compared with curves obtained from experimental data.

In Eq. 5.1 and Eq. 5.2 it is important to have an accurate estimate of the maximum compressive strength ($f_{\max}$) for confined sections (f'_{mc}) which is dependant to FRP wrap

confining pressure (f_l). In most confinement models for rectangular concrete sections, as it is shown in Figure 5.10, the unconfined area is represented by four second-degree parabolas with an initial slope of 45 degree. This model was first proposed in Matthys et al. (1999). The confining pressure on the rectangular masonry section can be calculated by Restrepol and De Vin (1996):

$$f_l = \frac{2E_f t_f}{D_e}\varepsilon_f \qquad 5.3$$

where, E_f = elastic modulus of FRP; t_f = thickness of FRP; D_e = equivalent to diameter of rectangular section. Considering Figure 5.10, parameter D_e is equal to (Lam and Teng, 2003):

$$D_e = \sqrt{B^2 + H^2} \qquad 5.4$$

where, B and H are dimensions or the rectangular section (Figure 5.10), and ε_f = tensile strain in FRP jacket. For calculating $f_{\max}$, the tensile strains at peak compressive strength (ε_{fc}) of tested prisms are concerned. The average values of $\varepsilon_{fc} / \varepsilon_{fu}$ presented in table 5.3 are used for estimating confining pressure (f_l) in this study. The relationship among confining pressure (f_l), volumetric ratio of FRP material (ρ_{FRP}), and maximum compressive strength of tested specimens ($f_{\max}$) is presented in Figure 5.11 which can be used for predicating $f_{\max}$ in Equations 5.1 and 5.2. Furthermore, similarly the relationship among ultimate strain of FRP-confined specimens (ε_{mcu}), confining pressure (f_l) and volumetric ratio of FRP material (ρ_{FRP}) is presented in Figure 5.12.

5.7 Comparison between the proposed stress-strain relationship of unconfined grouted concrete masonry with similar studies

In Figure 5.13, the proposed equations in this study are compared with stress-strain relations proposed in Priestley and Elder (1983) and Dhanasekar and Shrive (2002) for unconfined grouted concrete masonry. In General, good agreement exists between finding of this study for unconfined grouted concrete masonry sections and the study conducted in Priestley and Elder (1983). The differences that can be observed among the stress-strain curves are mainly due to the differences in the characteristic of constituent materials (i.e. mortar, grout, and blocks) that are used in these studies and also the size of the tested specimens. In Table 5.4 the compressive strength of the unconfined grouted masonry assemblage of current study is compared with those tested in Priestley and Elder (1983) and Dhanasekar and Shrive (2002). While the compressive strength of the masonry assemblages tested in these two studies are close to each other, it should be considered that the equations of this study were driven by testing prisms with five-high prisms and the equations proposed in Dhanasekar and Shrive (2002) were obtained by testing stiffer specimens made of three-high stack-bonded prisms.

5.8 Validation of the proposed stress-strain relationship for unconfined and CFRP-confined concrete masonry

To validate the proposed stress-strain relationship, experimental results obtained from testing six reinforced concrete masonry (RCM) columns (discussed in Chapter 4) were used, and the maximum flexural capacity recorded during the tests are compared with what is calculated from section analysis using Equations 5.2 and 5.3 for unconfined

and CFRP-confined sections. In Table 5.5, columns designations and their volumetric ratio of CFRP reinforcement (ρ_{FRP}) are given.

For flexural capacity calculations, the steel bars stress-strain relationship defined as follows (Priestley, 2007):

$$f_s = E_s.\varepsilon_s \quad \text{For: } \varepsilon_s < \varepsilon_{sy} \tag{5.5}$$

$$f_s = f_{sy} \quad \text{For: } \varepsilon_{sy} < \varepsilon_s < \varepsilon_{sh} \tag{5.6}$$

$$f_s = f_{sy} + (f_{su} - f_{sy})\left[2\frac{\varepsilon_s - \varepsilon_{sh}}{\varepsilon_{su} - \varepsilon_{sh}} - \left(\frac{\varepsilon_s - \varepsilon_{sh}}{\varepsilon_{su} - \varepsilon_{sh}}\right)^2\right] \quad \text{For: } \varepsilon_{sh} < \varepsilon_s < \varepsilon_{su} \tag{5.7}$$

where, E_s = modulus of elasticity , ε_{sy} = yield strain, ε_{sh} = strain-hardening strain, f_{sy} and f_{su} are yield and ultimate stresses, respectively.

To predict the section flexural capacity of unconfined and wrapped RCM columns subjected to axial and lateral loads, it is assumed that, as it shown in Figure 5.14, plane sections remain plane after deformations, tensile strength of masonry is neglected, confined masonry ultimate compressive strain were obtained from findings of this study and Figure 5.12, the effect of thickness of the composite material was ignored to simplify the calculations, and the compressive and tensile forces were calculated based on Equations 5.1 and 5.2 for concrete masonry and Equations 5.5 to 5.7 for steel bars.

In Figure 5.15, the stress-strain curves of CFRP-wrapped columns obtained from the model proposed in this study are shown. Using these curves for the section analysis, in Figure 5.16 the maximum recorded moment obtained from the tested RCM columns are compared with sections' resisting moment obtained from the analysis. The predicted values are approximately 93% of the measured flexural resistance, and the proposed curves provide good predictions of section flexural capacity.

5.9 Summary

In this chapter, the effect of CFRP wrapping of rectangular concrete masonry prisms on its compressive stress-strain behaviour has been investigated. Twelve concrete masonry prisms were wrapped with different CFRP content ratios and tested under increasing axial load. It is observed that CFRP confinement improves load-carrying capacity, reduces the post-peak slope of stress-strain curves, and increases the strains at peak strength (ε_{mc}), and at ultimate failure (ε_{mcu}). It is also observed that the recorded tensile strains along the prism height are greatly non uniform along the CFRP perimeter. Furthermore, based on the test results, a compressive stress-strain model for CFRP-confined concrete masonry blocks is proposed, it is shown that the proposed model provides good estimation of the compressive stress-strain relationship of CFRP-confined concrete masonry blocks as well as the confined compressive strength of masonry.

To validate the proposed stress-strain relationship, experimental results obtained from testing six reinforced concrete masonry (RCM) columns were used, and it is shown that there is a good correlation between analytical prediction of section flexural capacity and results obtained from experimental program. It should be noted that the above results are based on limited number of tests with specific parameters. For the model to be generalized, it needs to be calibrated using more future experimental results.

Table 5.1: Specimen Designation with volumetric ration, ρ_{FRP}, of CFRP material

Specimen	Designation	ρ_{FRP}
Concrete **M**asonry Prisms : 3 Control Prisms	CM-0	0
Concrete **M**asonry Prims with **1** layer of **C**FRP **W**raps: 3 Prisr	CM-CW-1	0.42
Concrete **M**asonry Prims with **2** layers of **C**FRP **W**raps: 3 Pris	CM-CW-2	0.85
Concrete **M**asonry Prisms with **1** layer of **C**FRP **S**trips: 3 Prisn	CM-CW-1S	0.17

Table 5.2: Experimental results of the 12 tested prisms

Specimen	ρ_{FRP}	f'_{mo} or f'_{mc} (MPa)	ε_{mo} or ε_{mc}	ε_{mu} or ε_{mcu}^{*}	Strengthening Ratio $f'_{mc}/(f'_{mo})_{AV}$
CM-0a	0	10.28	0.0017	0.0018	-
CM-0b	0	8.14	0.0017	0.0025	-
CM-0c	0	9.89	0.0017	0.0025	-
AV	-	9.44	0.0017	0.0023	
SD	-	0.93	0.0000	0.0003	
COV (%)	-	9.86	0.43	14.42	
CM-CW-1a	0.42	12.18	0.0021	0.0027	1.29
CM-CW-1b	0.42	12.88	0.0020	0.0026	1.36
CM-CW-1c	0.42	10.69	0.0020	0.0030	1.13
AV	-	11.92	0.0020	0.0028	1.26
SD	-	0.91	0.0000	0.0002	0.0967
COV (%)	-	7.66	2.35	6.19	7.66
CM-CW-2a	0.85	13.16	0.0020	0.0021	1.39
CM-CW-2b	0.85	12.59	0.0020	0.0028	1.33
CM-CW-2c	0.85	12.58	0.0020	0.0038	1.33
AV	-	12.78	0.0020	0.0029	1.35
SD	-	0.27	0.0000	0.0007	0.0287
COV (%)	-	2.12	0.28	24.71	2.12
CM-CW-1Sa	0.17	11.07	0.0019	0.0024	1.17
CM-CW-1Sb	0.17	10.85	0.0020	0.0024	1.15
CM-CW-1Sc	0.17	9.99	0.0018	0.0019	1.06
AV	-	10.64	0.0019	0.0022	1.13
SD	-	0.47	0.0001	0.0002	0.0494
COV (%)	-	4.38	6.03	10.82	4.38

* Strain at CFRP rupture and brittle crushing of concrete

Table 5.3: $\varepsilon_f / \varepsilon_{fu}$ values on the external FRP confinement

Specimen	Average of $\varepsilon_f/\varepsilon_{fu}$				$[\varepsilon_f/\varepsilon_{fu}]_{Av}$	$[\varepsilon_f/\varepsilon_{fu}]_{Av,all}$	$[\varepsilon_f/\varepsilon_{fu}]_{SD,all}$	$[\varepsilon_f/\varepsilon_{fu}]_{cov,all}$ (%)
	0.8H	0.6H	0.4H	0.2H				
CM-CW-1#1	0.03	0.05	0.08	-	0.05			
CM-CW-1#2	0.22	0.25	0.07	-	0.18	0.10	0.06	60.97
CM-CW-1#3	0.02	0.04	0.11	-	0.06			
CM-CW-2#1	0.05	0.15	0.19	-	0.13			
CM-CW-2#2	0.06	0.09	0.16	-	0.10	0.11	0.02	16.73
CM-CW-2#3	0.03	0.14	0.09	-	0.09			
CM-CW-1S#1	0.34	0.18	0.2	0.11	0.21			
CM-CW-1S#2	0.3	0.45	0.27	0.14	0.29	0.23	0.04	18.64
CM-CW-1S#3	0.22	0.12	0.21	0.22	0.19			

* All Strain values in above table are obtained at maximum strength

Table 5.4: Comparison between compressive strength of constituent materials in current study and studies conducted by Priestly and Elder (1983) and Dhanasekar and Shrive (2002)

	Mortar (MPa)	**Grout** (MPa)	**Concrete blocks** (MPa)	**Unconfined Grouted Assemblage (f'_{mo})** (MPa)
Current study	20.7	21.6	15.3	9.3
Priestly and Elder (1983)	11.4	27.8	38.2	26.2
Dhanasekar and Shrive (2002)	N.A.	N.A.	N.A.	10.8

* 28 days strength are given

Table 5.5: Designation of RCM columns and volumetric ration of used CFRP material

Specimen	**Designation**	ρ_{FRP}
Reinforced **M**asonry **C**olumn : Control Specimen	RMC-0	0
Reinforced **M**asonry **C**olumn with **1** layer of **C**FRP **W**raps	RMC-CW-1	0.27
Reinforced **M**asonry **C**olumn with **2** layers of **C**FRP **W**raps	RMC-CW-2	0.54
Reinforced **M**asonry **C**olumn with **3** layers of **C**FRP **W**raps	RMC-CW-3	0.81
Reinforced **M**asonry **C**olumn with **1** layer of **C**FRP **S**trips	RMC-CW-1S	0.16
Reinforced **M**asonry **C**olumn with **1** layers of **C**FRP **W**rap at **P**lastic hinge	RMC-CW-1P	0.1

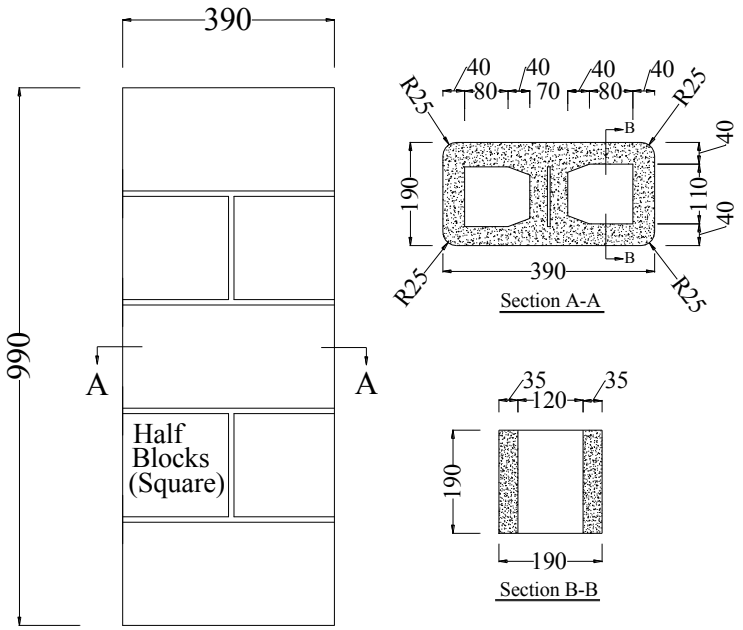

Elevation & Block Dimensions

Figure 5.1: Dimensions (in mm) of masonry prisms and their concrete masonry blocks

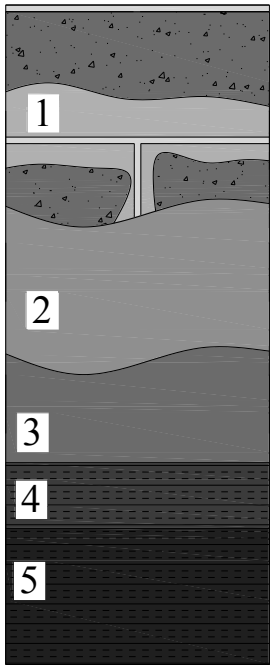

Elevation

1. Plaster over joints
2. Primer
3. Epoxy resin
4. CFRP sheets
5. Epoxy resin

Sequence of applied materials

Figure 5.2: CFRP installation process

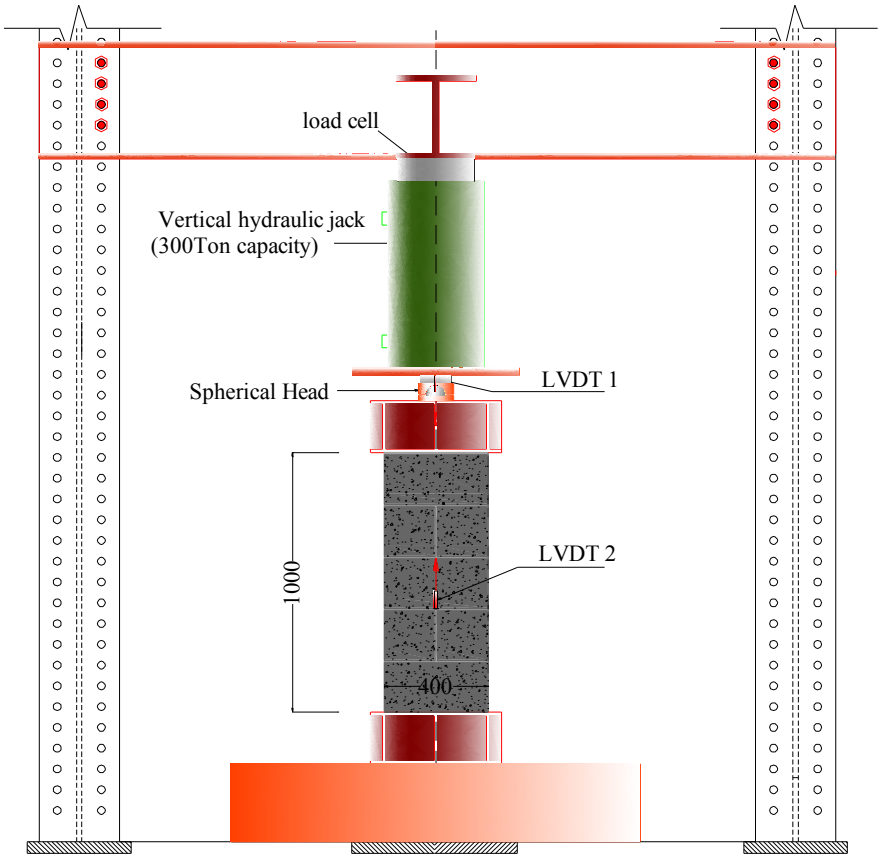

Figure 5.3: Test setup

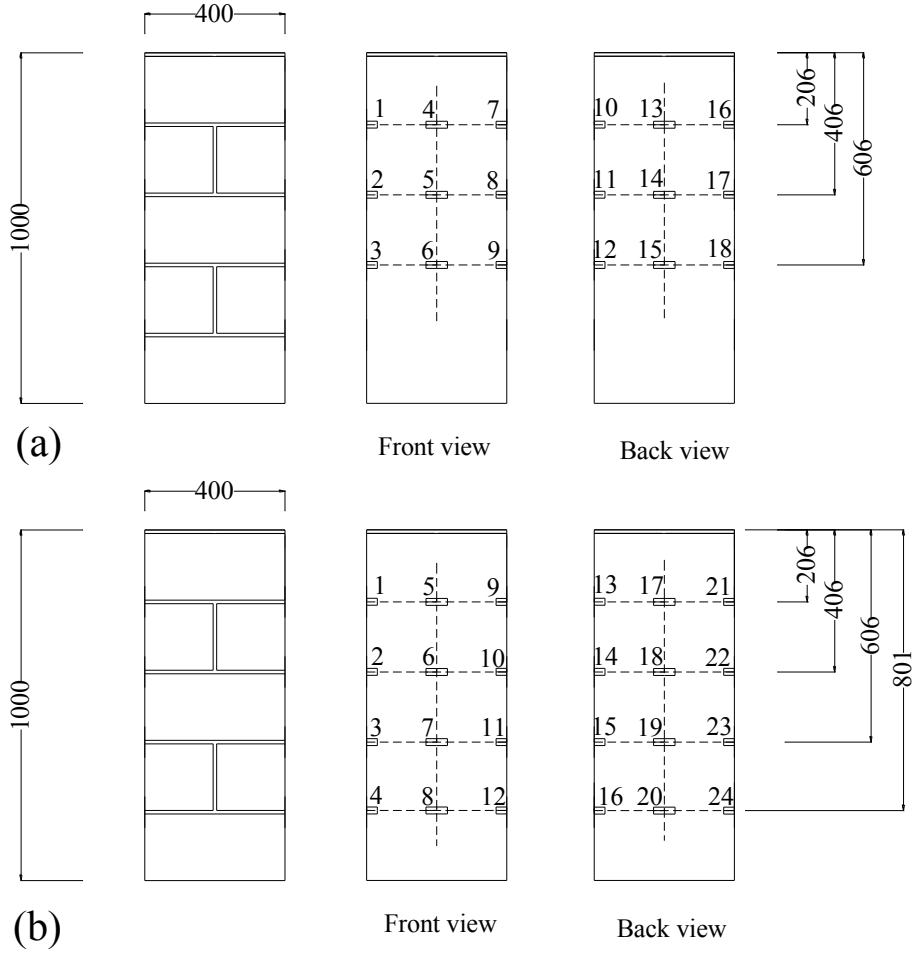

Figure 5.4: Layout of strain gauges: (a) Prism groups of CM-CW-1 and CM-CW-2, (b) Prism group of CM-CW-1S (Dimensions are in mm)

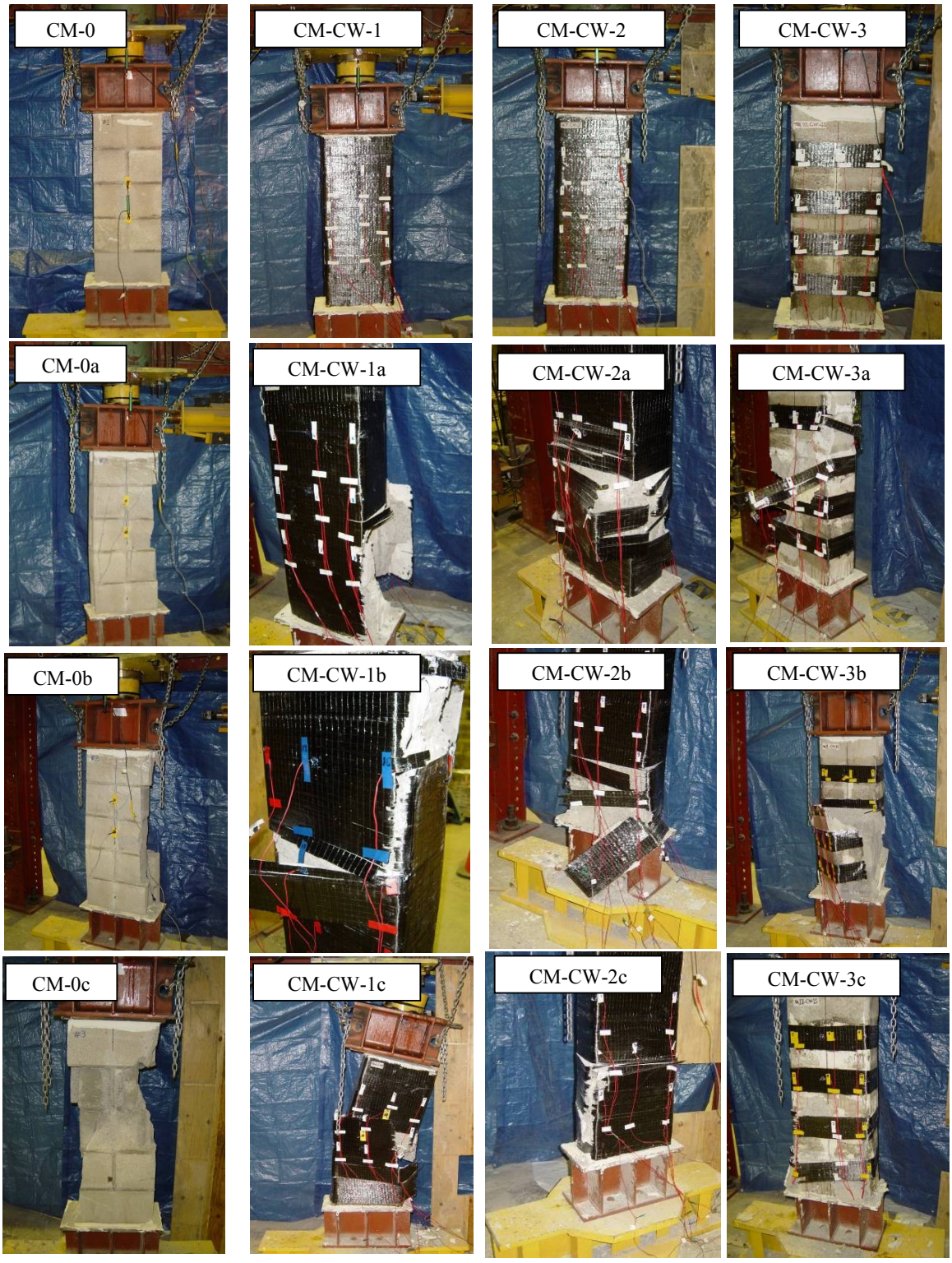

Figure 5.5: Prisms before applying compressive force (first row), and tensile rupture of CFRP wrap and failure of concrete masonry (second, third and fourth rows)

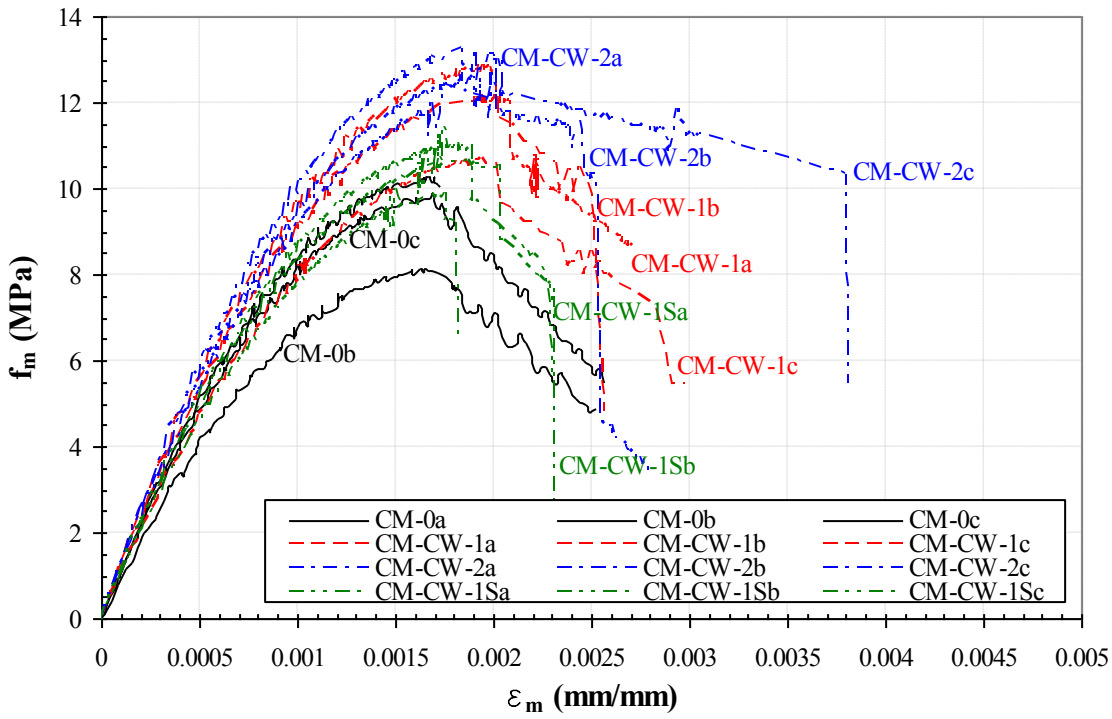

Figure 5.6: Axial stress-strain relationship of the 12 tested prisms

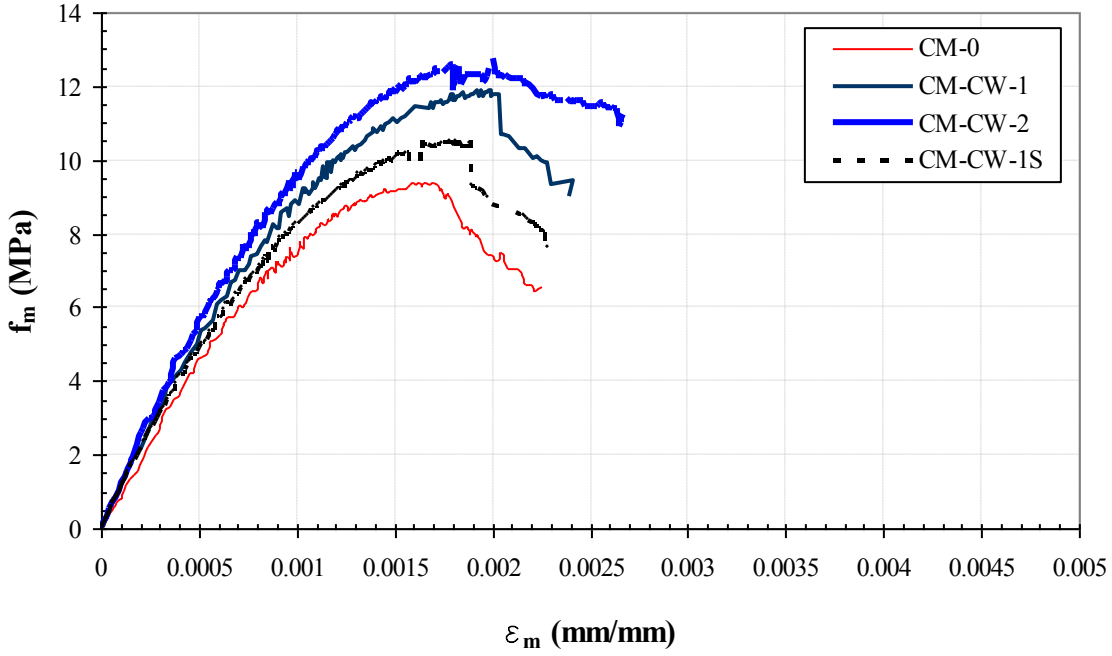

Figure 5.7: Comparisons between average stress-strain curves of all tested prisms

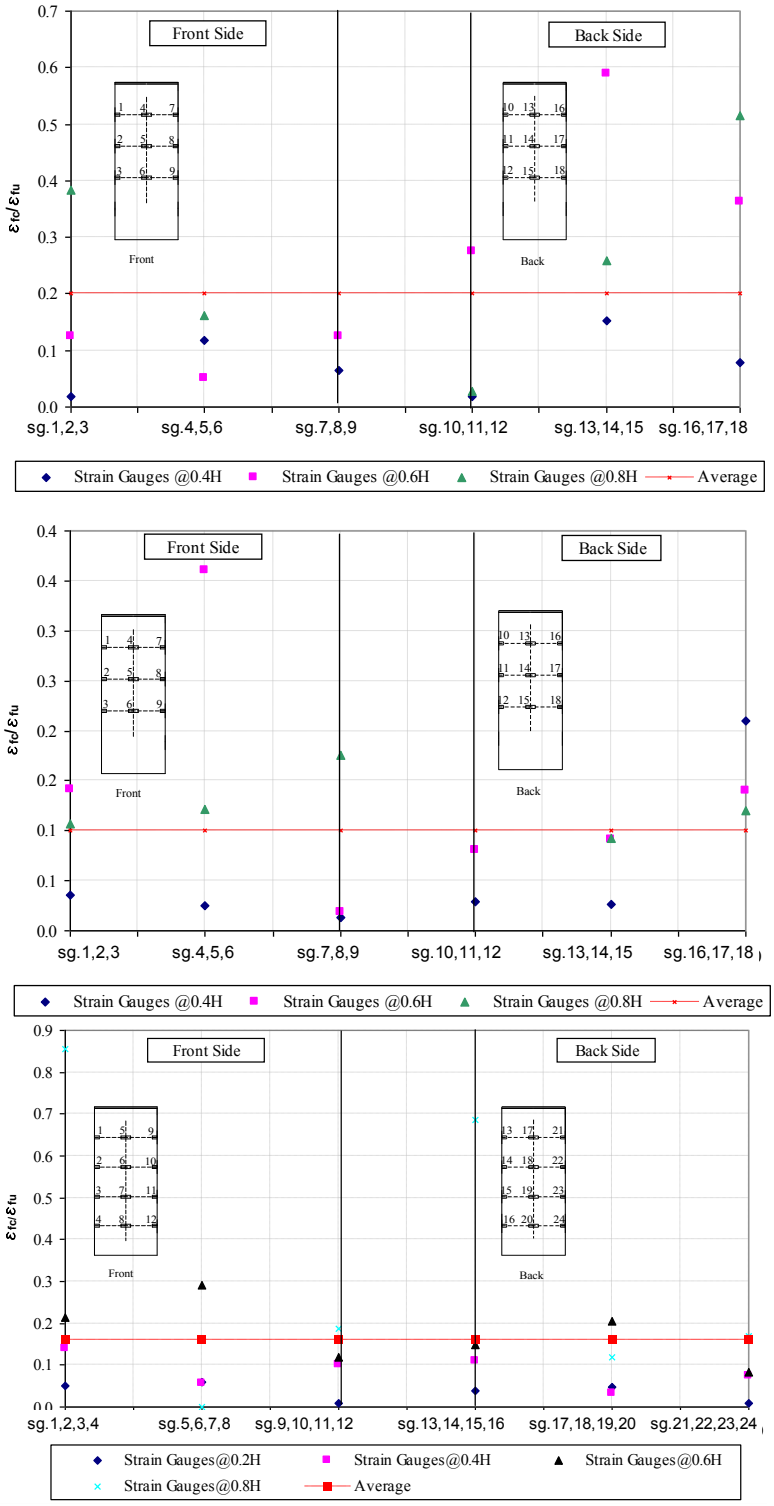

Figure 5.8: Tensile strains profile at peak compressive strength for specimens (1) CM-CW-1b, (2) CM-CW-2c, and (3) CM-CW-1Sc

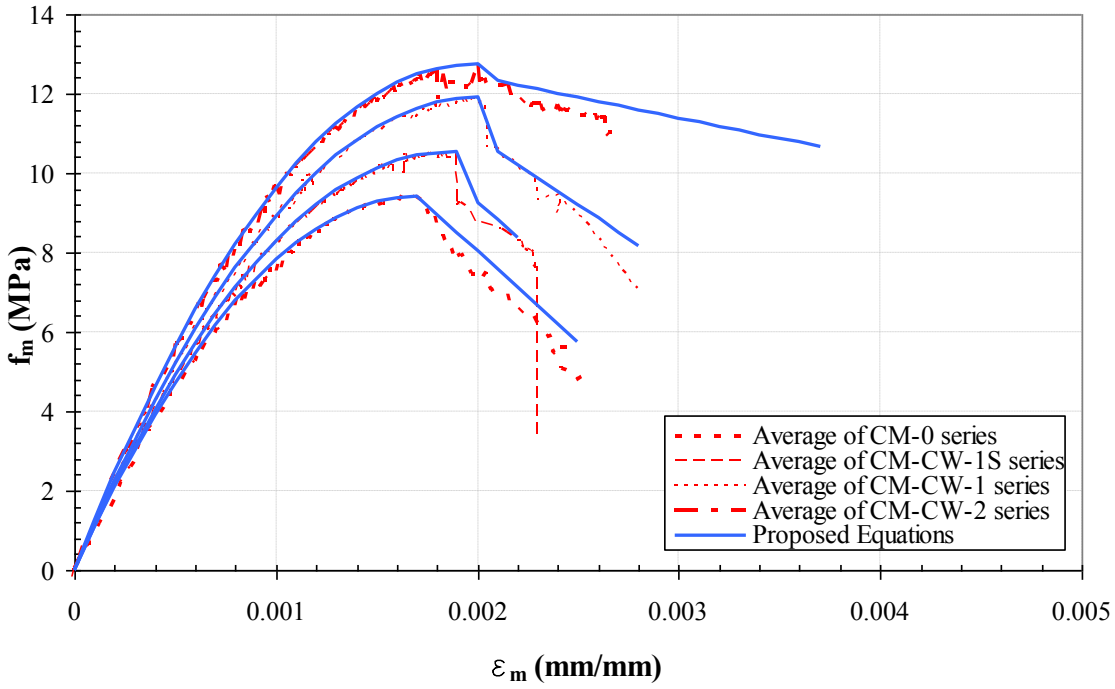

Figure 5.9: Analytical and average experimental stress-strain curves

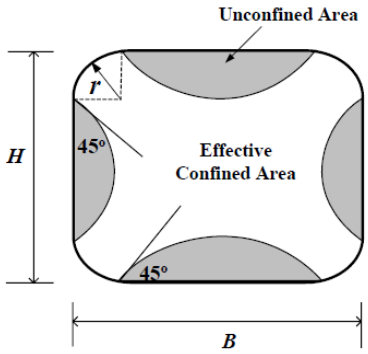

Figure 5.10: Typical model of effective confined area for concrete sections (Restrepol and Vino, 1996)

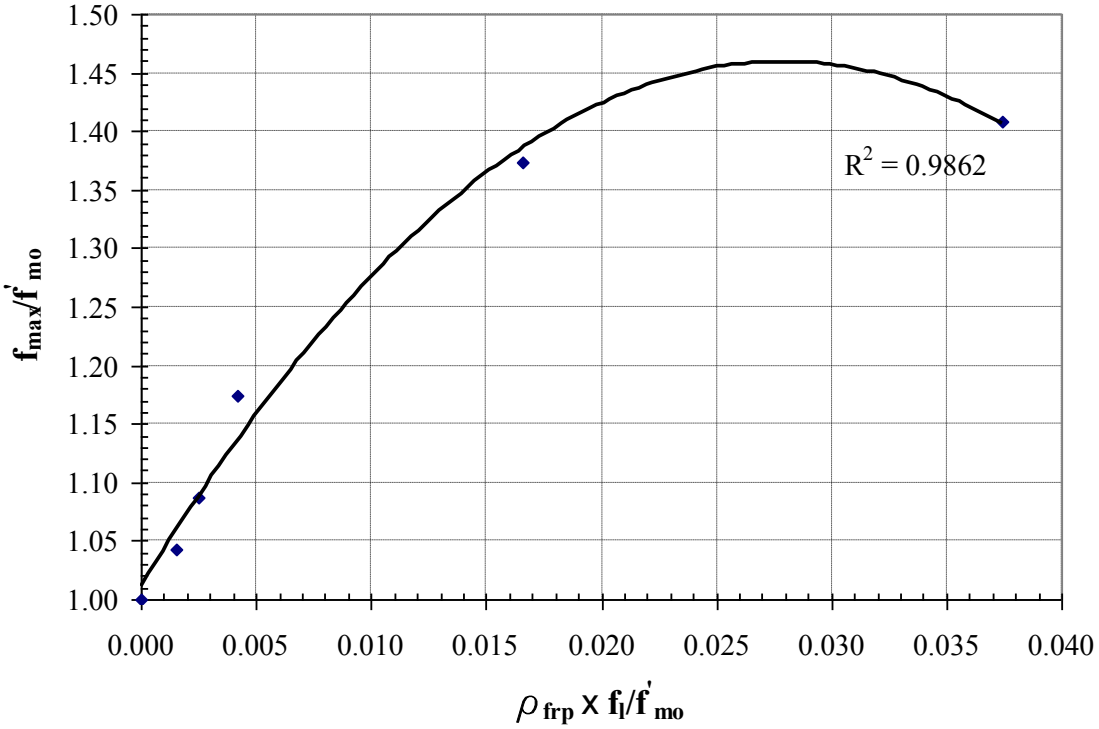

Figure 5.11: Predicting maximum compressive strength of FRP-confined specimens ($f_{\max}$) based on confining pressure (f_l) and volumetric ratio of FRP material (ρ_{FRP})

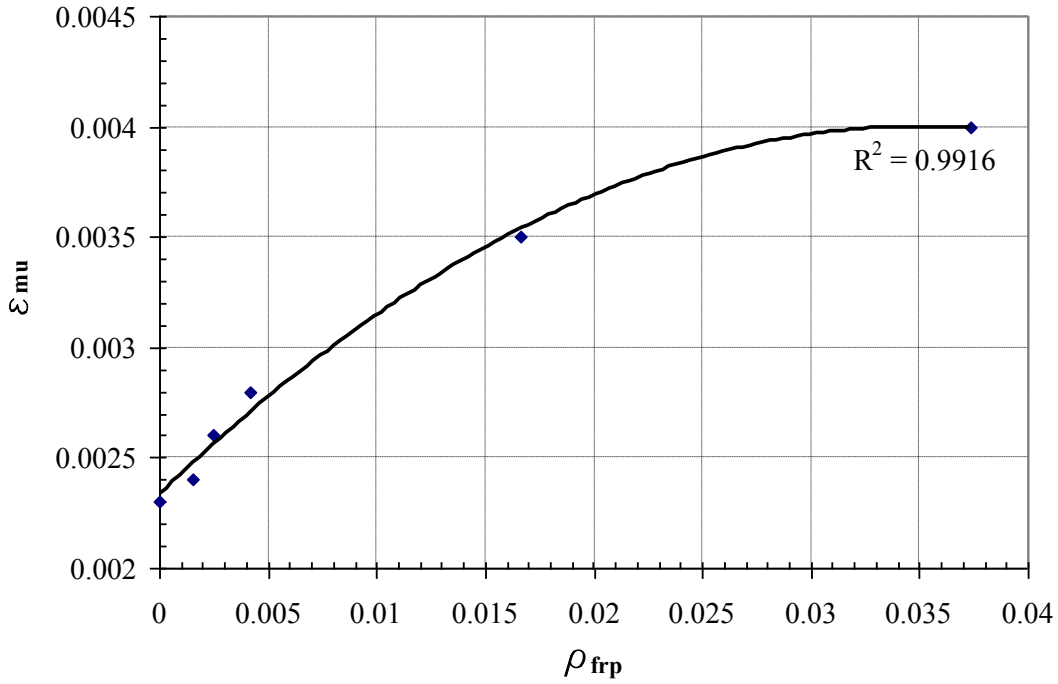

Figure 5.12: Predicting ultimate strain of FRP-confined specimens (ε_{mcu}) based on confining pressure (f_l) and volumetric ratio of FRP material (ρ_{FRP})

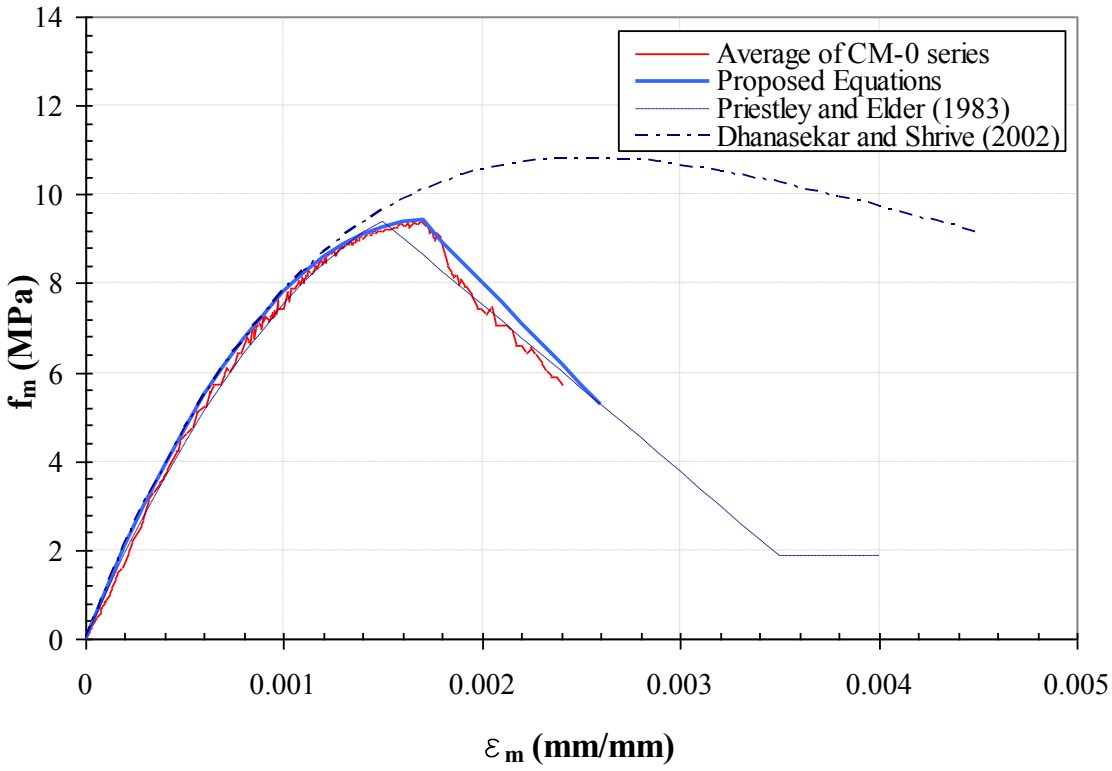

Figure 5.13: Comparison of stress-strain relation of experimental and different analytical methods for unconfined concrete masonry section

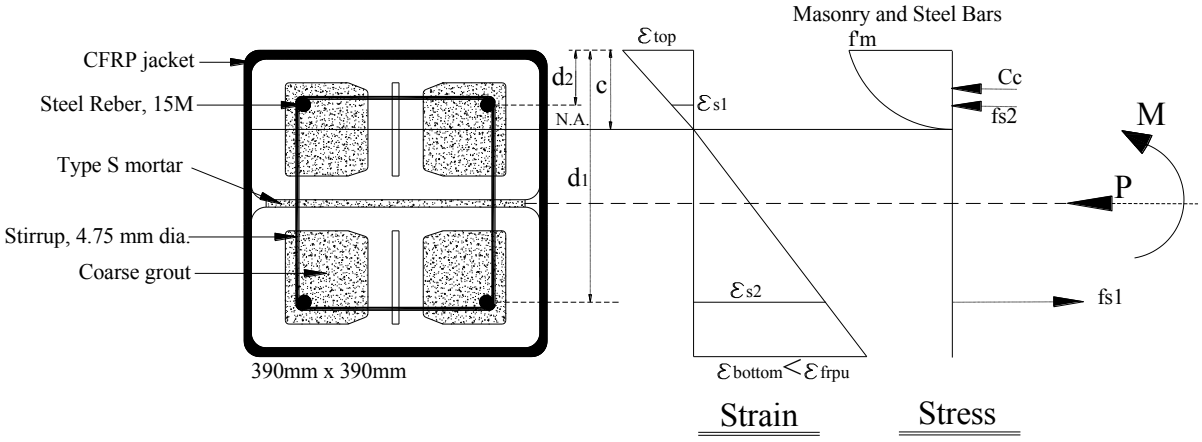

Figure 5.14: Strain, stresses, internal, and external forces in CFRP-wrapped reinforced concrete masonry specimen

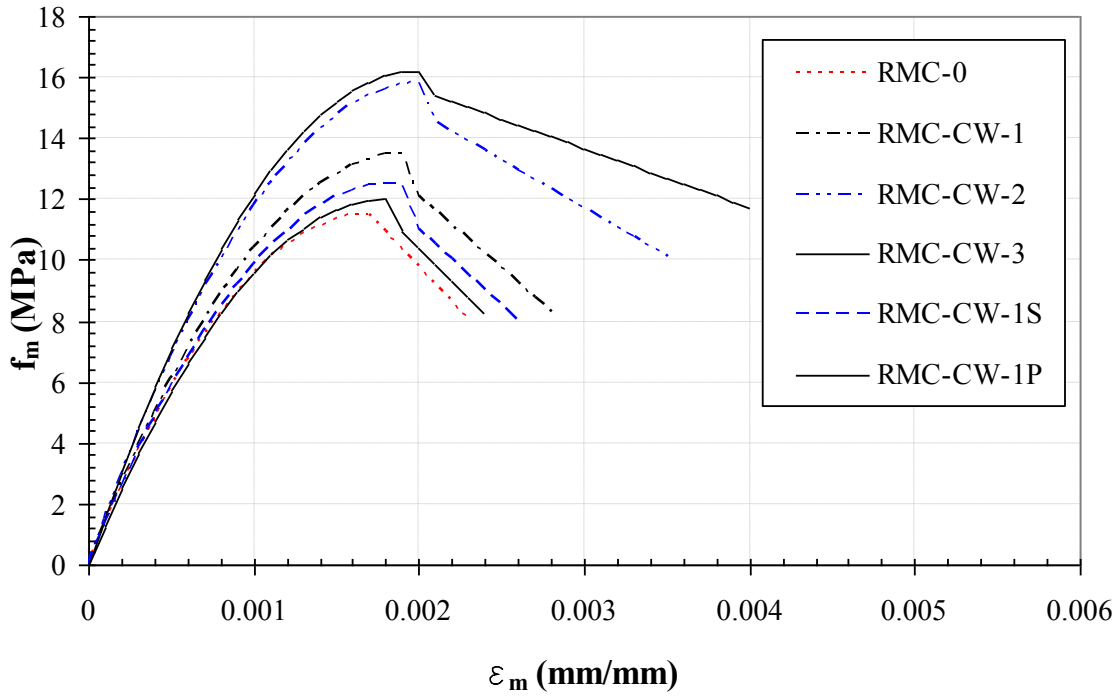

Figure 5.15: Stress-strain curves of the 6 tested full-scale RCM columns

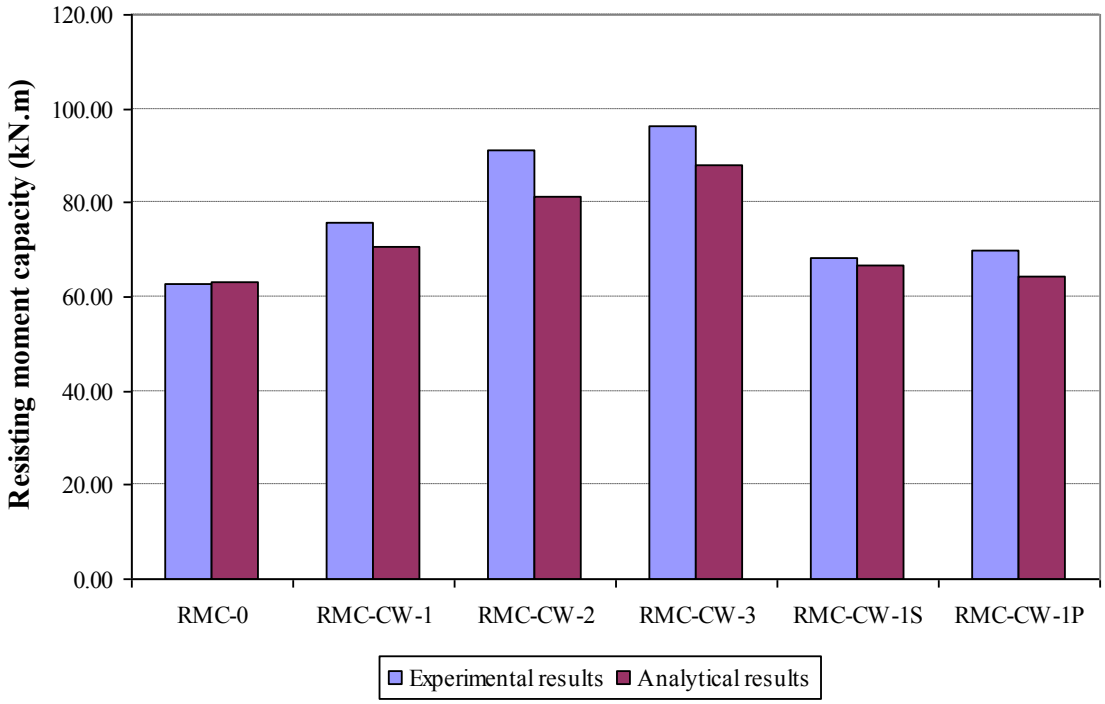

Figure 5.16: Comparison between experimental and analytical moment carrying capacity of the six tested RCM columns using the proposed model

CHAPTER 6

DEVELOPMENT OF NONLINEAR MACRO MODEL

6.1 Introduction

This chapter focuses on developing a macro model to simulate the cyclic lateral load-deformation response of FRP-strengthened reinforced concrete masonry (RCM) columns with limited computational effort. To obtain data regarding the hysteretic behaviour of the RCM columns, such as strength and stiffness degradation, the results obtained from testing the nine full-scale columns (chapter 4) were utilized. Also the experimental data was used for validating the monotonic and hysteretic models developed in this chapter. In predicting monotonic behaviour, the flexural and longitudinal bar slip contribution are considered. A three-parameter model proposed by Park et al. (1987) was used as a guideline for defining the hysteretic model of RCM columns in this study. In general, a good correlation was observed between the experimentally measured and the analytically proposed monotonic and hysteretic models.

6.2 Background and problem definition

The prediction of lateral load carrying capacity and deformability of masonry columns is usually based on the analogy with RC structural elements. However, mathematical modeling of nonlinear seismic behaviour of masonry structural elements is relatively complicated, mainly because masonry is a non-homogeneous and anisotropic building material, consisting of masonry units, mortar, steel reinforcement, and grout. Therefore, for RCM columns, similar to the case of masonry walls, mathematical models

developed for RC elements should be modified in order to take into account specific mechanical properties relevant to masonry materials (Tomazevic and Lutman, 1996).

There have been extensive research efforts in modeling of monotonic and hysteretic behaviour of RC columns and walls (Clough and Johnston 1966, Takeda et al. 1970, Takayanagi and Schnobrich 1976, and Saatcigolu and Derecho 1979). The hysteretic rules for the newer models are developed such that they consider the effect of flexure, shear, and bond slip contributions separately (Ozcebe and Saatcioglu 1989, Alsiwat and Saatcioglu 1992). More recently, few attempts were made to investigate the interaction and combination of flexure, shear, and bond slip components (Elwood and Moehle 2005, Mostafaei and Kabeyasawa 2007). However, the accuracy of these models is not necessarily verified for each individual component using experimental data, and the models prediction were compared with the total lateral response of columns.

In studying the behaviour of masonry members, different models have been developed to model lateral load-displacement relationships for masonry walls. Wakabayashi and Nakamura (1984) combined arch and truss mechanism in order to predict lateral load-displacement skeleton curve in the case of shear failure of reinforced masonry walls. Tassios (1984) proposed a combination of dowel, pullout, and friction mechanisms to model the skeleton curve as well as cyclic hysteretic behaviour. Brenardini et al. (1984) proposed a global implicit dimensionless analytical hysteretic model on the basis of experimental results of cyclic tests of reinforced masonry walls. Tanrikulu et al (1992) modeled hysteretic behaviour of plain masonry walls failing in shear by parameter functions, shear modulus and its viscous counterpart, and determined their loading and unloading characteristics by experiments. Tomazevic and Lutman,

(1996), on the basis of experimental observation, modified the hysteretic model that was initially developed by Park et al. (1987) to represent the nonlinear hysteretic behaviour of reinforced masonry walls.

In this study, data regarding the hysteretic behaviour of the tested RCM columns, such as strength, and stiffness degradation was used for calibration of nonlinear macro models to predict the backbone load-deformation response under monotonic loads as well as the full hysteretic response under cyclic lateral excitations.

6.3 Monotonic models

The monotonic lateral force-displacement relationship serves as primary backbone curve for the pertinent cyclic force-displacement relationships. Also, this curve is used to define the boundary for hysteretic loops.

A typical behaviour of RCM columns subjected to vertical and lateral loads is shown in Figure 6.1. The percentage and the yield strength of the longitudinal steel, the compressive strength of the confined concrete masonry, the shape and the size of the cross-section, and the level of the axial load affect the deformation of the RCM columns (Assa and Dhanasekar, 2002). In this study, two deformation components were considered in estimating the total lateral displacement, namely deformation due to flexure and deformation due to reinforcement slippage.

As the seismic response of the tested FRP-retrofitted RMC columns were dominated by the flexural behaviour, the shear components of deformations are neglected. Also, Assa and Dhanasekar (2002) recommended that, unless the cross-section

of the masonry column is more like a "blade column" (or it resembles a wall), shear deformations will be small and could be neglected.

6.3.1 Flexural deformation

Because the RCM columns are subjected to axial load levels that results in low normal stresses, flexure is considered as the predominant mechanism where failure is tension-controlled. Flexural deformation of a RCM column section can be calculated through a moment-curvature analysis considering nonlinearity. For moment-curvature analysis, it is imperative to define that the nonlinear stress-strain relations of the constituent materials.

As there are limited data available in the literature for quantifying the change in stress-strain characteristics of rectangular concrete masonry section when confined with FRP wraps, as explained in the previous chapter, twelve 5-block high prisms were constructed and tested under increasing axial load. The detailed characteristics of the stress-strain relationship of FRP wrapped concrete masonry can be found in the previous chapter, and expressed by Equations 5.1 to 5.4 and Figures 5.11 and 5.12. Since the GFRP wrapped columns behaved very similar to CFRP wrapped ones (as it is shown in Figure 4.6 of chapter 4), the Equations 5.1 to 5.4 can be used for the GFRP-strengthened columns if instead of FRP volumetric ratio (ρ_{FRP}), the coefficient equal to $\rho'_{FRP}.\frac{E_s}{E_{GFRP}}$ is utilized.

For steel rebars, a model that is conventionally being used in the seismic design is considered. The stress-strain curves for reinforcing steel in monotonic tension and

compression are assumed to be identical, and are given in Equations 5.5 to 5.7 in Chapter 5.

The flexural displacements can be calculated by integrating the curvature distribution over the height of the column. Flexural deformations are calculated from a plastic hinge model as shown in Figure 6.2:

$$\Delta_f = \Delta_y + (\phi - \phi_p) h_P \left(h - h_p\right) \qquad 6.1$$

where, Δ_y = flexural deformation at yield ($=\phi_y h^2/3$), ϕ = curvature at the base of the column, ϕ_y = base curvature at yield, h = height of the column, and h_p = height of the plastic hinge. Similar to the assumption that is commonly used for reinforced concrete columns, the height of the plastic hinge for the tested concrete masonry columns was assumed to be equal to the depth of the cross section (Assa and Dhanasekar, 2002). Moreover, from the FRP wrap strain gauges readings obtained from tested columns; it was observed that while maximum tensile strains in CFRP jacket occurred at 200 mm above footing and column interface, the tensile strains were almost negligible above 400 mm above the base which confirms that the assumption of plastic hinge equal to the depth of the cross section is valid. More details about this observation are provided in chapter 4. The results of the obtained flexural deformations combined with bond-slip deformations are presented in Figure 6.4 for all nine columns. The columns designation and also equivalent volumetric ratio of FRP material (ρ'_{FRP}) of each column is presented in Table 4.1 in chapter 4.

6.3.2 Bond-slip deformation

There is a potential for the occurrence of bond-slip due to the insufficient bond transfer because of limited contact surface area of the steel bars or insufficient anchorage in lightly reinforced RCM columns. As the tested RCM columns in this study are subjected to low level of axial load, this phenomenon is more evident. Figure 6.3 clearly shows the occurrence of bond slip at high lateral drifts for the columns C-CW-3, RMC-W-1S, and RCM-CW-1P. The bars' pullout mechanism represents the base rigid body rotation and the associated pullout of the reinforcing steel. This pullout is caused by the cumulative slippage along the column height and the foundation block (Assa and Dhanasekar 2002). The bar slip model used in this study was developed by Sezen and Setzler (2008) and modified to be used for grouted RCM columns.

A reinforcing bar embedded in grout can be modeled by assuming linear elastic behaviour and a uniform bond stress over the development length of the reinforcing rebar. From equilibrium of forces, the required elastic development length (l_d) can be determined as:

Before yielding of rebars: $l_d = f_s d_b / (4u_b)$ 6.2

After yielding of rebars: $l_d^{'} = (f_s - f_y) d_b / (4u_b^{'})$ 6.3

where, d_b = rebar diameter, f_s = steel tensile stress, and f_y = yield strength. The model assumes two different constant bond stresses between the grout and reinforcing steel along the embedment length of the bar. The elastic bond stress, u_b, is taken as $1.0\sqrt{f_m^{'}}$ or $1.0\sqrt{f_{mc}}$ MPa and the inelastic bond stress, $u_b^{'}$, is taken as $0.5\sqrt{f_m^{'}}$ or

$0.5\sqrt{f_{mc}}$ MPa, where $f_m^{'}$ and f_{mc} are peak compressive strength of unwrapped and CFRP-wrapped columns respectively.

Since the bond stress is uniform in the elastic and inelastic portions of the embedded bar, the strain distribution will be linear in each range. The bar slip can be derived by integrating the strains, ε_s, over the bar development length. Once the slip of a reinforcing bar is known, the rotation of the column caused by slip can be determined. For the proposed model, it is assumed that slip will occur in bars under tension only, and that the rotation will be about the neutral axis. The slip rotation can be calculated by dividing the bar slip by width of the open crack. The lateral displacement at the tip of a cantilever column is calculated as the product of the column height *h* and slip rotation as it follows:

$$\Delta_{slip} = \frac{h}{d-c}\int_0^{l_d} \varepsilon(x)dx = \frac{\varepsilon_s f_s d_b h}{8u_b(d-c)} \quad : \text{for } \varepsilon_s \le \varepsilon_y \qquad 6.4$$

$$\Delta_{slip} = \frac{h}{d-c}\int_0^{l_d+l_d^{'}} \varepsilon(x)dx = \frac{d_b.h}{8u_b(d-c)}\left[\varepsilon_s f_y + 2(\varepsilon_s+\varepsilon_y)(f_s-f_y)\right] \quad : \text{for } \varepsilon_s > \varepsilon_y \qquad 6.5$$

where, ε_y = yield strain, *d* = depth of the cross section, and *c* = neutral axis depth. The total lateral response of a RCM column can be modeled by combining flexure and rebars slip response as springs in series, where the force in each spring is the same and the total deformation is the sum of the individual spring deformations (Sezen and Chowdhury, 2009). As shown in Figure 6.4, the combined effect of flexural and bond-slip deformation resulted in an envelope curve that is in good agreement with the backbone curve obtained from experimental results. It is worth mentioning that flexural deformations were the dominant component of the total displacement before and after

peak response. Moreover, it was observed that for all tested specimens the calculated lateral displacements in the rising branch of the lateral force-displacement curves are greater than the experimental values. Assa and Dhanasekar (2002) suggested that the main reason for this difference is the presence of base concrete footing with heavy reinforcement which provided additional confinement of the specimen. The analytical model does not consider this type of confinement and hence it predicts lower lateral loads for all specimens.

6.4 Hysteretic Models

On the basis of experimental observations in this study, the three-parameter model proposed in the computer program IDARC by Park et al. (1987) was chosen as the base hysteretic model. Several modifications are introduced to make it suitable for representing the nonlinear behaviour of RCM columns. The model takes into account the strength and stiffness degradation due to increasing damage at large deformations, which is an important feature of RCM columns subjected to seismic loads. For simplicity in the proposed model, the calculated primary curve defines the strength degradation curve in hysteretic cycles. Model of stiffness degradation is defined based on experimental observations, and the following general equation was used for estimating stiffness values of RCM columns:

$$k = (2.1\rho'_{FRP} \cdot \frac{E_S}{E_{FRP}} + 3.2)\delta^{(0.23\rho'_{FRP} \cdot \frac{E_S}{E_{FRP}} - 1.04)} \qquad 6.6$$

where, k is column stiffness (kN/mm), δ is lateral drift (%), ρ'_{FRP} is equivalent volumetric ratio of FRP reinforcement, E_{FRP} is modulus of elasticity of CFRP or GFRP

material, and E_S is modulus of elasticity of steel (200 GPa). More information regarding Equation (6.6) is presented in the chapter 4.

As shown in Figure 6.5, the skeleton curve is a simple symmetric curve, determined by there pairs of values of lateral load and displacement ($F_{cr}, d_{cr}, F_{\max}, d_{\max}, F_u, d_u$), which define the cracking point, maximum resistance, and ultimate limit state of the behaviour of a column respectively. Also information regarding to the yield point (F_y, d_y) is included for defining the shape of hysteretic loops. In the analysis, cracking load (F_{cr}) can be calculated from:

$$F_{cr} = \frac{I_g}{0.5hH}\left(\frac{P}{A_g} + f_t\right) \qquad 6.7$$

where A_g = gross section area, I_g = gross section moment of inertia, h = column's height, H = section width, P = axial force, and f_t = the modulus of rupture of the concrete masonry where in this research obtained from testing 7-block prisms (details are explained in the chapter 3). Moreover, lateral displacement at the cracking point (d_{cr}) is equal to $\frac{2}{3}\phi_{cr}(h)^2$. (Note that since displacements are very small at this level, the longitudinal bar-slip deformations are neglected).

To define the yield point, a simplified assumption was made based on the observed experimental results. It was observed that the number of FRP layers does not affect the yield state of the columns, and in all columns yield started at similar level of lateral drift of 1.0-to-1.2%. Therefore, the same value of lateral drift was used to define the yield point, whereas its corresponding yield force, F_y, was obtained from the calculated

primary curve. Maximum force for each cycle, $F_{\max}$, was also obtained from calculated primary curve for each level of maximum displacement, $d_{\max}$. In the analysis, the hysteretic loops are calculated up to the point that maximum lateral force , $F_{\max}$, reached to 80% of peak lateral force in the backbone curve, and this value and corresponding displacement are defined as ultimate values (F_u, d_u).

Considering Figure 6.5, the following points define the shape of the skeleton curve and its hysteretic loops:

- Point A: Cracking state of the concrete masonry section (F_{cr}, d_{cr})
- Point B: Maximum lateral drift and the corresponding lateral force ($F_{\max}, d_{\max}$) for each loop obtained from primary curve. Furthermore, as it was mentioned in the previous section, due to confining presence of the concrete footing, the calculated lateral displacements in the rising branch of the lateral force-displacement curves are smaller than the observed experimental values. Therefore, a correction factor of 1.2 is implemented for lateral force values along the loading path A-2-B in the loops with the maximum displacements less than yield point, i.e. for the loops with $d_{\max} < d_y$. Note that this correction factor diminishes when the confining presence of the base is decreased.
- Point C: Defines the unloading path B-3-C. The lateral force at point C is described by $F_C = C_F F_{\max}$. Factor C_F is unloading stiffness shape factor and equal to:

$$C_F = -0.2 \text{ : For } d_{\max} \le d_y \qquad 6.8a$$

$$C_F = \frac{\rho'_{FRP}}{3}.\frac{E_s}{E_{FRP}} : \text{For } d_{\max} > d_y \qquad 6.8b$$

where, ρ'_{FRP} is equivalent volumetric ratio of CFRP reinforcement. Lateral diplacement at point C (d_C) is defined based on stiffness degradation formula described in Equation (6.6):

$$d_C = d_{\max} - \frac{F_{\max} - F_C}{k.e^{0.015d_{\max}}} \qquad 6.9$$

where k in Equation 6.9 is calculated from Equation 6.6, and $d_{\max}$ is the maximum lateral displacement in (mm) corresponding to δ, the lateral drift(%) .

- Point D: For loops with $d_{\max} \le d_y$, point D is removed from the cycles. However, for loops with $d_{\max} > d_y$, it is assumed that lateral Force at Point D is equal to $F_C = C_F F_{\max}$ with $C_F = -0.2$ similar to point C. Lateral displacement at point D (d_D) is equal to the cracking displacement, i.e. $d_D = -d_{cr}$
- Point E: assuming that the cyclic loops are symmetric in push and pull directions, lateral force and displacement at point E equal to $F_{\max}$ and $d_{\max}$ with the negative sign.
- Point F: Considering the symmetrical form of cyclic loops, lateral displacement at point F defined similar to the point C. however, different lateral force is defined for point F in compare to point C. After careful observation of experimental results, the following expression was adopted for lateral force at point F:

$$F_F = 0 \qquad : \text{For } d_{\max} \le d_y \qquad 6.10a$$

$$F_F = -\frac{d_y}{d_{\max}} d_C \ : \text{For } d_{\max} > d_y \qquad 6.10b$$

Figures 6.6 to 6.11 show the comparison of experimental and hysteretic response of tested specimens obtained using the proposed model.

As can be seen in Figures 6.6 to 6.14, a good correlation exists between the experimentally obtained hysteretic loops and the proposed analytical model for FRP-wrapped reinforced masonry columns subjected to axial and cyclic loads. Furthermore, it is noteworthy to mention that pinching of cyclic loops is incorporated by degradation of stiffness in the model by varying the slopes of the unloading and reloding branches within the same loop.

6.5 Conclusions

In this chapter, on the basis of findings in chapter 4 and 5, an analytical model was proposed to simulate nonlinear cyclic behaviour of RCM and FRP-confined RCM columns. First, monotonic backbone force-deformation curves were obtained by considering the effect of flexural and longitudinal rebars bond-slip contribution. To get the primary curves, moments-curvature and lateral load-displacement analysis of the RCM columns subjected to axial load and lateral loads were conducted by using the concept of formation of plastic hinge at the base of the column.

In the moment-curvature analysis, stress-strain relation of CFRP-confined concrete masonry was required, and it was obtained from a companion experimental study which consisted of testing twelve 5-blocks high concrete masonry prisms under axial increasing compressive load. Since the proposed stress-strain relations are given for the whole rectangular/square RCM section consisting of confined and unconfined zones, it provided significant convenience in the moment-curvature and section analysis.

The proposed monotonic model was validated using the experimental results of six RCM columns. Five of the RCM columns were wrapped with different number of layers or at different locations with CFRP sheets. The columns were tested under constant axial force and cyclic lateral loads.

Furthermore, on the basis of the experimental results, a three-parameter model proposed by Park et al. (1987) was used as a guide line for defining the hysteretic model of RCM columns in this study. The symmetrical skeleton curve was determined by evaluating there pairs of values of lateral load and displacement at the cracking point, maximum resistance, and ultimate limit state of the behaviour of a column. Moreover, by setting several rules for calculating cyclic loops, the proposed model was capable of providing efficiency in computational efforts. Finally, it was shown that, in general, a good agreement exists between proposed hysteretic model and obtained experimental results.

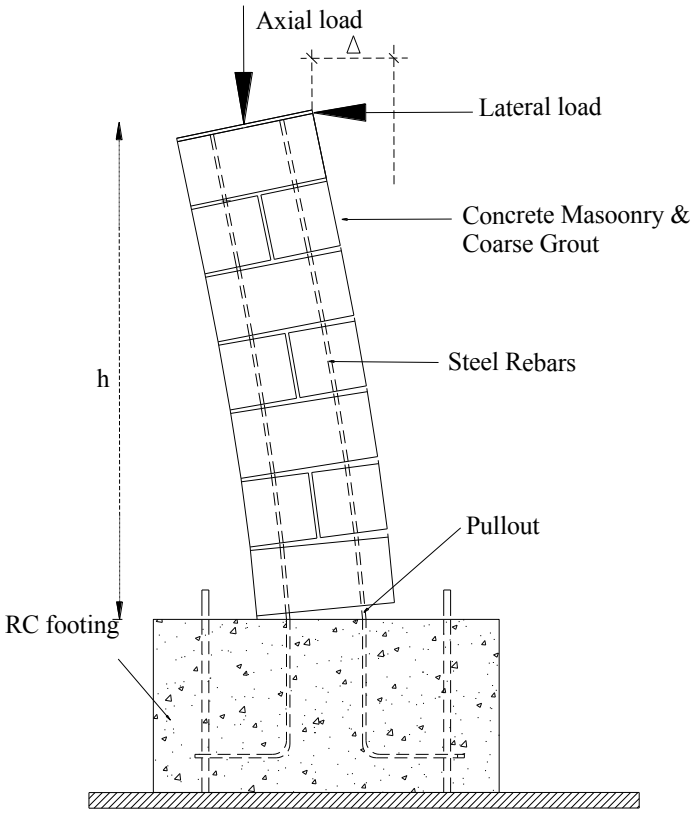

Figure 6.1: Behaviour of RCM column under axial and lateral loads

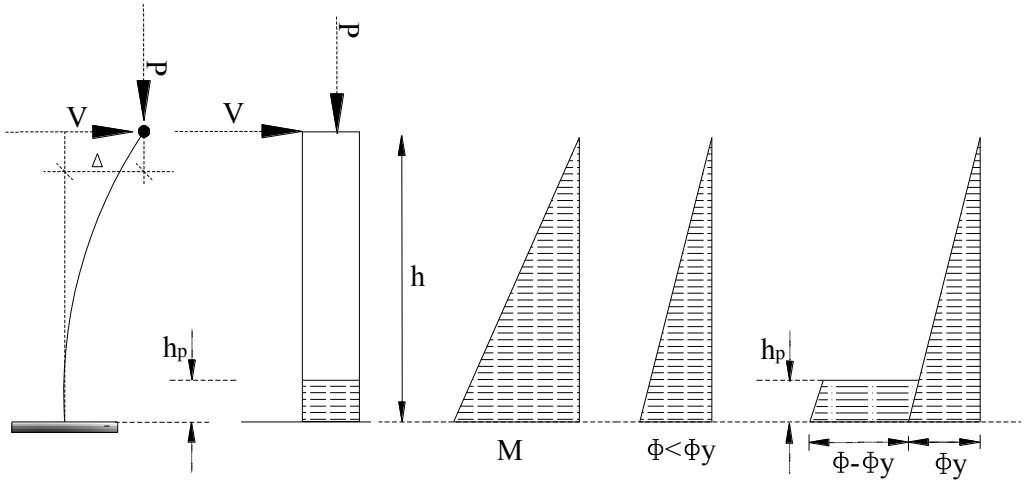

Figure 6.2: Obtaining displacement from idealization of curvature distribution before and after yield

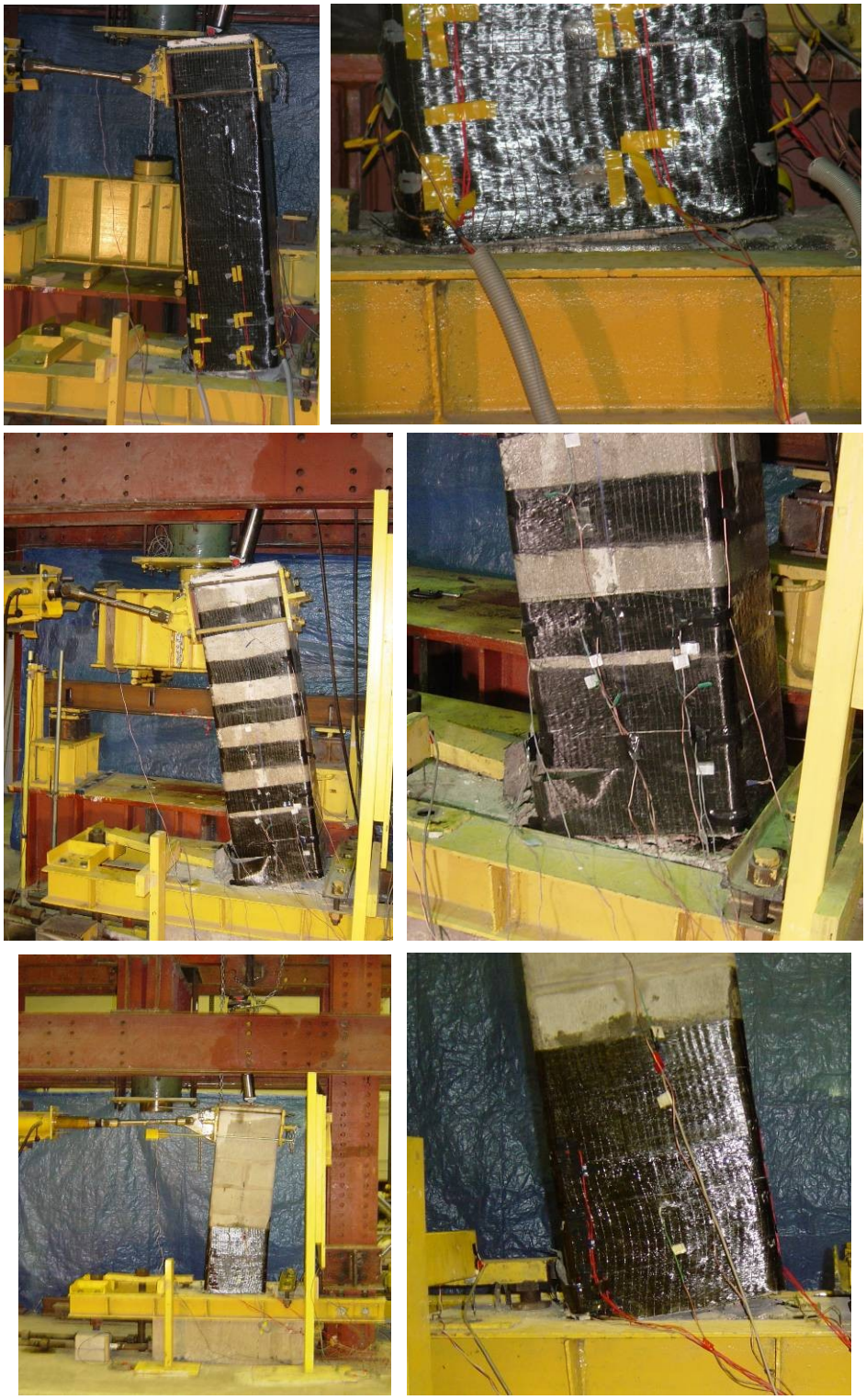

Figure 6.3: Occurrence of bond-slip at column-footing interface at high lateral drifts in columns C-CW-3, RMC-W-1S, and RCM-CW-1P

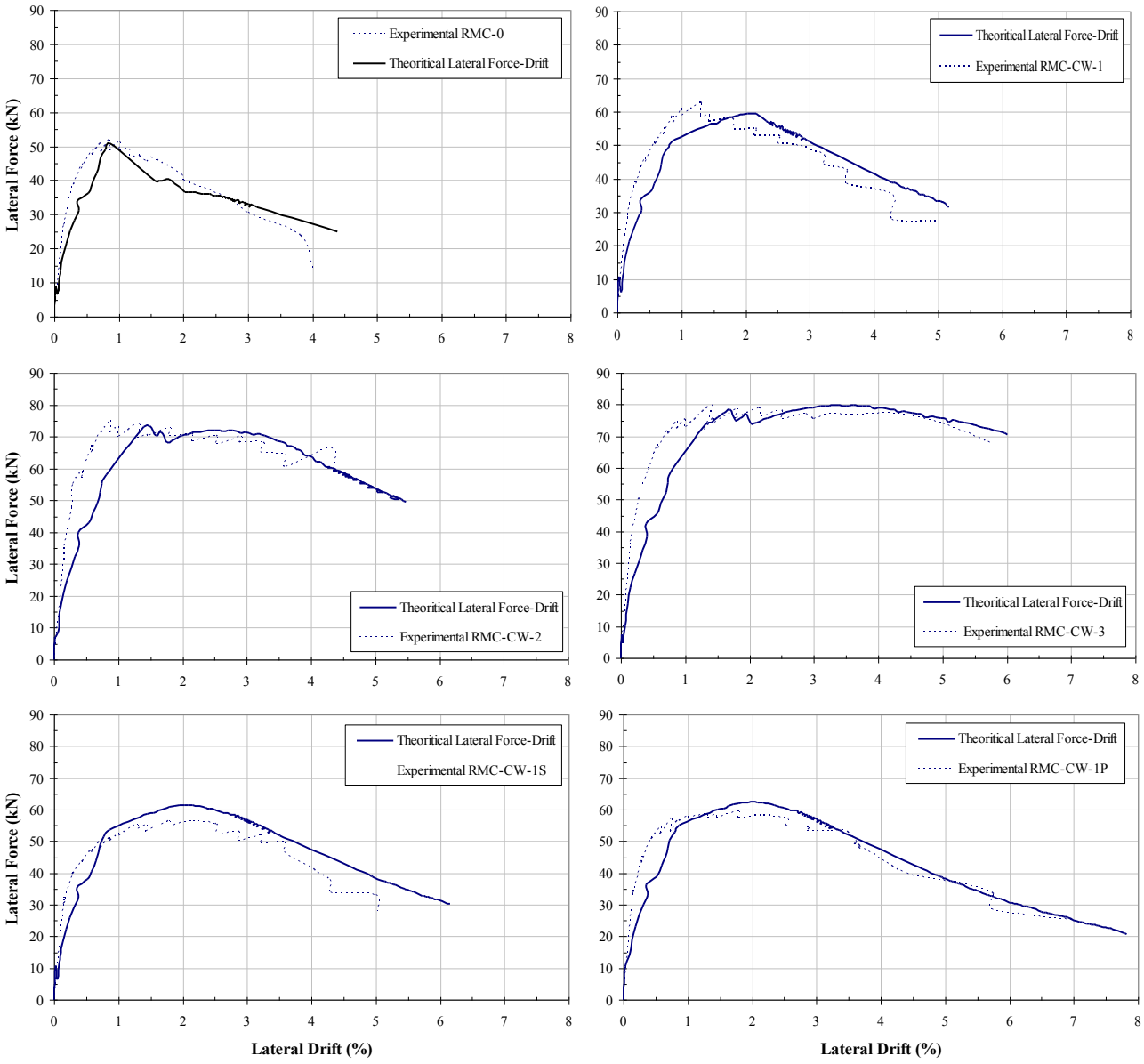

Figure 6.4: Comparison between calculated analytical (combination of flexure and bond-slip effects) and experimental envelope curves for the nine tested RCM columns (continued)

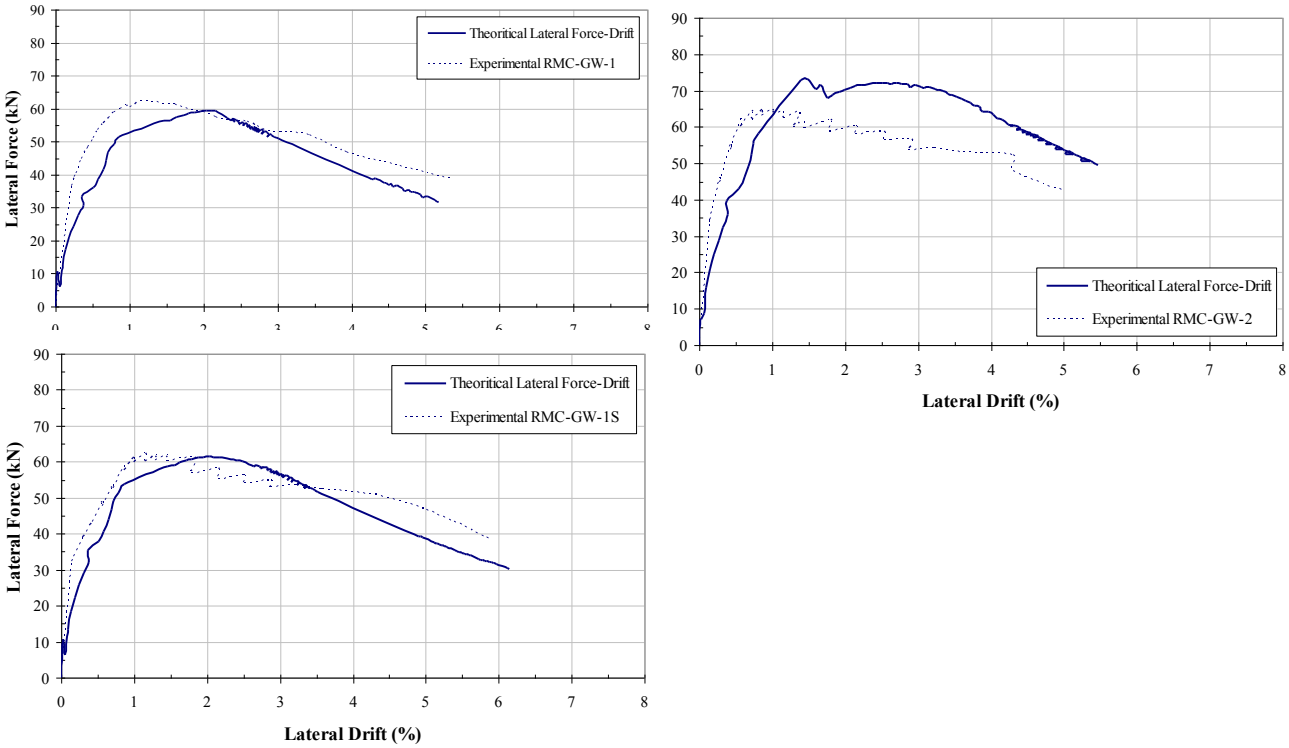

Figure 6.5: Comparison between calculated analytical (combination of flexure and bond-slip effects) and experimental envelope curves for the nine tested RCM columns

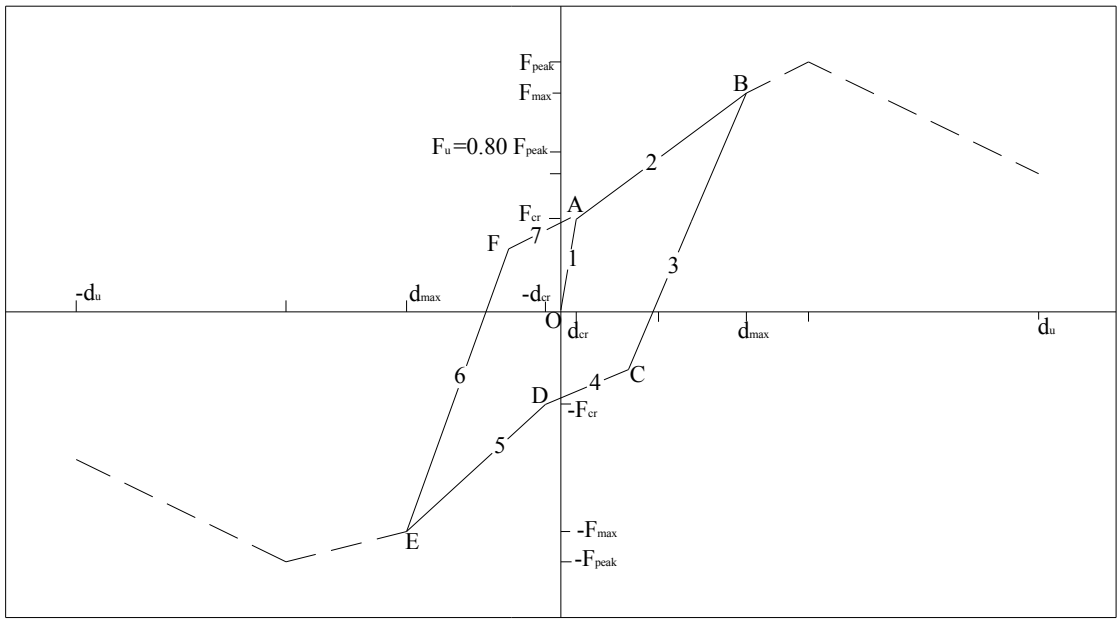

Figure 6.6: Definition of Hysteretic Rules

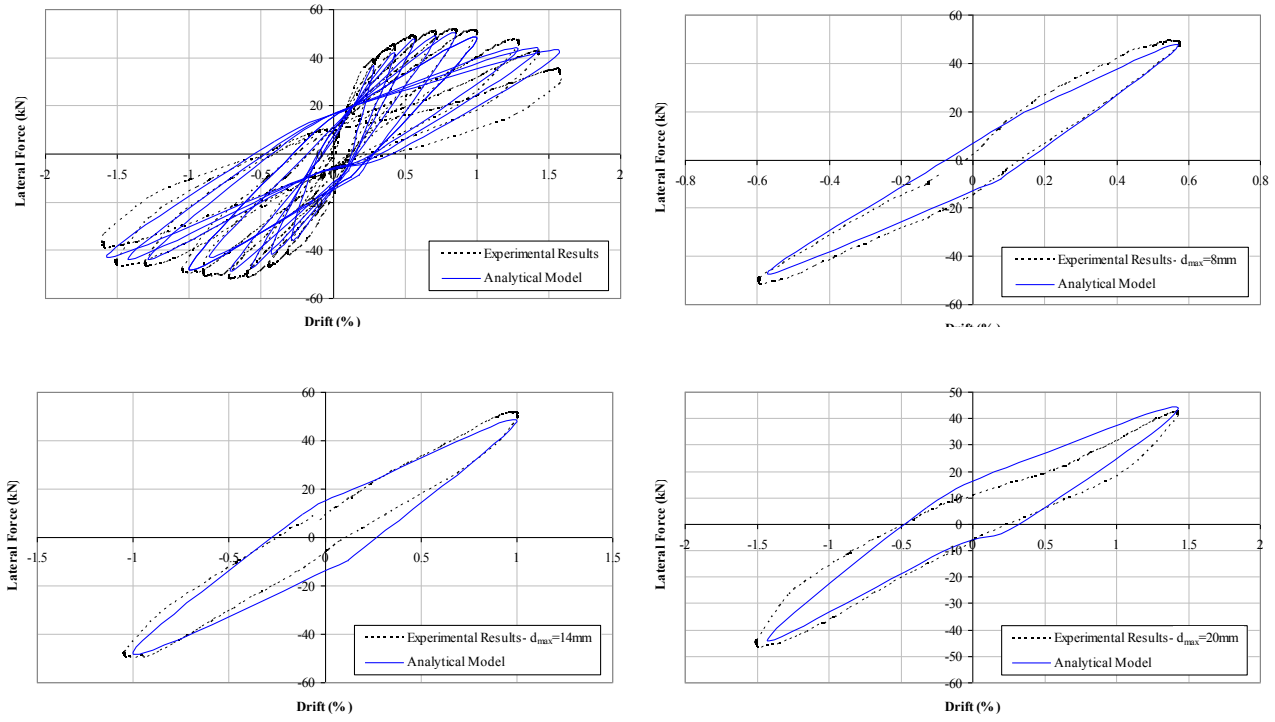

Figure 6.7: Comparison between experimental and calculated hysteretic loops for column RMC-0

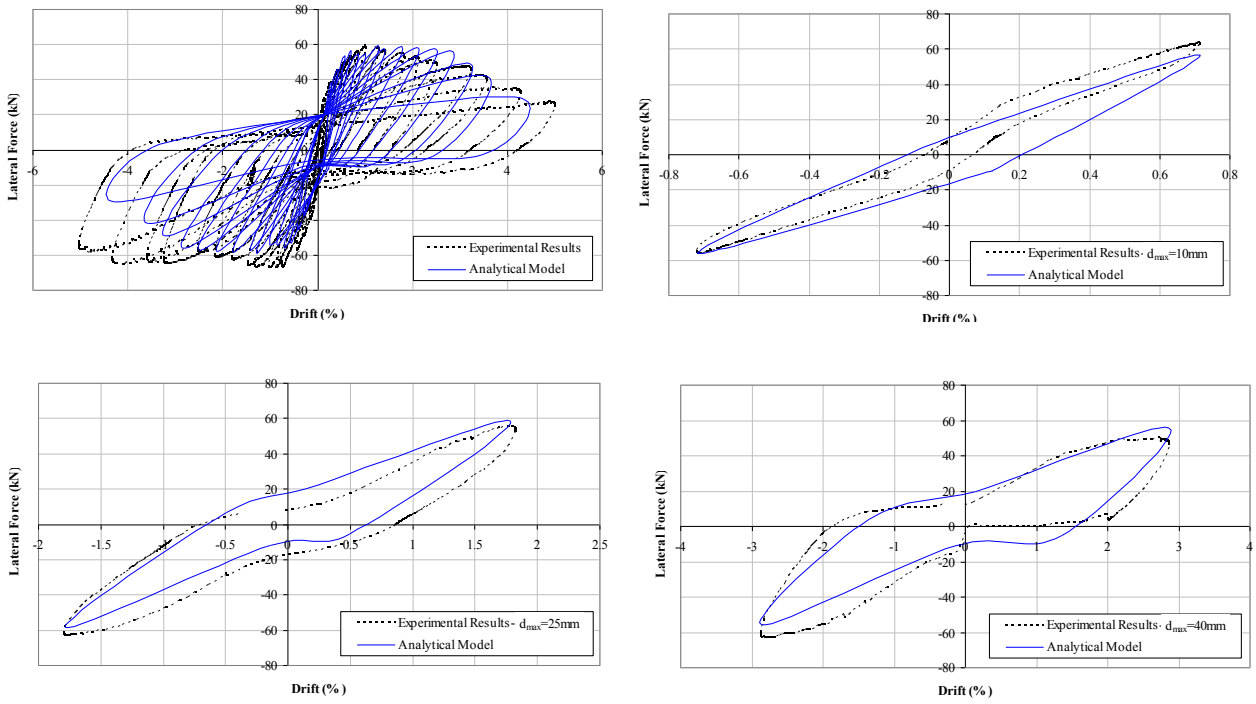

Figure 6.8: Comparison between experimental and calculated hysteretic loops for column RMC-CW-1

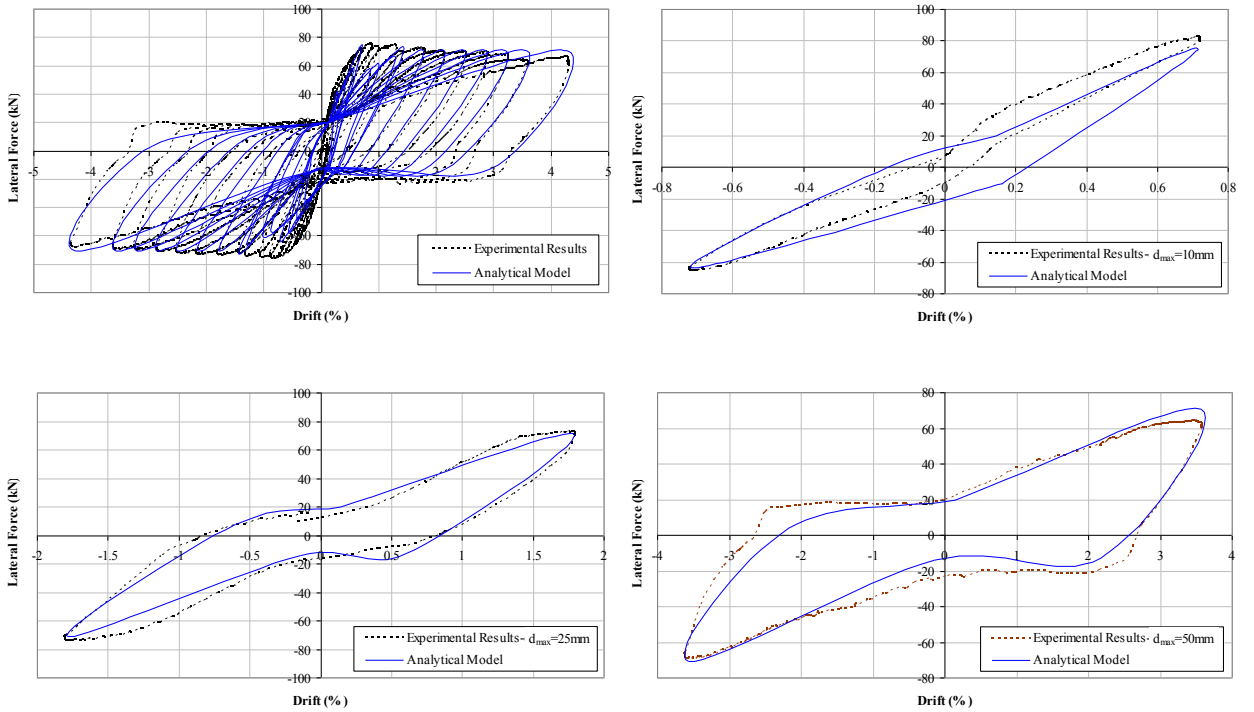

Figure 6.9: Comparison between experimental and calculated hysteretic loops for column RMC-CW-2

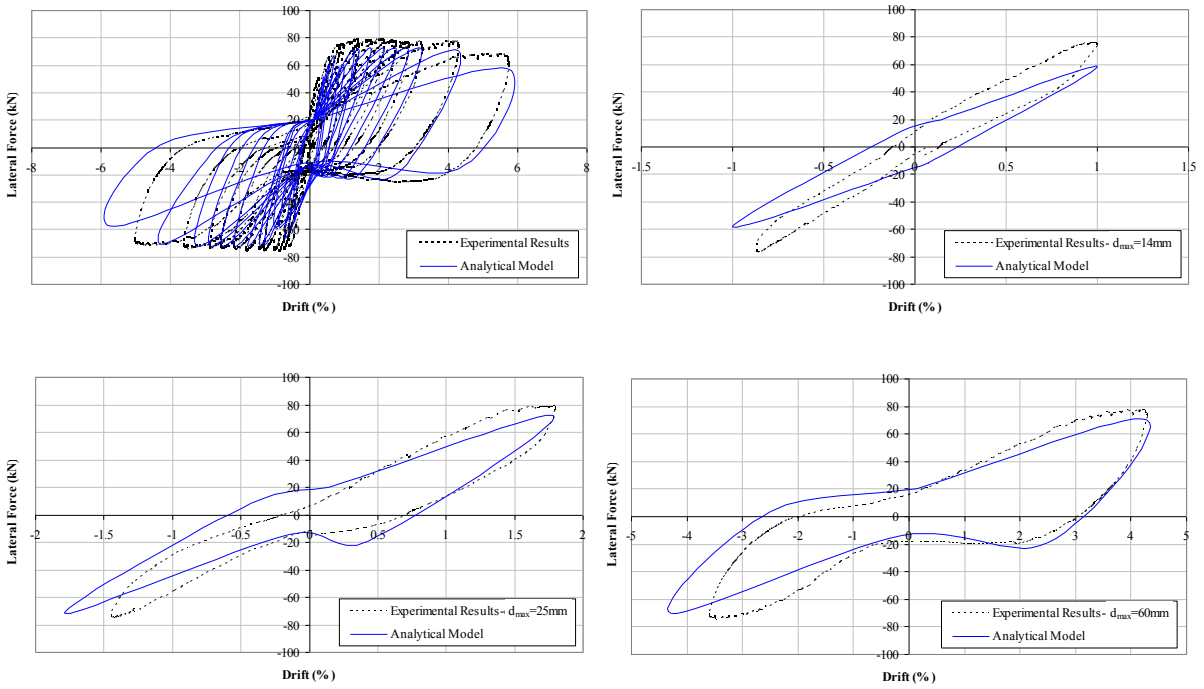

Figure 6.10: Comparison between experimental and calculated hysteretic loops for

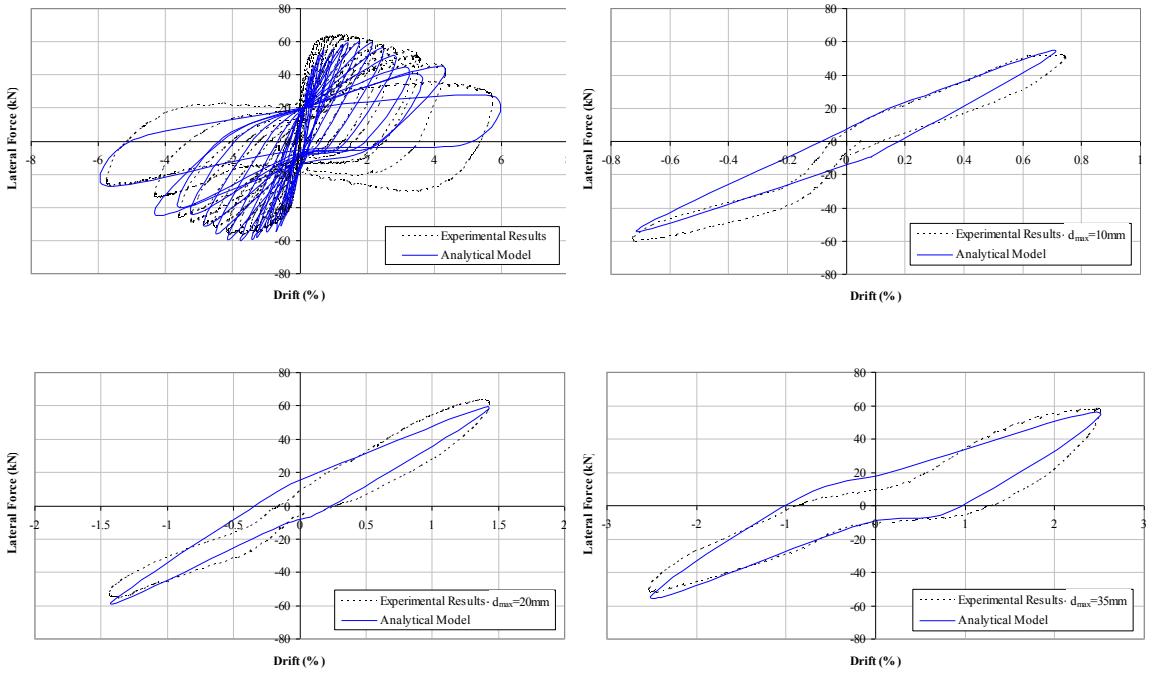

Figure 6.11: Comparison between experimental and calculated hysteretic loops for column RMC-CW-1S

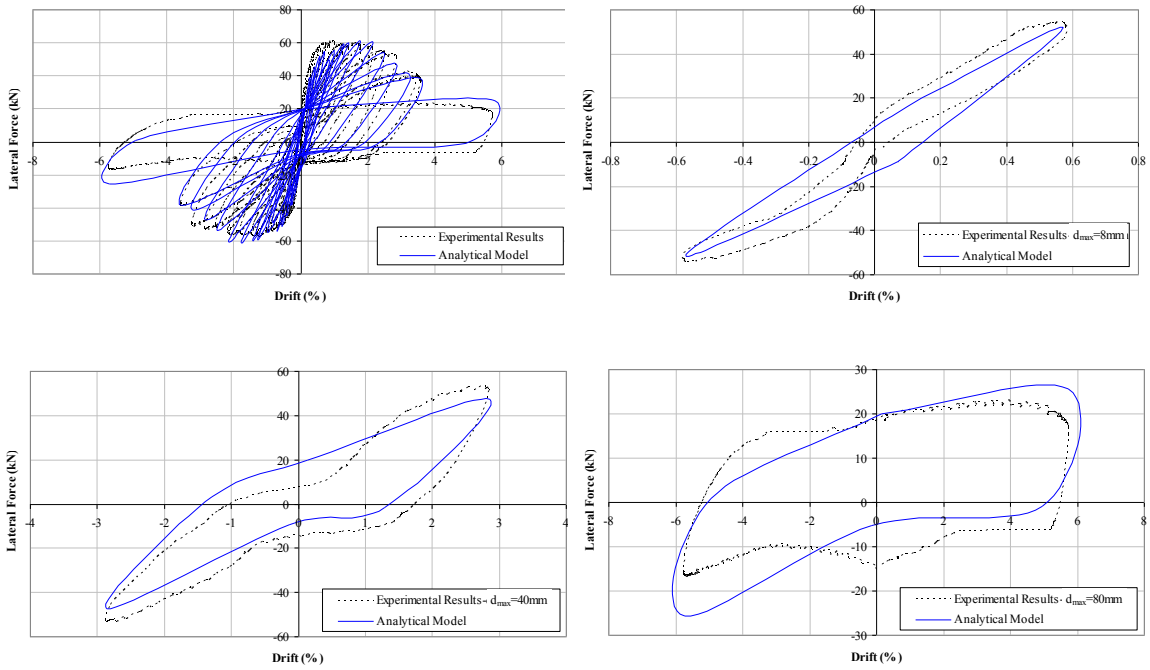

Figure 6.12: Comparison between experimental and calculated hysteretic loops for column RMC-CW-1P

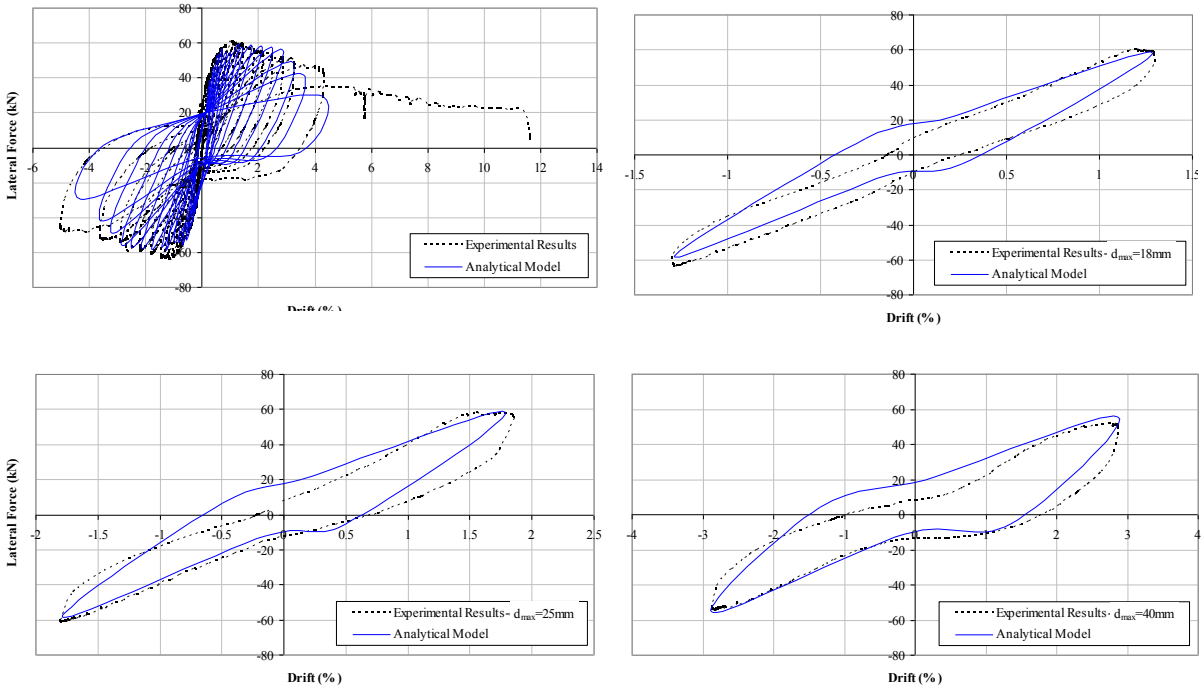

Figure 6.13: Comparison between experimental and calculated hysteretic loops for column RMC-GW-1

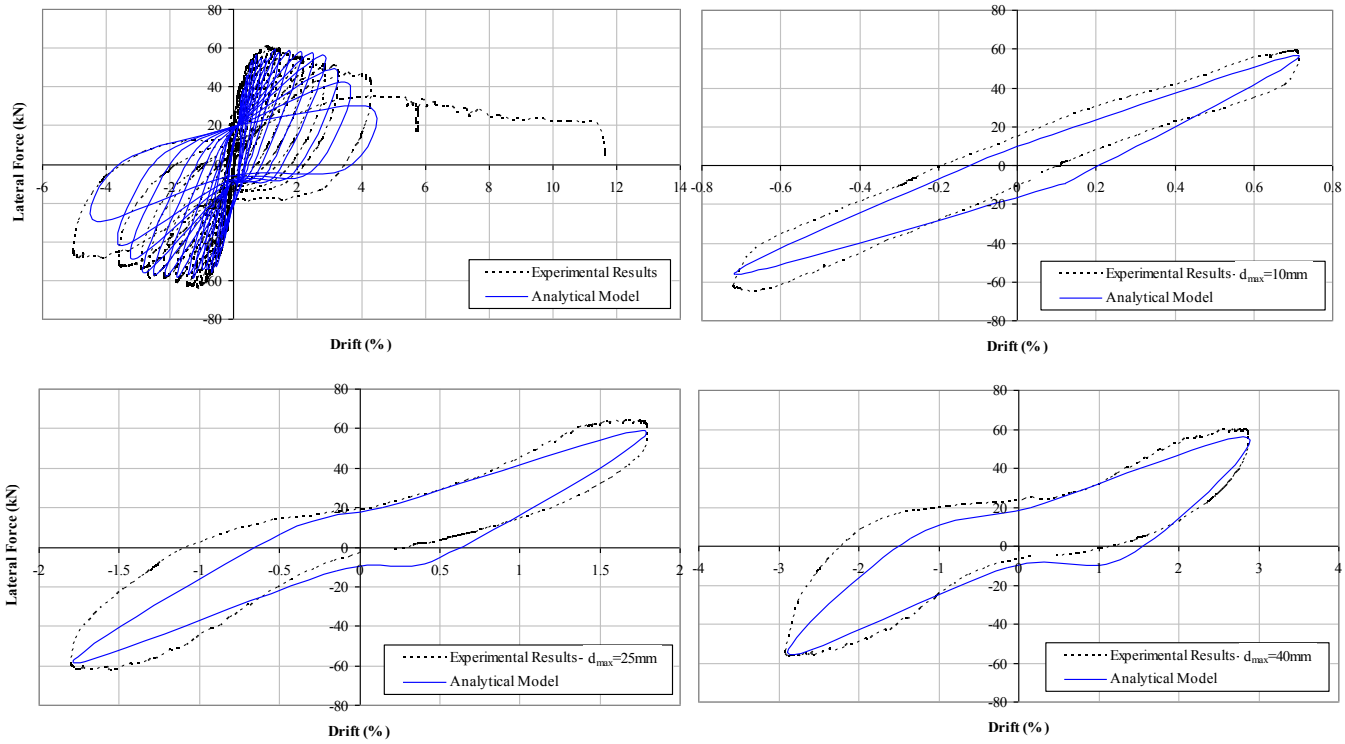

Figure 6.14: Comparison between experimental and calculated hysteretic loops for column RMC-GW-2

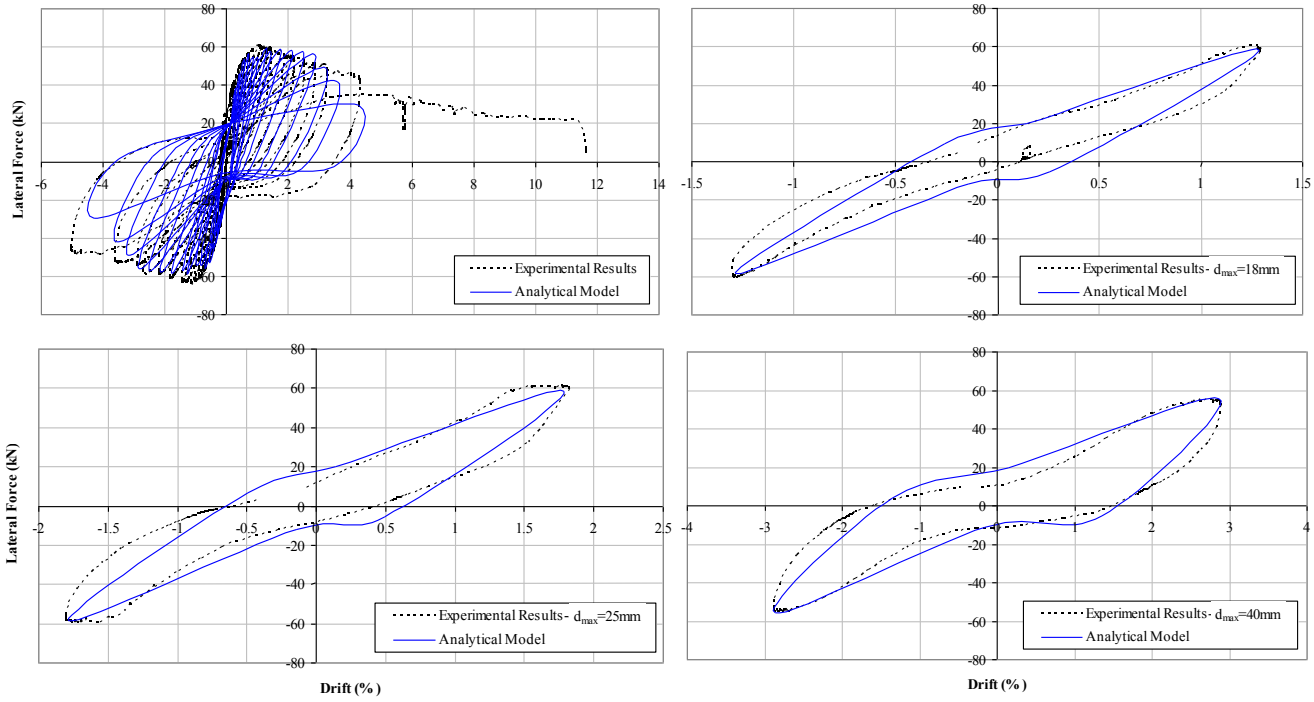

Figure 6.15: Comparison between experimental and calculated hysteretic loops for column RMC-GW-1S

CHAPTER 7

CONCLUSIONS AND RECOMMENDATIONS

7.1 Summary and conclusions

The background and need for research are explained in Chapter 1, and based on that the objectives of the study were defined. This research had two main objectives. The first objective was to examine experimentally the overall seismic performance of FRP-confined rectangular reinforced concrete masonry (RCM) columns subjected to axial and lateral load excitations, and to generate enough experimental data to develop a non-linear macro model to predict the behaviour of RCM columns. The second objective was to develop an accurate analytical model based on experimental tests to represent stress-strain relation of the CFRP-confined concrete masonry in axial compression which was needed for development of non-linear macro model.

A literature review is provided in Chapter 2. The literature review focused on techniques for increasing confinement in reinforced masonry columns (RMC). Different techniques in increasing confinement were explained. Furthermore, previous approaches in predicting stress-strain behaviour of concrete masonry and also the methods for evaluating the FRP confinement effect in increasing the strength of masonry columns/sections are briefly discussed. At the end of Chapter 2, the current Canadian codes and standards in the field of masonry were introduced.

Phase one of the experimental program consisting of the tests for obtaining the properties of concrete blocks, steel reinforcement, CFRP or GFRP materials, mortar,

grout, compressive strength and flexural strength of masonry assemblage are explained in Chapter 3. Modulus of elasticity assemblage (E_m) is obtained with two different approaches; compressive strength of masonry assemblage ($f_m^{'}$) is obtained from testing 5 five-block high prisms, and then E_m calculated using CSA S304.1-04 (clause 6.5.2). In second approach, E_m is calculated from testing 5 seven-block high prisms under four-point loading and measuring mid-span deflections of the specimens. Test setup preparation for the second phase of experimental program is also explained in chapter 3. In the second phase of experimental program, nine full scale reinforced masonry columns were constructed and wrapped with different number of layers of CFRP or GFRP material or schemes and tested under combined effect of axial and cyclic lateral loads.

In Chapter 4, the effectiveness of CFRP and GFRP confinement in increasing the lateral load carrying capacity, displacement ductility, stiffness, and energy dissipation of RCM columns with square cross section was assessed. This experimental research led to the following findings:

- Wrapping the reinforced masonry control column along its full-height with 1, 2 or 3 layers of CFRP sheets increased the lateral load carrying capacity of the column by about 30%, 46%, and 53%, respectively, while wrapping it with 1 and 2 layers of GFRP sheets increased its lateral load bearing capacity by about 23 and 25%, respectively.
- Wrapping the reinforced masonry control column along its full-height with 1, 2 or 3 layers of CFRP sheets increased the displacement ductility of the column by about 115% and 260%, and 273%, respectively, while wrapping it with 1 and 2 layers of GFRP sheets increased its displacement ductility by about 81% and

105%, respectively.

- Wrapping the reinforced masonry control column along its full-height with 1 or 2 layers of CFRP sheets, increased the cumulative energy dissipation capacity of the column at 5% drift by about 32% and 74%, respectively, while wrapping it with 1 and 2 layers of GFRP sheets, increased the cumulative energy dissipation capacity at 5% drift by about 1% and 26%, respectively.
- It is observed that wrapping the RCM columns at the plastic hinge zone and mortar joints prevents cracking of the columns under the lateral and cyclic loads even at very high lateral drifts. In general, the experimental hysteretic loops in columns RMC-CW-1P, RMC-CW-1S, and RMC-GW-1S were very similar to the ones with one continuous layer of FRP along the height (columns RMC-CW-1, RMC-GW-1) with slightly less increase (about 12%) in lateral load carrying capacity. However, it was observed that this pattern of wrapping is not as effective as continuous wrapping for improving the ductile behaviour of the RCM columns.
- It is observed that by wrapping the RCM columns at plastic hinge zone, no cracks occurred above the wrapped zone when the columns were subjected to cyclic loads, and that the failure occurred through CFRP rupture and crushing of concrete masonry units and it took place at the column's base at very high lateral drifts (10% drift).
- Failure of columns wrapped at the plastic hinge only (RMC-CW-1P) or at the plastic hinge zone and with strips at the mortar bed joints (RMC-CW-1S)

occurred due to premature rupture of CFRP wrap. In these columns, CFRP failure occurred at very high lateral drift of 10%.

In chapter 5, the effect of CFRP wrapping of rectangular concrete masonry prisms on its compressive stress-strain behaviour was investigated. Twelve concrete masonry prisms were wrapped with different CFRP content ratios and tested under increasing axial load. Based on the test results, a compressive stress-strain model for CFRP-confined concrete masonry blocks is proposed. The results of the experimental and analytical findings are summarized as follows:

- The CFRP confinement improves the load-carrying capacity, reduces the post-peak slope of stress-strain curves, and increases the strains at peak strength (ε_{mc}), and at capacity failure (ε_{mcu}) of axially loaded masonry prisms.
- The proposed model provides good estimation of the compressive stress-strain relationship of FRP-confined concrete masonry blocks as well as the confined compressive strength of masonry.

Finally in Chapter 6, and based on the findings in chapter 4 and 5, an analytical model was developed in order to simulate nonlinear cyclic behaviour of RCM, as well as CFRP- and GFRP-confined RCM columns. First, monotonic backbone force-deformation curves were obtained by considering the effect of flexural and longitudinal rebars bond-slip contribution. To get the primary curves, moments-curvature and lateral load-displacement analysis of the RCM columns subjected to axial load and lateral loads were conducted by using the concept of formation of plastic hinge at the base of the column. In the moment-curvature analysis, stress-strain relation of FRP-confined concrete masonry obtained in this research (Chapter 5) was used. Since the proposed stress-strain relations

are given for the whole rectangular/square RCM section consisting of FRP-confined and unconfined zones, it provided significant convenience in the moment-curvature and section analysis.

The proposed monotonic model was validated using the experimental results of the tested RCM columns. Furthermore, on the basis of the experimental results, a three-parameter model was proposed to define the hysteretic model of RCM columns in this study. The symmetrical skeleton curve was determined by evaluating there pairs of values of lateral load and displacement at the cracking point, maximum resistance, and ultimate limit state of the behaviour of a column. Moreover, by setting several rules for calculating cyclic loops, the proposed model was capable of providing efficiency in computational efforts. Finally, it was shown that, in general, a good agreement exists between the predictions of the proposed hysteretic model and the obtained experimental results of full-scale reinforced masonry columns wrapped with CFRP and GFRP.

7.2 Recommendations for future work

Based on the proposed models and the research results illustrated in this dissertation, several potential research topics are suggested for future studies.

One of the limitations of any research in masonry field is the wide variety that exists in construction of the masonry elements. The selection of the constituent materials and components like blocks, bricks, mortar, grout and also strengthening materials (i.e. steel reinforcement, CFRP or GFRP with different properties), shape of the members (for example, studying rectangular or circular masonry columns), location, and role of the masonry member in the whole structure all can be subject of detailed studies. RCM

columns with different levels of axial compression can also be considered in this category of research.

Since in many cases masonry columns are a part of lateral load carrying system of the masonry building, and are located besides the openings and masonry walls, it is necessary to investigate the interaction and behaviour of the columns beside the walls and presence of the opening with different sizes. The usage of reduced scale (half-scale or one-third scale) masonry units can be considered as a practical approach in this type of experimental investigation.

Furthermore, CFRP and GFRP wrapped RCM columns with short shear span (i.e. piers) can be tested to develop more accurate shear design expressions.

In this study, 12 concrete masonry prisms were wrapped with different CFRP content ratios and tested under increasing axial load. Based on the test results, a compressive stress-strain model for CFRP-confined concrete masonry blocks is proposed. Similar experimental program with more variables is required to develop a more accurate stress-strain model for GFRP-confined concrete masonry blocks.

Finally, in this study a macro model was developed to simulate the cyclic lateral load-deformation response of CFRP-strengthened reinforced concrete masonry (RCM) columns. Based on this model, the following studies can be conducted:

- A parametric study to measure the influence of model parameters, may clarify the range and validity of the various proposed model parameters.
- It is required to develop a modified shear model for the assessment of (strengthened) short masonry columns behaviour.

- The macro model needs to be integrated into a general purpose nonlinear dynamic analysis program in order to study the effect of having realistically calibrated models in the analysis.

REFERENCES

Aiello, M. A., Micelli, F., and Valente, L. (2007). "Structural Upgrading of Masonry Columns by Using Composite Reinforcement", *Journal of Composites for Construction, ASCE*; 11(6), p. 650-658.

Aiello M. A., Micelli, F., and Valente Luca (2009), "Structural FRP Confinement of Square Masonry Columns." *Journal of Composites for Construction,* ASCE; 13(2), p.148-156.

Alsiwat, J. M., and Saatcioglu, M., (1992). "Reinforced Anchorage Slip under Monotonic Loading," *Journal of Structural Engineering, ASCE,* 118(9), p. 2421-2438.

Assa, B., Dhanasekar, M., (2002). "A Numerical Model for Flexural Analysis of Short Reinforced Masonry Columns Including Bond-Slip," *Journal of Computers and Structures*; 80, p. 547-558.

ASTM C140-02 (2002). "Standard Test Methods for: Sampling and Testing Concrete Masonry Units and Related Units" Vol. 04.05, West Conshohocken, Pa., p.98-108.

ASTM C270-02 (2002). "Standard Specification for: Mortar for Unit Masonry, American Society of Testing and Materials." Vol. 04.05, West Conshohocken, Pa., p.146-157.

ASTM C780-02 (2002). "Standard Test Method for Preconstruction and Construction Evaluation of Mortars for Plain and Reinforced Unit Masonry." Vol. 04.01, West Conshohocken, Pa., p.464-480.

ASTM C476-02 (2002). "Standard Specification for: Grout for Masonry, American Society of Testing and Materials." Vol. 04.05, West Conshohocken, Pa., p.290-292.

ASTM C1314-02 (2002). "Standard Test Method for Compressive Strength of Masonry Prisms." Vol. 04.05, West Conshohocken, Pa., p.860-867.

ASTM E518-02 (2002*)*. "Standard Test Method for Flexural Bond Strength of Masonry." Vol. 04.05, West Conshohocken, Pa., p.1183-1187.

Bernardini, A., Giuffre, A., and Modena, C., (1984). "Reinforced Hollow Clay Brick Masonry Walls under Seismic Actions", *8th World Conference on Earthquake Engineering*, N.J., 4, p. 679-686.

Binici, B. (2008). "Design of FRPs in Circular Bridge Column Retrofits for Ductility Enhancement," Journal of Engineering Structures, 30(3), 766-776.

Canadian Standards Association (CSA). (2004). "A179-04: Mortar and Grout for Unit Masonry." Mississauga, Ontario, Canada.

Canadian Standards Association (CSA). (2004). "S304.1-04: Design of Masonry Structures." Mississauga, Ontario, Canada.

Canadian Standard Association (CSA). (2009). "S806-09: Design and Construction of Building Components with Fibre-Reinforced Polymers," Mississauga, Ontario, Canada.

Canadian Standard Association (CSA). (2004b), "Mortar and Grout for Unit Masonry." A179-04, Mississauga, Ontario, Canada.

Canadian Standards Association (CSA). (2004). "S304.1-04: Design of Masonry Structures." Mississauga, Ontario, Canada.

Clough, R. W., and Johnston, S. B. (1966). "Effect of Stiffness Degradation on Earthquake Ductility Requirements," *Proc., Japan Earthquake Energy Symposium,* Tokyo, Japan, p. 195-198.

Corradi, M., Grazini, A., Borri, A. (2007). "Confinement of Brick Masonry Columns with CFRP Materials," *Journal of Composite Science and Technology*, 67(9):1772-1783.

De Lorenzis, L., Tepfers, R. (2003). "Comparative Study of Models on Confinement of Concrete Cylinders with Fiber-Reinforced Polymer Composites." *Journal of Composites for Construction,* 7(3), p.219-237.

Dhanasekar, M., and Shrive, N. G. (2002). "Strength and Deformation of Confined and Unconfined Grouted Concrete Masonry." *ACI Structural Journal*, 99(6), p.819-826.

Drysdale Robert G., Hamid Ahmed A. (2005). "Masonry Structures; Behaviour and Design," Canada Masonry Design Centre.

Elwood, J. K., and Moehle, J. P. (2005). "Drift Capacity of Reinforced Concrete Columns with Light Transverse Reinforcement," *Earthquake Spectra*, 21(1), p. 71-89.

FEMA 273/274. (1997). "NEHRP guidelines for the seismic rehabilitation for buildings," Fed. Emergency Management. Agency, Washington D.C. 340p/395p.

Fyfe Company LLC. (2009). Tyfo® SCH-11UP Composite using Tyfo® S Epoxy User`s Guide, http://www.fyfeco.com, retrieved January 2009.

Galal, K., Arafa, A., and Ghobarah A. (2005). "Retrofit of RC Square Short Columns," *Journal of Engineering Structures*, 27, p. 801–813.

Iacobucci, R. D. (2001). "Seismic Upgrade and Repair of Square Reinforced Concrete Columns with CFRP Jackets," *MS thesis*, University of Toronto, Toronto.

ICBO. (1997). "*Uniform Building Code"*, Vol. 2. International Conference of Building Officials, Whittier, California

Intelligent Sensing for Innovative Structures (ISIS), (2008). "FRP Rehabilitation of Reinforced Concrete Structures," ISIS Canada Educational Module, Design Manual No. 4, Department of Civil Engineering, University of Manitoba, Winnipeg, Manitoba, Canada, March 2008.

Khalaf M., Hendry W. Arnold, Fairbrain R. Daniel (1993). "Reinforced Block-work Masonry Columns," *ACI Structural Journal*, Vol. 90(5), p. 496-504.

Kog Y. C., Ong K.C.G, Yu C.H., Sreekanth, A.P.V. (2001). "Reinforced Concrete Jacketing for Masonry Columns with Axial Loads," *ACI Structural Journal*, Vol. 98(2), p. 105-115.

Krevaikas, Theofanis D., and Traintafillou, C. Thanasis (2005). "Masonry Confinement with Fiber-Reinforced Polymers." *Journal of Composites for Construction*, 9(2), p.128-135.

Lam. L. and Teng J. G., (2003). "Design-oriented stress-strain model for FRP-confined concrete." Construction and Building Materials Journal, 17(6-7), p. 471-489.

Lee, C-S. (2006). "Modeling of FRP-Jacketed RC Columns Subject to Combined Axial and Lateral Loads." PH.D dissertation, University of California, San Diego.

Ludovico, M., D'Ambra, C., Prota, A., and Manfredi, G. (2010). "FRP Confinement of Tuff and Clay Brick Columns: Experimental Study and Assessment of Analytical Models." *Journal of Composites for Construction* 14(5), p.583-597.

Mander, J.B., Priestley, M.J.N. and Park, R. (1988). “Theoretical Stress-Strain Model for Confined Concrete,” *Journal of Structural Engineering*, ASCE, 114(8):1804-1826.

Masia, M.J., Shrive, N.G. (2003). “Carbon Fibre Reinforced Polymer Wrapping for the Rehabilitation of Masonry Columns,” *Canadian Journal of Civil Engineering*; 30: 734–744.

Matthys, S., Taerwe, L., and Audenaert, K., (1999). “Tests on Axially Loaded Concrete Columns Confined by Fiber Reinforced Polymer Sheet Wrapping.” *Proc. FRPRCS-4*, Baltimore, 1999, p.217-228.

Micelli F., De Lorenzis L. and La Tegola A., (2004), "FRP-confined masonry columns under axial loads: analytical model and experimental results". *Masonry International Journal*, Ed. British Masonry Society, 17(3), p.95-108.

Mitchell, D., Patrick Paultre, P., Tinawi, R., Saatcioglu, M., Tremblay, R., Elwood, K., Adams, J.,and DeVall, R. (2010). “Evolution of seismic design provisions in the National building code of Canada”, *Canadian Journal of Civil Engineering*, 37(9), p.1157-1170.

Miyauchi, K., Nishibayashi, S., and Inoue, S. (1997). “Estimation of Strengthening Effects with Carbon Fiber Sheet for Concrete Column,” *Proc., FRPRCS-3*, Sapporo, Japan, 1997; Vol. 1: 217-224.

Mostafaei, H., and Kabeyasawa, T. (2007). “Axial-Shear-Flexure Interaction Approach for Reinforced Concrete Columns,” *ACI Structural Journal,* 104(2), p. 218-226

National Building Code of Canada, *NBCC2010* (2010), Volume 1, Part 4: Structural Design, Table 4.1.8.9, p. 4-26.

NCMA. (1994). TEK 9-1: Mortars for Concrete masonry, National Concrete Masonry Association. Herndon, Virginia.

NRCC. (1941). National Building Code of Canada, Associate Committee on the National Building Code, *National Research Council of Canada*, Ottawa, ON.

NRCC. (1953). National Building Code of Canada, Associate Committee on the National Building Code, *National Research Council of Canada*, Ottawa, ON.

NRCC. (1960). National Building Code of Canada, Associate Committee on the National Building Code*, National Research Council of Canada*, Ottawa, ON.

NRCC. (1965). National Building Code of Canada, Associate Committee on the National Building Code, *National Research Council of Canada*, Ottawa, ON.

NRCC. (1970). National Building Code of Canada, Associate Committee on the National Building Code, *National Research Council of Canada*, Ottawa, ON.

NRCC. (1975). National Building Code of Canada, Associate Committee on the National Building Code, *National Research Council of Canada*, Ottawa, ON.

NRCC. (1977). National Building Code of Canada, Associate Committee on the National Building Code, *National Research Council of Canada*, Ottawa, ON.

NRCC. (1980). National Building Code of Canada, Associate Committee on the National Building Code, *National Research Council of Canada*, Ottawa, ON.

NRCC. (1985). National Building Code of Canada, Associate Committee on the National Building Code, *National Research Council of Canada*, Ottawa, ON.

NRCC. (1990). National Building Code of Canada, Associate Committee on the National Building Code, *National Research Council of Canada*, Ottawa, ON.

NRCC. (1995). National Building Code of Canada, Associate Committee on the National Building Code, *National Research Council of Canada*, Ottawa, ON.

NRCC. (2005). National Building Code of Canada, Associate Committee on the National Building Code, *National Research Council of Canada*, Ottawa, ON.

NRCC. (2010). National Building Code of Canada, Associate Committee on the National Building Code*, National Research Council of Canada*, Ottawa, ON.

Ozbakkaloglu, T., Saatcioglu, M. (2006). "Seismic Behavior of Square High-strength Concrete Columns Confined with steel and Fiber-reinforced Polymer Tubes," *Journal of Composites for Construction*, 10(6), p. 533-549.

Ozcebe, G., Saatcioglu, M., (1989). "Hysteretic Shear Model for Reinforced Concrete Members," *Journal of Structural Engineering*, *ASCE*, 115(1), p. 132-148

Park, Y.J., Reinhorn, A.M., and Kunnath, S.K., (1987). "IDARC: Inelastic Damage Analysis of Reinforced Concrete Frame – Shear Wall Structures," *Tech. Rep. NCEER-87-0008*, Nat. Ctr. for Earthquake Engineering Res., Buffalo, N.Y.

Park, R. (1989). "Evaluation of Ductility of Structures and Structural Assemblages from Laboratory Testing," *Bull New Zeal Nat Soc Earthquake Eng*; 22(3).

Parvin, A., Altay, S., Yalcin, C., Kaya, O., (2010). "CFRP Rehabilitation of Concrete Frame Joints with Inadequate Shear and Anchorage Details," *ASCE Journal of Composite for Construction;* Vol. 14 (1), p. 72-82.

Paultre, P., and Legeron, F. (2008). "Confinement Reinforcement Design for Reinforced Concrete Columns," *Journal of Structural Engineering.*, 134(5), p. 738.

Priestly M. J. N. and Elder D. (1983). "Stress-strain Curves for Unconfined and Confined Concrete Masonry." *ACI Journal*, 80(3), p.192-201.

Priestley M. J. N., Calvi G.M., Kowalsky M. J. (2007). "Displacement-Based Seismic Design of Structures," *IUSS Press*, Pavia, Italy.

Restrepol J. and De Vino B. (1996) "Enhancement of the Axial Load Carrying Capacity of Reinforced Concrete Columns by Means of Fiberglass-Epoxy Jacket." *Second International Conference Advanced Composite Materials in Bridges and Structures*, CSCE, Quebec, Canada, 1996: p.547-553.

Rocca, Silvia (2007). "Experimental and Analytical Evaluation of FRP-confined Large Size Reinforced Concrete Columns," Ph. D thesis, University of Missouri-Rolla.

Saatcioglu, M., and Derecho, A. T., (1979). "Dynamic Inelastic Response of Coupled Shear Walls as Affected by Axial Forces," *Proc., Nonlinear Design of Concrete Structures., CSCE-ASCE-ACI-CEB Int. Symposium.,* Univ. of Waterloo Press, Waterloo, Ontario, Canada, p. 639-670.

Seible, F, Priestley, M.J.N., Hegemier, G.A., Innamorato, D. (1997). "Seismic Retrofit of RC Columns with Continuous Carbon Fiber Jackets," *Journal of Composite for Construction*; 1(2):52–62.

Sezen, H., and Setzler, E. J. (2008). "Reinforcement Slip in Reinforced Concrete Columns," *ACI Structural Journal,* 105(3), p. 280-289

Sezen, H., and Chowdhury, T., (2009). "Hysteretic Model for Reinforced Concrete Columns Including the Effect of Shear and Axial Load Failure," *Journal of Structural Engineering, ASCE*, 135(2), p. 139-146.

Shaheen E., Shrive N.G., (2005). "Strengthening of masonry columns with sprayed glass fiber reinforced polymer (SGFRP)", *10th Canadian Masonry Symposium*, Banff, Alberta.

Sheikh, S. A., and Yua, G. (2002). "Seismic Behavior of Concrete Columns Confined with Steel and Fiber-reinforced Polymers," *ACI Structural Journal,* 99(1), p. 72-81.

Shrive, P.L., Azarnejad, A., Tadros, G., McWhinnie, C., and Shrive, N.G. (2003). "Strengthening of Concrete Columns with Carbon Fibre Reinforced Polymer Wrap," *Canadian Journal of Civil Engineering;* 30:543–54.

Takeda, T., Sozen, M. A., and Nielsen, N. N., (1970). "Reinforced Concrete Response to Simulated Earthquakes," *Journal of Structural Division,* ASCE, 96(4), p. 2557-2573.

Takayanagi, T., and Schnobrich, W. C., (1976). "Computed Behaviour of RC Shear Walls," *SRS No. 434*, Univ. Illinois, Urbana, I11.

Tanrikulu, A. K., Mengi, Y., and McNiven, H. D., (1992). "The Nonlinear Response of Unreinforced Masonry Buildings to Earthquake Excitations," *Earthquake Engineering and Structural Dynamics,* 21(11), p. 965-985.

Tassios, T., (1984). "Behaviour of Walls Including Infilled Frames Under Cyclic Loading", *CIB Symposium on Wall Structures, International Center for Building Systems*, Warsaw, Poland.

Tegola A., Miglliacci A., Ronca P. and Micaletto S. (2003). "Innovative Confinement Technique and Modeling of Masonry Columns," *Ninth North American Masonry Conference*, South Caroline, USA, p. 292-303.

Tomazevic, M., Lutman, M. (1996). "Seismic Behaviour of Masonry Walls: Modeling of Hysteretic Rules," Journal of Structural Engineering, Vol. 122, No. 9, P. 1048-1054.

UBC. (1935). Uniform Building Code 1935. *International Conference of Building Officials (ICBO)*, Long Beach, California.

Vision 2000 Committee (1995). "Performance based seismic engineering of buildings," *Structural Engineers Association of California (SEAOC)*, Sacramento, California.

Wakabayashi, M., and Nakamura, T. (1984). Reinforcing Principle and Seismic Resistance of Brick Masonry Walls, *8th World Conference on Earthquake Engineering*, N.J., 5, p. 661-667.

Xiao, Y., and Wu, H. (2000). "Compressive Behaviour of Concrete Confined by Carbon Fiber Composite Jackets," *Journal of Material in Civil Engineering*; 12(2): 139-146.

Youd, TL., Bardet, J., and Bray, JD.(2000). "1999 Kocaeli, Turkey, Earthquake Reconnaissance Report," *Earthquake Spectra*, Supplement A to Volume 16, p. 152-170.

APPENDIX A: SECTION ANALYSIS OF CONTROL CONCRETE MASONRY COLUMN

In this section, Control column (RMC-0) designed using current Canadian (CSA S304.1-04). CSA S304.1-04 uses rectangular stress block approach in order to determine the flexural capacity of concrete masonry sections.

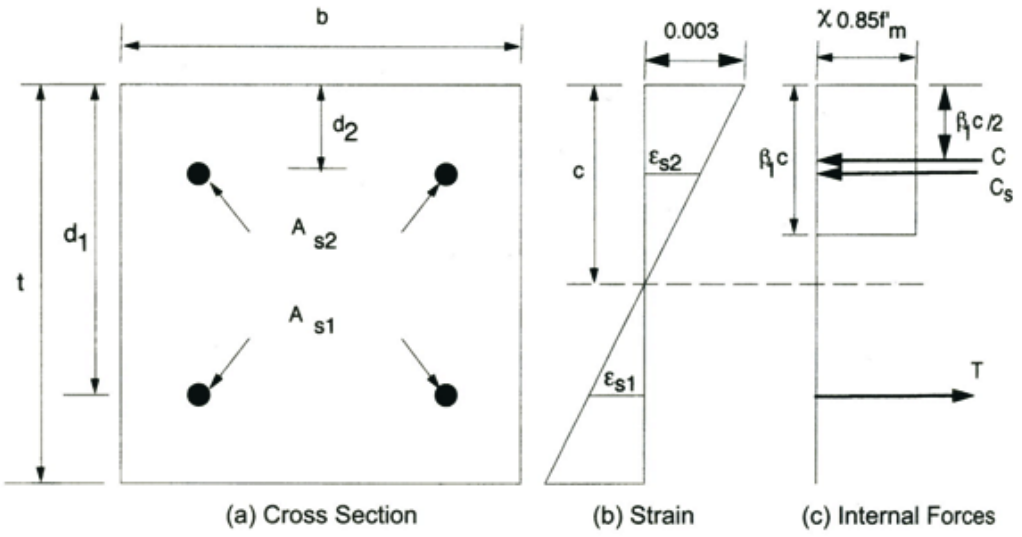

Figure A.1: Analysis of column cross section at ultimate limit state (Drysdale and Hamid, 2005)

Considering Figure A.1 as a guide, in this project:

$t = 390 \ \ mm$

$d_1 = 260 \ \ mm$

$d_2 = 130 \ \ mm$

$b = 390 \ \ mm$

$f_y = 400 \ \ MPa$: For steel bars

$A_s = 200 \times 2 = 400 \ \ mm^2$: 2-M15

$\beta_1 = 0.80$: For masonry design

$\chi = 1$: For compression normal to the bed joint in a member

$C = 0.85\phi_m \chi f_m^{'} b \beta_1 c$

$f_m^{'} = 11.5 \ \ MPa$

$T_1 = C_s = \phi_s A_s f_y$

$\phi_m = \phi_s = 1$: For calculating nominal resisting moment M_{rn}

Therefore, Compressive and tensile forces in concrete masonry and steel are:

$C = 0.85 \times 1 \times 11.5 \times 0.390 \times 0.8c$

$T = A_s f_y = 400 \times 400 \times 10^{-3} = 160(kN): \ \varepsilon_{s1} > 0.002 \Rightarrow f_y = 400 \ \ MPa$

$C_s = \varepsilon_m . \dfrac{c - d_2}{c} . A_{s2} . E_s$: Assuming c<130 mm and $E_s = 200 \ \ GPa$

Note that Column RMC-0 is subjected to constant axial force of 200 kN. Therefore, considering section equilibrium:

$C - (C_s + T) = 200 \ \ kN$

Depth of neutral axis (c) is obtained by an iterative process, as it is shown in following table:

Table A.1: Iterative process for calculating neutral axis depth (c)

c (mm)	**C (kN)**	**ε_{s1}**	**ε_{s2}**	**f_{s1} (MPa)**	**f_{s2} (MPa)**	**T (kN)**	**C_s (kN)**	**C-C_s-T (kN)**	**M_{rn} (kN.m)**
90	274.5	0.00567	0.00133	400	266.7	160	106.7	7.8	47.1
100	305	0.0048	0.0009	400	180	160	72	73	53
110	335.5	0.00409	0.00055	400	109.1	160	43.6	131.8	58.2
120	366	0.0035	0.00025	400	50	160	20	186	62.9
122.72	374.2	0.00336	0.00018	400	35.6	160	14.2	200	64.1

Therefore, Nominal resisting moment M_{rn} can be estimated:

$$M_n = C\left(\frac{t}{2} - \frac{\beta_1 c}{2}\right) + \sum C_{s_i}\left(\frac{t}{2} - d_i\right) + \sum T_i\left(d_i - \frac{t}{2}\right) = 64.08 \text{ kN.m}$$

For calculating cracking moment M_{cr}, f_t obtained from 7-blocks tests is used. Therefore:

$$f_t = 1.2 \ MPa$$

$$M_{cr} = \frac{I_g}{0.5H}\left(\frac{P}{A_g} + f_t\right) = \frac{(0.39)^4/12}{0.5*0.39}\left(\frac{200}{(0.39)^2} + 1.2\times10^3\right) = 24.9 \ kN.m$$

Furthermore, nominal shear capacity of concrete masonry section calculated as follows:

$$V_r = \phi_m(v_m b_m d_v + 0.25P_d)\gamma_g + (0.6\phi_s A_v f_y) \le 0.4\sqrt{f'_m} b_w d_v \gamma_g = 0.4\sqrt{12}\times.39\times312 = 168.6 \ kN$$

$$V_{rn} = (v_m b_w d_v + 0.25P_d)\gamma_g + (0.6A_v f_y \frac{d_v}{s})$$

For calculating V_n:

$$\phi_m = \phi_s = 1$$

$A_v = 2\times\frac{\pi}{4}\times(4.75\times10^{-3})^2 = 3.54\times10^{-5} \ m^2$: Cross-sectional area of horizontal shear reinforcement

f_y=240 MPa: mild steel

S = 200 mm: vertical spacing of stirrups

$d_v > 0.8l_w = 0.8\times390 = 312$ mm : effective depth for shear calculations

$$0.6A_v f_y \frac{d_v}{s} = 0.6\times3.54\times10^{-5}\times240\times10^3\times\frac{312}{200} = 7.92 \ kN$$

b_w = 390 mm: actual thickness of the column

γ_g = 1: factor to account for partially grouted or ungrouted walls/columns constructed of units that are not solid. It is 1 for fully grouted walls/ columns.

P_d = 200 kN: axial compressive load on a section

$$v_m = 0.16(2 - \frac{M_f}{V_f d_v})\sqrt{f_m^{'}}$$

$f_m^{'} = 12 \ MPa$: Masonry compressive strength

M_f: Factored moment at the section considered

V_f: Factored shear at the section considered

$\frac{M_f}{V_f d_v} = \frac{V_f h}{V_f d_v} = \frac{h}{d_v} = 1$: A value not less than 0.25 nor not more than 1.0

Therefore, it is obtained:

$V_n = 125 \ kN$

Note that using UCSD model introduced in chapter 7 $V_m = 102.4 \ kN$ is calculated.

APPENDIX B: DETAILED BEHAVIOUR OF THE TESTED COLUMNS

1. Column RMC-0

Prior to the application of lateral load, control column was first loaded with a constant axial compressive force of 200 kN, corresponding to approximately 11% of the axial load bearing capacity. Observations during the test showed that the first crack was formed at 0.7% drift level. The cracks were widened during the subsequent cycles at the same displacement. Between 1.0% and 5% drift levels, new cracks appeared and continued to widen. The yielding of vertical rebars started after 1% lateral drift. The new diagonal cracks caused decrease in the load bearing capacity. The maximum lateral load reached during the test was 52 kN at the 0.7% drift level (see Figure B.1).Column RMC-0 was considered failed when lateral load capacity reduced to less than 80% of maximum recorded lateral load. Therefore, the failure occurred at 1.5% drift when lateral load capacity decreased to less than 40 kN. In order to achieve ultimate failure of the column, test was continued, and spalling of concrete blocks was observed at the base of the column at 4.0% drift level as it is shown in Figure B.2. After completion of 2.0% lateral drift level, column was only pushed until the end of the test at 5% drift level.

Figures B.3 and B.4 show the strains in the ties at $1/7^{th}$ and $4/7^{th}$ of the column's height, respectively. From the Figures B.3 and B.4, it is noticed that for the same level of lateral drift, strain in the bottom tie are bigger in the magnitudes in compare to recorded strains at the mid height ($4/7^{th}$) of the column. The recorded strains in the bottom tie are bigger than strains at the mid height because of the expansion of section in plastic hinge

zone of the column (the bottom 400 mm) which creates tensile strain in transverse reinforcement and consequently reduces the shear capacity at the bottom part of the column. In general, in all columns the contribution of the lateral shear strength from steel mechanism provided by ties was low (due to using small size steel rods-4.75mm diameter- for ties).

2. Column RMC-CW-1

In this test, due to the confinement provided by one layer of CFRP wrap, it was not possible to monitor cracking or spalling of the original masonry column; however, in plastic hinge zone minor rupture of CFRP wrap and crushing of the blocks was observed at high level of lateral loads (Figure B.6-3). Similar to previous tests, axial load was kept on constant value of 200 kN. The lateral load did not increase after the drift level of 1.5% and reduced gradually after. The maximum lateral load reached during the test was 68 kN at the 1% drift level (see Figure B.5). Column considered failed at 2.8% drift level when lateral load reduced to less than 80% of the maximum recorded lateral load. Test was stopped at 5% drift level, due to technical problems.

Figure B.7 shows the strains in the tie at $1/7^{th}$ of the column height. As it is shown in Figure B.8, recorded tensile strains at $1/7^{th}$ of the height in column RMC-CW-1 are significantly less than measured tensile strains at $1/7^{th}$ of the height in column RMC-0 due to confinement provided by one layer of CFRP wrap in column RMC-CW-1. Moreover, measured strains obtained from one of the four vertical rebars are shown in Figure B.9. Note that in this Figure measured strains are recorded up to 3% drift when the installed strain gauge stopped functioning. Figure B.10 shows the tensile strain

measurements on CFRP wrap via lateral load. Strains are recorded at one of the bull-nose corners at one-seventh of the height.

3. Column RMC-CW-2

In this test, due to the confinement provided by 2 layers of CFRP wraps no cracking or spalling was observed on the surface of the column (Figure B.12). After removing the CFRP sheets, it was observed that cracks had been occurred at the intersection of the foundation and column. Lateral load did not increase after the drift of 1% and reduced gradually after. Axial load was kept on 200 kN during the test. The maximum lateral load reached during the test was 76 kN at the 0.9% drift level (see Figure B.11). Due to technical problems, it wasn't possible to continue the lateral drift beyond 6% drift, and up to this point no rupture or damage were occurred on CFRP wraps; however, local debonding of the wrap were observed. Note that after reaching to 5% drifts level, the specimen was only pushed until the end of this test.

Figure B.13 shows the strains in the tie at $1/7^{th}$ of the column height. Similar to column RMC-CW-1, measured tensile strains at $1/7^{th}$ of the height in column RMC-CW-2 are significantly less than measured tensile strains at $1/7^{th}$ of the height in column RMC-0 due to confinement provided by two layers of CFRP wrap. Measured strains obtained from one of the four vertical rebars are shown in Figure B.14. Note that in this Figure measured strains are recorded up to 5% drift when the installed strain gauge stopped functioning. Figure B.15 shows the tensile strain measurements on CFRP wrap via lateral load. Strains are recorded at flat surface of wrap at one-seventh of the height. Finally, in Figure B.16, measured tensile strains of CFRP wrap along the height of column RMC-CW-2 at different drift levels are shown, and it can be seen that the

measured strains are the highest in plastic hinge zone and almost negligible in top at 1200 mm from the footing-column interface.

4. Column RMC-CW-3

In this test, 3 layers of CFRP wraps was provided and similar to column RMC-CW-2 no cracking or spalling was observed on the surface of the column (Figure B.17). After removing the CFRP sheets, it is observed that the cracks had been occurred at the intersection of foundation and column. Lateral load did not increase after drift of 1.5% and started decreasing gradually after 4% drift (see Figure B.18). Similar to previous tests, axial load was kept on 200 kN during the test. As it is shown in Figure B.18, the maximum lateral load reached during the test was 79.7 kN at 1.5% drift level. Test continued until 10% lateral drift and up to this point no rupture or damage were occurred on CFRP wraps; however, local debonding of wrap were observed. Due to test setup limitations and safety concerns, it was not possible to continue the test up to ultimate failure. Note that after 5% drifts level, the specimen was only pushed until the end of the test.

Figure B.19 shows the strains in the tie at $1/7^{th}$ of the column height. Similar to columns RMC-CW-1 and RMC-CW-2, measured tensile strains at $1/7^{th}$ of the height in column RMC-CW-3 are significantly less than measured tensile strains at $1/7^{th}$ of the height in column RMC-0 due to confinement provided by three layers of CFRP wraps. However, it is also noted that recorded tensile strains at this location for column RMC-CW-3 are almost half of recorded tensile strains in column RMC-CW-1. Figure B.20 shows the recorded tensile strains in the tie placed at the mid height of the section, and it can be seen that measured tensile strains at mid height are almost one-third of recorded

strains in the tie placed at plastic hinge zone. Measured strains obtained from one of the four vertical rebars are shown in Figure B.21.

Figure B.22 shows the tensile strain measurements on CFRP wrap via lateral load. Strains are recorded at flat surface of wrap at one-seventh of the height. Finally, Figure B.23 compares the measured tensile strains of CFRP wrap at two-seventh of the height of column RMC-CW-3 with measured tensile strains of CFRP wrap at one-seventh of the height, and at it is shown tensile strains of the wrap above the plastic hinge zones are significantly less than recorded tensile strains in plastic hinge zone; moreover, these readings provide a good approximation of the height of the plastic hinge zone which can be used in analytical calculations.

5. Column RMC-CW-1S

In this test, it is tried to optimize used CFRP material; therefore, instead of wrapping the column continuously along the height, only plastic hinge zone (bottom 300 mm) and mortar joints were wrapped with CFRP strips, as it is shown in Figure B.24-1. Only one layer of CFRP was used for strengthening of column RMC-CW-1S such that the obtained results for this column can be compared with results attained from column RMC-CW-1. Similar to previous four tests, axial load was kept 200 kN during the test. The lateral load did not increase after the drift level of 1.2% and reduced gradually after (see Figure B.25). The maximum lateral load reached during the test was 63 kN which is 8% less than maximum recorded lateral load for column RMC-CW-1. Column RMC-CW-1S was considered failed at 3.5% lateral drift when lateral load reduced to less then 80% of the maximum recorded lateral load. After 5% drift, column was only pushed, and

ultimate failure was occurred at 10% drift with sudden rupture of CFRP wrap and crushing of concrete masonry, as it is shown in Figure B.24-3.

Figure B.26 shows the strains in the tie at 1/7th of the column height. Similar to columns RMC-CW-1, RMC-CW-2, and RMC-CW-3 measured tensile strains at 1/7th of the height in column RMC-CW-1S are significantly less than measured tensile strains at 1/7th of the height in column RMC-0 due to confinement provided by one layers of CFRP wrap. Moreover, it is also noted that recorded tensile strains at this location for column RMC-CW-1S are almost at the same level of recorded tensile strains in column RMC-CW-1.

6. Column RMC-CW-1P

Since in testing column RMC-CW-1S no cracks were observed above plastic hinge zone, last test was conducted on a RCM column that was only wrapped at the base of the column as it is shown in Figure B.30-1.

Figure B.31 shows the obtained lateral load versus lateral drift for this column. In general, this column behaved very similar to column RMC-CW-1S, and maximum recorded lateral load during the test was 60 kN which is slightly less than maximum lateral loaded obtained from testing column RMC-CW-1S. At 5.7% lateral drift, as it shown in Figure B.30-2, CFRP jacket opened up at several locations along the height. No cracks were observed above the wrapped zone. Finally, similar to the previous test, the test was stopped at 10% drift when CFRP wrap rupture and crushing of the base occurred at the base of the column (see Figure B.30-3).

Figure B.32 shows the strains in the tie at 1/7th of the column height. Similar to previous columns measured tensile strains at 1/7th of the height in column RMC-CW-1P

are significantly less than measured tensile strains at $1/7^{th}$ of the height in column RMC-0 due to confinement provided by one layers of CFRP wrap. Moreover, it is also noted that recorded tensile strains at this location for column RMC-CW-1P are almost at the same level of recorded tensile strains in column RMC-CW-1. Moreover, in Figure B.32 the tensile strains in tie placed at $4/7^{th}$ are compared with the tensile strains in tie placed at bottom of the column. In general, this column behaved very similar to column RMC-CW-1S.

7. Column RMC-GW-1

In this test, GFRP sheets are used for strengthening purposes instead of CFRP material. Column RMC-GW-1 was wrapped with continuous layer GFRP material as it is shown in Figure B.33. Similar to previous test, axial load was kept constant and equal to 200 kN. Figure B.34 shows Lateral load versus drift (%) for column RMC-GW-1; moreover, in this Figure, the lateral load versus lateral drift of this column are compared with the column wrapped with one continuous layer of CFRP sheets (RMC-CW-1), and as it is shown in this Figure both columns behaved very similarly.

No cracking or GFRP rupture was observed even at the end of the test and high lateral drifts (10% drift). However, as it is shown in Figure B.33-3 longitudinal rebars pullout were observed at high lateral drifts. The lateral load did not increase after the drift level of 1.3% and reduced gradually after. The maximum lateral load reached during the test was 66 kN at the 1% drift level (see Figure B.34). Column considered failed at 2.8% drift level when lateral load reduced to less than 80% of the maximum recorded lateral load. Test was stopped at 11.6% drift level when the column could not sustain the axial loads.

Measured strains obtained from two of the four vertical rebars are shown in Figure B.35. Strains reading obtained from strain gauges installed over GFRP wrap were greatly scattered and in general lower than rupture strain values. Figure B.36 shows the tensile strain measurements on GFRP wrap via lateral load of the strain gauge with highest recorded strain values. This strain gauge was installed at one of the round corners and 200 mm above footing. As it is shown in Figure B.36, the ratio between highest recorded strain and rupture strain of GFRP material at 11% lateral drift equals to 0.67.

8. Column RMC-GW-2

In this test, due to the confinement provided by 2 layers of GFRP wraps no cracking or spalling was observed on the surface of the column (Figure B.37). Figure B.38 shows the obtained lateral force versus lateral drift hysteric curves; moreover, the results are compared with the hysteretic of the column wrapped with two layers of CFRP sheets. In general, the two columns behaved similarly, but the column with two layers of GFRP exhibited lower lateral load bearing capacity in compare to the column with 2 layers of CFRP wrap (see Figure B.38).

After removing the GFRP sheets, it was observed that cracks had been occurred at the bottom 200 mm of the column. Lateral load did not increase after the drift of 1% and reduced gradually after. Axial load was kept on 200 kN during the test. The maximum lateral load reached during the test was 65.2 kN at the 1% drift level (see Figure B.38). After reaching 5% lateral drift, the column was only pushed up to 11% lateral drift when it was not possible to sustain the axial load safely. Measured strains obtained from two of the four vertical rebars are shown in Figure B.39. Strains reading obtained from strain

gauges installed over GFRP wrap were greatly scattered and in general lower than rupture strain values. Figure B.40 shows the tensile strain measurements on GFRP wrap via lateral load. These strain gauges were installed at one of the round corners and at the 200, 400, and 600 mm above the footing.

9. Column RMC-GW-1S

Similar to the tests on CFRP wrapped columns, in this test, it is tried to optimize used GFRP material. Therefore, instead of wrapping the column continuously along the height, only plastic hinge zone (bottom 300 mm) and mortar joints were wrapped with GFRP strips, as it is shown in Figure B.41-1. Only one layer of GFRP was used for strengthening of column RMC-GW-1S such that the obtained results for this column can be compared with results attained from columns RMC-CW-1S and RMC-GW-1.

The lateral load versus drift results of this column are compared with columns with one continuous layer of GFRP material (RMC-GW-1) and column with strips of CFRP material (RMC-CW-1S) in Figures B.42 and Figures B.43 respectively. Similar to previous tests, axial load was kept 200 kN during the test. The lateral load did not increase after the drift level of 1.2% and reduced gradually after. No GFRP rupture was observed and no cracks were developed on the surface of the column during the test; therefore, as it is shown in Figure B.42, the column RMC-GW-1S behaved almost the same as column RMC-GW-1. The maximum lateral load reached during the test was 59.2 kN which is slightly less than maximum recorded lateral load for column RMC-GW-1. Furthermore, this column behaved very similar to column RMC-CW-1S (see Figure B.43); however, since no GFRP rupture or opening occurred, the degradation of lateral

forces were more gradual and without any abrupt decrease in lateral loads (unlike column RMC-CW-1S). Column RMC-GW-1S was considered failed at 4% lateral drift when lateral load reduced to less then 80% of the maximum recorded lateral load. After 5% dirft, column was only pushed until 12% lateral drift was reached and column could not carry the compressive loads safely.

Measured strains obtained from two of the four vertical rebars are shown in Figure B.44. Strains reading obtained from strain gauges installed over GFRP wrap were greatly scattered and in general lower than rupture strain values. Figure B.45 shows the tensile strain measurements on GFRP wrap via lateral load. These strain gauges were installed at one of the round corners and at the 200 and 400 mm above the footing. In compare to column with one continuous layer of GFRP (column RMC-GW-1), the recorded strains are greatly higher in column RMC-GW-1S.

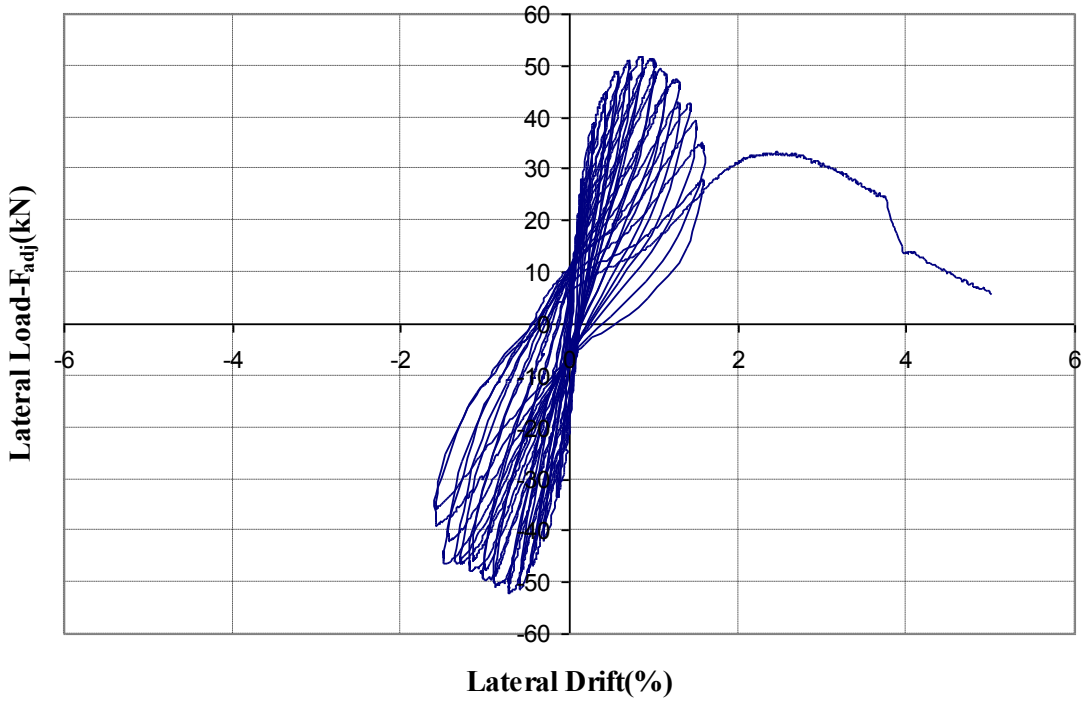

Figure B.1: Lateral load versus drift for column RMC-0

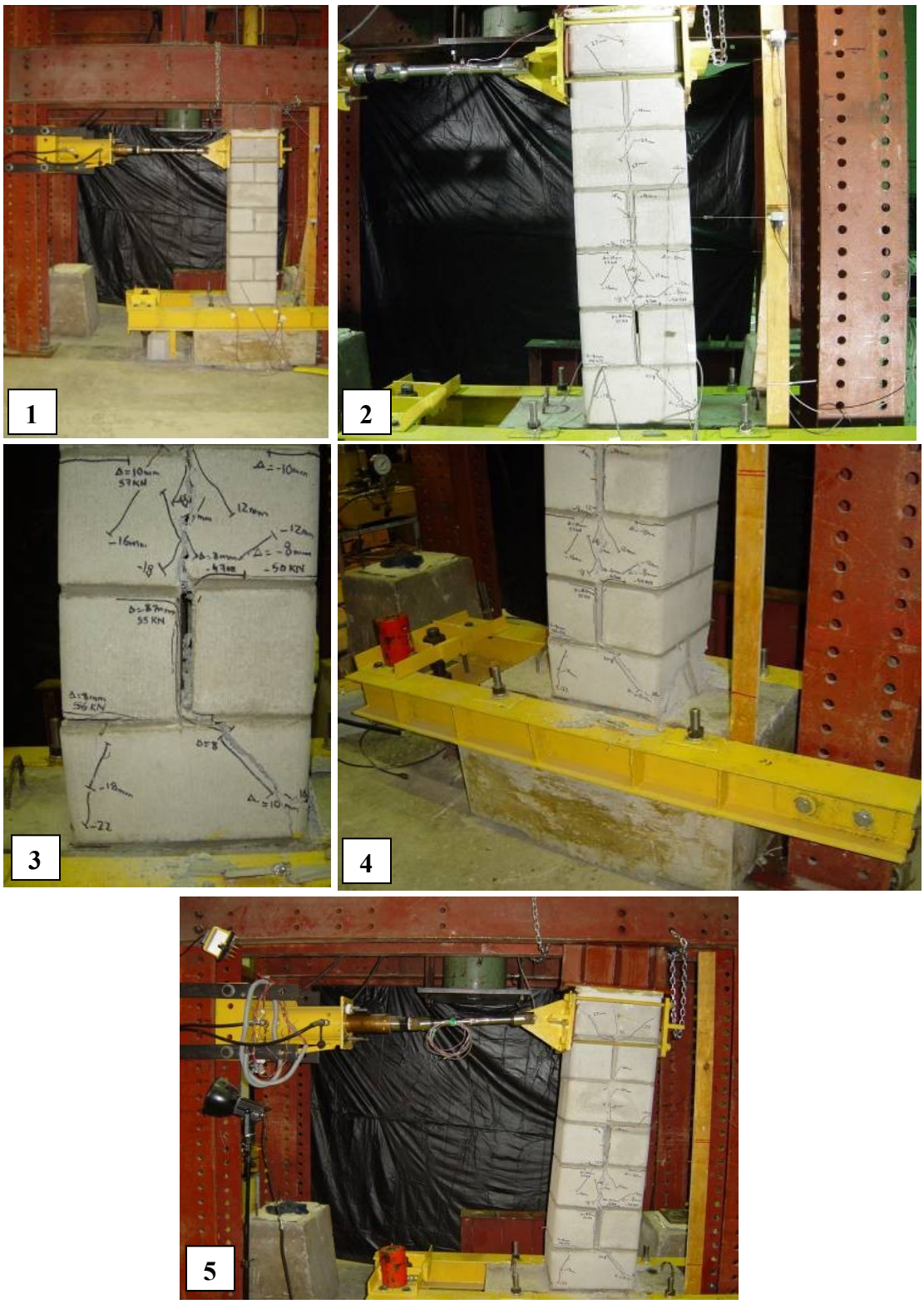

Figure B.2: (1) Control specimen before the test (2) Column at 2% drift level (3, 4) Sample of cracks and spalling at column's base (5) Column at 5% drift level

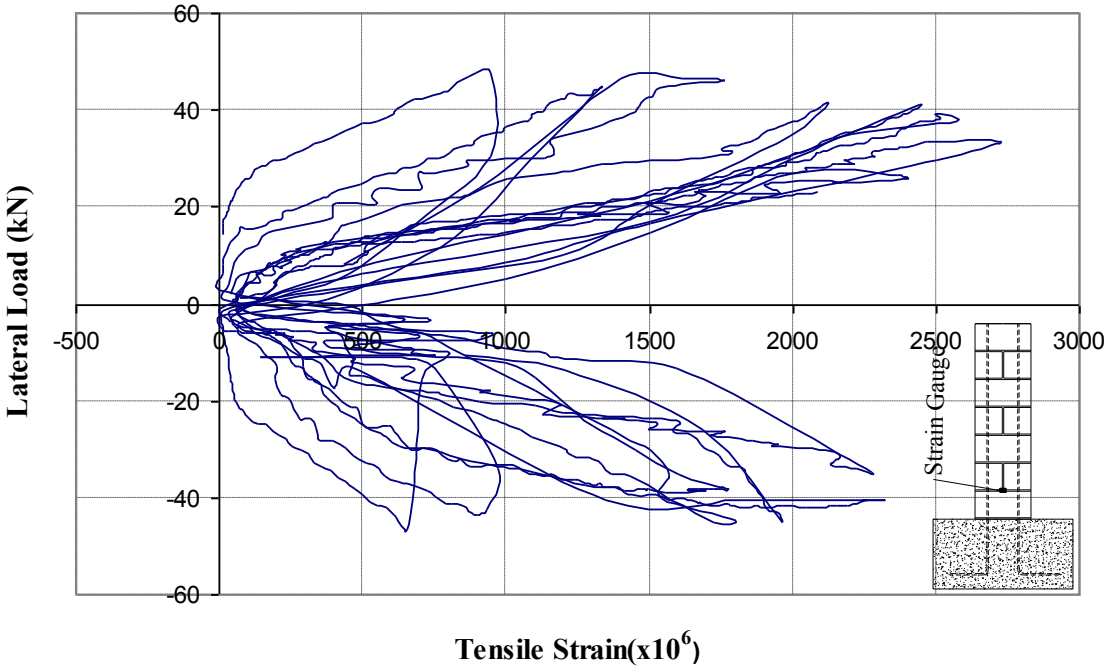

FigureB.3: Measured strain in the tie located at one-seventh of the height in column RMC-0

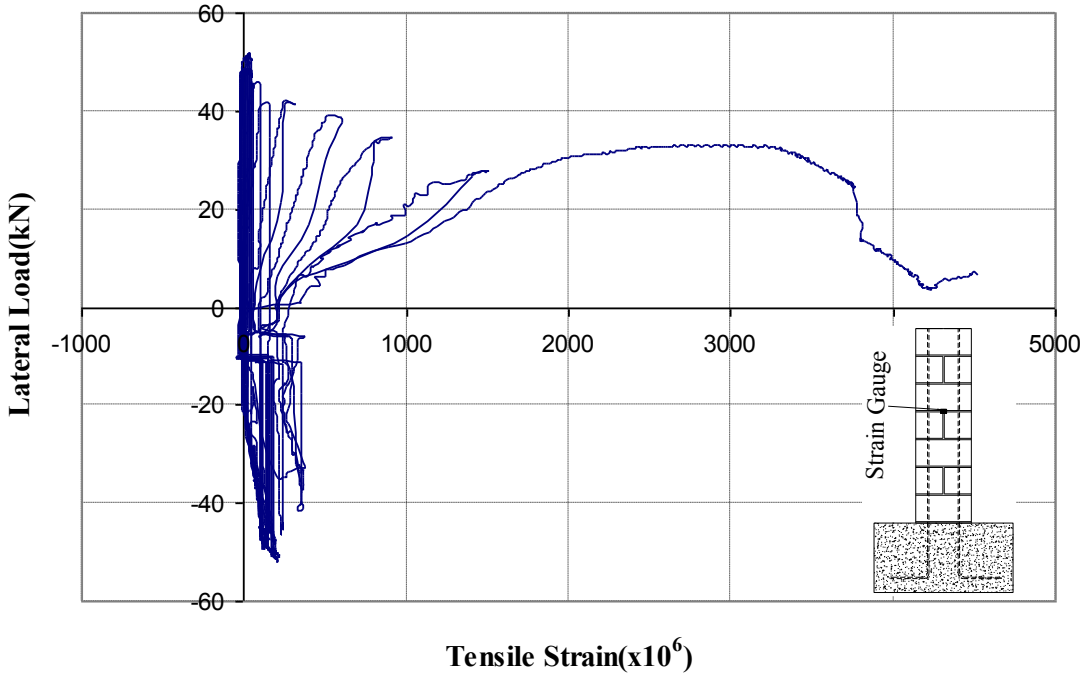

FigureB.4: Measured strain in the tie located at four-seventh of the height in column RMC-0

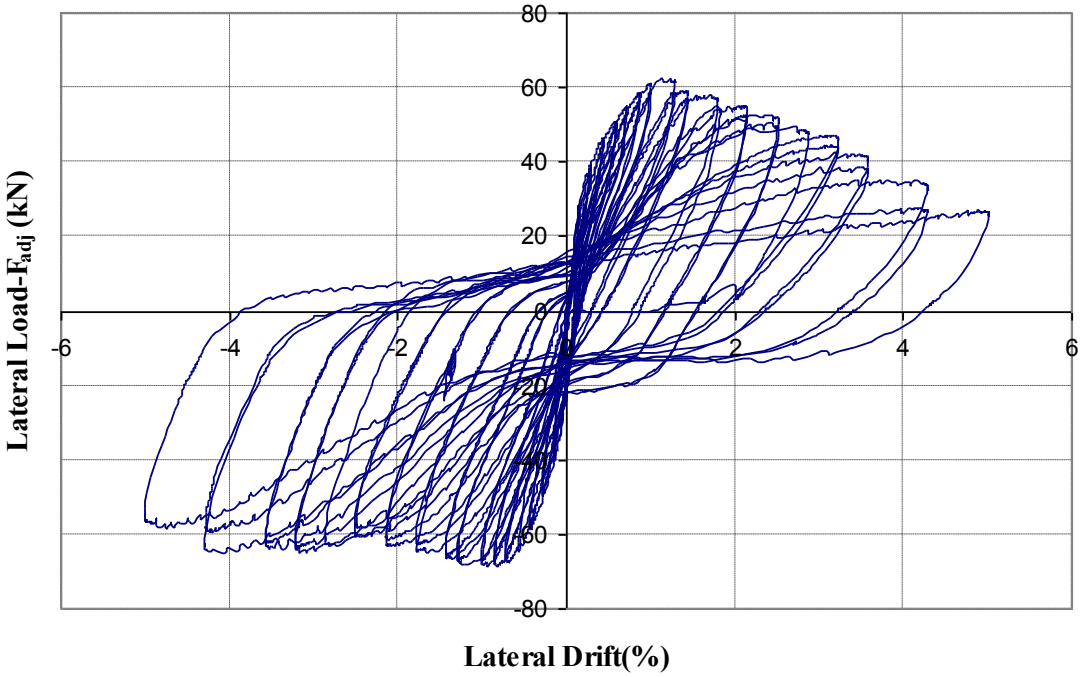

Figure B.5: Lateral load versus drift (%) for column RMC-CW-1

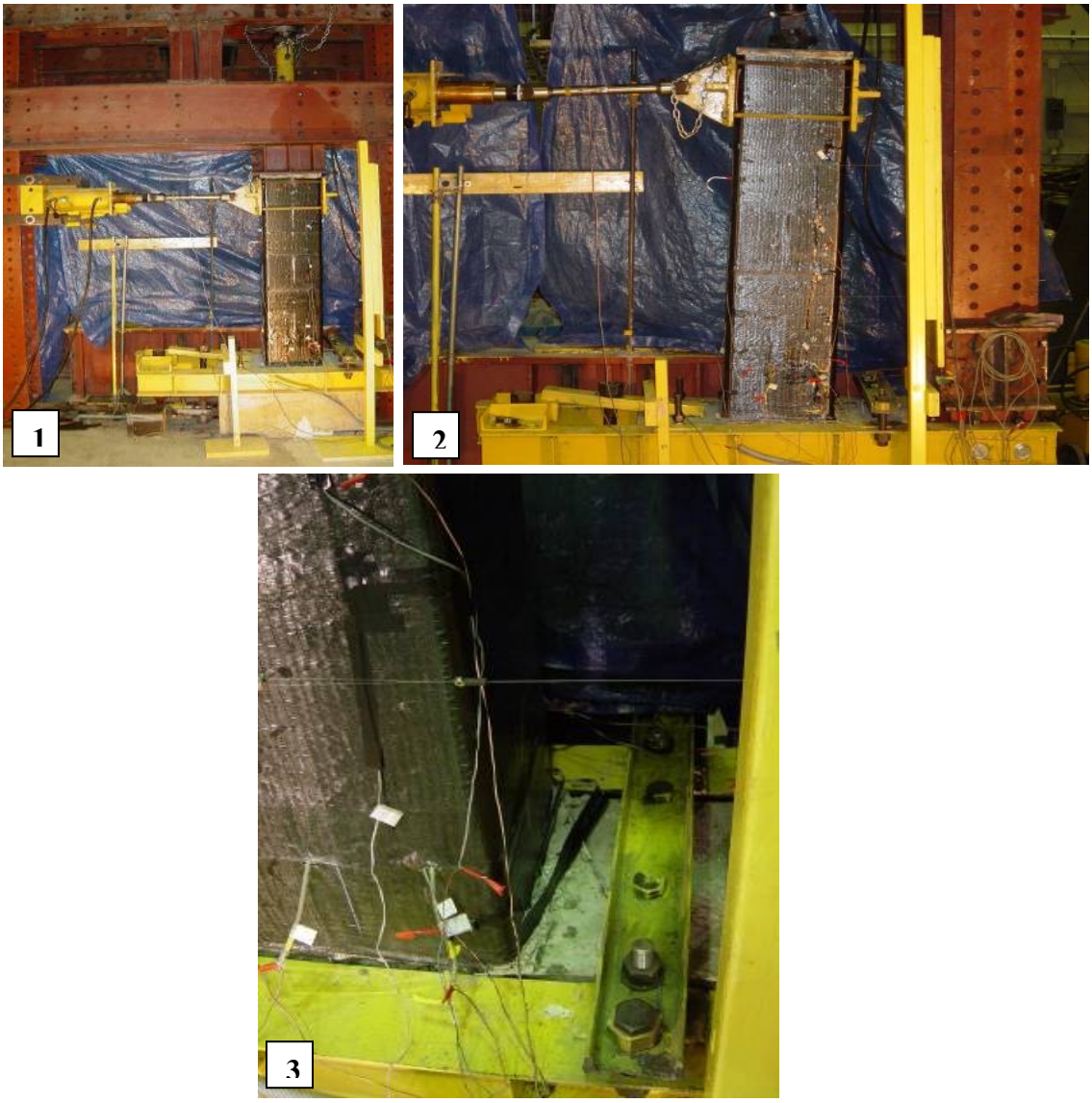

FigureB.6: (1) Column RMC-CW-1 before the test (2) Specimen at 5% drift level (3) Wrap rupture near the base

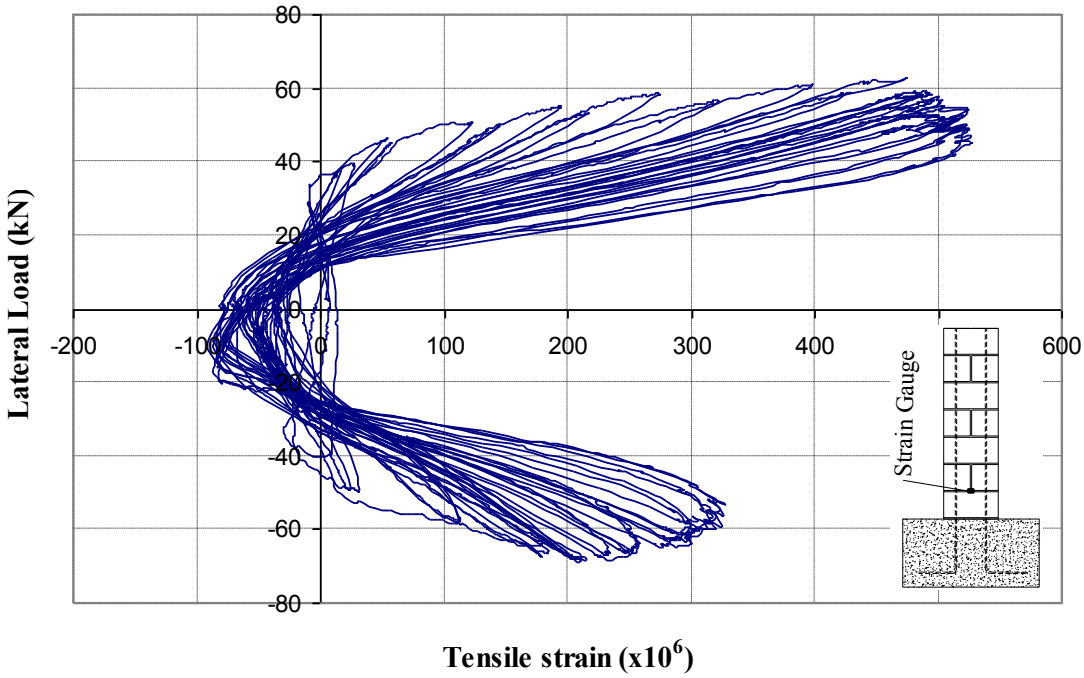

Figure B.7: Measured strain in the tie located at one-seventh of the height in column RMC-CW-1

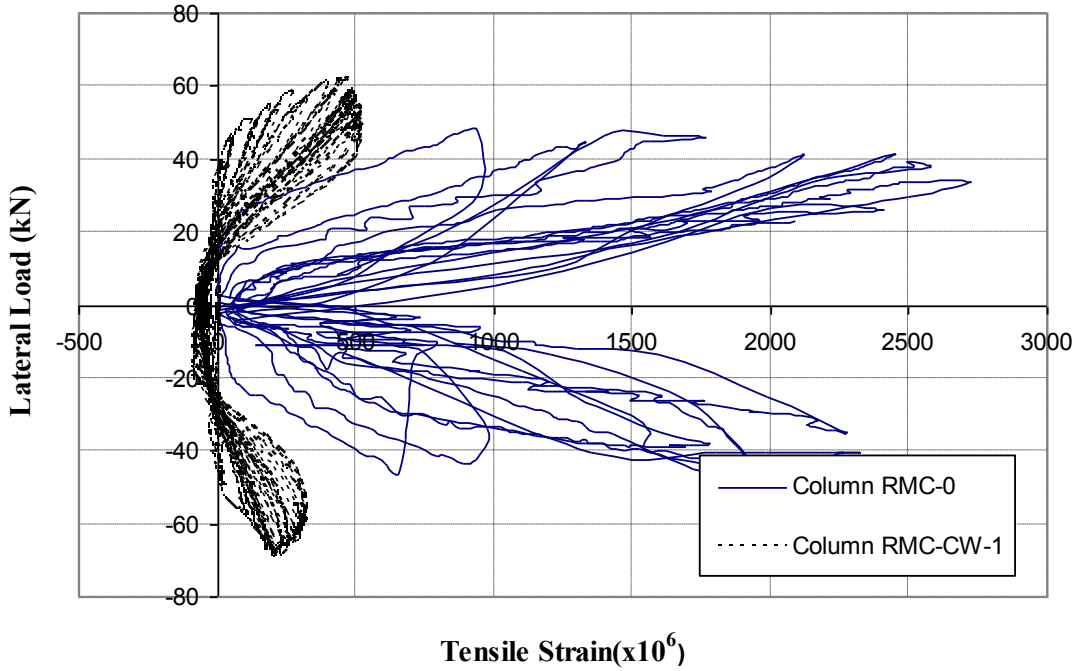

Figure B.8: Measured strains in tie located at one-seventh of the height in columns RMC-0 and RMC-CW-1

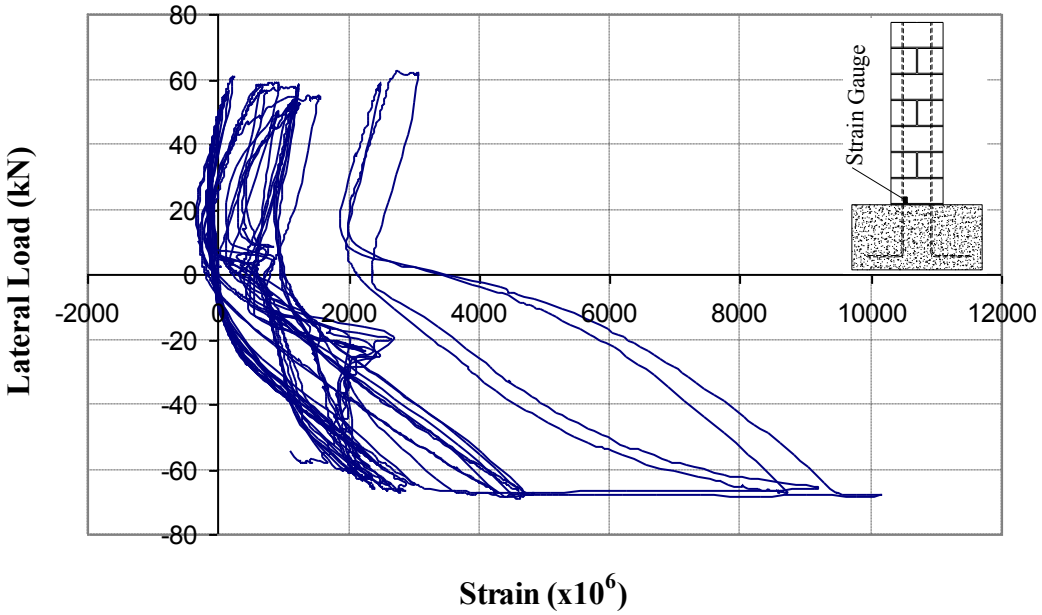

Figure B.9: Measured strains in one of the vertical bars in column RMC-CW-1

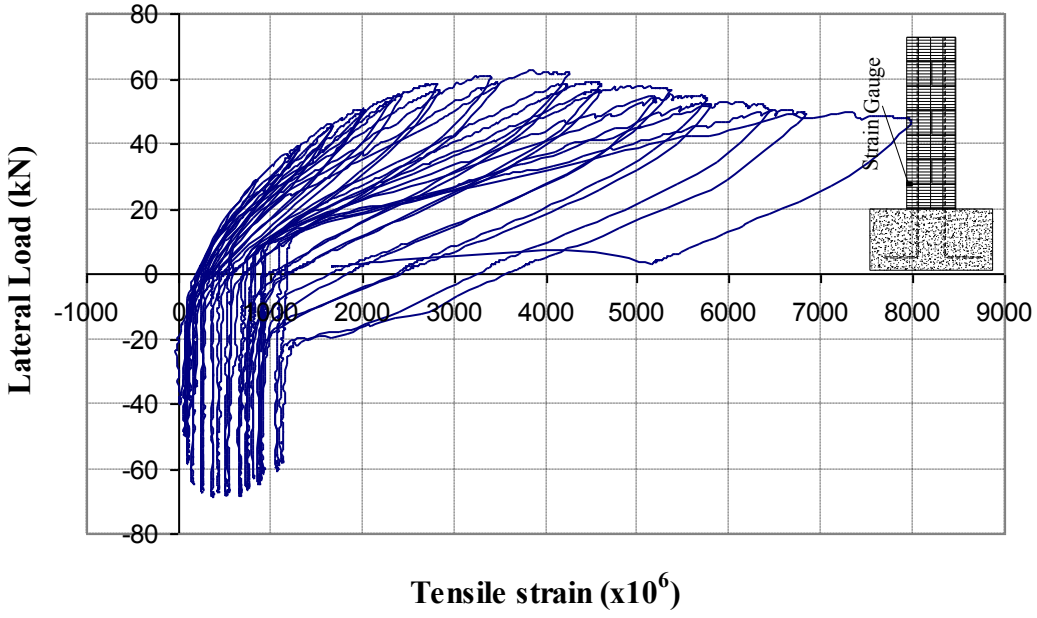

Figure B.10: Measured strains of CFRP wrap in one of the bull-nose corners at one-seventh of the column height.

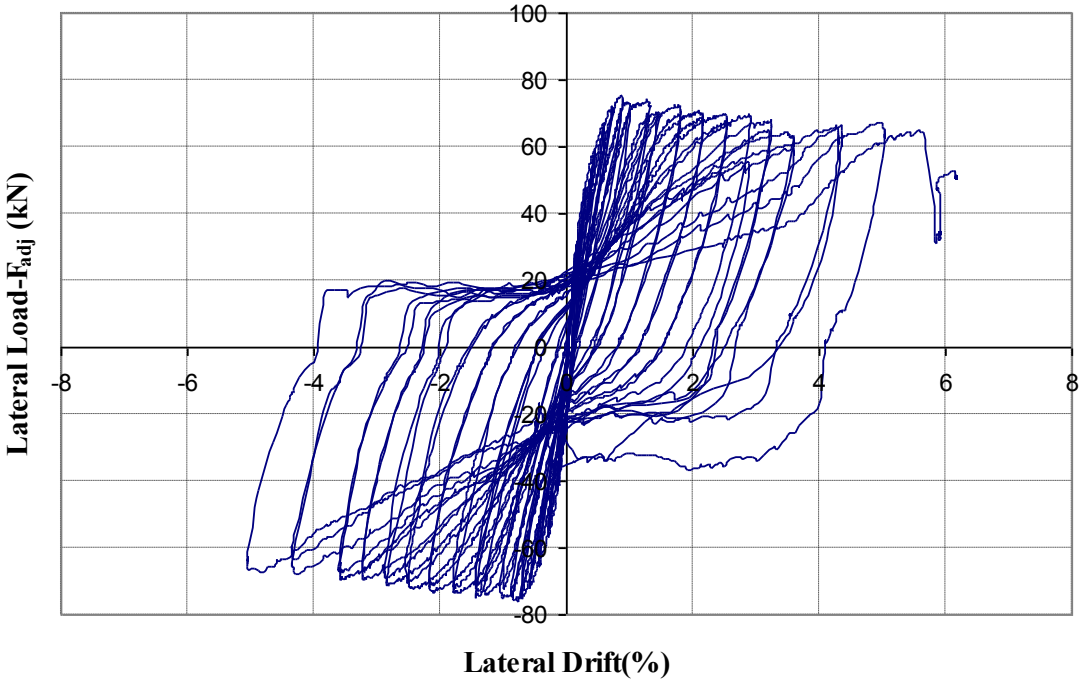

Figure B.11: Lateral load versus drift (%) for column RMC-CW-2

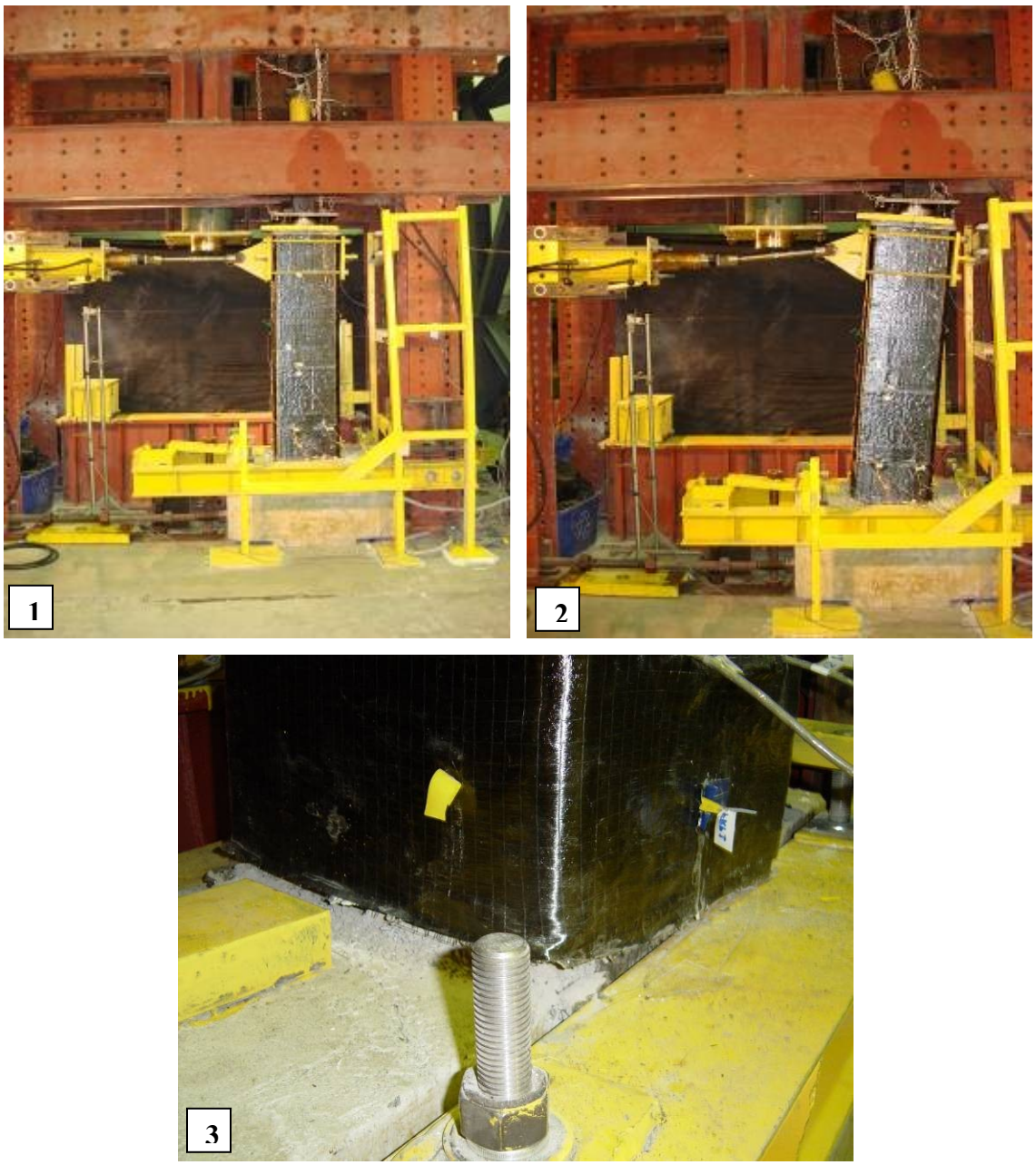

Figure B.12: (1) Wrapped column before the test (2) Specimen at 6% drift level (3) Column-footing interface at 6% drift

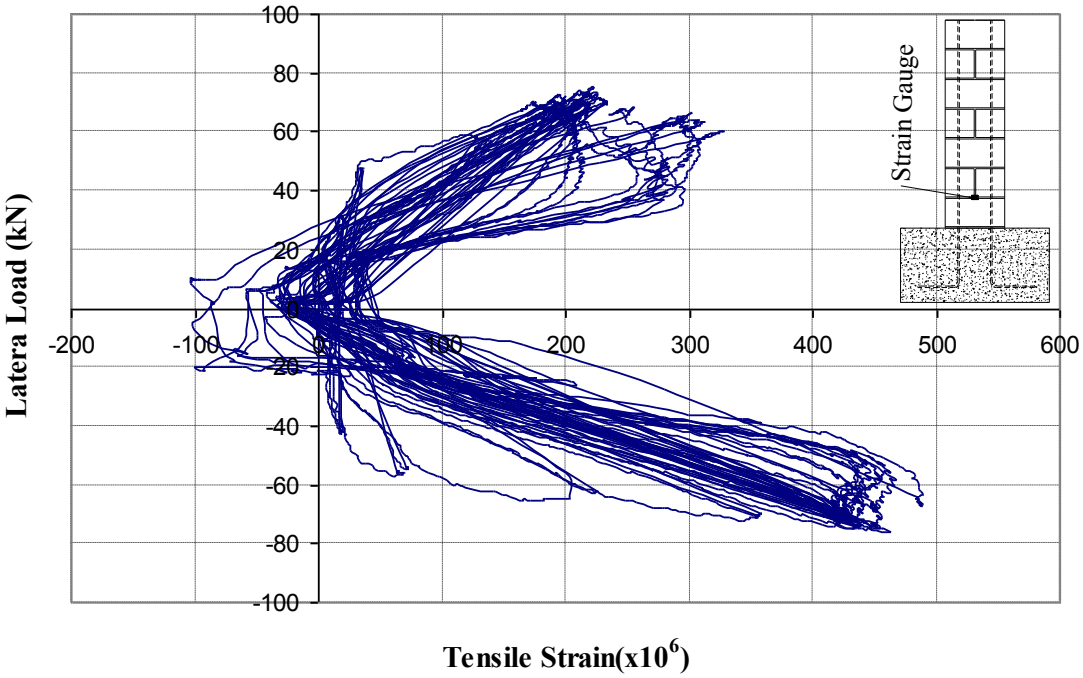

Figure B.13: Measured strain in the tie placed at one-seventh of the height in column

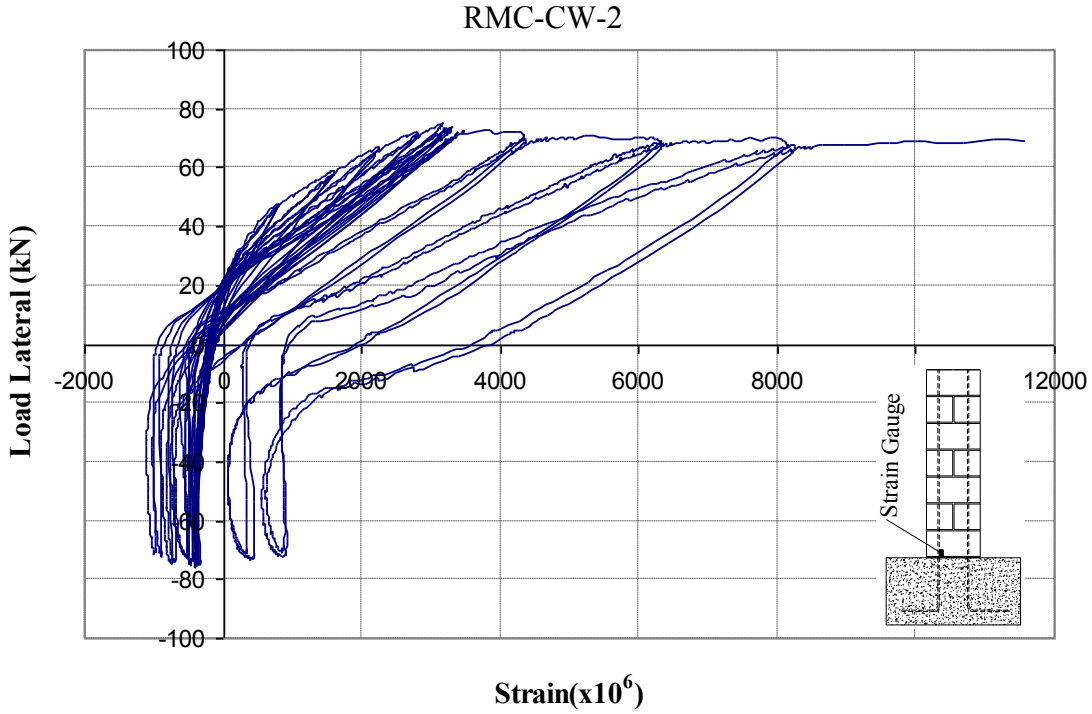

Figure B.14: Measured strain in one of the vertical bars in column RMC-CW-2

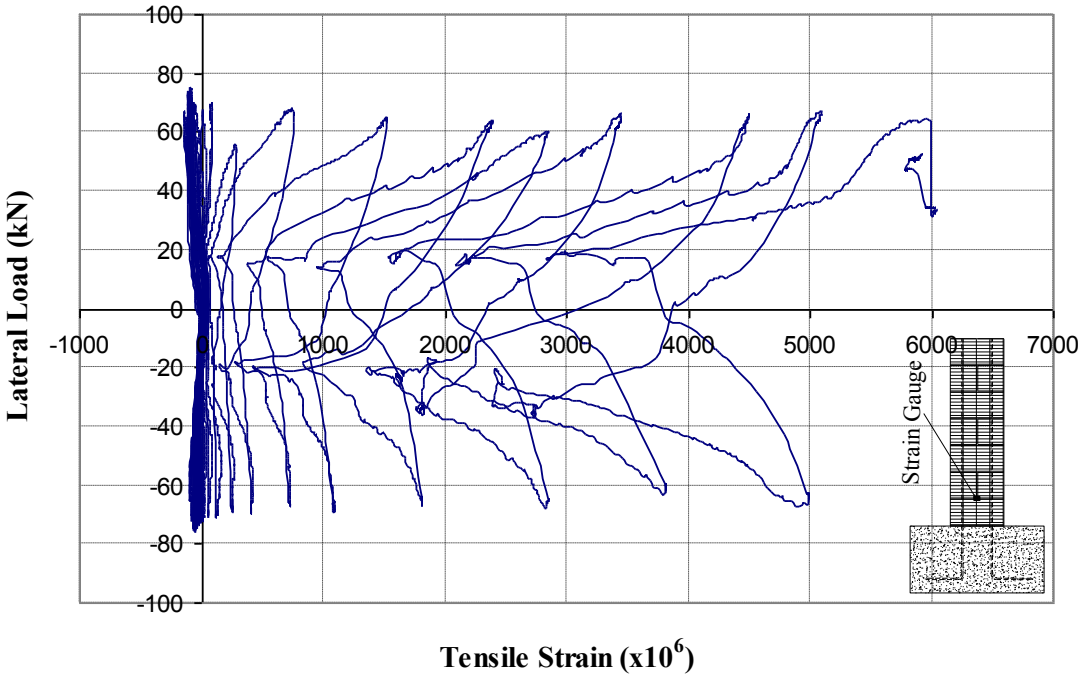

Figure B.15: Measured strains of CFRP wrap in the middle of flat surface at one-seventh of the column height.

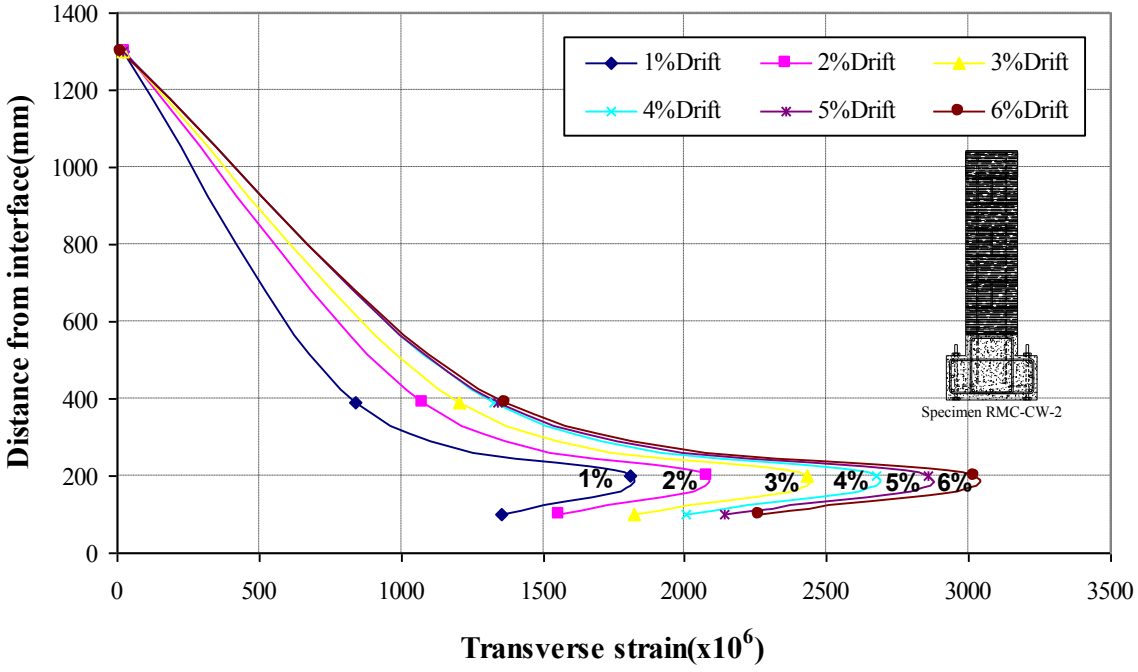

Figure B.16: Measured tensile strains of CFRP wrap along the height of column RMC-CW-2 at different drift level

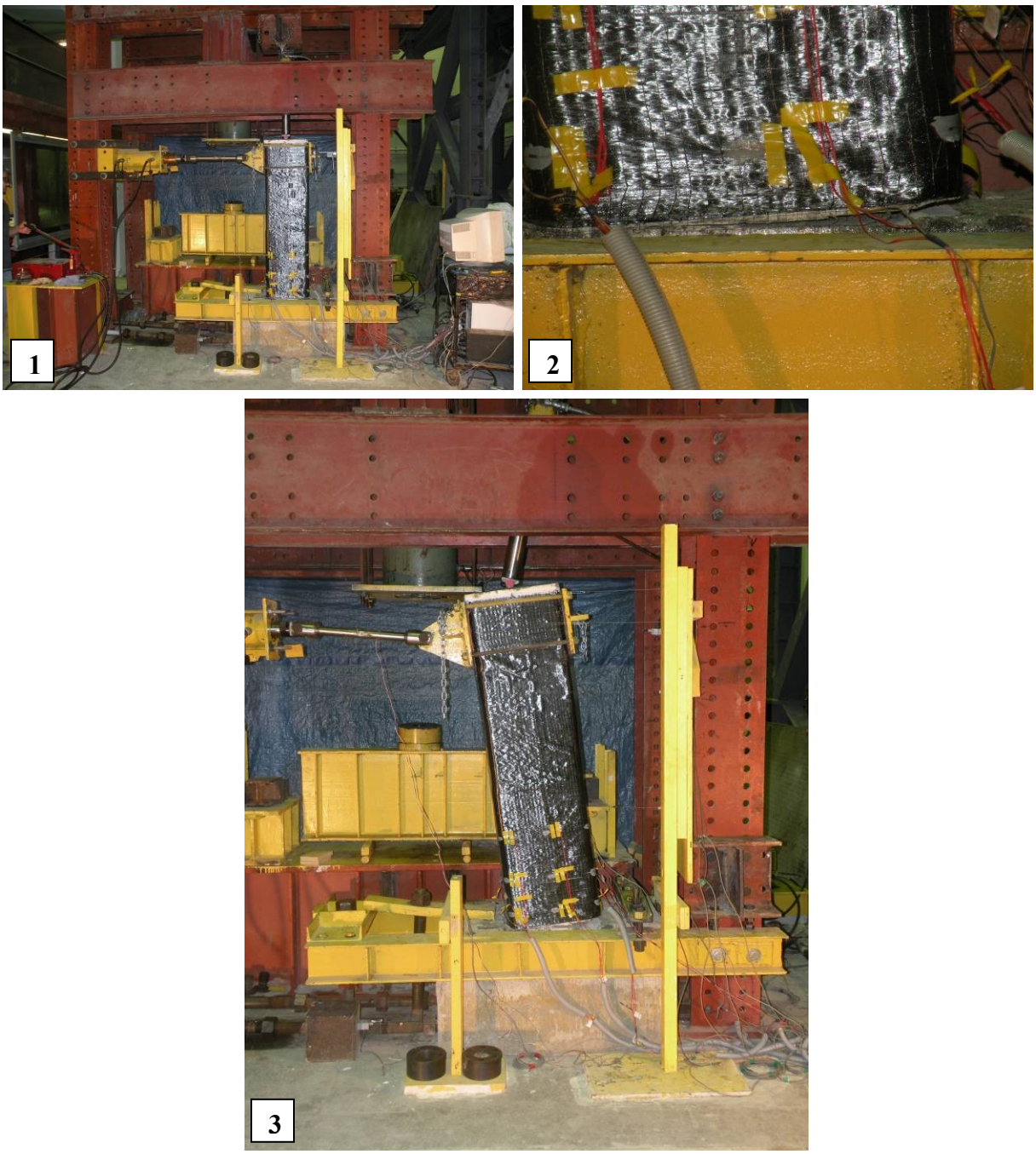

Figure B.17: 1) Test setup for column RMC-CW-3, 2) column footing interface at high drifts, 3) column at 10% lateral drift

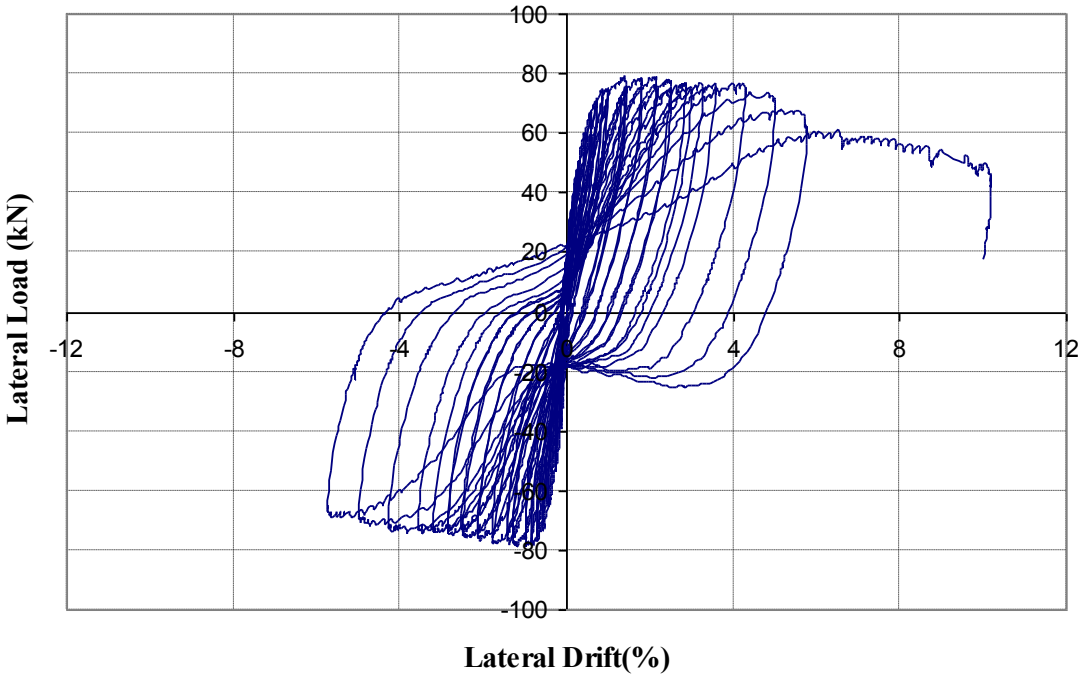

Figure B.18: Lateral load versus drift (%) for column RMC-CW-3

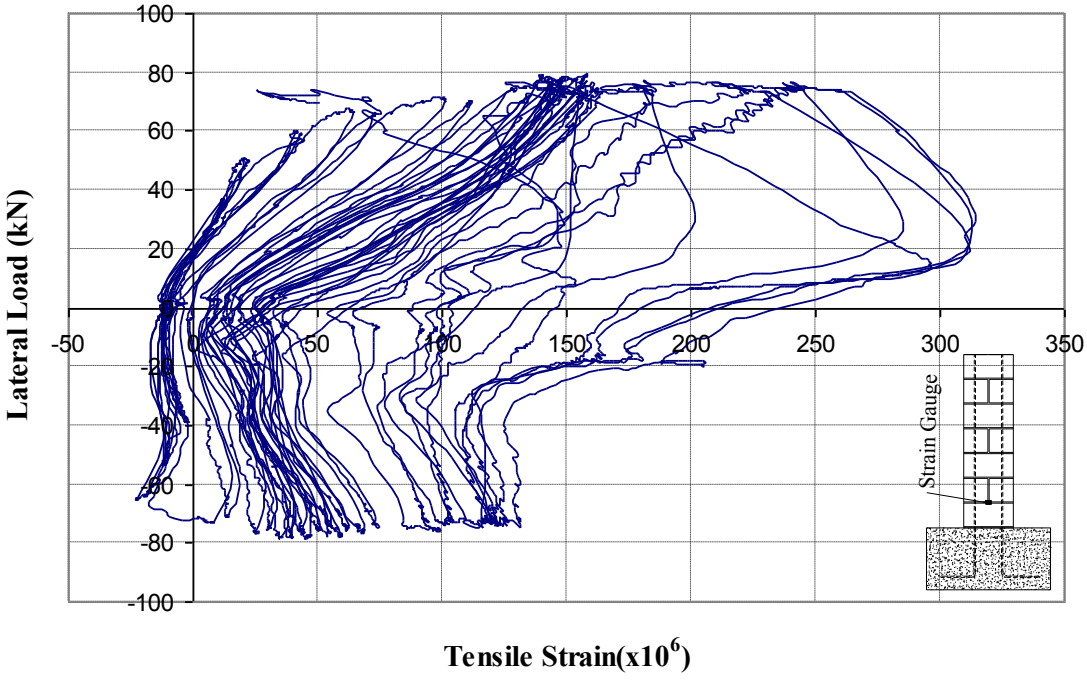

Figure B.19: Measured strains in the tie placed at one-seventh of the height in column RMC-CW-3

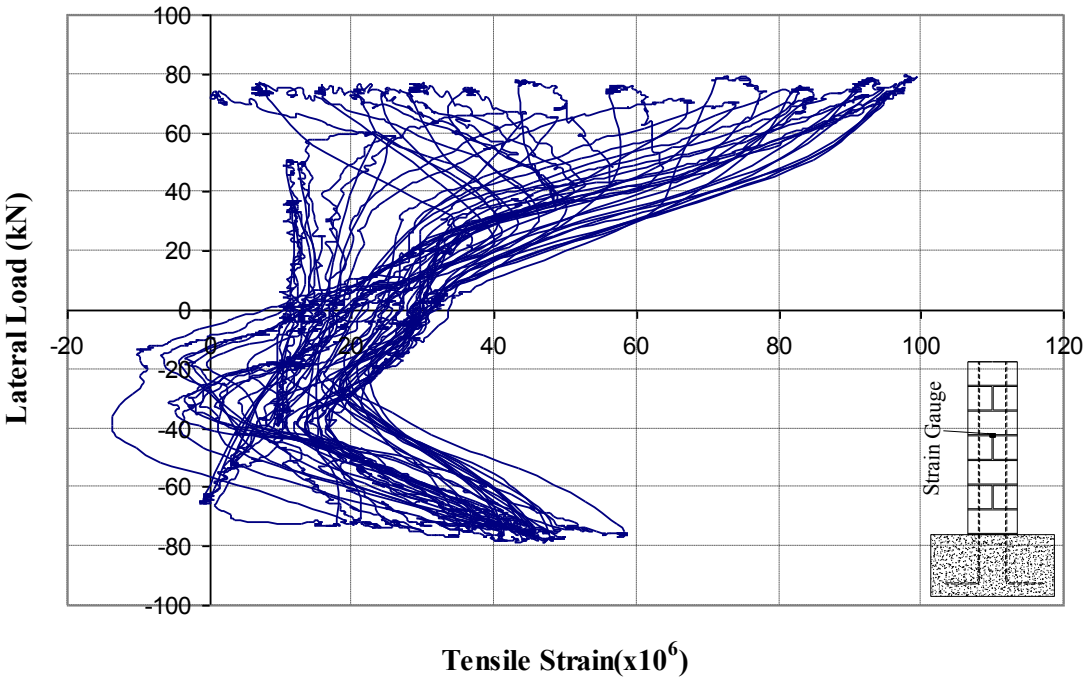

Figure B.20: Measured strain in the tie placed at middle of the height in column RMC-CW-3

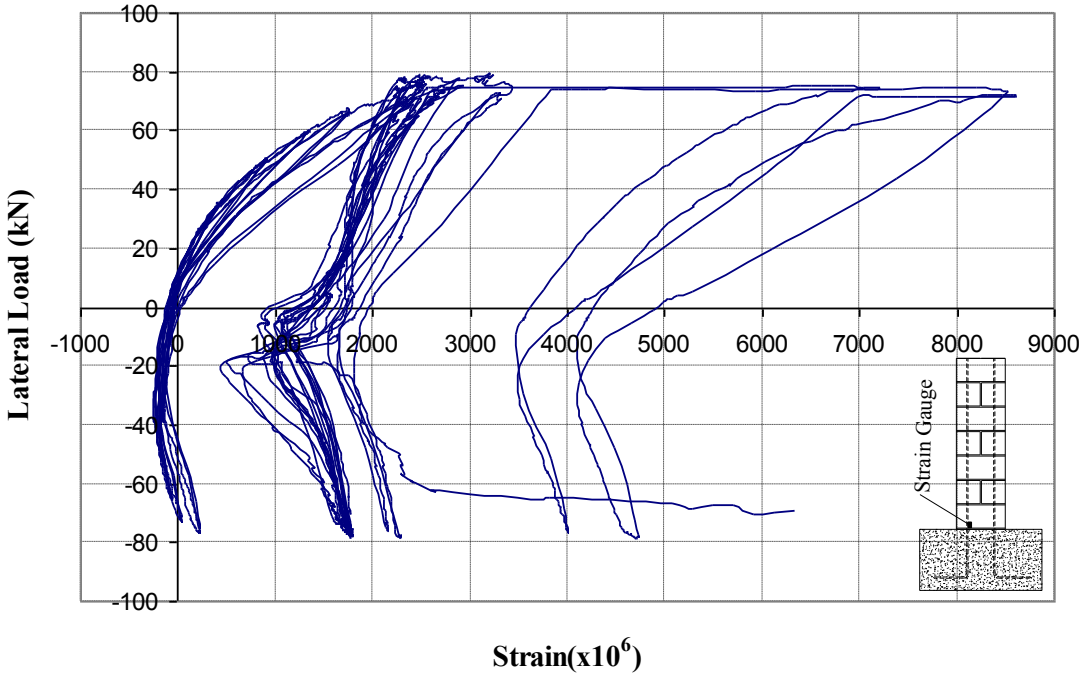

Figure B.21: Measured strain in one of the vertical bars in column RMC-CW-3

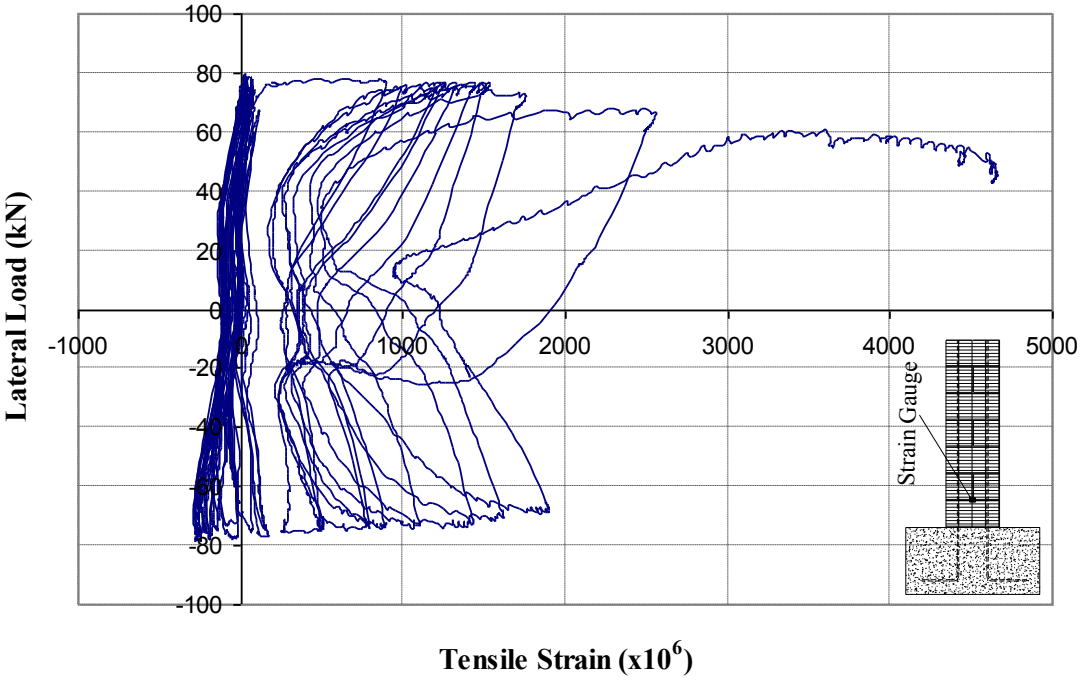

Figure B.22: Measured strains of CFRP wrap at the middle of flat surface located at one-seventh of the height in column RMC-CW-3

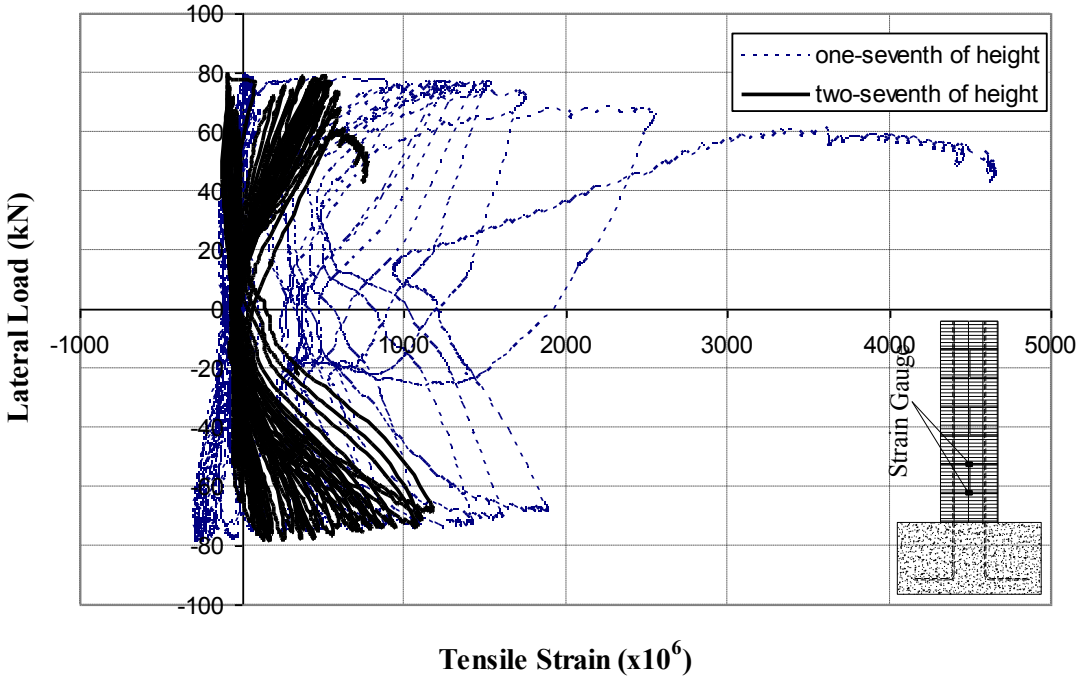

Figure B.23: Measured strains of CFRP wrap at two-seventh and one-seventh of the of the height in column RMC-CW-3

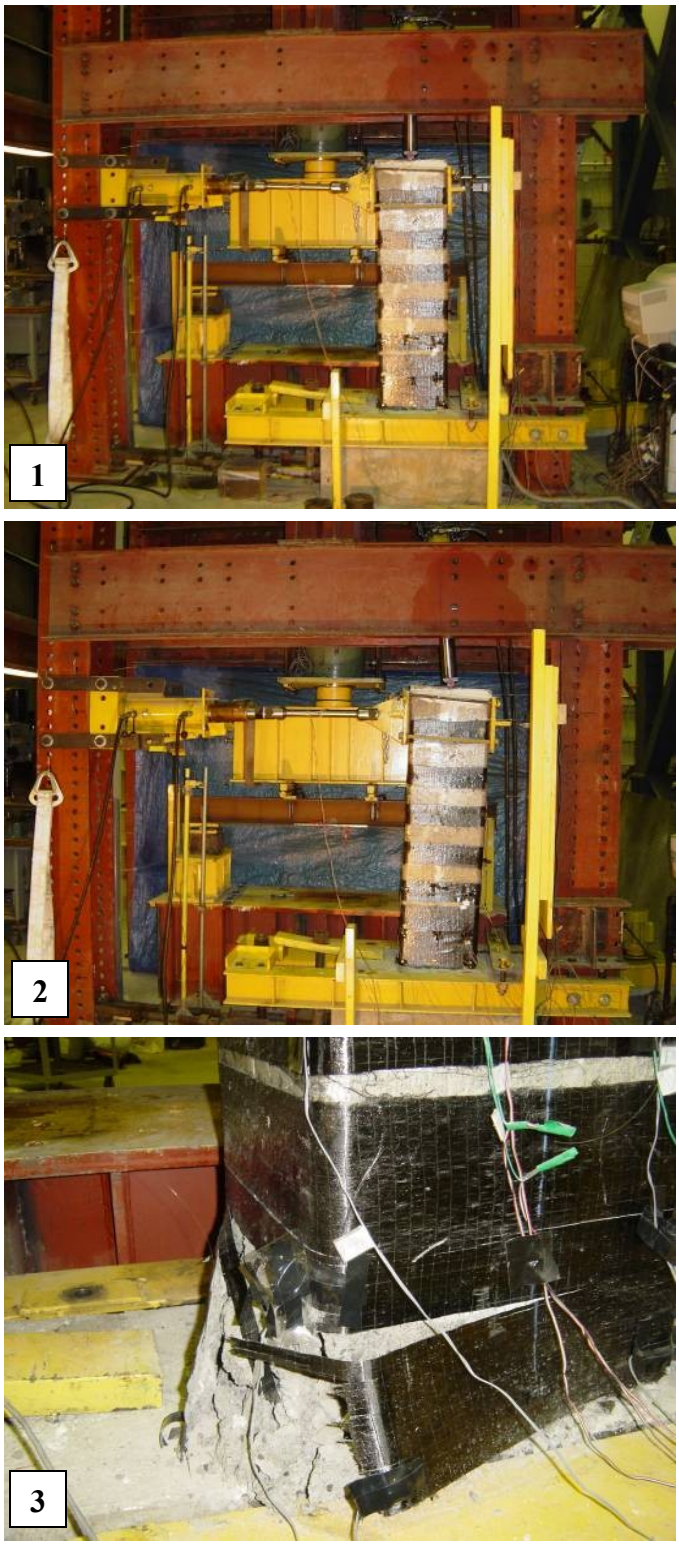

Figure B.24: 1) column RMC-CW-1S at 1% drift, 2) column at 3% drift, 3) Sudden rupture of CFRP wrap near footing and explosive crushing of concrete units at 10% drift

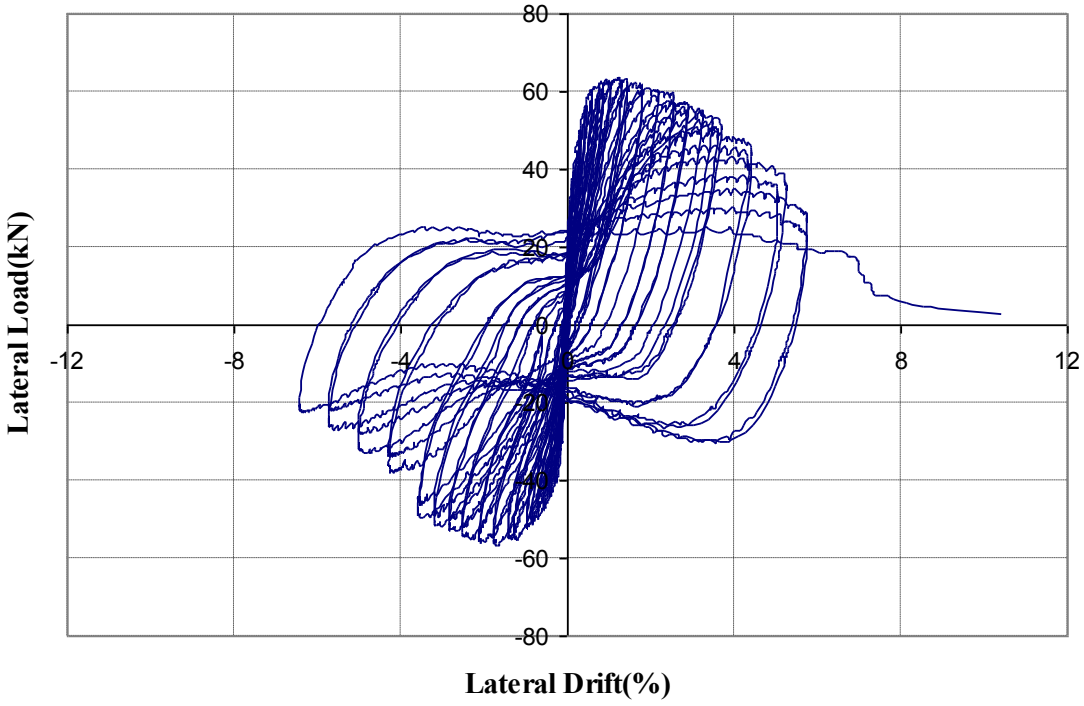

Figure B.25: Lateral load versus drift (%) for column RMC-CW-1S

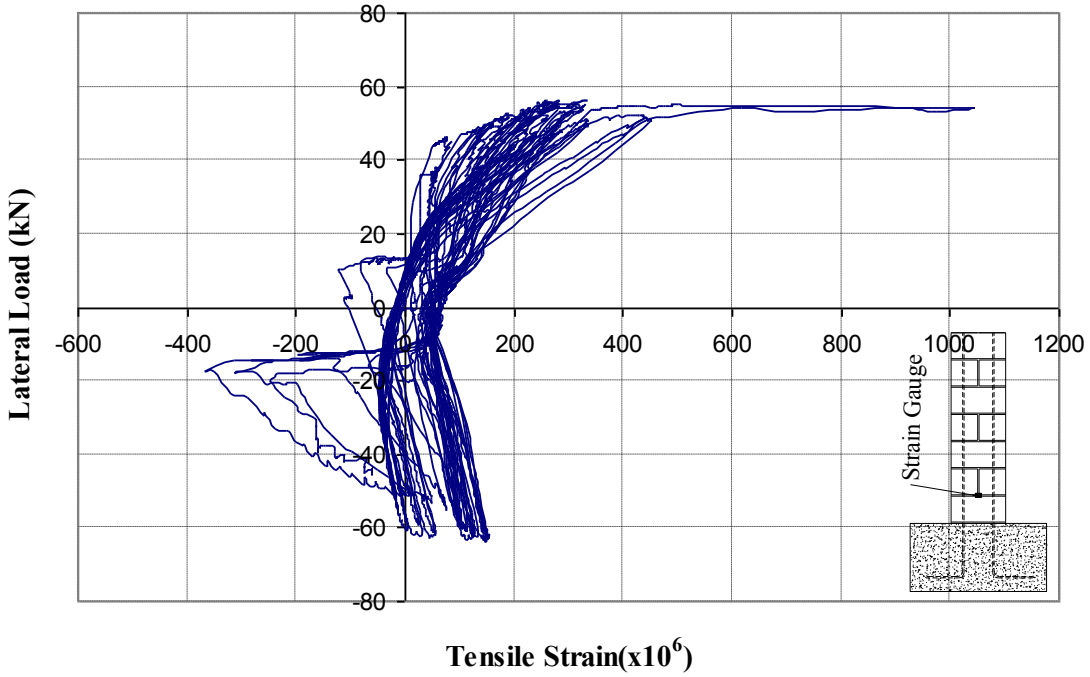

Figure B.26: Measured strains in the tie placed at one-seventh of the height in column RMC-CW-1S

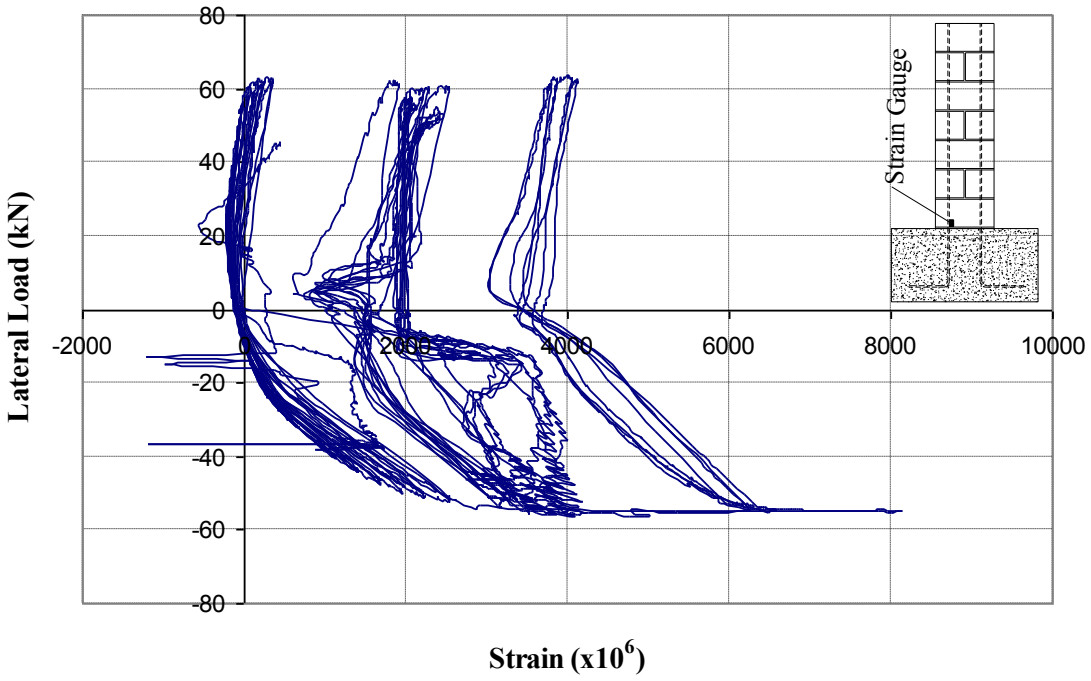

Figure B.27: Measured strain in one of the vertical bars in column RMC-CW-1S

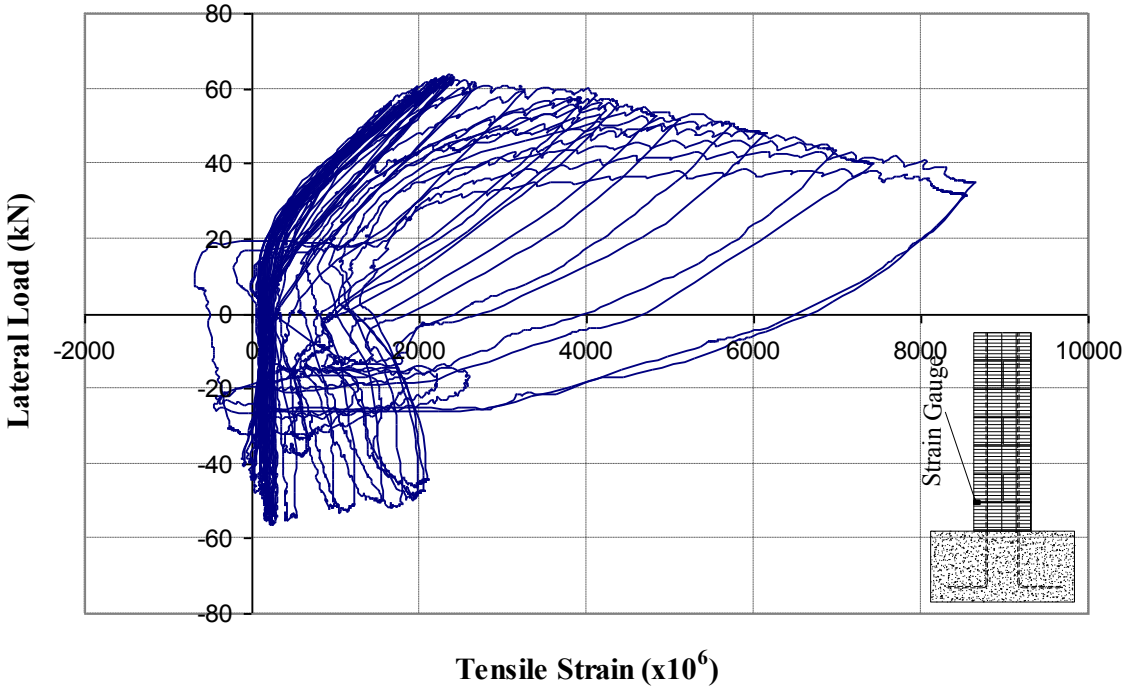

Figure B.28: Measured strains of CFRP wrap at a corner located at one-seventh of the column RMC-CW-1S height.

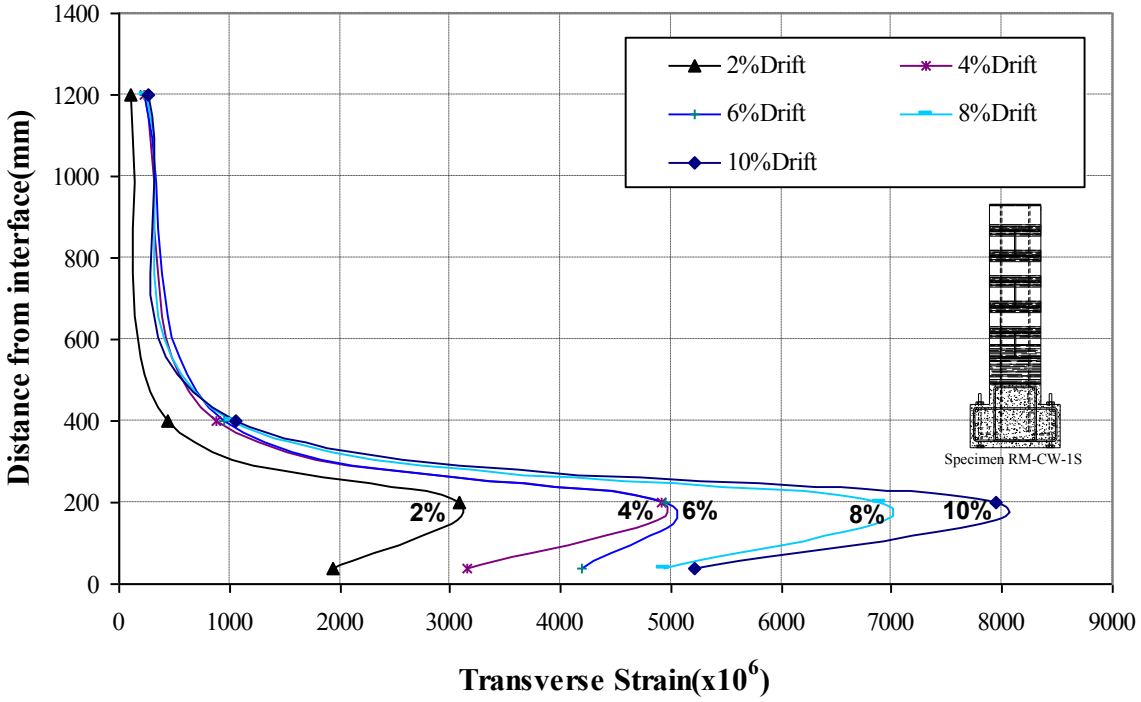

Figure B.29: Measured tensile strains of CFRP wrap along the column height at different drift levels

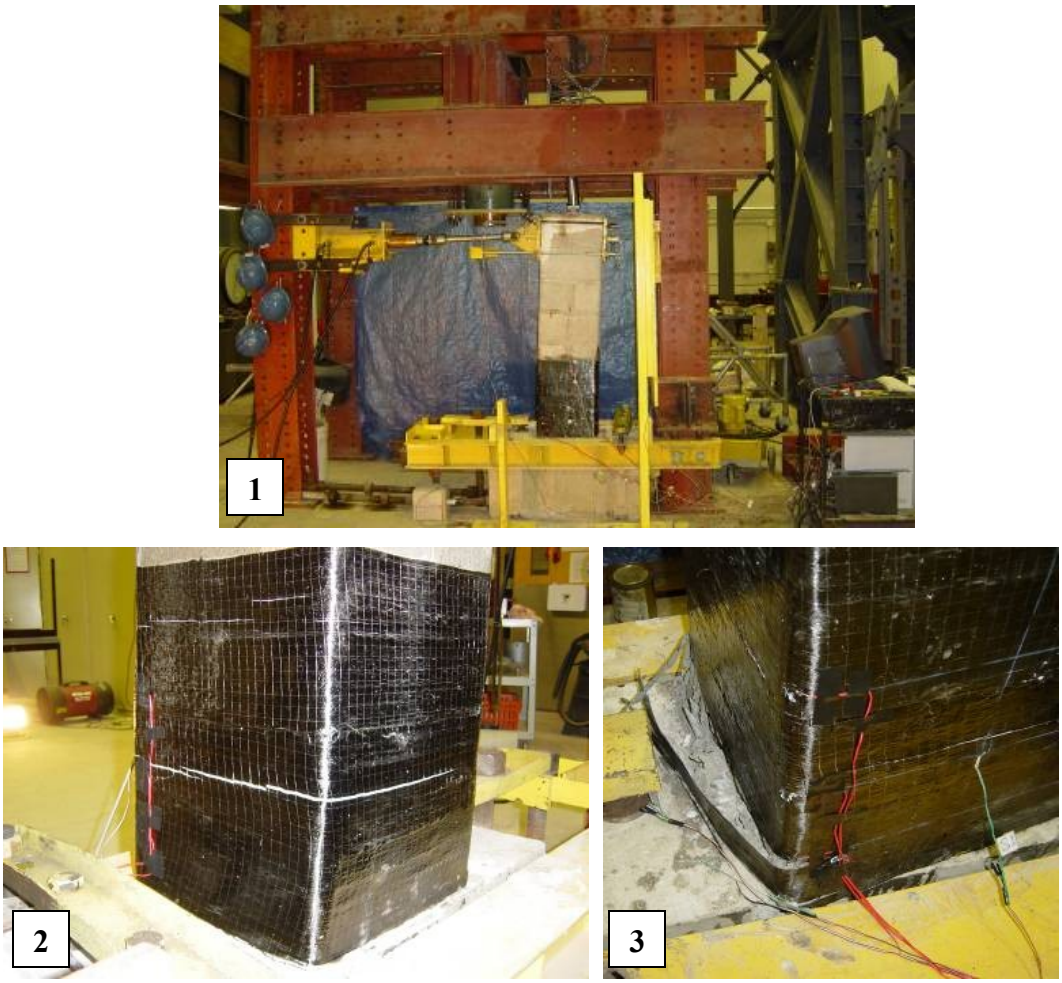

Figure B.30: 1) Column RMC-CW-1P at 3% lateral drift, 2) Column RMC-CW-1P: Local opening of CFRP jacket in several location 5.7% lateral drift, 3) CFRP wrap rupture and crushing of masonry blocks at 10% lateral drift in column RMC-CW-1P

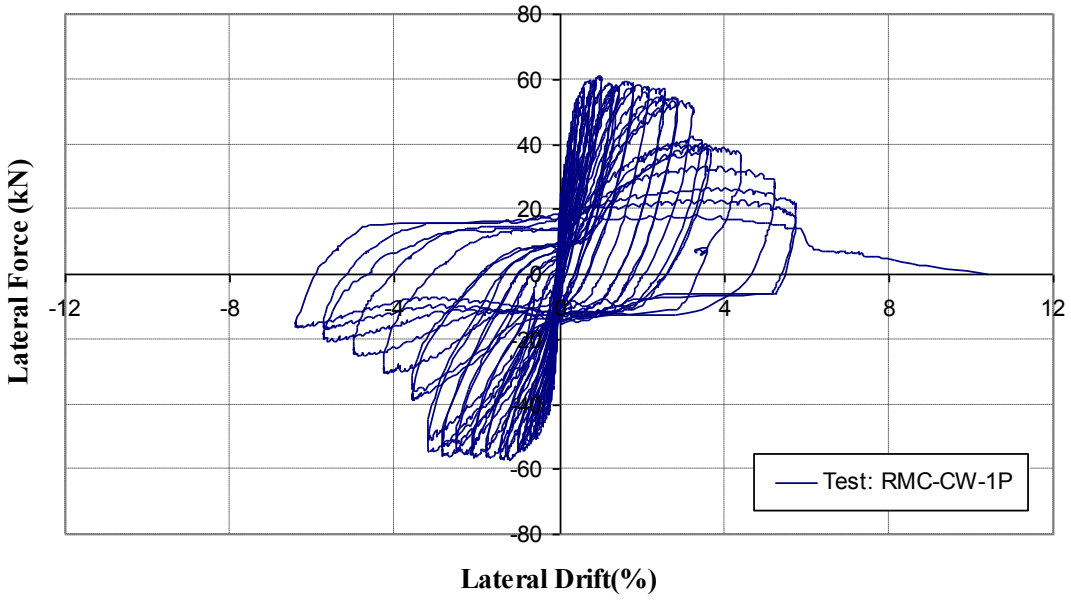

Figure B.31: Lateral load versus drift (%) for column RMC-CW-1P

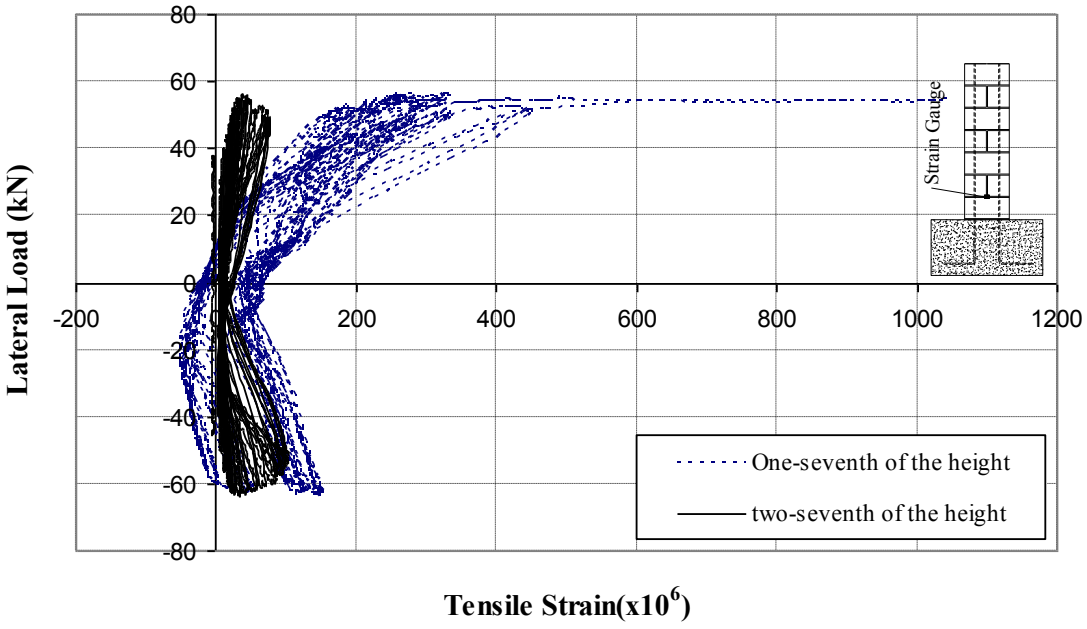

Figure B.32: Measured strains in the tie placed at one-seventh and four-seventh of the height in column RMC-CW-1P

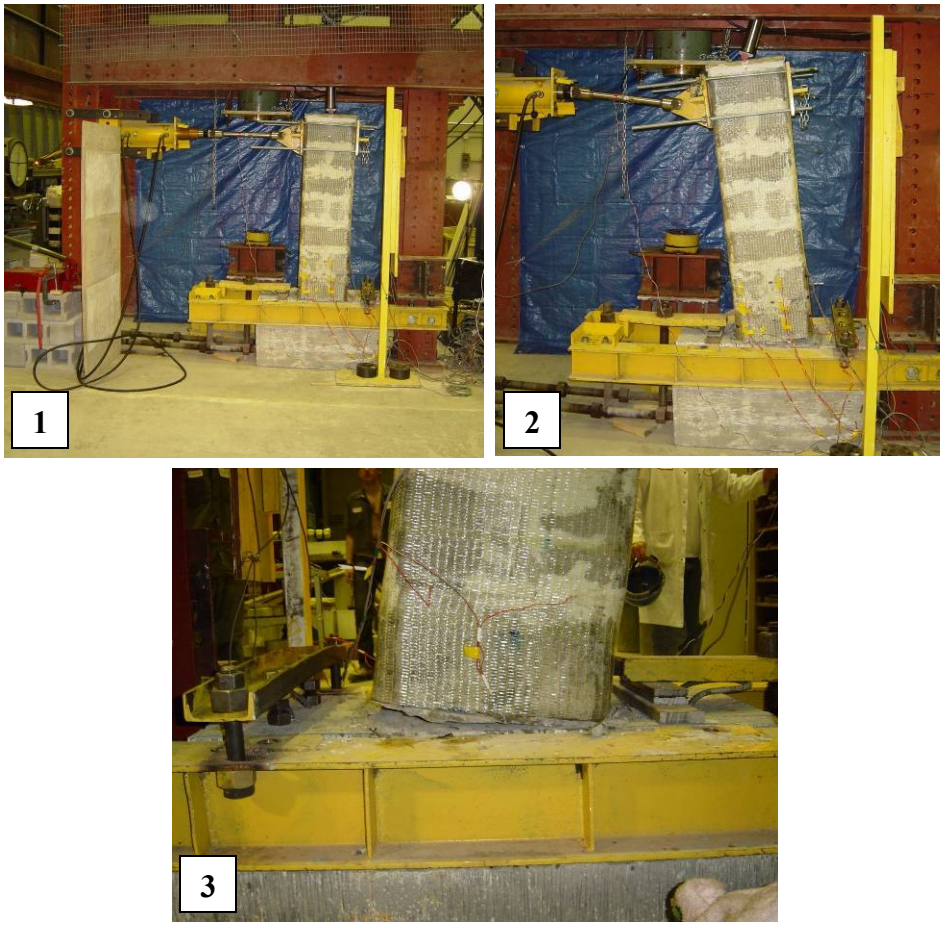

Figure B.33: 1) Column RMC-GW-1 before applying lateral loads, 2) Column RMC-GW-1 at 6% lateral drift, 3) column-footing interface at high lateral drift

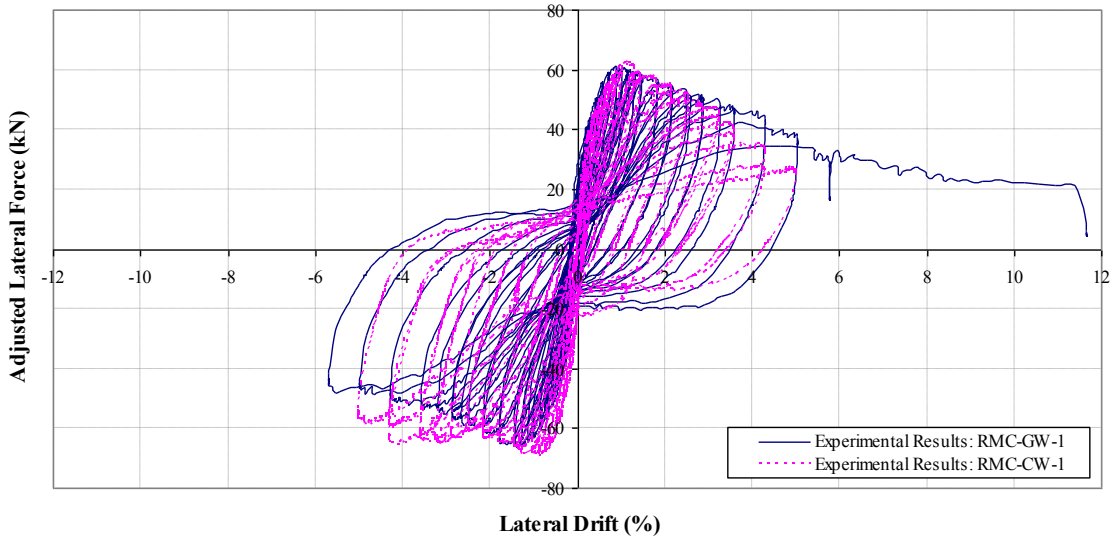

Figure B.34: Lateral load versus drift (%) for column RMC-GW-1

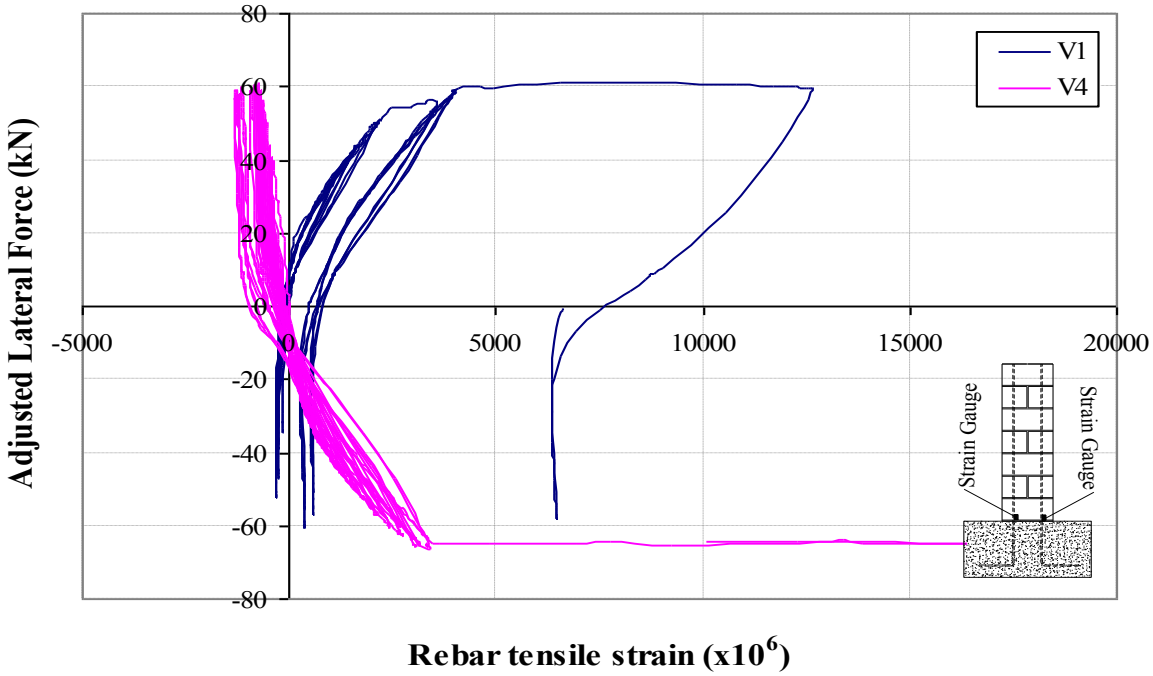

Figure B.35: Measured strain in two of the vertical bars in column RMC-GW-1

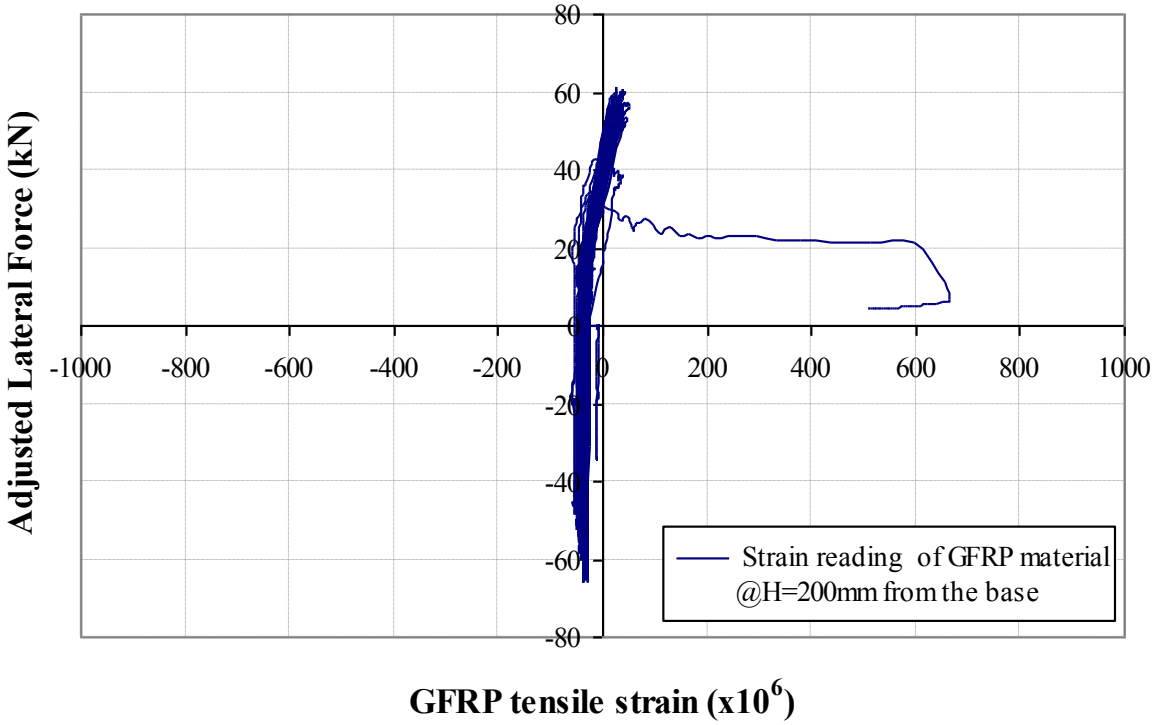

Figure B.36: Measured strain of GFRP wrap at 200 mm above footing and one of the corners of column RMC-GW-1

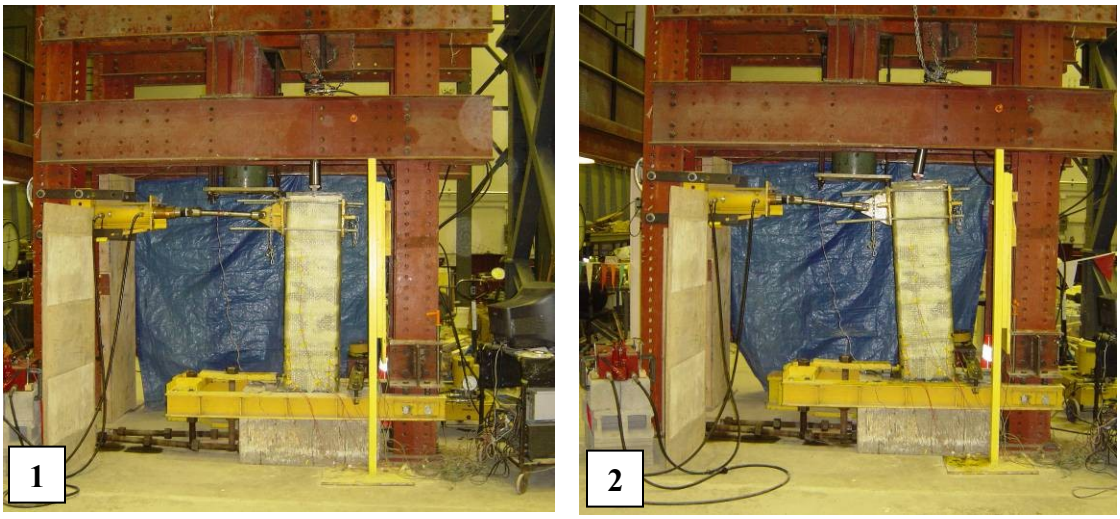

Figure B.37: 1) Column RMC-GW-2 before applying lateral loads, 2) Column RMC-GW-2 at 6% lateral drift.

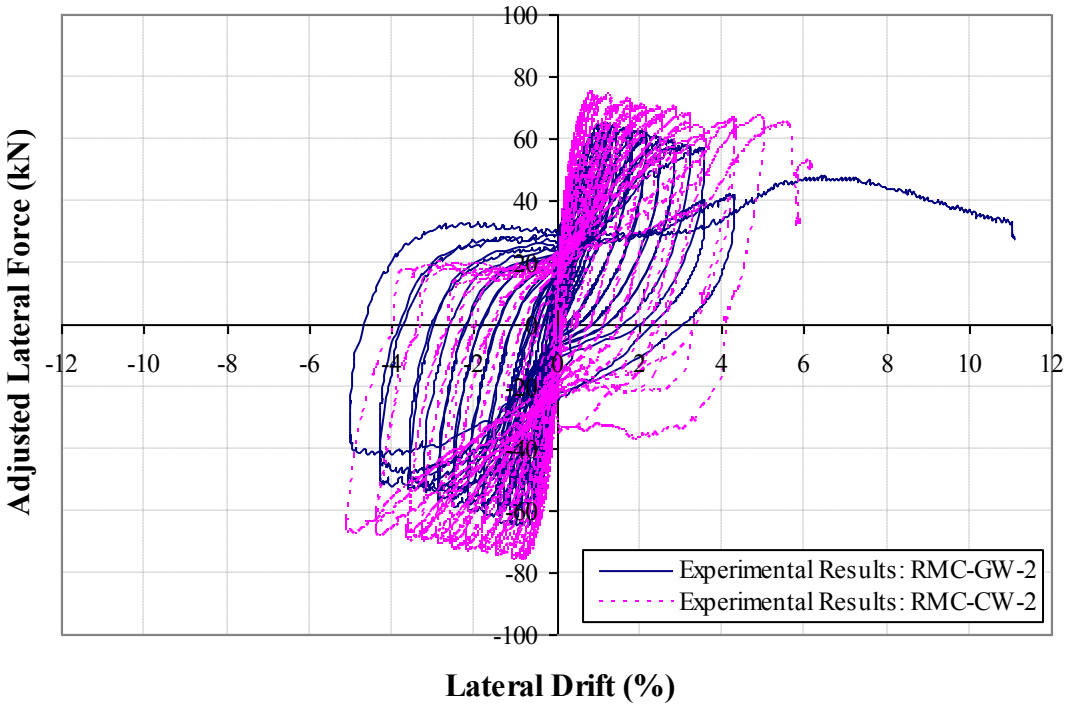

Figure B.38: Lateral load versus drift (%) for column RMC-GW-2 compared with column wrapped with 2 layers of CFRP (column RMC-CW-2)

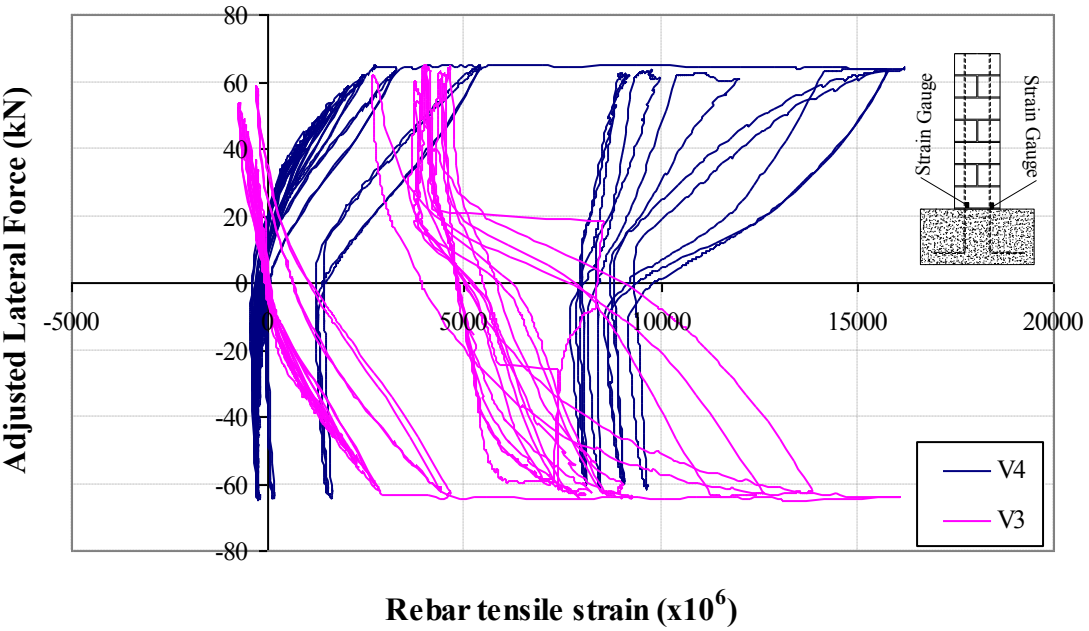

Figure B.39: Measured strain in two of the vertical bars in column RMC-GW-2

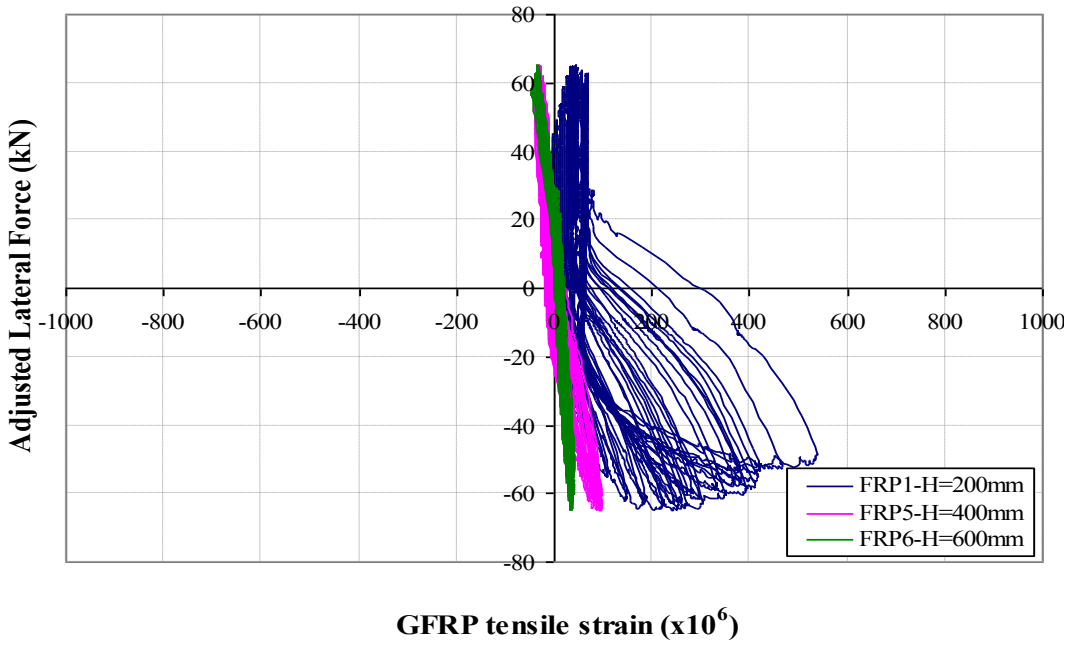

Figure B.40: Measured strain of GFRP wrap at 200,400, and 600 mm above the footing of column RMC-GW-2

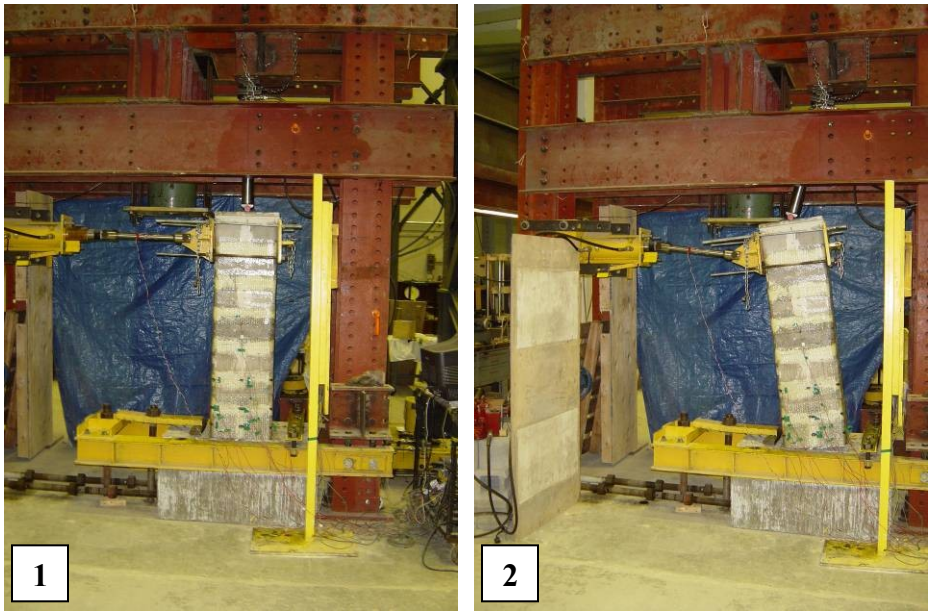

Figure B.41: 1) Column RMC-GW-1S before applying lateral loads, 2) Column RMC-GW-1S at 6% lateral drift.

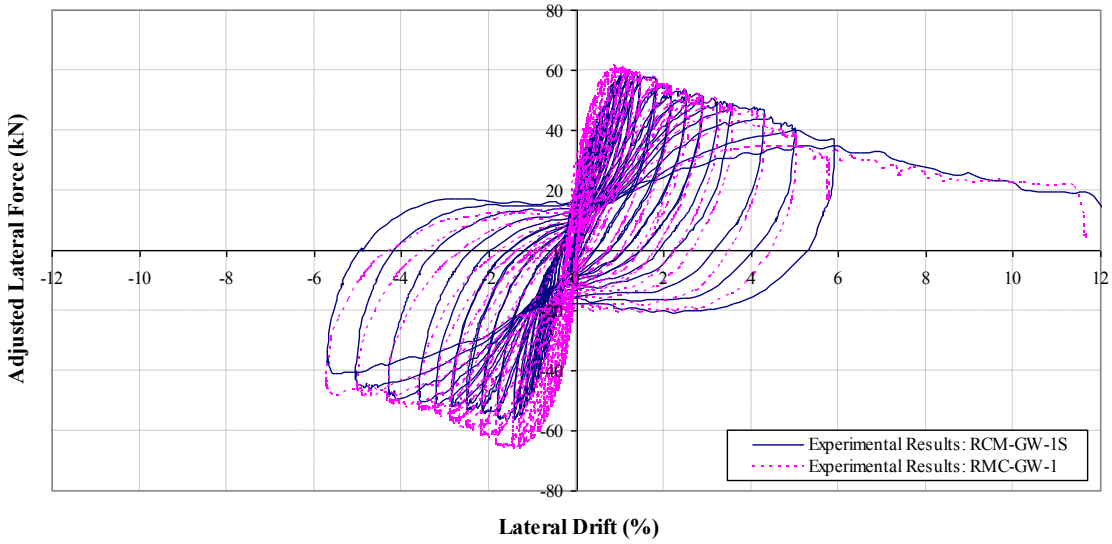

Figure B.42: Lateral load versus drift (%) for column RMC-GW-1S compared with column wrapped with 1 layers of CFRP (column RMC-CW-1)

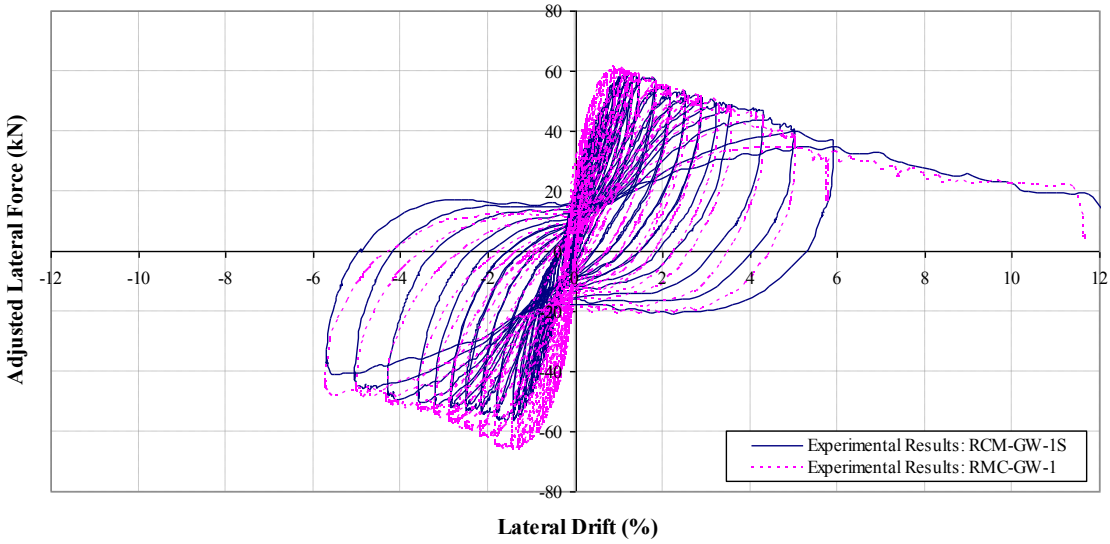

Figure B.43: Lateral load versus drift (%) for column RMC-GW-1S compared with column wrapped with strips of 1 layers of CFRP (column RMC-CW-1S)

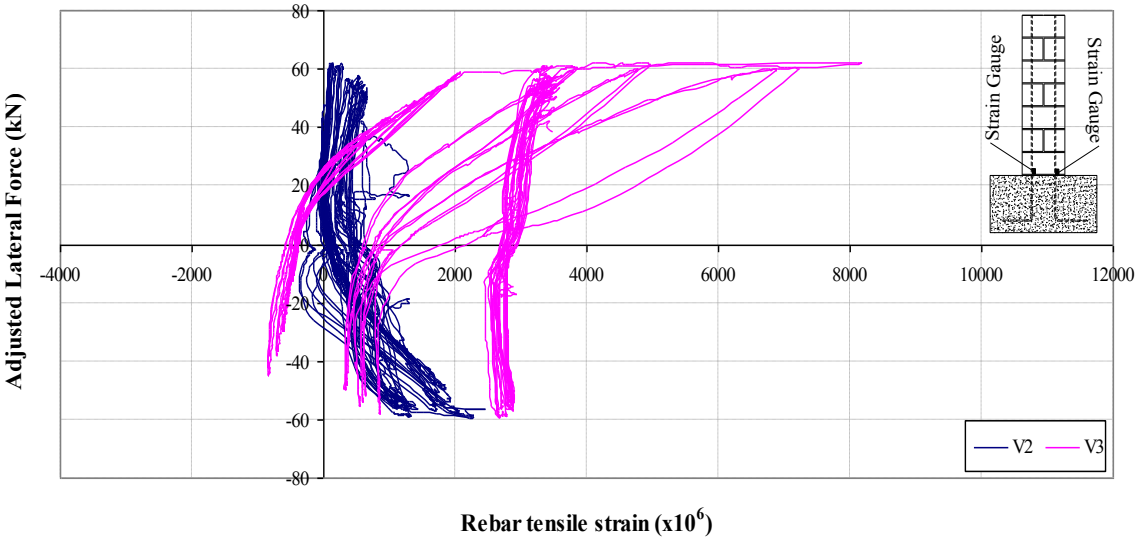

Figure B.44: Measured strain in two of the vertical bars in column RMC-GW-1S

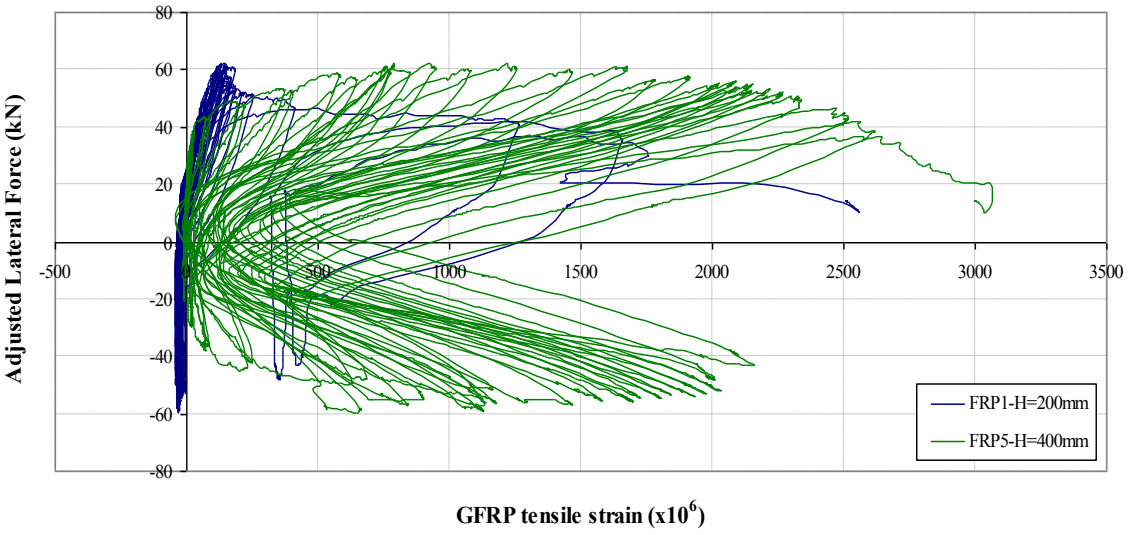

Figure B.45: Measured strain of GFRP wrap at 200and 400 mm above the footing of column RMC-GW-1S